NASA Contractor Report 3523

Wind Tunnel Tests of High-Lift Systems for Advanced Transports Using High-Aspect-Ratio Supercritical Wings

John B. Allen, Wayne R. Oliver,
and Lee A. Spacht

NASA

NASA Contractor Report 3523

Wind Tunnel Tests of High-Lift Systems for Advanced Transports Using High-Aspect-Ratio Supercritical Wings

John B. Allen, Wayne R. Oliver,
and Lee A. Spacht

McDonnell Douglas Corporation
Long Beach, California

NASA
National Aeronautics
and Space Administration

Scientific and Technical
Information Office

1982

CONTENTS

CONTENTS — (Concluded)

ILLUSTRATIONS

ILLUSTRATIONS — (Continued)

ILLUSTRATIONS — (Concluded)

SUMMARY

This report presents the results of the wind tunnel testing of an advanced-technology high-lift system for a wide body and a narrow body model of a fuel-efficient transport. These aircraft, derived from detailed system studies for a medium-range transport, incorporated high-aspect-ratio supercritical wings. Along with the wind tunnel results from an earlier phase of the program, these experimental results represent the first low-speed high-Reynolds-number wind tunnel data for such an advanced transport. Experimental data included the effects on the low-speed aerodynamic characteristics of slat, variable-camber Krueger (VCK), and fixed-camber Krueger (FCK) leading-edge devices, two-segment and single-segment trailing-edge flaps, nacelles, pylons, ailerons, spoilers, horizontal tail, and landing gear. Both Mach and Reynolds-number effects were also studied for selected configurations

The cruise wings achieved tail-off maximum lift coefficients near 1.6 and tail-off lift-drag ratios near 21. For the high-lift configurations, the values of maximum lift coefficient were significantly improved when compared with current aircraft values. Typical tail-off maximum lift coefficients for takeoff and landing configurations were 2.4 and 3.1, respectively. Corresponding tail-off lift-drag ratios were 15.4 and 9.8. These ratios represent significant improvement over those of previous-generation aircraft.

Aileron studies indicated that, for all flap settings, negative deflections (trailing edge up) were more effective than positive deflections (trailing edge down). The effect of spoiler deflection on roll characteristics indicated improved effectiveness as the flap deflection was increased. Symmetrical spoiler deflections, for both takeoff and landing flaps, showed the spoiler to be very effective in reducing lift and incremental drag. The landing gear caused a slight reduction in maximum lift coefficient for the landing configuration.

Analysis of the data has identified areas where continued efforts could result in further improvements. These areas include pitching moments for the high-lift configuration, and ground effect characteristics. Specific test items are suggested for this continued development.

FOREWORD

This document presents the results of a contract study performed for the National Aeronautics and Space Administration (NASA) by the Douglas Aircraft Company, McDonnell Douglas Corporation. This study was part of Phase II of the Energy Efficient Transport (EET) project of the Aircraft Energy Efficiency (ACEE) program.

Acknowledgments for their support and guidance are given to the NASA technical monitor for the contract, T.G. Gainer of the Energy Efficient Transport Project Office at the Langley Research Center; to the NASA Project Manager, R.V. Hood, and to J.R. Tulinius, the on-site NASA representative; also to R.T. Whitcomb of the Langley Research Center for his concept of the supercritical wing.

Acknowledgments are also given to the director and staff of the NASA Ames and Langley Research Centers, at which facilities the test programs were conducted. The cooperation and discussions concerning high-lift development for high-aspect-ratio supercritical wings of R.J. Margason and H.L. Morgan of the NASA Langley STAD Low-Speed Aerodynamics Branch were greatly appreciated.

The Douglas personnel who made significant contributions to this work were:

M. Klotzsche	ACEE Program Manager
A.B. Taylor	EET Project Manager
J.G. Callaghan	Branch Chief, Configuration Design and Development, Aerodynamics Subdivision
D.E. Ellison	Branch Chief, Stability, Control and Flying Qualities, Aerodynamics Subdivision
W.R. Oliver	Task Manager for initial-phase Aerodynamic Design (Report Author)
G.G. Myers	Aerodynamic Design
L.A. Spacht	Aerodynamic Design (Report Author)

J.B. Allen	Task Manager for final-phase Aerodynamic Design (Report Author)
J.D. Cadwell	Branch Chief, Aerodynamics Wind Tunnel Model Group
R.J. Commons	Aerodynamics Wind Tunnel Model Group
F.B. Baugh	Aerodynamics Wind Tunnel Model Group
D.H. Broderson	Aerodynamics Wind Tunnel Model Group
L.B. Scherer	Aerodynamics Wind Tunnel Model Group
G.K. Ige	Aerodynamics Wind Tunnel Model Group
R.C. Leeds	Aerodynamics Wind Tunnel Model Group

INTRODUCTION

The present investigation was made in connection with the high-lift studies of Reference 1 and the cruise performance studies of Reference 2. During the Reference 2 work, Douglas developed the high-aspect-ratio supercritical wing for the DC-X-200, a 200-passenger wide body configuration proposed as a next generation transport. The results of that study were used to design a wing with minimum drag creep for the Advanced Technology Medium Range (ATMR) transport, a 176-passenger narrow body configuration. Both investigations showed that supercritical wing technology could significantly reduce fuel consumption and direct operating costs; they also established a sound technology base for future development work.

The high-lift system reported in Reference 1 was developed for the DC-X-200. A model of a DC-X-200 with various leading- and trailing-edge high-lift devices was tested. The results indicated that although the system gave better performance than the high-lift systems on current transports, even greater improvements are to be gained by developing the system further. Moreover, the takeoff and landing configurations tested had undesirable pitch-up at angles of attack near stall. Further investigation was needed to alleviate the pitch-up and improve the performance.

The present investigation was undertaken to continue the high-lift development for the DC-X-200 (the effort reported in Reference 1), and to extend the development to the ATMR configuration with its narrower body and more advanced wing. Part I of this report describes the investigation of the DC-X-200 high-lift system. The same 4.7-percent scale model tested during the high-lift study was tested in the the present investigation, but with a number of the leading- and trailing-edge modifications that it was hoped would improve the performance. These included:

1. A leading-edge fixed-camber Krueger which would be mechanically simpler than the variable-camber Krueger investigated in the work of Reference 1.

2. A two-segment flap replacing the flaperon tested on the Reference 1 model.

3. A variable-camber Krueger with a reduced deflection.
4. A mixed leading-edge configuration (a slat outboard and a fixed-camber Krueger inboard).
5. A two-piece leading-edge device, each piece having a different deflection.
6. Changes in the slat trim, both next to the fuselage and around the engine pylons.
7. A short-chord fixed-camber Krueger for the inboard wing to improve the pitching-moment characteristics.
8. A sealed leading-edge slat to improve the takeoff lift-drag ratio.

The model was tested in two different tunnels-- the NASA Langley Research Center V/STOL Tunnel in October and November 1979 and the NASA Ames Research Center 12-Foot Tunnel in July 1980. When tested in the Langley V/STOL Tunnel this model was designated the LB-486C; when tested in the Ames 12-Foot Tunnel it was designated the LB-486B. These designations are used throughout this report.

Part II of this report describes the ATMR investigation, in which the emphasis was placed on determining the effects of the narrow body configuration and the advanced wing geometry. These tests were made using a 5.59-percent scale model (designated LB-507A) in the Ames 12-Foot Tunnel in January and Febuary 1981. The objective of the LB-507 program was to evaluate the low-speed aerodynamic characteristics of the narrow body model, including the following:

1. The cruise wing characteristics.
2. The influence of takeoff and landing slat configurations on the aerodynamic characteristics.
3. Longitudinal stability characteristics (with and without the horizontal tail).
4. Nacelle/pylon and landing gear effects.
5. Spoiler and lateral control effectiveness.
6. Mach and Reynolds number effects.
7. Lateral-directional characteristics for selected configurations.

The data obtained during the three tunnel tests included data on the six-component forces and moments. The data obtained in the NASA Ames 12-Foot Tunnel included data on pressures measured at appropriate stations on the wing, slats, and flaps, and flow visualization photographs taken using a mini-tuft technique (Reference 3). The tests in the Langley V/STOL Tunnel were made at a Reynolds number of about 1.1×10^6; those in the Ames 12-Foot Tunnel at Reynolds numbers from 1.1×10^6 to about 5.5×10^6.

The longitudinal aerodynamic characteristics presented in this paper are referred to in the stability-axis system. Force data are reduced to coefficient form based on the trapezoidal wing area. All dimensional values are given in both International System of Units (SI) and U.S. Customary Units, the principal measurements and calculations using the latter. The model configuration notation is defined in the appendixes.

Coefficients and symbols used herein are defined as follows:

AR	wing aspect ratio
b	wing span
c	wing chord
c_H	horizontal stabilizer chord
C_D	drag coefficient
C_L	lift coefficient
$C_{L\alpha} = 0$	lift coefficient at 0^0 angle of attack
$C_{L_{MAX}}$	maximum lift coefficient
C_ℓ	rolling-moment coefficient
$(\Delta C_\ell)_{\Delta\beta = -5^0}$	change in yawing-moment coefficient with a change in sideslip angle from 0^0 to -5^0
C_M	pitching moment coefficient
C_n	yawing-moment coefficient
$(\Delta C_n)_{\Delta\beta = -5^0}$	change in yawing-moment coefficient with a change in sideslip angle from 0^0 to -5^0
$C_{p_{min}}$	minimum pressure coefficient
$C_{p_{TE}}$	pressure coefficient measured at the trailing edge of the element
c_V	vertical stabilizer chord
c_W	wing root chord

FCK	fixed-camber Krueger (flap)
FRP	fuselage reference plane
H_{MAC}	mean aerodynamic chord of the horizontal tail
i_H	incidence angle between the horizontal tail and the fuselage reference plane, positive trailing edge down (deg)
(L)	left wing panel
L/D	lift-drag ratio
L_H	distance between the 25-percent MAC point on the wing and the 25-percent MAC point on the horizontal tail
L_V	distance between the 25-percent MAC point on the wing and the 25-percent MAC point on the vertical tail
MAC	mean aerodynamic chord
MACH	Mach number
MS	model station
(R)	right wing panel
O.H.	overhang
RN_{MAC}	Reynolds number based on MAC
S_H	horizontal tail area
S_{REF}	reference wing area
S_V	vertical tail area
S_W	wing area
TED	trailing edge down
TEU	trailing edge up
TS	tunnel station
VCK	variable camber Krueger (flap)
V_s	Stalling Speed - the minimum steady flight speed at which the airplane is controllable
WRP	wing reference plane

WUSS	wing under slat surface
X,Y,Z	spanwise, chordwise, and vertical fuselage stations, respectively
X_H, Y_H	spanwise and chordwise horizontal-tail stations, respectively
X_W, Y_W	spanwise and chordwise wing stations, respectively
Y_V, Z_V	chordwise and vertical vertical-tail stations, respectively
$\alpha C_{L_{MAX}}$	angle of attack at $C_{L_{MAX}}$
α_{FRP}	angle of attack of the fuselage reference plane, positive nose up (deg)
$\alpha C_L = 0$	angle of attack for zero lift
$\Delta\beta$	change in yaw (sideslip) angle
Γ	dihedral angle
Γ_H	horizontal-tail dihedral angle
η	ratio of X_W to semispan
δF_{AFT}	aft flap deflection angle, positive for trailing edge down (deg)
δFCK	flexible-camber Krueger flap deflection angle, positive for trailing edge down (deg)
$\delta FLAP$	flap deflection angle, positive for trailing edge down (deg)
δLE	general leading-edge device flap deflection angle, positive for trailing edge down (deg)
$\delta SLAT$	leading-edge slat deflection angle, positive for trailing edge down (deg)
δF_{MAIN}	main flap deflection angle, positive for trailing edge down (deg)
δSP	spoiler deflection angle (symmetrical), negative for trailing edge up (deg)

δ_{VCK} variable-camber Krueger flap deflection angle, positive for trailing edge down (deg)

Λ sweep angle

λ taper ratio

PART I
WIDE BODY
DC-X-200-TYPE MODEL
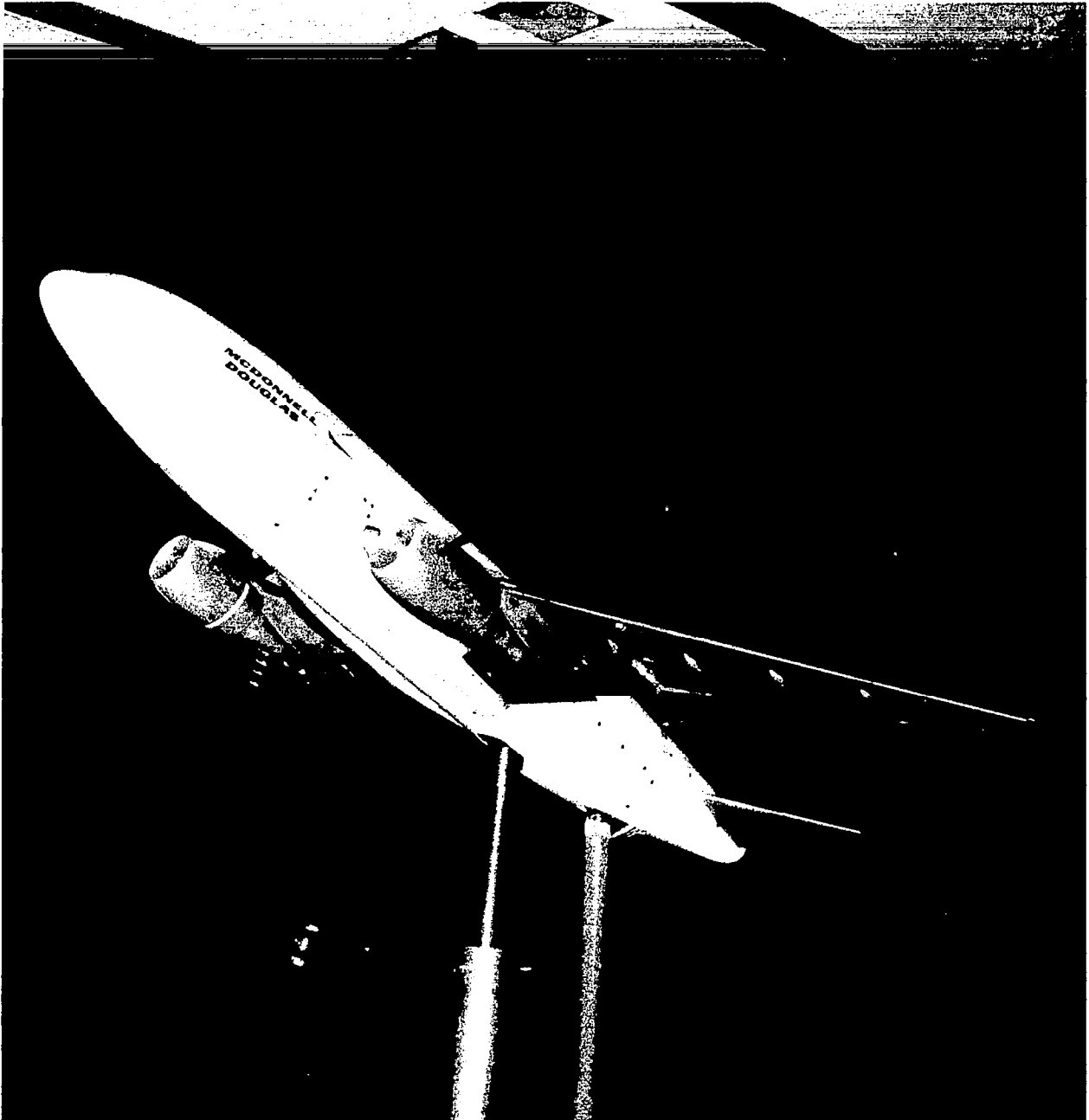
**LB-486C MODEL
INSTALLED IN
LANGLEY V/STOL TUNNEL**

PART I

WIDE BODY DC-X-200-TYPE MODEL

LB-486B,C MODEL DESCRIPTION

The wind tunnel model used for the program was a 4.7-percent representation of the DC-X-200 aircraft, and was the same as that used in Phase I of the EET Project study. The model is depicted in Figure 1. The configuration notation data, dimensional data, and grid position definitions are presented in Appendixes A, B, and C, respectively. The model was designed as a primary high-lift configuration that included a variable-camber Krueger (VCK). Secondary configurations employed either slats or fixed-camber Kruegers (FCK) along the leading edge. Combinations of an FCK inboard with a slat outboard were also tested.

The primary trailing-edge configuration employed inboard and outboard two-segment flaps. Between these two flaps was a flaperon, essentially a single-slotted flap, that could be articulated in the same manner as the

DIMENSIONS IN CENTIMETERS (INCHES) MODEL SCALE

36.530 (14.382) POD LOCATION

1.8°

70.236
(27.652)

87.076 (34.282)

222.08 (87.435)

28.293 (11.139) DIA

82.301 (32.402)

39.700
(15.630)

198.77 (78.255)
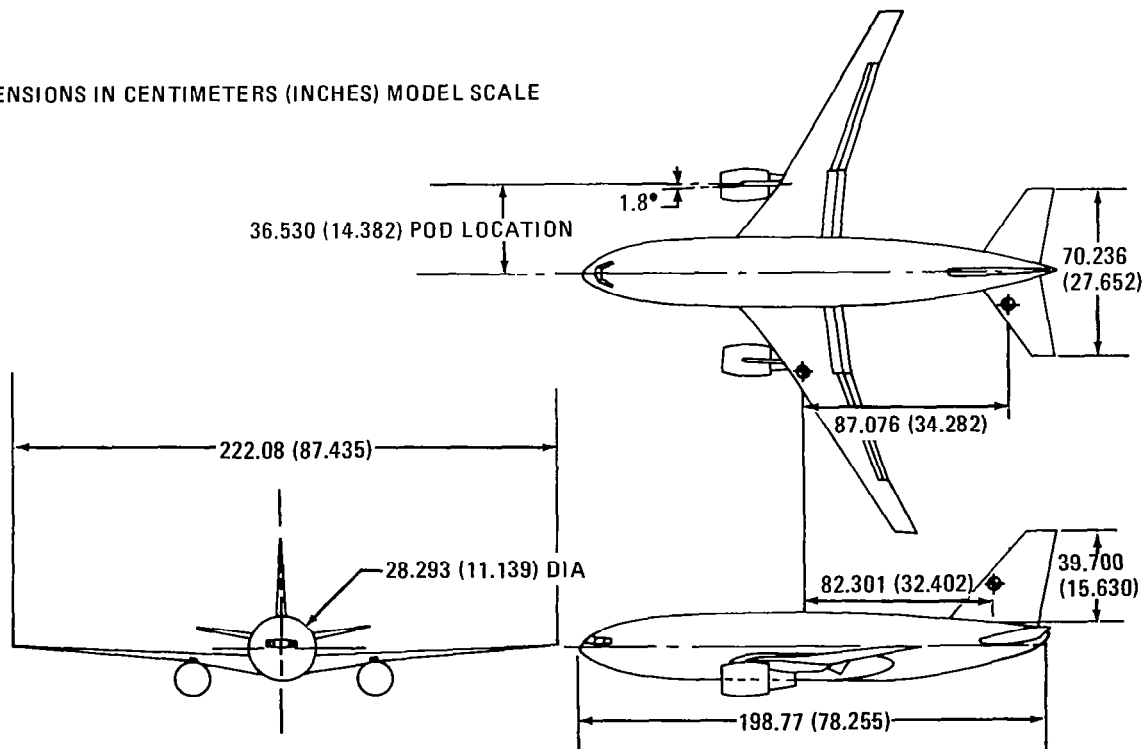
FIGURE 1. HIGH-LIFT LOW-SPEED WIND TUNNEL MODEL

main flap for the high-lift conditions, but that incorporated a high-speed, short-chord aileron in the retracted, or cruise, configuration. At the high-lift condition, this aileron was locked in an undeflected position. This permitted an 80-percent continuous flap span resulting in an improved span loading for high-lift conditions. The various high-lift components are depicted in Figure 2.
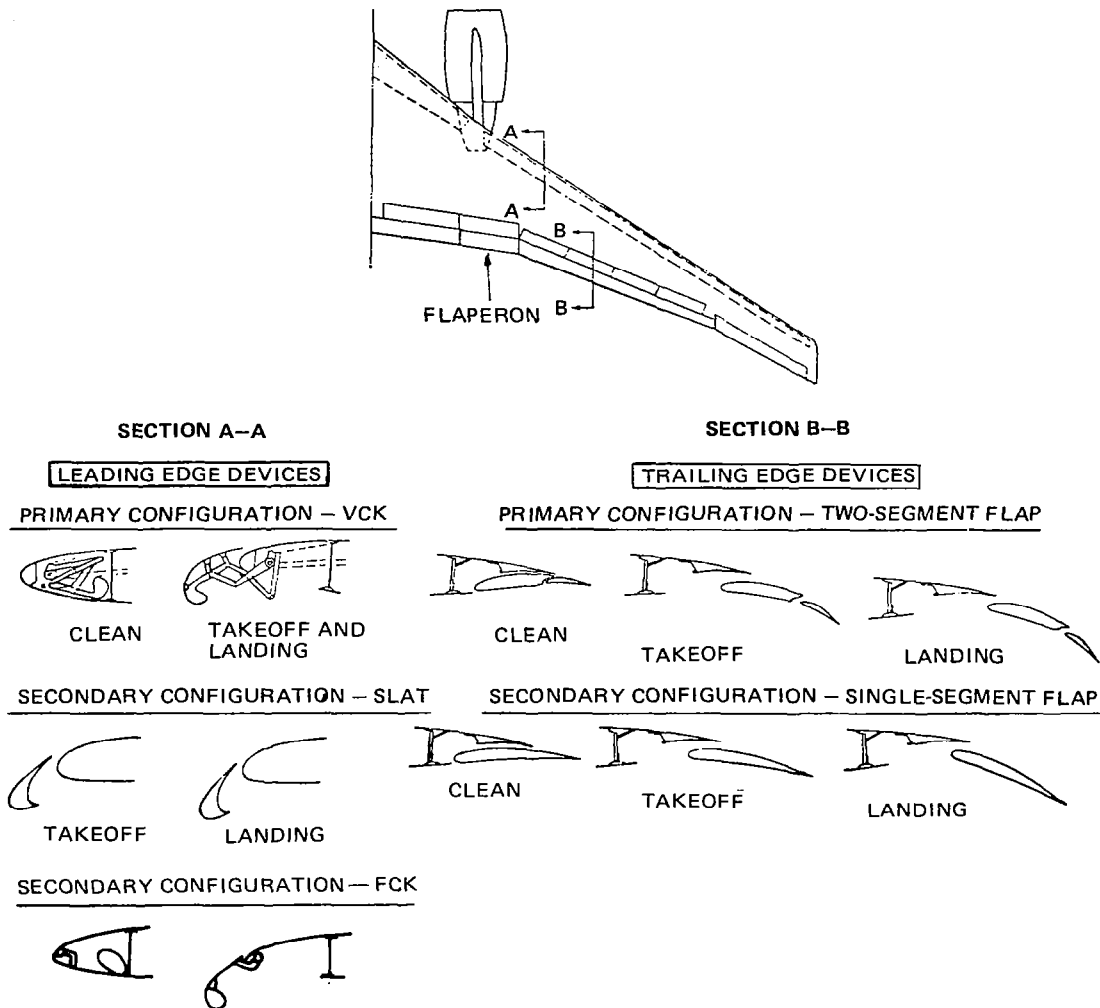
FIGURE 2. HIGH-LIFT COMPONENTS EVALUATED IN EXPERIMENTAL TEST PROGRAM

The model also included an aileron on the left wing panel, spoilers, and a remote-drive horizontal stabilizer deflection capability. Other model components included nacelles, pylons, landing gear, and a cruise wing trailing edge (i.e., flaps retracted). The fuselage consisted of DC-10 model nose and aft fuselage shell sections, and a top center section and wing/fuselage fillet developed for Phase I testing.

A fuselage core was adapted for attachment of the fuselage shell sections, support of two 5-module scanivalve systems, support of a bubble pack plate, and attachment of the wing and the vertical and horizontal stabilizers. A fuselage internal pitch system was installed in the core. This system permited the fuselage to be pitched from $\alpha_{FRP} = 0^0$ to $+10^0$ while the internal balance remained at $\alpha_{FRP} = 0^0$. The other pitch angles were obtained by using the external pitch system. This system provided more accurate drag measurements between 0^0 to 10^0.

The wing geometry and planform dimensions are shown on the wing diagram (Figure 3). The wing was designed to simulate the aircraft wing under a 1-g load. It incorporated the following features:

1. A cruise leading edge removable at the front spar. This leading edge was tested with and without simulated VCK stowage wells. Also provided was a WUSS (wing under slat surface) leading edge for the slat configuration.

2. A VCK, FCK, and slat leading-edge flap device with variable deflection and position capability.

3. A two-segment trailing-edge flap supported at five deflection angles by fixed brackets simulating the airplane flap linkage. Variable position capability was provided for the main flap.

4. A manually set aileron, left side only, and spoilers both sides.

5. Approximately 400 static pressure orifices installed in the VCK, slat, wing, and flaps.

The geometry of the horizontal stabilizer is shown in Figure 4. The horizontal stabilizer was removable for testing tail-off. Each side of the stabilizer was fabricated in one piece without elevators. A remote control system was used to vary the stabilizer incidence between $+5^0$ and -15^0.

The vertical stabilizer planform is shown in Figure 5. The stabilizer was fabricated as one piece without rudders and was removable to provide a tail-off configuration.

S_{REF}	= 0.4696 m² (5.055 SQ FT)
AR	= 10.5020
TAPER RATIO	0.1407

DIMENSIONS IN CENTIMETERS (INCHES) MODEL SCALE

WING ORIGIN
Y = 121.984 (48.025)

+Y$_W$

14.140
(5.567)

11.677
(4.597)

X_W = 36.367
(14.318)

(C/4)MAC
Y = 160.280 (63.102)
X_W = 41.580 (16.370)
Y_W = 38.296 (15.077)

28.744
(11.317)

X_W = 43.411
(17.091)

37.761
(14.867)

14.788 (5.822)

20.950 (8.248)

FRONT SPAR PLANE

51.895
(20.431)

X_W = 89.020
(35.047)

6.954 (2.738)

8.692 (3.422)

INBOARD SPOILERS

+X$_W$

INBOARD TWO-SEGMENT FLAP

X_W = 111.274
(43.809)

57.731
Y_W = (22.729)

2.317 (0.912)

OUTBOARD SPOILERS

30.793 (12.123)

5.562 (2.190)

43.411 (17.091)

Y_W = 74.895
(29.486)

Y_W = 72.773
(28.651)

OUTBOARD TWO-SEGMENT FLAP

9.270
(3.650)

VIEW IN WING REFERENCE PLANE

REAR SPAR PLANE

LOW-SPEED AILERON

FIGURE 3. WING (W$_{3B}$) DIAGRAM

S_H = 0.1298 m^2 (1.397 FT^2)

AR = 3.80

λ = 0.350

SWEEP $\dfrac{C_H}{4}$ = 30^0

Γ = 10.0^0

DIMENSIONS IN CENTIMETERS (INCHES)
MODEL SCALE

X_H 35.659 (14 039)

Y = 231.87 (91.287)

30°

27.384 (10.781)

PIVOT AXIS 58.85
PERCENT C_R
$\dfrac{4.536\ (1.786)}{\text{ABOVE FRP}}$
Y_H = 16.11 (6.344)

c/4 MAC

X_H = 14.74 (5.804)
Y_H = 15.49 (6.097)

MAC$_H$ = 19.91 (7.839)

+X_H

+Y_H

9.596 (3.778)

THEORETICAL
TRAILING EDGE

MODEL ACTUAL TRAILING EDGE
(CUT BACK TO ACHIEVE 0.03 (0.010)
THICK TRAILING EDGE)
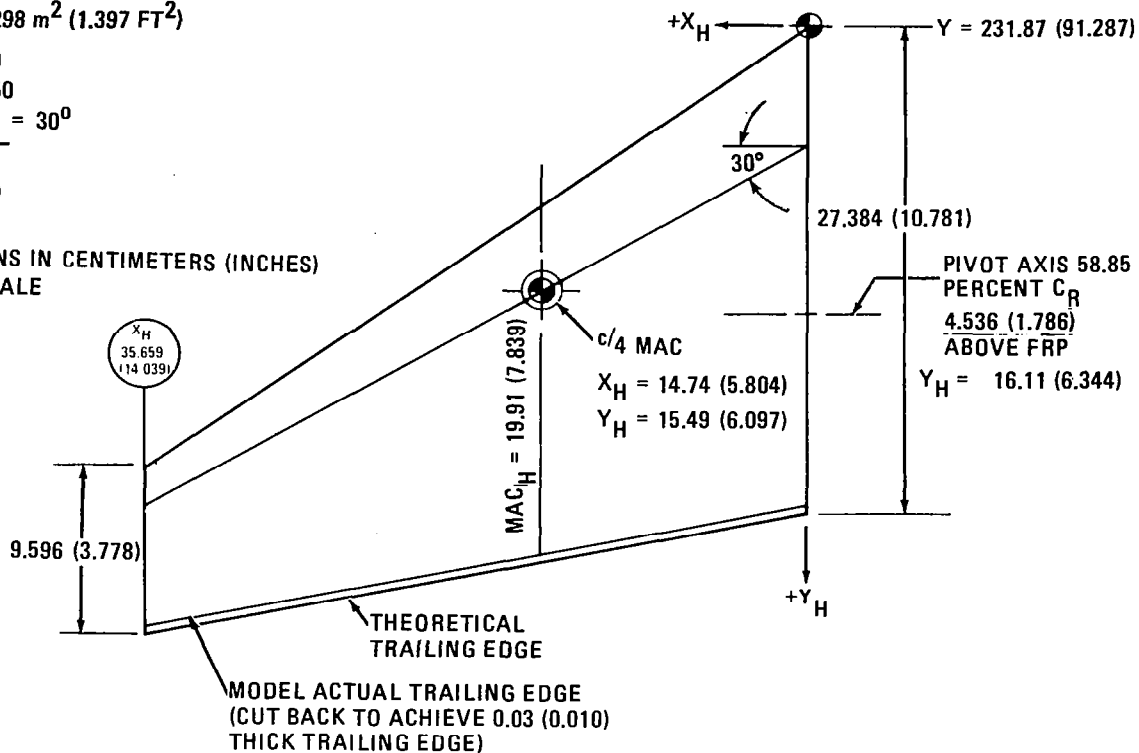
FIGURE 4. HORIZONTAL STABILIZER (H$_{1A}$) DIAGRAM

S_V = 0.09850 m^2 (1.0603 FT^2)

AR = 1.600

λ = 0.35

SWEEP $\dfrac{C_V}{4}$ = 35°

DIMENSIONS IN CENTIMETERS (INCHES)
MODEL SCALE

12.87
(5.065)

Y = 221 72 (87 292)

$\dfrac{C}{4}$ MAC

Y_V = 20.86 (8.212)
Z_V = 16.66 (6.561)

MAC$_V$ = 26.731 (10.524)

39.700
(15.630)

+Z_V

THEORETICAL
TRAILING EDGE

35°

ACTUAL MODEL TRAILING
EDGE (CUT BACK TO
ACHIEVE 0.03 (0.010)
THICK TRAILING EDGE)

+Y_V

VERT
STABILIZER
ORIGIN

36.759
(14.472)
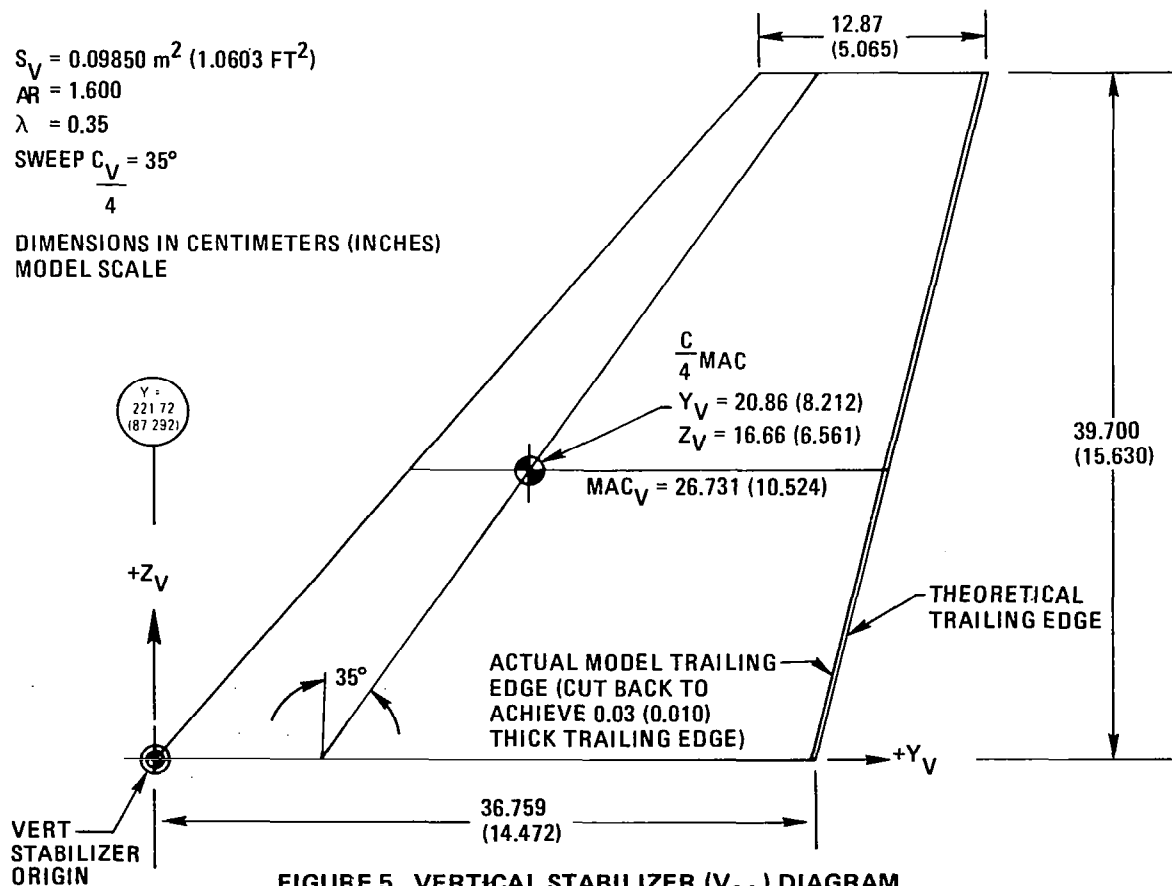
FIGURE 5. VERTICAL STABILIZER (V$_{1A}$) DIAGRAM

Flow-through nacelles (Figure 6) from a DC-10 model were used and were attached to the wing by pylons. The pylon plane of symmetry had a 1.8° toe-in relative to the airplane plane of symmetry (measured in the FRP) and was perpendicular to the FRP with the wing in a rigged position with a dihedral angle of 4.05°. Nacelle strakes were attached to the nacelle for most tests.

DIMENSIONS IN CENTIMETERS (INCHES)
MODEL SCALE

4.30 (1.69)

3.25 PERCENT CHORD

4.78 (1.88) MINIMUM

NEW DC-X-200 PYLON (P$_{2A}$)

ENGINE CENTERLINE AT + 1.6° INCIDENCE TO THE FRP

EXISTING DC-10 GE NACELLE (N$_{2A}$)
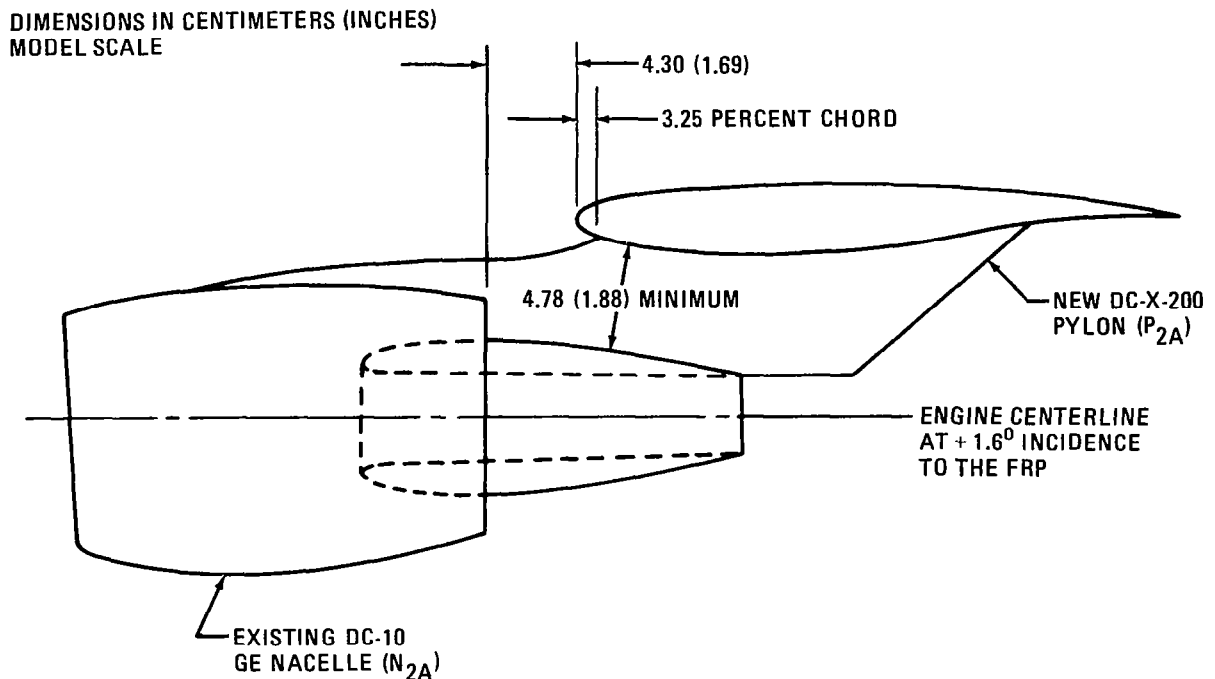
FIGURE 6. NACELLE/PYLON (N$_{2A}$ P$_{2A}$) DIAGRAM

The nose gear simulated the DC-10 nose gear in structure and location. The main landing gear simulates the airplane gear configuration with oleos extended. Extended main gear wheel well cavities were not simulated. A retracted main landing gear configuration was also provided.

The definitions of gap, overhang (O.H.), and deflection used to position the leading-edge high-lift devices are illustrated in Figure 7. The deflection angles were measured in a streamwise plane oriented normal to the wing reference plane (WRP). Definitions for main and aft flap gap, O.H., and deflections are shown in Figure 8. The same definitions were used for both the flaperon and the main flap. The variable test positions tested are defined and identified in the grid notations table of Appendix C.

SLAT
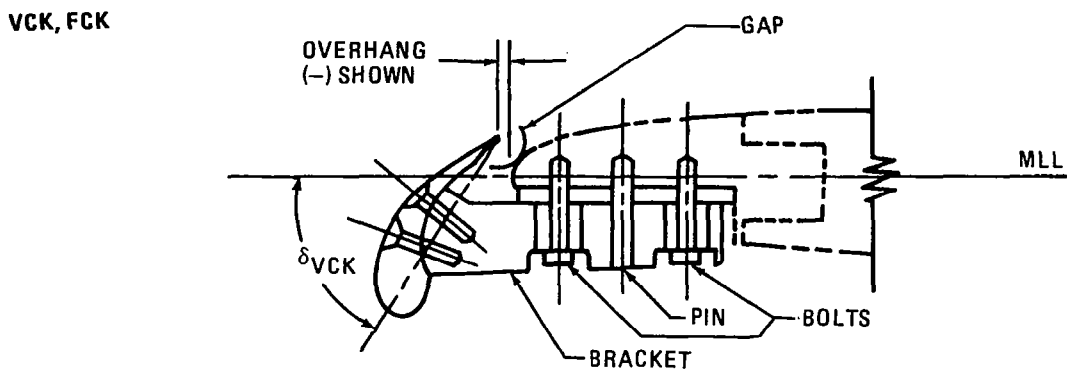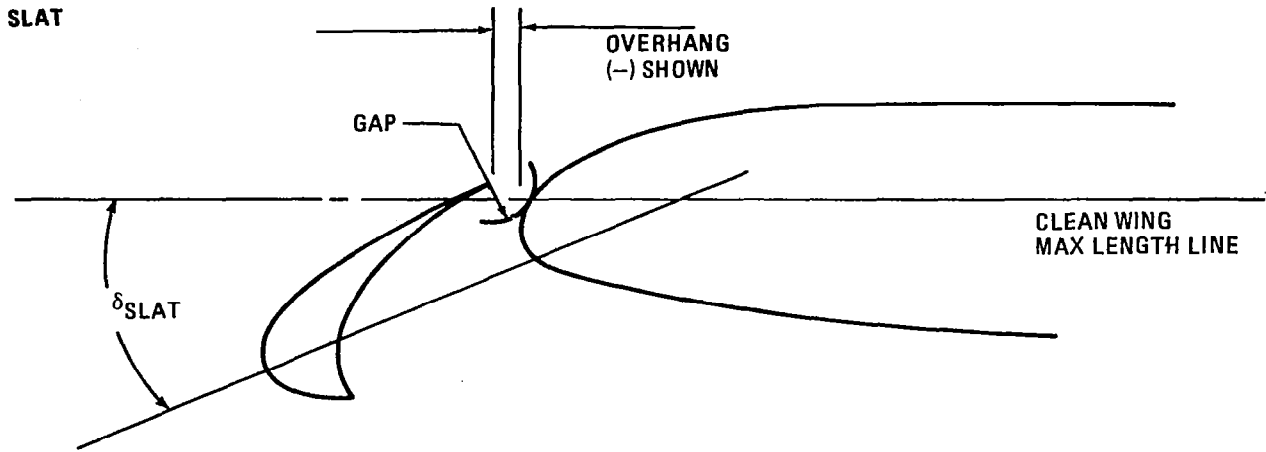
FIGURE 7. LB-486 LEADING EDGE DEVICE GAP, OVERHANG, AND DEFLECTION DEFINITIONS
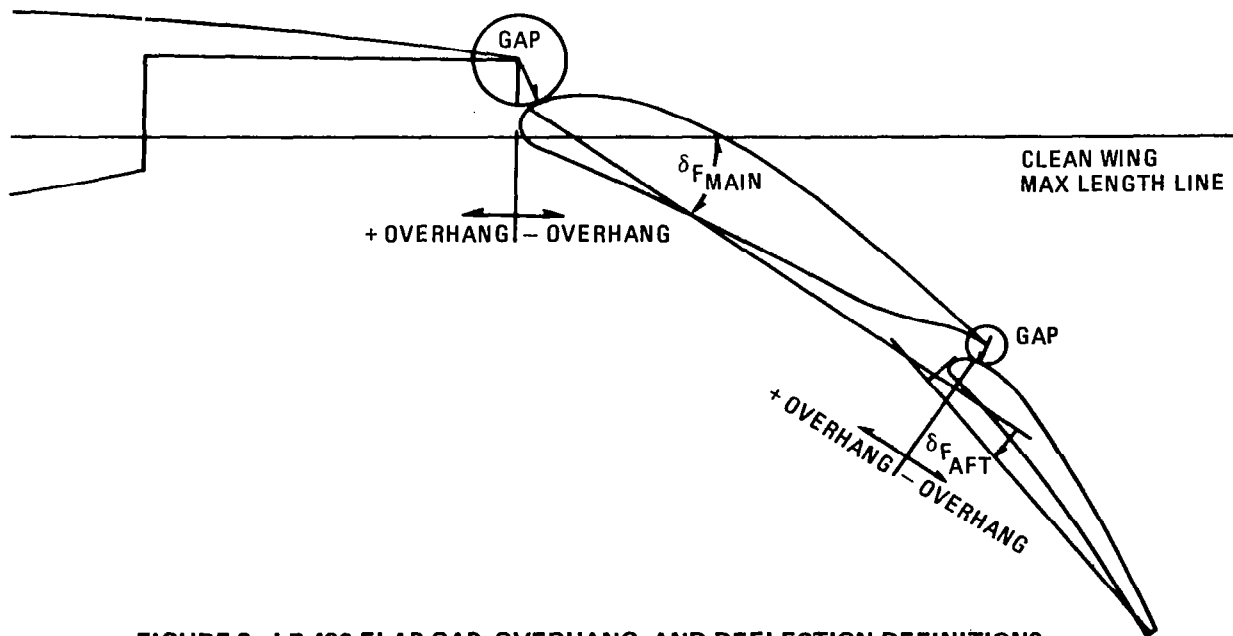
FIGURE 8. LB-486 FLAP GAP, OVERHANG, AND DEFLECTION DEFINITIONS

LB-486B,C INSTRUMENTATION

Aerodynamic forces on the model were measured using the Ames Task Mark II
10.16-cm (4-in.) diameter internal balance at the Ames 12-Foot Pressure Wind
Tunnel (LB-486B test). For the NASA Langley V/STOL Wind Tunnel
(LB-486C test), the balance used was the Langley 5.08-cm (2-in.) diameter
internal balance.

In the Ames test, electrolytic alignment bubbles housed in the fuselage nose
were used to measure the angle of attack of the fuselage reference plane.
From angles of attack of -6^0 to 0^0, the model was pitched by the
external pitch drive. From 0^0 to $+10^0$ angles of attack, the fuselage
was pitched using the fuselage internal pitch drive while maintaining the
balance at 0^0. For angles of attack of 10^0 to 34^0, the fuselage was
pitched using the external pitch drive with a 10^0 angle maintained between
the balance axis and the fuselage axis.

In the Ames test the horizontal stabilizer incorporated remote drive and
dual-position potentiometer for changing tail incidence during a run. In
the NASA V/STOL test, a NASA-furnished electronic inclinometer was used to
determine angle of attack. The horizontal-tail incidence in the V/STOL test
was set at 0^0.

LB-486B,C MODEL INSTALLATION

The model was installed in the NASA Ames 12-Foot Pressure Wind Tunnel on the
tandem support system shown in Figure 9. The model was pivoted about the
main strut pivot point and was powered by the aft pitch strut. The entire
strut system was nonmetric (i.e., air loads on the strut are not sensed by
the balance). The struts entered the fuselage as far aft as practical to
minimize the aerodynamic interference effects on the model.
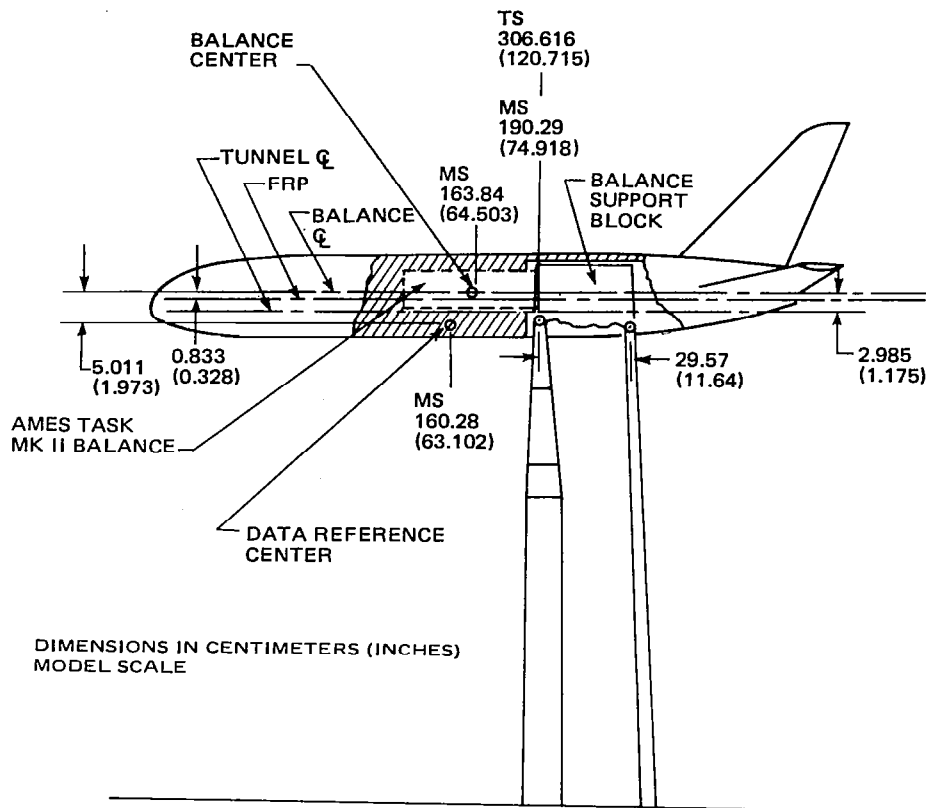
FIGURE 9. MODEL INSTALLATION IN THE NASA AMES 12-FOOT PRESSURE WIND TUNNEL

The same support system (Figure 10) was utilized during the NASA Langley V/STOL test program. It was adapted to the existing V/STOL Tunnel structure; extensions for the main and pitch struts were added to the basic tandem strut system. The extensions permitted the model to be located near the vertical position of the tunnel centerline.

REVIEW OF PHASE I RESULTS

During Phase I, the aerodynamic characteristics of the clean wing, VCK, slat, and flaps were defined experimentally. The lift and pitching-moment curves for the clean wing are shown in Figure 11. These curves indicate that the cruise wing, as defined for Phase I, was subject to outboard stall, although it is likely that the curves overstate the tendency for stall because of the Reynolds number effect. Because of the short tip chord of the wind tunnel model, the highest Reynolds number condition resulted in a tip chord Reynolds number of only 1.9 million. Figure 12 shows that higher
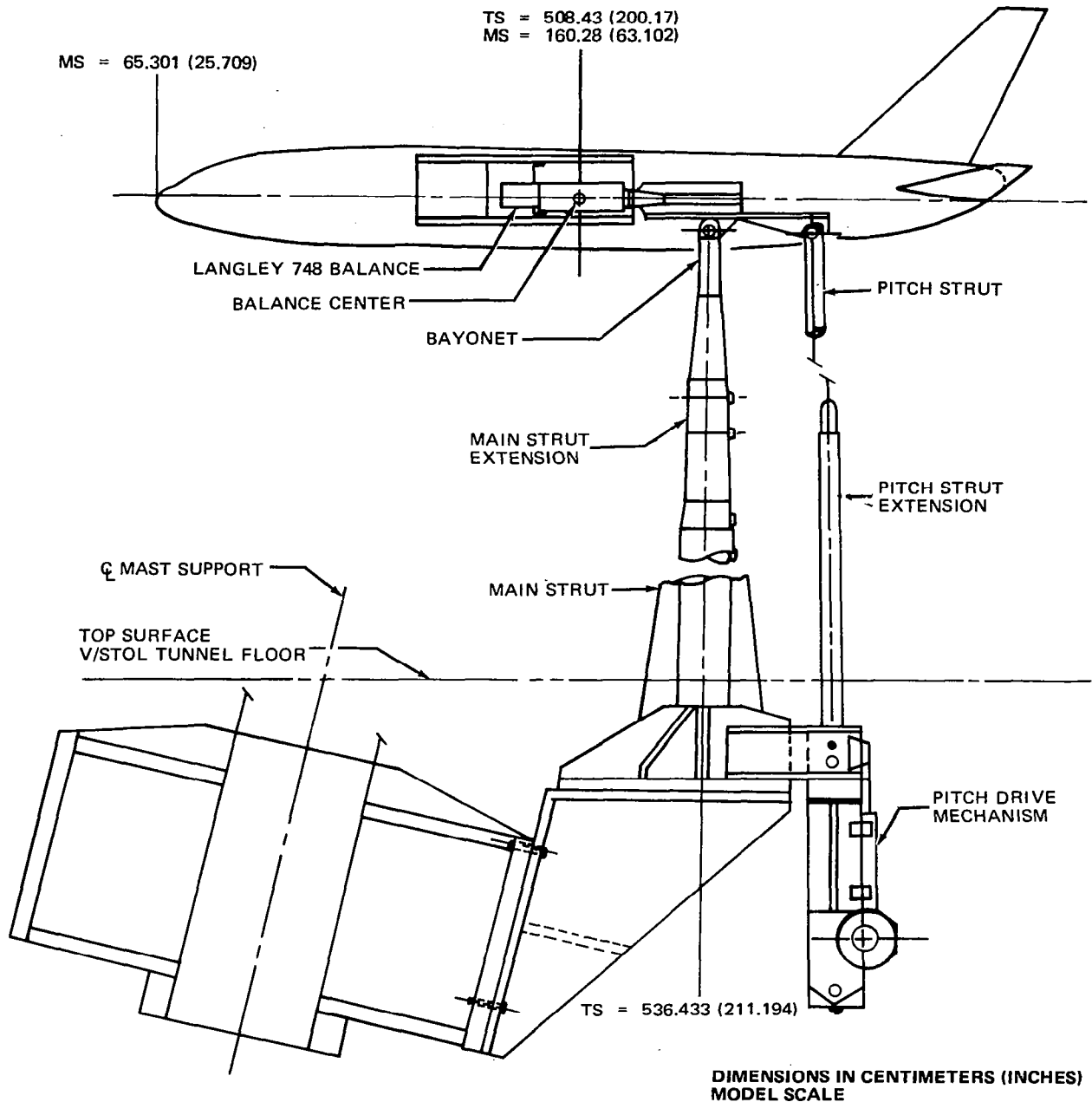
FIGURE 10. MODEL INSTALLATION IN THE NASA LANGLEY V/STOL WIND TUNNEL

stall angles and larger values of section $C_{L_{MAX}}$'s for the outboard wing panel might have been obtained if the test could have been made at a higher Reynolds number. Later high-aspect-ratio supercritical wing designs have shown improvements in stall angles and $C_{L_{MAX}}$.

MODEL LB-486A

CONFIGURATION $S_1N_{2A}P_{2A}Z_{1A}V_{1A}H_{1A}$

MACH = 0.20

$RN_{MAC} = 5.12 \times 10^6$

i_H	SYM	RUN
OFF	O	23
0°	□	34
−5°	◇	35
−10°	△	36

LIFT COEFFICIENT

PITCHING-MOMENT COEFFICIENT

ANGLE OF ATTACK-DEG

ANGLE OF ATTACK-DEG
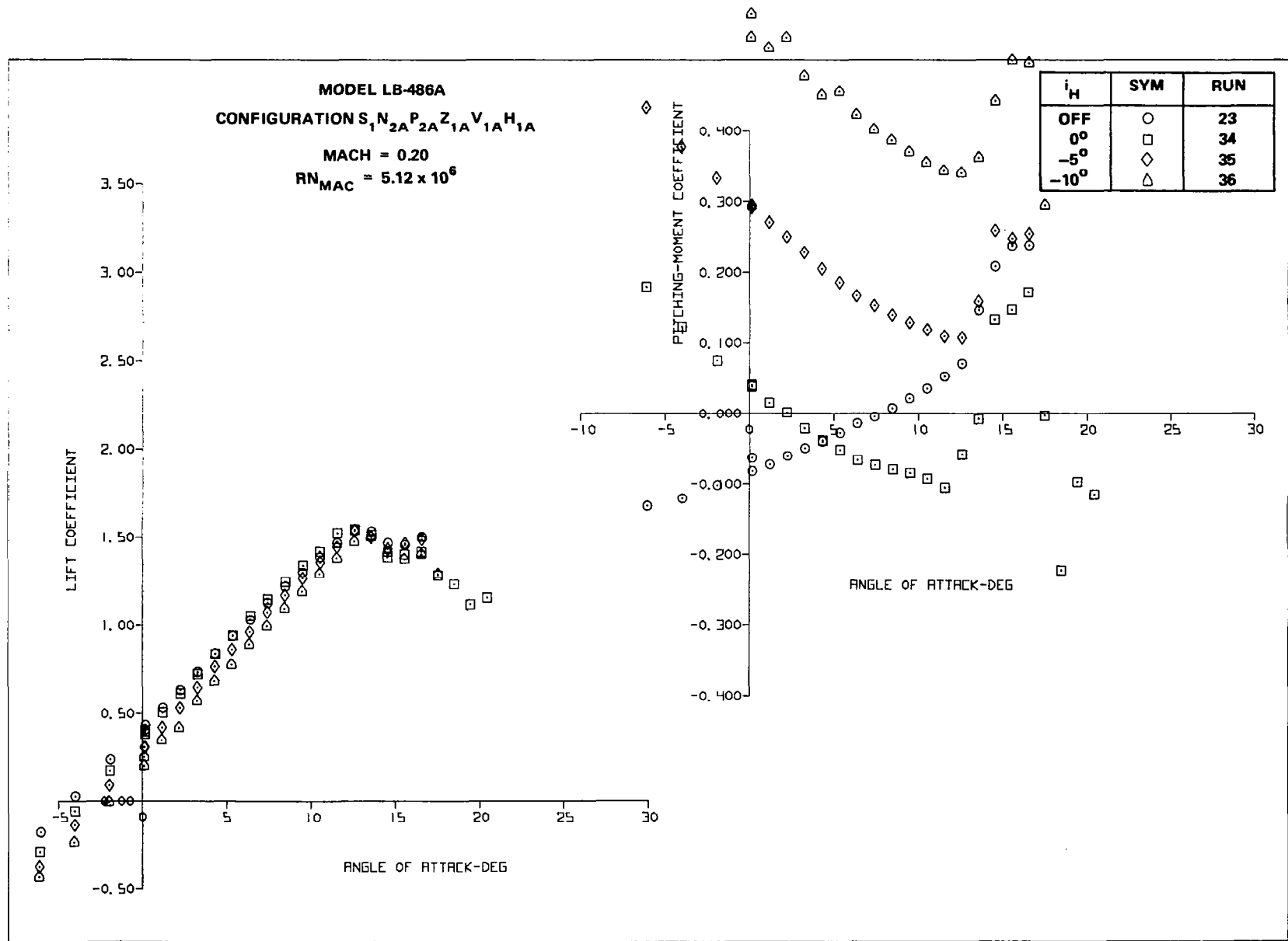
LIFT AND PITCHING MOMENT

FIGURE 11. TAIL-ON CHARACTERISTICS FOR THE CRUISE WING WITH NACELLES, PYLONS, AND STRAKES ATTACHED

MODEL LB-486A
CONFIGURATION $S_1 N_{2A} P_{2A} Z_{1A}$
MACH = 0.20
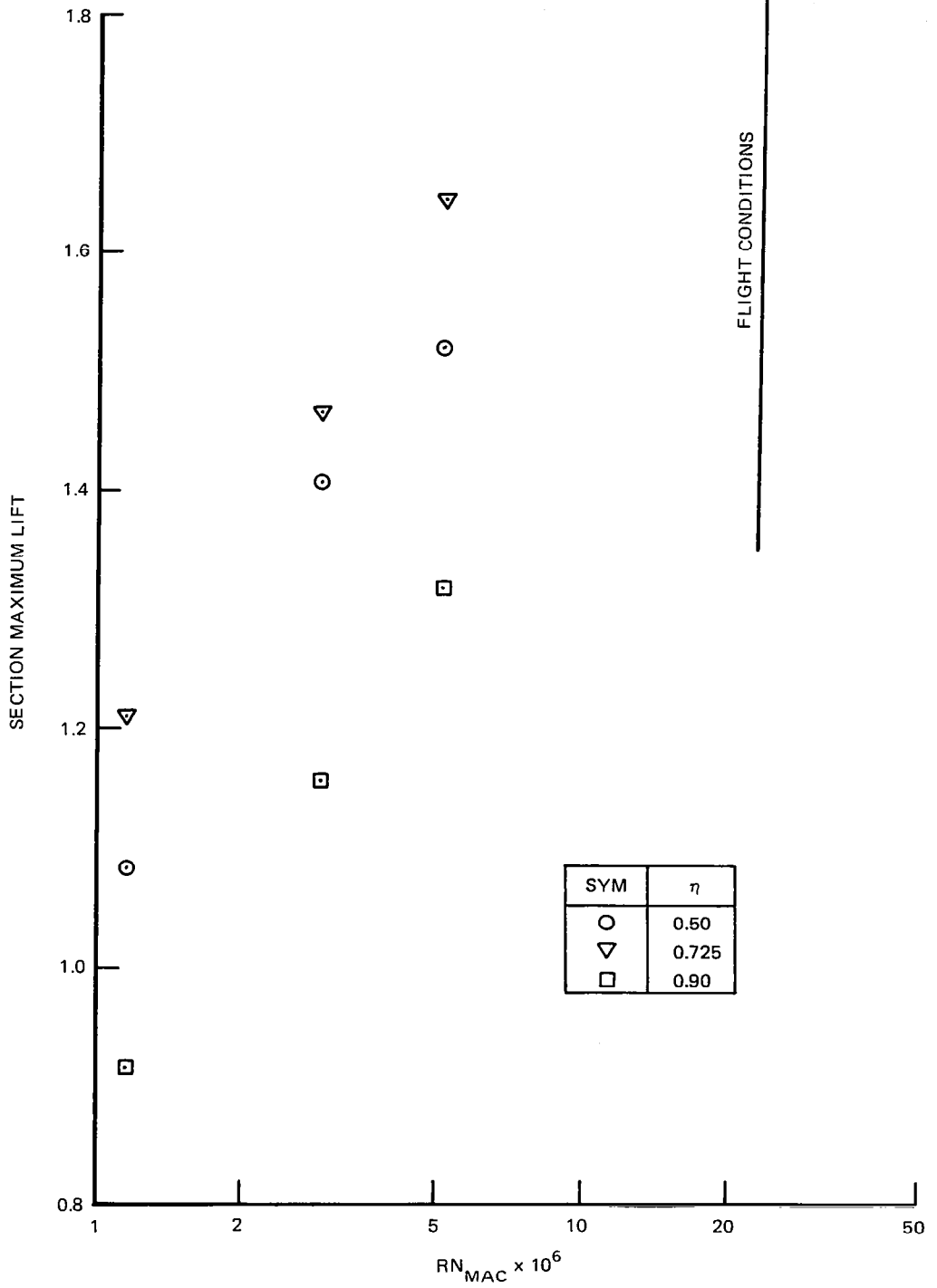
FIGURE 12. EFFECT OF REYNOLDS NUMBER ON CLEAN-WING SECTION MAXIMUM LIFT

Figures 13 and 14 show the lift and pitching-moment characteristics for the primary VCK and slat configurations tested. While the $C_{L_{MAX}}$ and L/D ratio for the slat configurations were marginally better than those of the VCK configurations, use of the VCK resulted in superior stall characteristics. Configurations including slats exhibited both pre-stall and post-stall nose-up tendencies. While the VCK configurations showed post-stall nose-up trends, the pre-stall characteristics were good. Nearly all of the work accomplished on this model during Phase II was directed toward improving the low-speed stall characteristics by making adjustments in leading-edge device position and type.

The trailing-edge flap studies of Phase I indicated that the changes in performance due to gap and overhang variations were not as significant as the corresponding variations for the leading-edge devices. As expected, the two-segment flap was superior to the single-segment flap in $C_{L_{MAX}}$ and flap lift increments. Trimmed polar comparisons indicated that the single-segment and two-segment flaps resulted in equivalent L/D envelopes for takeoff flap settings. For equivalent values of approach speed, the L/D values for the two-segment flap were superior to those of the single-segment flap. Because of these definitive results, little additional flap optimization work was conducted on the wide-body model during Phase II. In addition to the high-lift work, Phase I testing also defined the effectiveness of the spoilers and ailerons.

MODEL LB-486A

CONFIGURATION $S_4H_{1A}V_{1A}$

MACH = 0.20

$RN_{MAC} = 5.12 \times 10^6$

$\delta_{VCK} = 45E/45G$

$\delta_{FLAP} = 5C/10B$

i_H	SYM	RUN
OFF	⊙	116
0°	▣	121
−5°	◇	122

LIFT COEFFICIENT

PITCHING-MOMENT COEFFICIENT

ANGLE OF ATTACK-DEG

ANGLE OF ATTACK-DEG
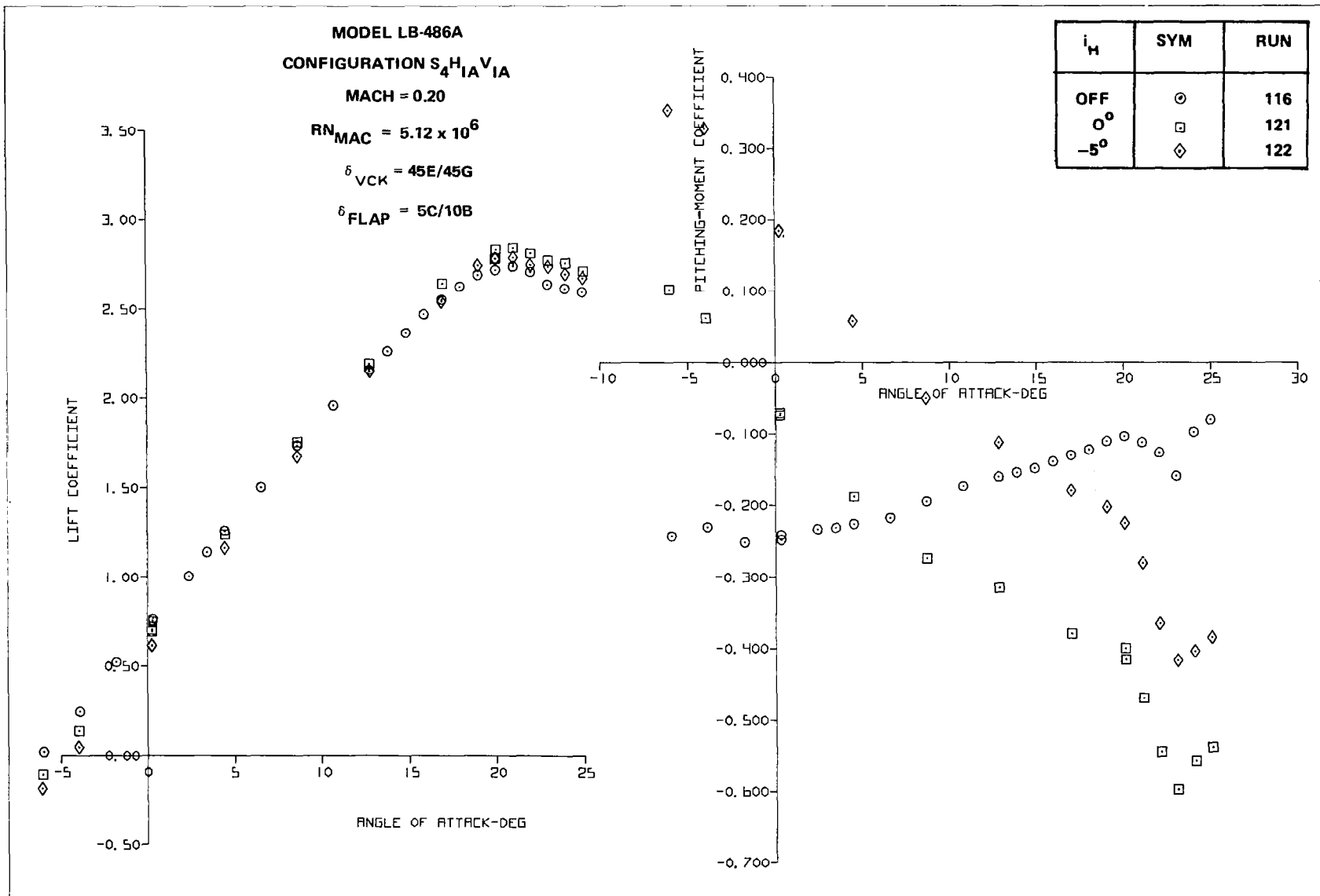
LIFT AND PITCHING MOMENT

FIGURE 13. TAIL-ON AND TAIL-OFF AERODYNAMIC CHARACTERISTICS OF THE VCK WITH TWO-SEGMENT TAKEOFF FLAPS CONFIGURATION
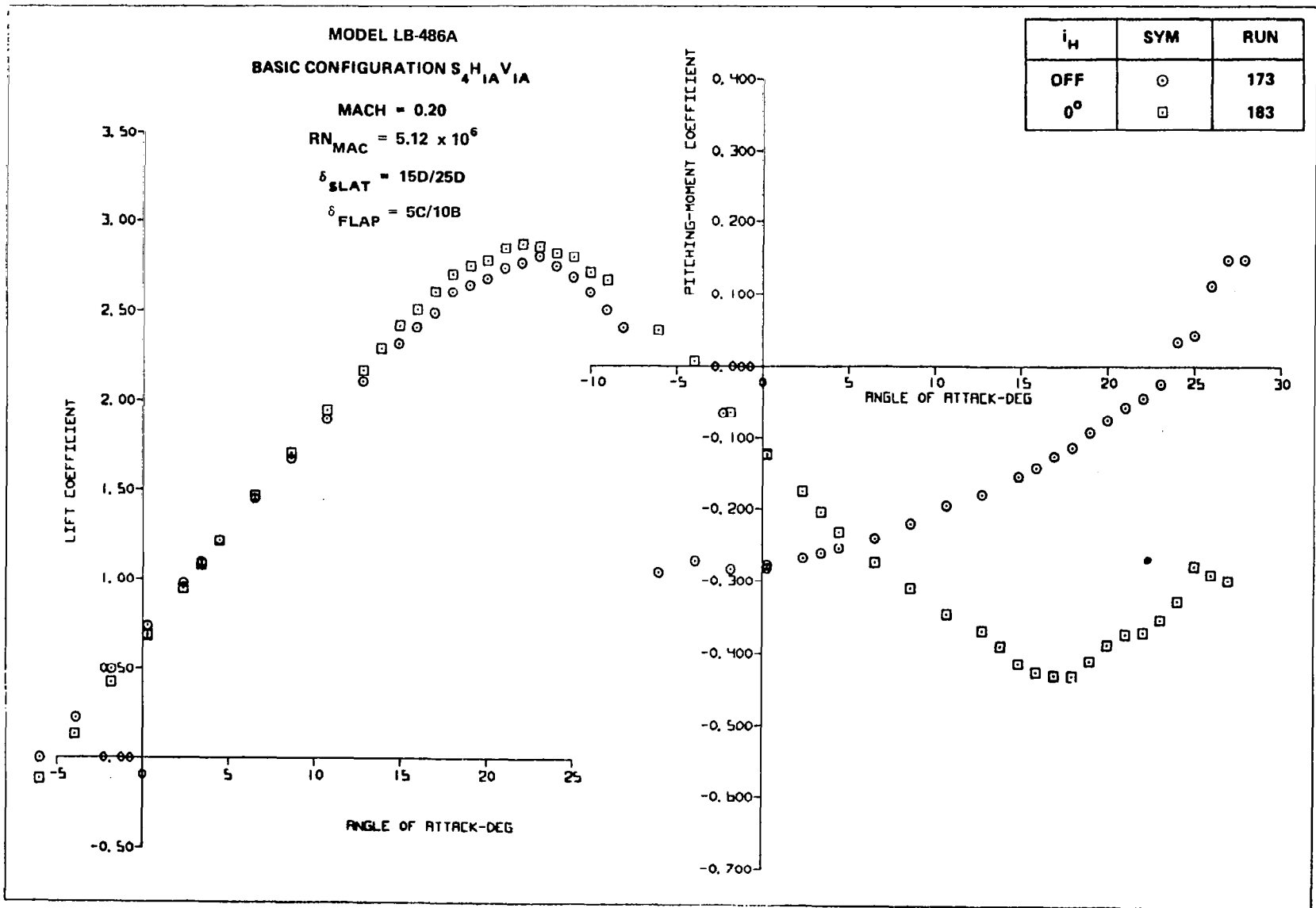
FIGURE 14. TAIL-ON AND TAIL-OFF AERODYNAMIC CHARACTERISTICS OF THE SLAT WITH TWO-SEGMENT TAKEOFF FLAPS CONFIGURATION

Most of the work on the wide body model during Phase II was directed toward improving the pitching-moment characteristics of the wing, without causing an excessive loss in $C_{L_{MAX}}$. The approach consisted of either increasing the stalling angle of the outboard wing panel, or tuning the stall angle of the inboard wing to be just below that of the outboard wing. Additionally, to prevent post-stall pitch-up, it was desirable that the stall inboard be due to separation at the leading edge of the high-lift device, thereby increasing the rate of lift loss inboard relative to that outboard. Configurations tested included a VCK with a reduced deflection, trimmed slats inboard, a normal-chord and a short-chord FCK, a differential flap deflection, and a two-segment flaperon. In addition to the study of these configurations designed to improve $C_{L_{MAX}}$ and/or pitching-moment trends, the improvement in takeoff L/D performance due to sealed slats was evaluated, the penalty associated with use of a high-speed aileron was determined, and data obtained at the Langley and Ames tunnels were compared.

Reduced VCK Deflection

Phase I results (LB-486A) showed equivalent $C_{L_{MAX}}$ values for the slat and VCK configurations. However, the lower minimum pressure coefficients on the VCK indicated that a reduction in deflection might delay leading-edge separation and result in increased maximum lift. A VCK deflection of $\delta_{VCK} = 33^0$ compared to the Phase I value of $\delta_{VCK} = 45^0$ was therefore selected for the LB-486C test at the NASA Langley V./STOL Facility. Results of this test indicated that it was not possible to obtain increased $C_{L_{MAX}}$ due to the low Reynolds number (1.14 million) available in this tunnel. Further examination of the configuration was made at a higher Reynolds number (5.89 million) during the Ames 12-Foot Tunnel entry (LB-486B). The same results as in LB-486C were observed. The reduced deflection resulted in a lower outboard stall angle than the 45^0 deflection. The basic 45^0, 33^0, and 45^0/33^0 (inboard/outboard) VCK deflection lift and pitching-moment data are shown in Figure 15. The corresponding drag values indicated L/D values at 1.3V_s of 9.52, 10.0, and 9.0 for the 45^0, 33^0, and 45^0/33^0 VCK deflections, respectively.

MODEL LB-486B

CONFIGURATION B_{2A} W_{3B} X_{2B} N_{2A} P_{2A} Z_{1A}

MACH = 0.20

RN_{MAC} = 5.12 x 10^6

δ_{FLAP} = 25K/12C

δ_{VCK}	SYM	RUN
45E/45G	O	7
33L/33P	□	8
45E/33J	◇	11

LIFT COEFFICIENT

PITCHING-MOMENT COEFFICIENT

ANGLE OF ATTACK-DEG

ANGLE OF ATTACK-DEG

NSTC
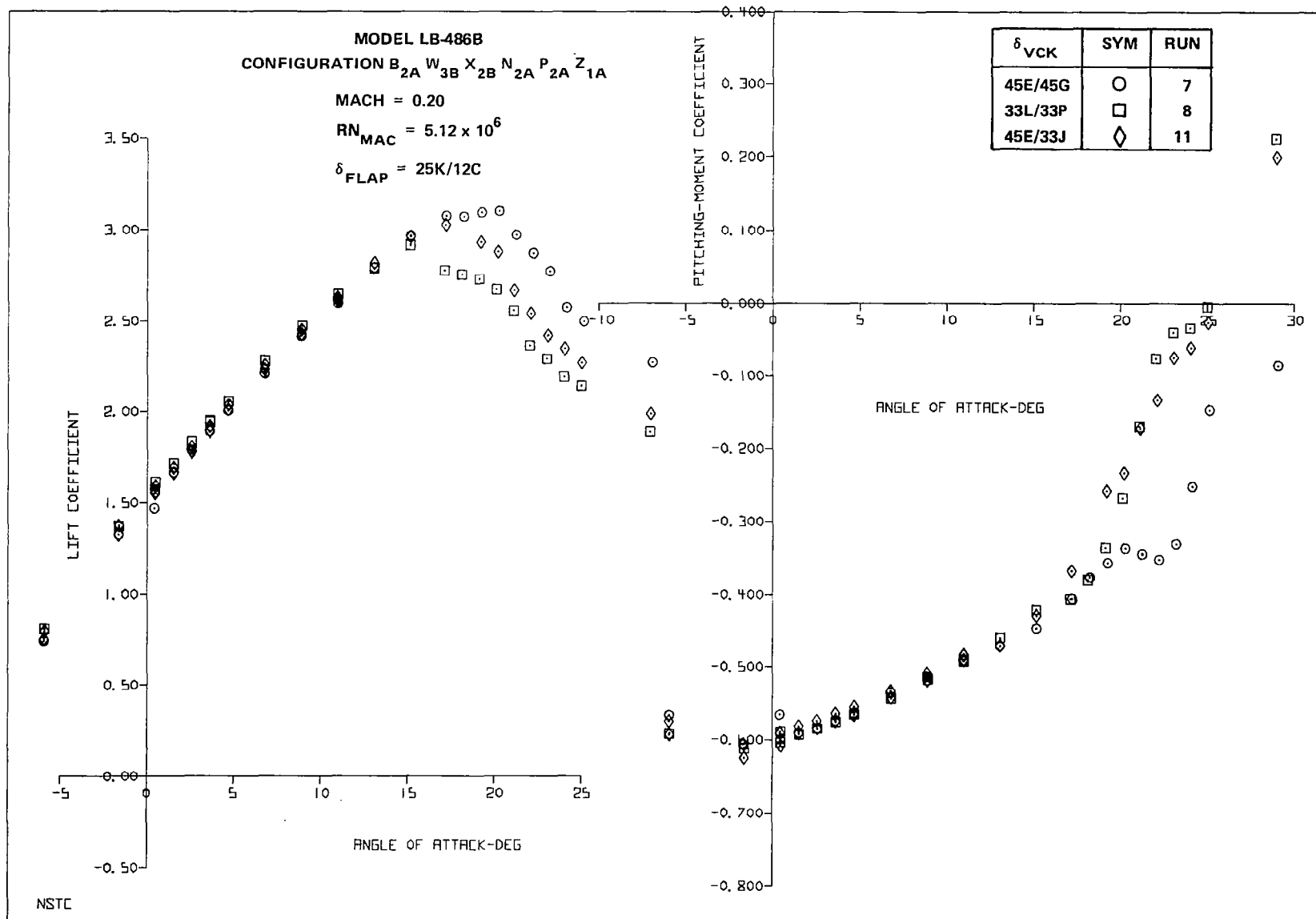
A. LIFT AND PITCHING MOMENT

FIGURE 15. EFFECT OF VCK DEFLECTION
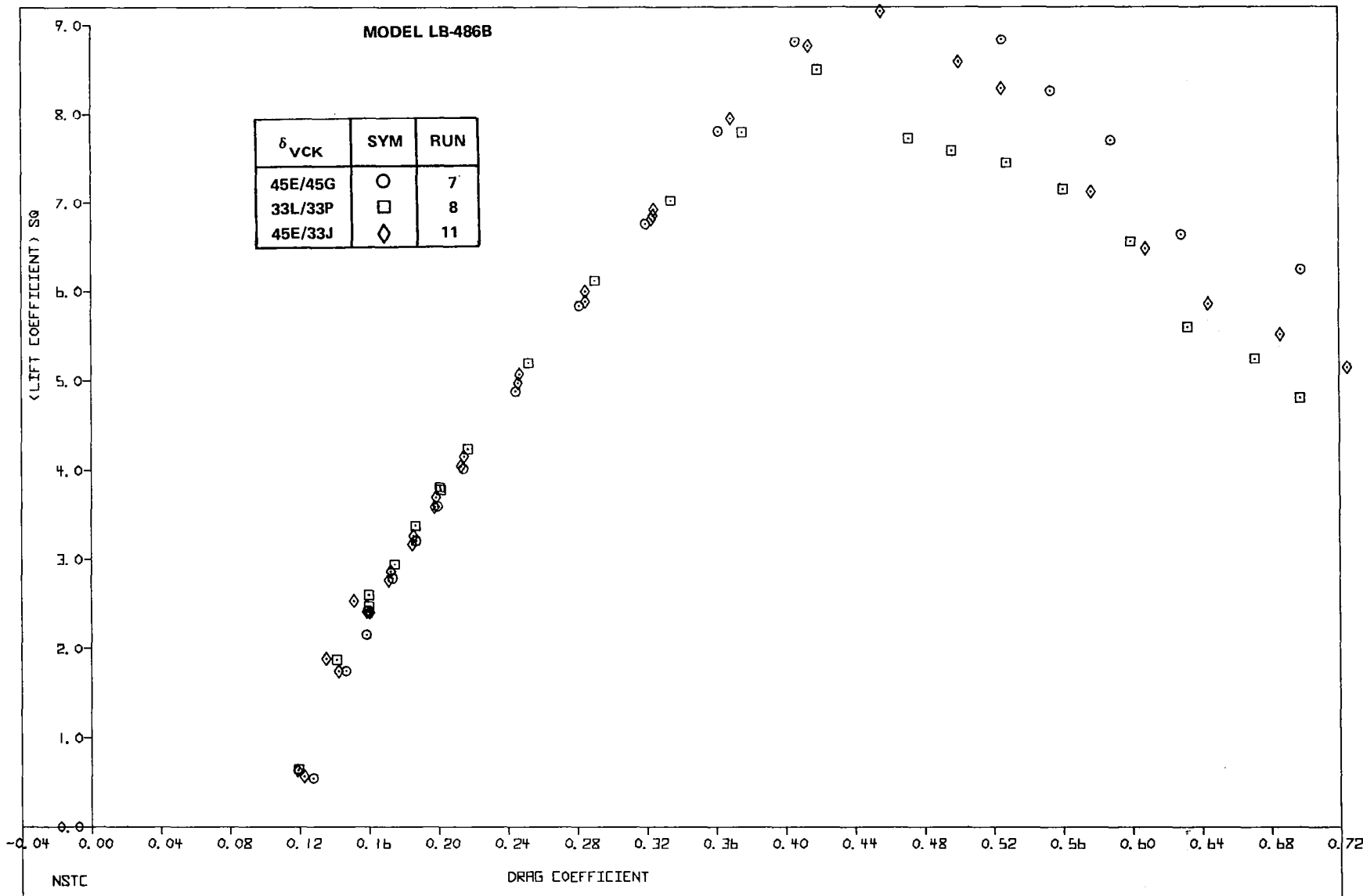
B. DRAG

FIGURE 15. EFFECT OF VCK DEFLECTION

Sealed Slats

In the Phase I LB-486A tests, a landing slats/takeoff flaps combination was investigated since it would simplify the high-lift system mechanically to have only one slat position for both takeoff and landing. The results showed, however, that the landing slat reduced L/D when used with either a clean trailing edge ($\delta_{FLAP} = 0^0$) or the basic takeoff flap deflection ($\delta_{FLAP} = 5^0/10^0$). To improve the L/D for this combination a sealed (i.e., zero gap) inboard and outboard slat configuration was investigated. The configuration was tested first with a 5^0 slat deflection inboard and a 20^0 deflection outboard. Then because previous analysis had shown a retracted slat might improve the pitching-moment characteristics, it was also tested with a 0^0 deflection inboard and a 20^0 deflection outboard. The results are presented in Figure 16. Because the loads on the sealed slat were expected to be high, it was not tested at the high Reynolds number. The results indicate that, as expected, the $5^0/20^0$ configuration had adverse pitch-moment characteristics. These were improved by retracting the inboard slat, without reducing $C_{L_{MAX}}$.

Also shown in Figure 16 is the landing slat configuraton with takeoff flaps. The $C_{L_{MAX}}$ penalty associated with the sealed slat is obvious. Figure 16 shows the $0^0/20^0$ slat configuration gave slightly higher L/D than the $5^0/20^0$ slat configuration, tail-on. Tail-off L/D's for clean, sealed, and slotted configurations are compared in Figure 17. The improved tail-off L/D values for the sealed configuration at $5^0/10^0$ flap deflection are illustrated. High Reynolds number data for the clean trailing edge with sealed slat configuration were not obtained.

An inboard sealed slat deflection of 5^0 was tested with landing flaps and an outboard landing slat position. Results indicated a substantial $C_{L_{MAX}}$ degradation and post-stall nose-down pitching-moment trends (Figure 18). LB-486A testing included a 15^0 inboard sealed slat position; the results showed no adverse effects on $C_{L_{MAX}}$ and no change in pitching-moment characteristics. An inboard sealed or small-gap slat configuration at an intermediate inboard slat deflection is a candidate for future low-speed studies.

MODEL LB-486B

CONFIGURATION B_{2A} W_{3B} N_{2A} P_{2A} Z_{1A} H_{1A} V_{1A}

MACH = 0.20

δ_{FLAP} = 5C/10

RN_{MAC}	δ_{SLAT}	SYM	RUN
2.89 x 10^6	5 SEALED/20 SEALED	◯	42
2.89 x 10^6	CLEAN/20 SEALED	☐	46
5.11 x 10^6	15 SLOTTED/25 SLOTTED	▽	41

PITCHING-MOMENT COEFFICIENT

LIFT COEFFICIENT

ANGLE OF ATTACK-DEG

ANGLE OF ATTACK-DEG

NSTC
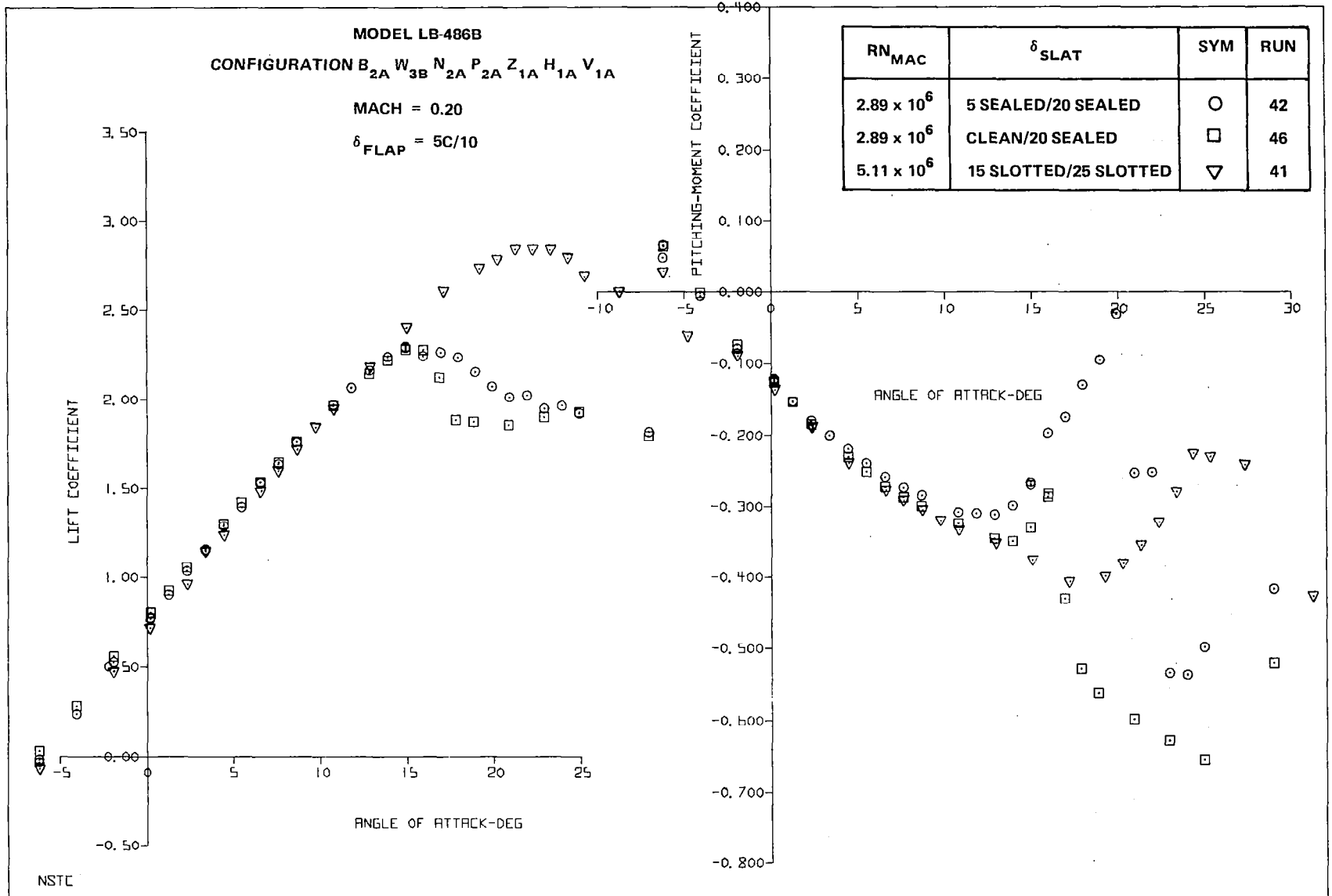
A. LIFT AND PITCHING MOMENT

FIGURE 16. EFFECT OF SEALED SLATS

FIGURE 16. EFFECT OF SEALED SLATS

MODEL LB-486

CONFIGURATION $B_{2A} W_3 X_{2B} N_{2A} P_{2A} Z_{1A}$

MACH = 0.20

RN_{MAC} = 2.58 x 10^6

TEST	δ_{SLAT}	δ_{FLAP}	SYM	RUN
LB-486A	CLEAN/CLEAN	0/0	▢	24
LB-486A	15 SLOTTED/25 SLOTTED	5/10	○	178
LB-486B	CLEAN/20 SEALED	5/10	▽	51
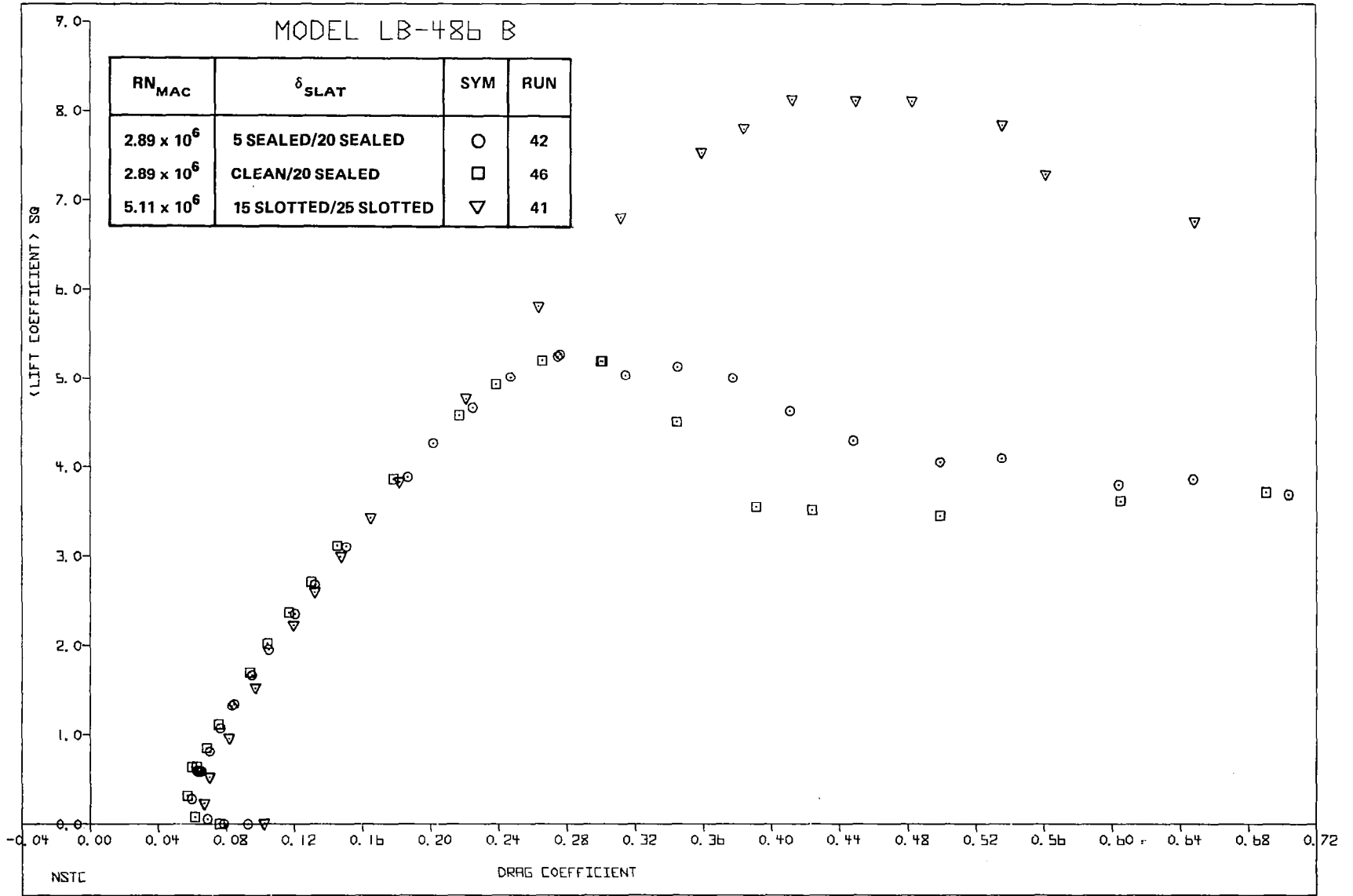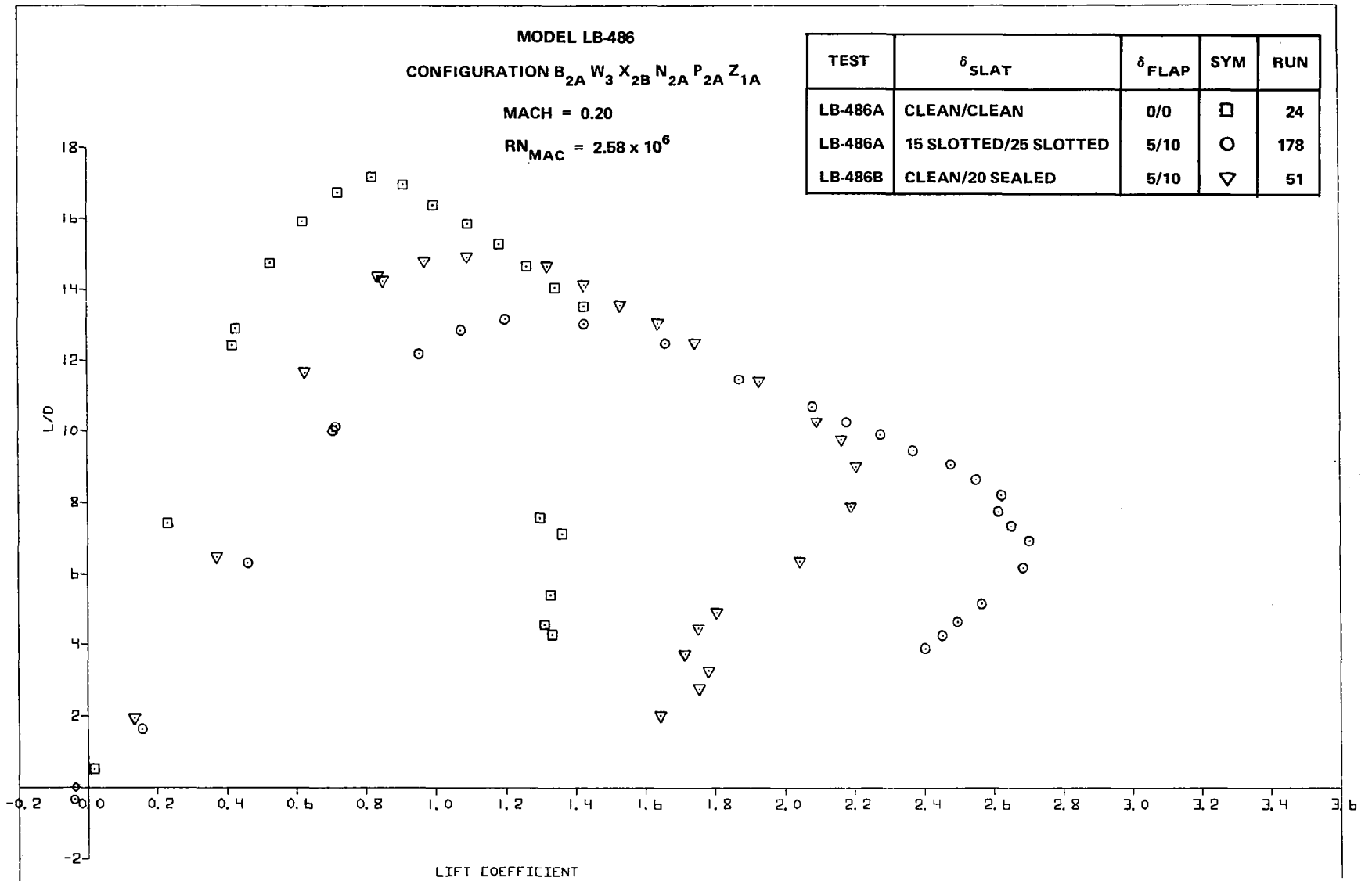
FIGURE 17. L/D COMPARISONS FOR CLEAN WING, SEALED SLAT, AND LANDING SLAT CONFIGURATIONS
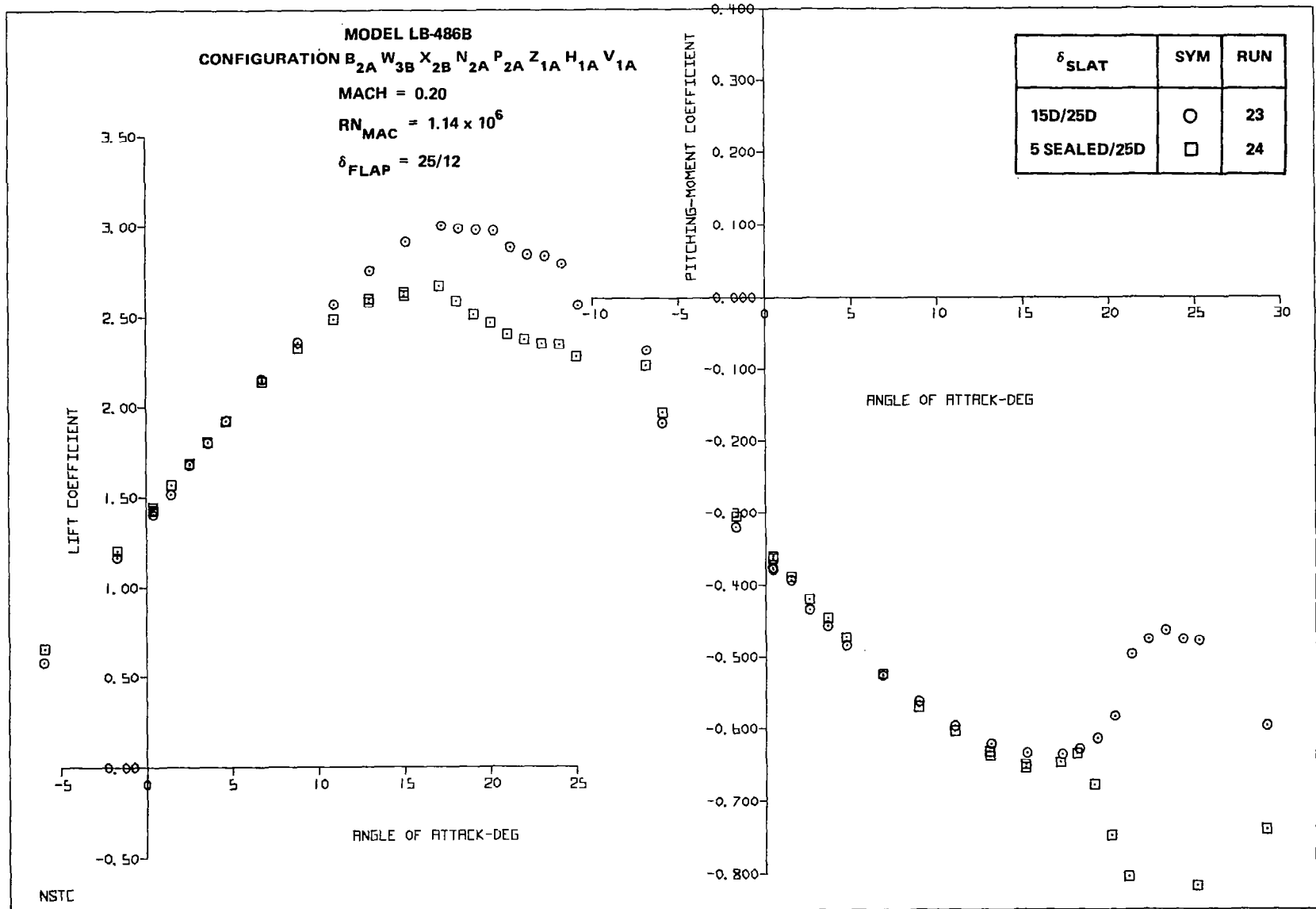
A. LIFT AND PITCHING MOMENT

FIGURE 18. EFFECT OF INBOARD SEALED SLAT WITH LANDING FLAPS
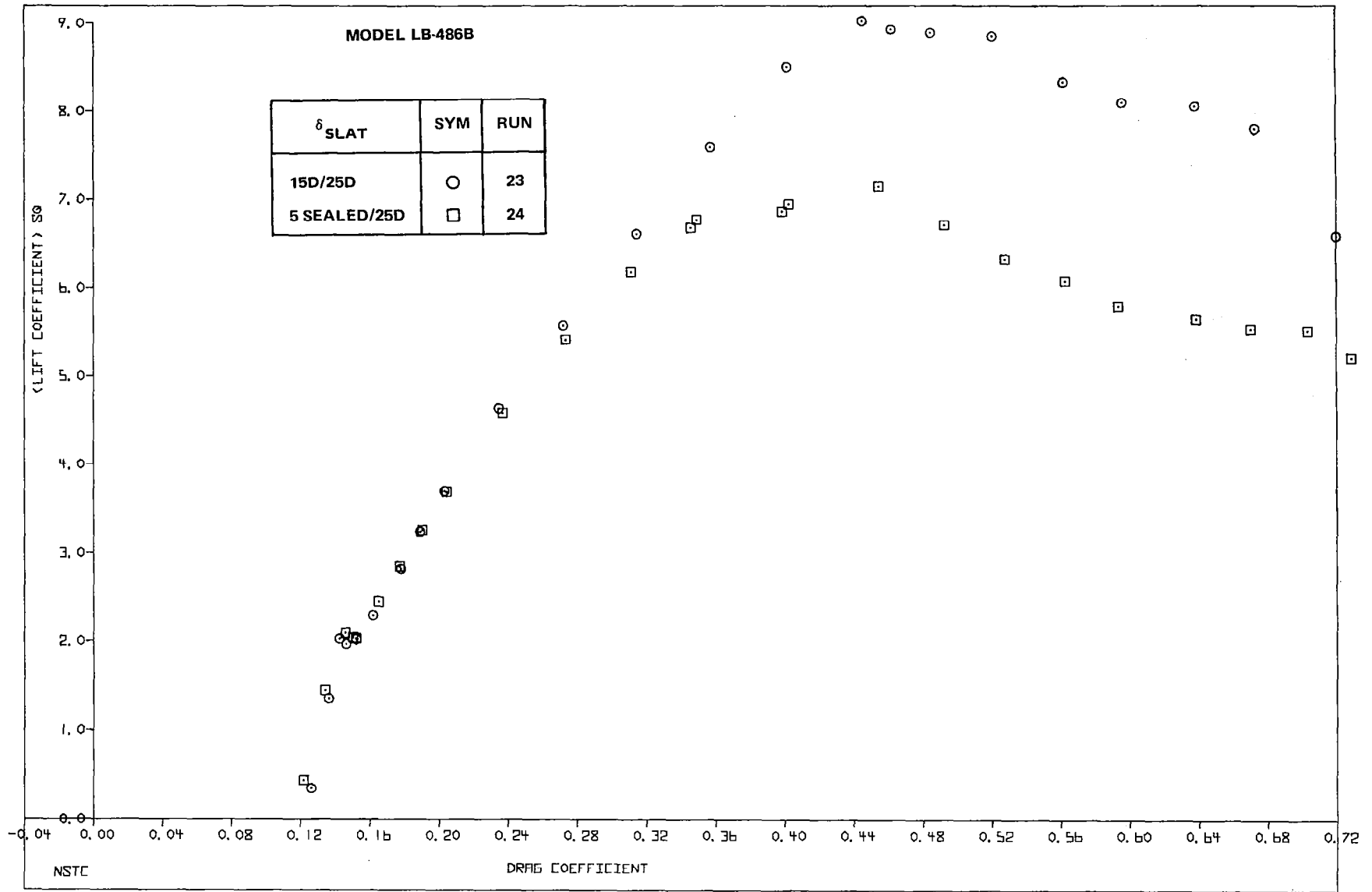
FIGURE 18. EFFECT OF INBOARD SEALED SLAT WITH LANDING FLAPS

Fixed-Camber Krueger

A fixed-camber Krueger (FCK) is an attractive high-lift device option, especially inboard, because of its mechanical simplicity and the need to stall the inboard wing panel just before the outboard panel stalls. The capability of a very efficient slat or VCK is not needed. As shown in Figure 19, the full-span FCK produced lift and pitching-moment characteristics equivalent to those of the full-span slat and full-span VCK configuration. Use of an FCK inboard with a slat outboard, however, resulted in improved pitch characteristics (Figure 20). Even though the FCK/slat combination caused pitch-up to start at a lower angle of attack than the FCK/FCK combination, pre-stall nose-up tendencies were greatly reduced, and could possibly be eliminated with additional tuning. Post-stall characteristics continued to be unsatisatifactory, indicating a lack of leading-edge separation on the FCK.

To further improve pitching-moment characteristics, a short-chord FCK was fabricated and tested during the LB-486B series. The chord ratio for this device was 0.068, extrapolated to the side of the fuselage, and 0.105 at the leading-edge break (pylon position). The comparable values for the slat were 0.1803 and 0.1295, respectively. The bulb shape was tailored such that an inboard, leading-edge stall would be obtained. FCK deflections of 50^0 and 70^0 were evaluated with zero gap and overhang. Examination of the trailing-edge pressures indicated that a premature inboard stall was being obtained. Favorable pitch characteristics at stall were obtained (Figure 21), but at the expense of a substantial reduction in $C_{L_{MAX}}$ values of -0.457 and -0.412, respectively, for the two FCK deflections. Shims were fabricated at the tunnel to obtain a small gap and negative overhang for this leading-edge device. The best FCK/slat configuration resulted in higher maximum lift values and better pitching-moment trends then did the full-span slat configuration (Figure 22). Tail-off drag values indicated L/D values at $1.3V_s$ of 9.71 and 9.77 for the FCK and basic slat configuration, respectively.

MODEL LB-486C

CONFIGURATION B_{2A} W_{3B} X_{2B} N_{2A} P_{2A} Z_{1A}

MACH = 0.20

RN_{MAC} = 1.14 x 10^6

δ_{FLAP} = 25/12

LE DEVICE	SYM	RUN
SLAT	O	19
FCK	□	42
VCK	◇	66

LIFT COEFFICIENT

ANGLE OF ATTACK (DEG)

PITCHING-MOMENT COEFFICIENT

ANGLE OF ATTACK (DEG)
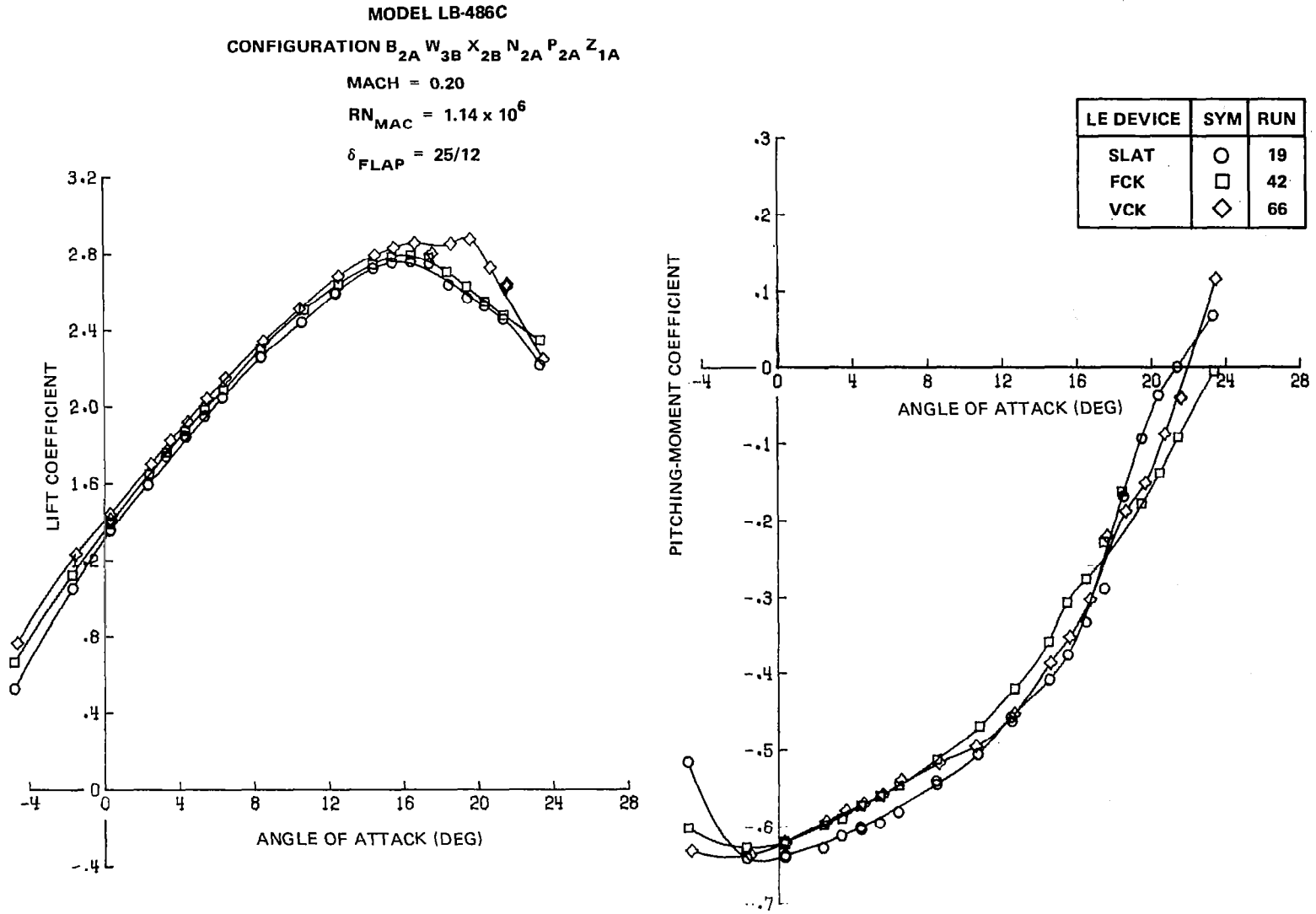
A. LIFT AND PITCHING MOMENT

FIGURE 19. EFFECT OF LEADING EDGE DEVICE WITH LANDING FLAPS
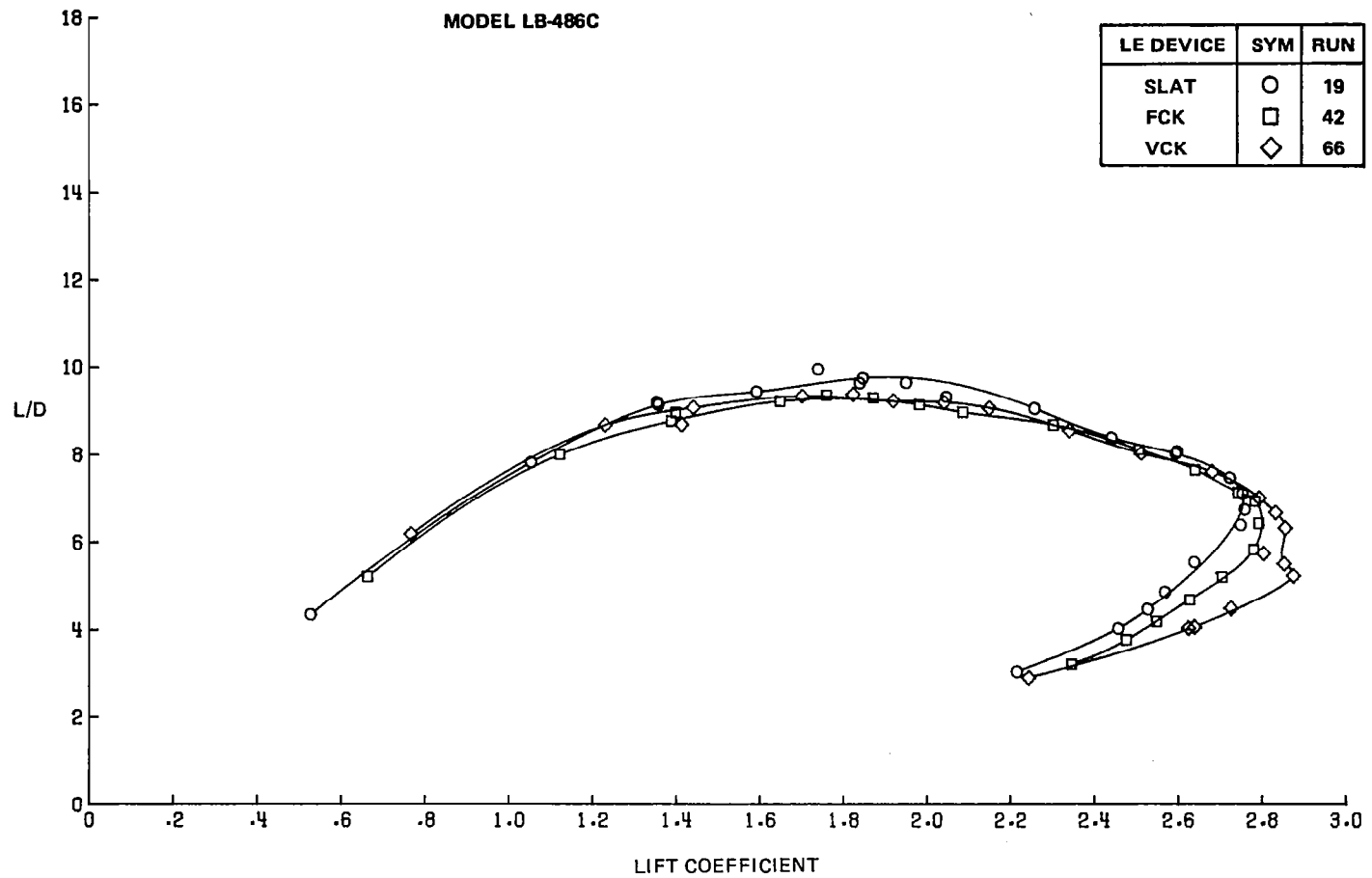
B. LIFT-DRAG RATIOS

FIGURE 19. EFFECT OF LEADING EDGE DEVICE WITH LANDING FLAPS

MODEL LB-486C

CONFIGURATION B_{2A} W_{3B} X_{2B} N_{2A} P_{2A} Z_{1A} V_{1A} H_{1A}

MACH = 0.20

RN_{MAC} = 1.14 x 10^6

δ_{FLAP} = 25/12

LE DEVICE	SYM	RUN
FCK/FCK	O	77
FCK/SLAT	□	52
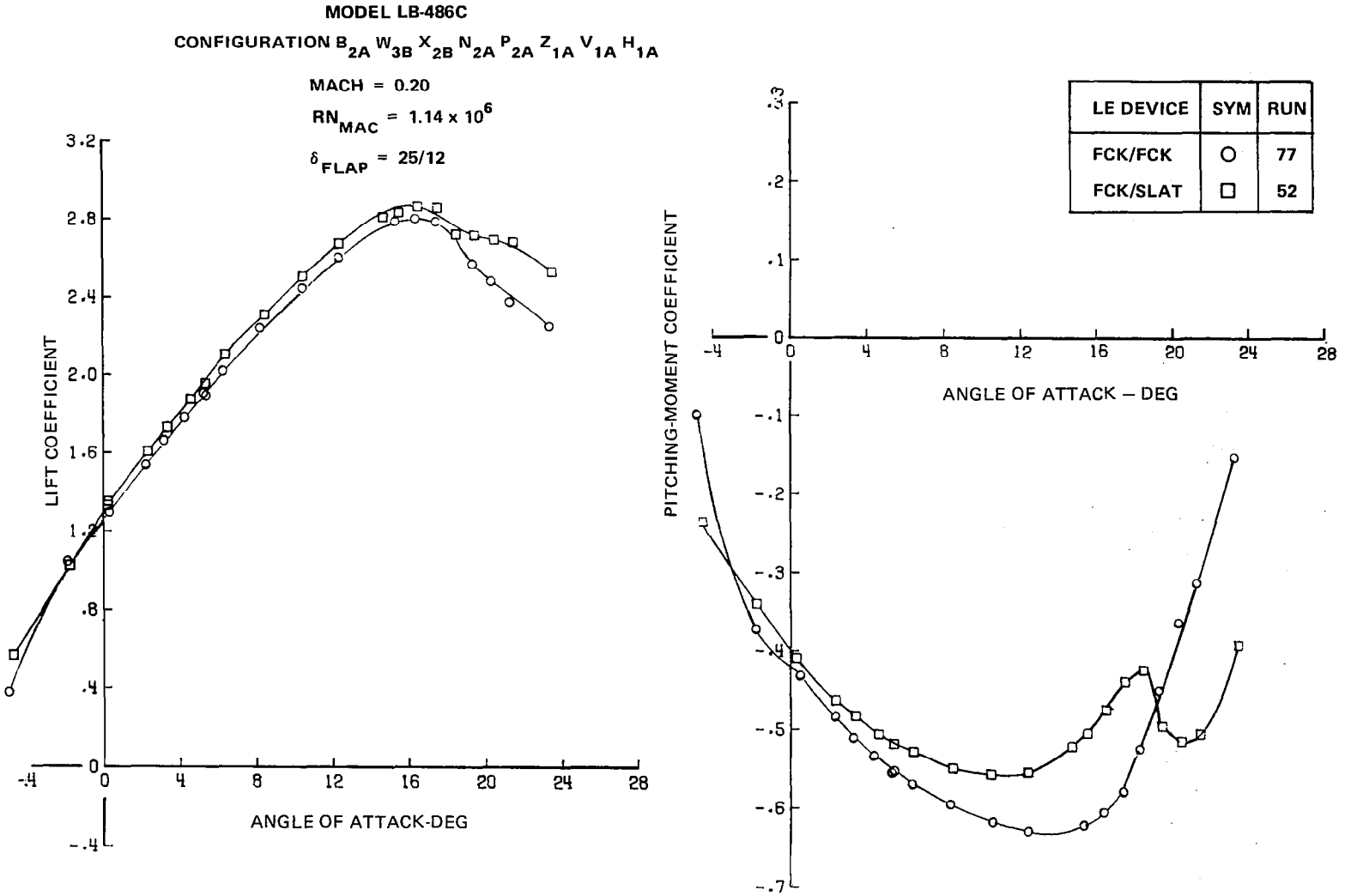
A. LIFT AND PITCHING MOMENT

FIGURE 20. COMPARISON OF FULL-SPAN FCK AND FCK/SLAT COMBINATION

MODEL LB-486C
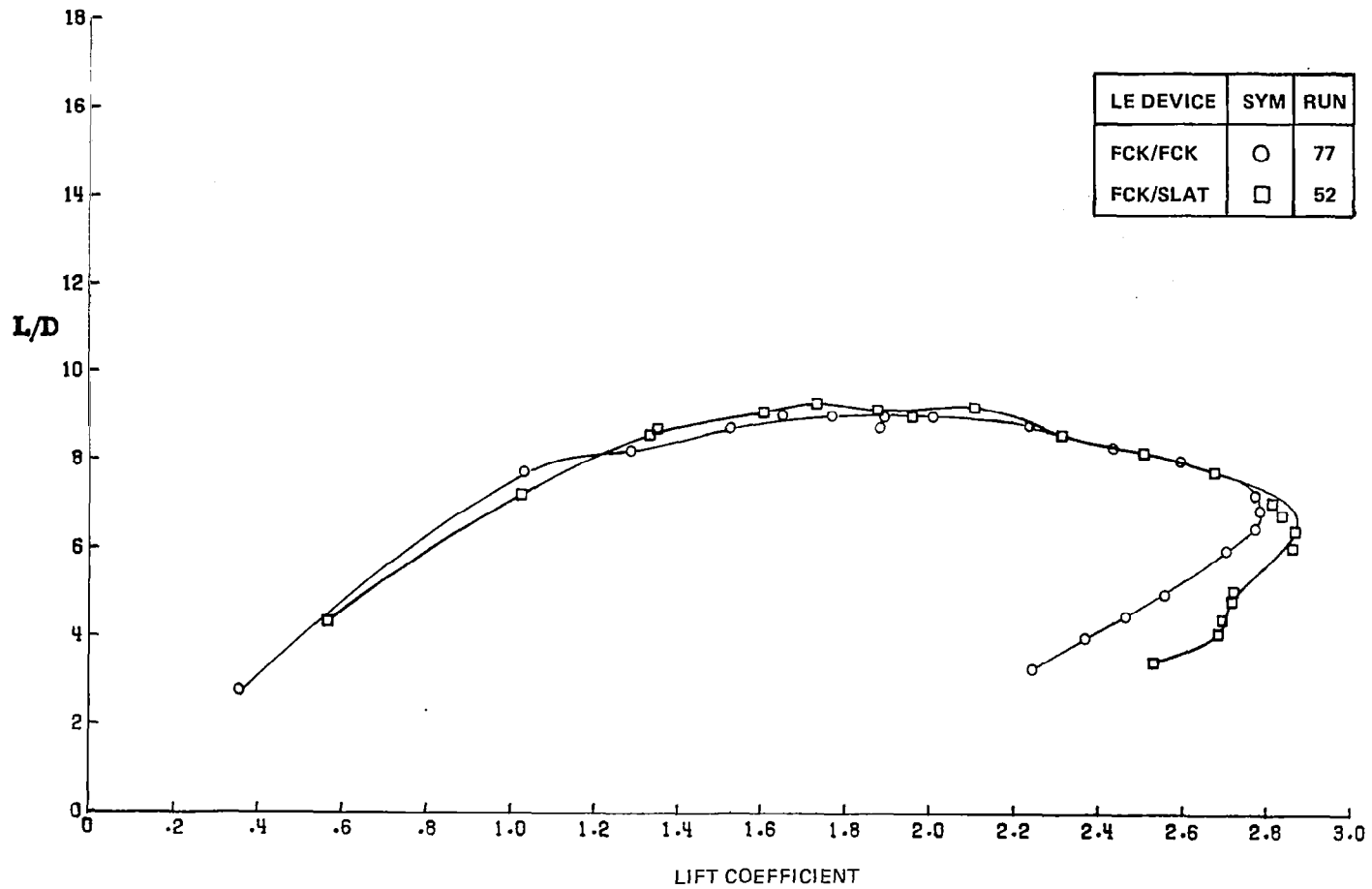
B. LIFT-DRAG RATIO

FIGURE 20. COMPARISON OF FULL-SPAN FCK AND FCK/SLAT COMBINATION

43

MODEL LB-486B

CONFIGURATION $B_{2A} W_{3B} X_{2B} N_{2A} P_{2A} Z_{1A} V_{1A} H_{1A}$

MACH = 0.20

RN_{MAC} = 5.1 x 10^6

i_{TAIL} = $0°$

$\delta_{FCK}/\delta_{SLAT}$	SYM	RUN
50A/25D	O	33
70C/25D	□	34
70D/25D	◇	35

PITCHING-MOMENT COEFFICIENT

ANGLE OF ATTACK-DEG

LIFT COEFFICIENT

ANGLE OF ATTACK-DEG

NSTC
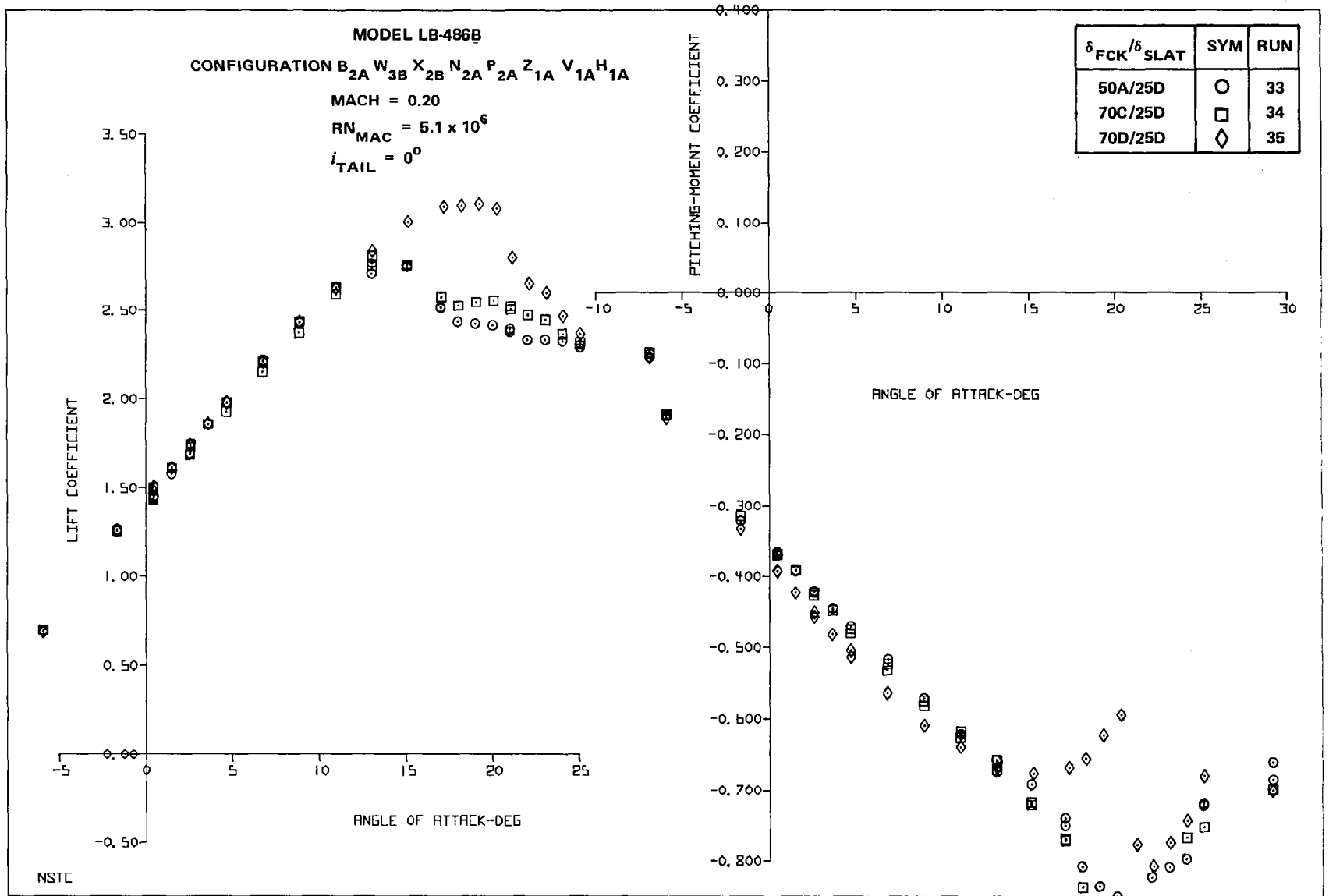
A. LIFT AND PITCHING

FIGURE 21. GRID STUDY FOR SHORT-CHORD FCK/SLAT COMBINATION

B. DRAG

FIGURE 21. GRID STUDY FOR SHORT-CHORD FCK/SLAT COMBINATION

MODEL LB-486B

CONFIGURATION B_{2A} W_{3B} X_{2B} N_{2A} P_{2A} Z_{1A} V_{1A} H_{1A}

MACH = 0.20

$RN_{MAC} = 5.11 \times 10^6$

$\delta_{FLAP} = 25/12$

$i_{TAIL} = 0^\circ$

LE DEVICE	δ_{LE}	SYM	RUN
SLAT/SLAT	15D/25D	O	25
FCK/SLAT	70D/25D	□	35

PITCHING-MOMENT COEFFICIENT

ANGLE OF ATTACK-DEG

LIFT COEFFICIENT

ANGLE OF ATTACK-DEG

NSTC

A. LIFT AND PITCHING MOMENT
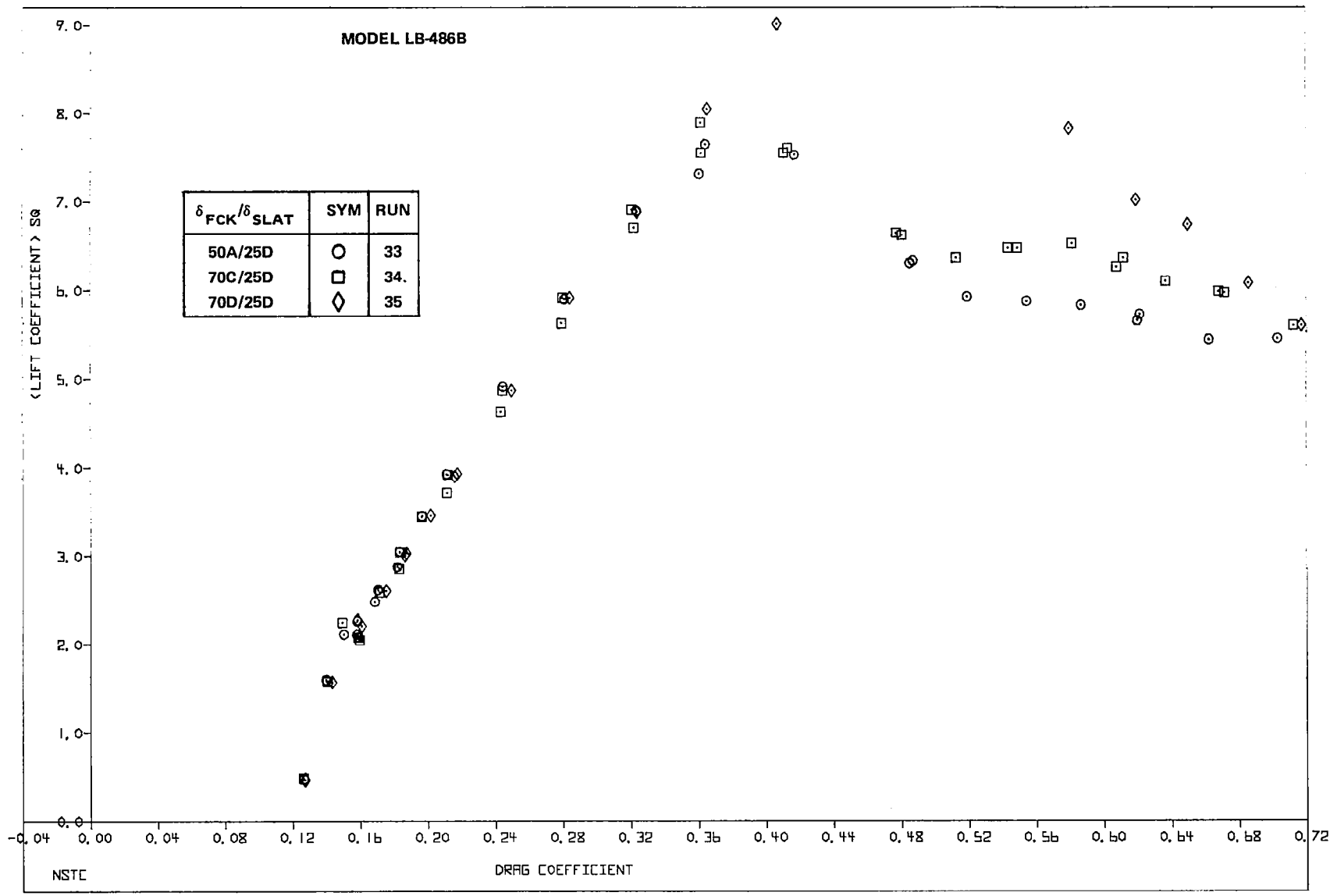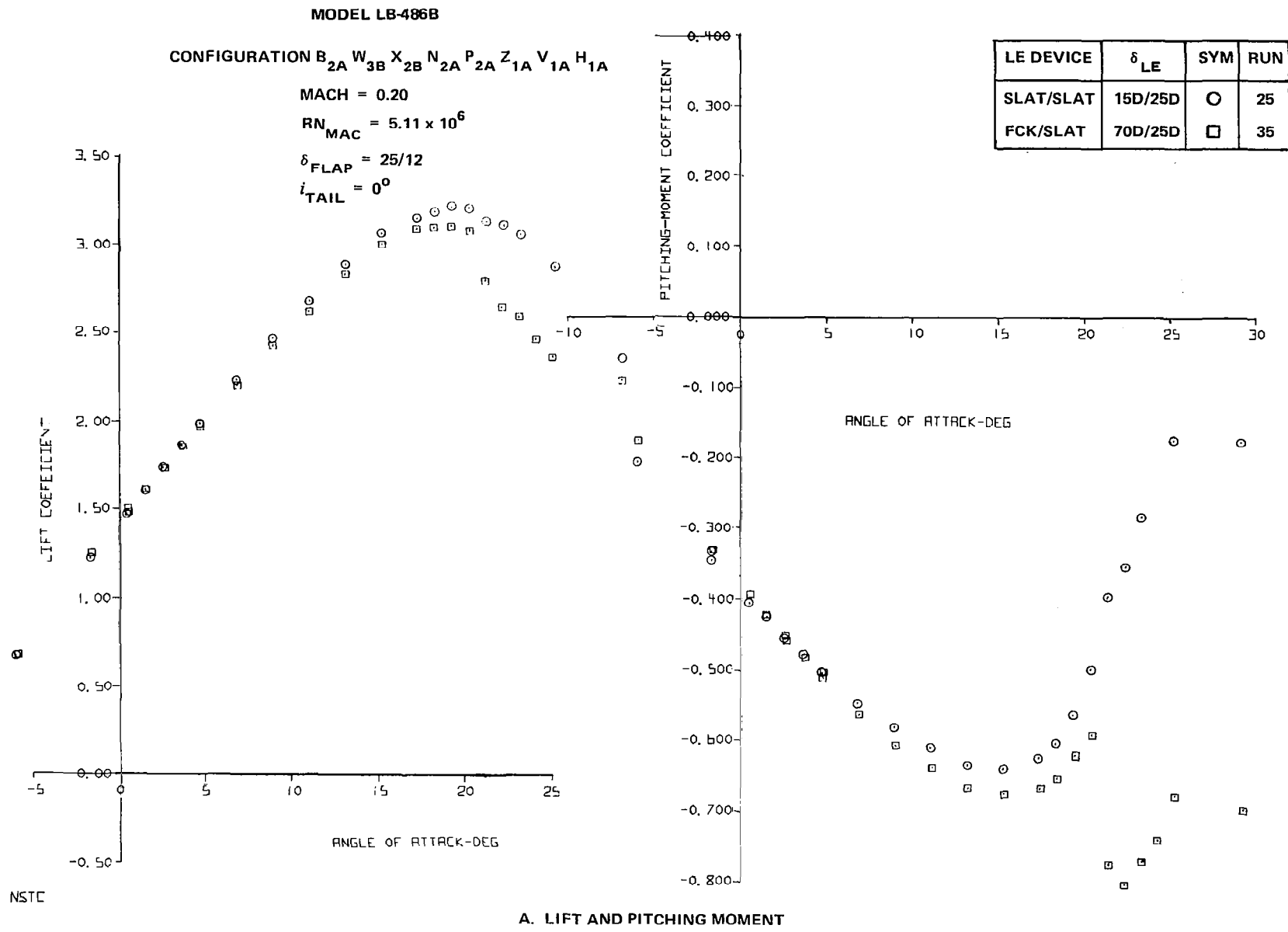
FIGURE 22. COMPARISON OF FULL-SPAN SLAT AND SHORT-CHORD FCK/SLAT COMBINATION
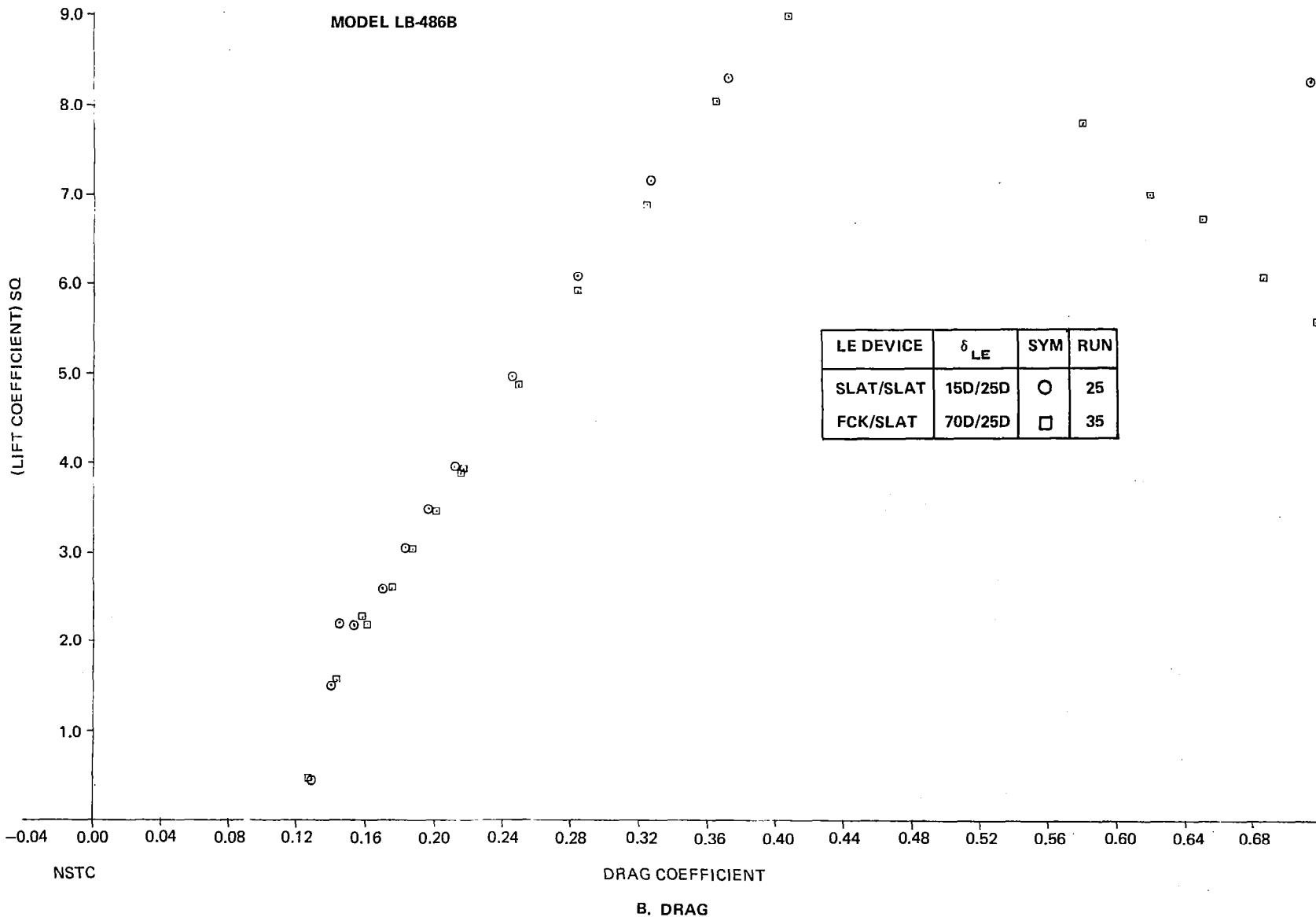
FIGURE 22. COMPARISON OF FULL-SPAN SLAT AND SHORT-CHORD FCK/SLAT COMBINATION

Slat Trim Effects

The lift and pitching-moment characteristics for the revised slat trim are presented in Figure 23. The basic trim consisted of a side-of-fuselage inboard trim and a sealed over-the-pylon configuration (i.e., continuous over the pylon). This base case resulted in a $C_{L_{MAX}}$ value of 3.2. Figure 23 also illustrates two other trim variations which showed a $C_{L_{MAX}}$ reduction of approximately 0.20. For the first variation, the slat trim was moved outboard 2.25 cm (1 in.) from the fuselage side. This resulted in improved pitch characteristics at the stall angle, but pitch-up at post-stall conditions. In the second variation, in addition to the revised inboard slat trim an over-the-pylon island (i.e., undeflected slat) trim was tested. Pitching-moment characteristics similar to those of the basic trim resulted but with reduced magnitude of pitch-up. Small effects were noted on L/D performance for the two slat-trim revisions. Examination of Figures 22 and 23 indicates a lower $C_{L_{MAX}}$ and more adverse post-stall behavior for the slat trim configuration than the short-chord FCK.

High-Speed Aileron

In order to determine the benefit of a flaperon, a configuration using a high-speed aileron in place of the flaperon was tested at the maximum landing flap deflection of $35°/12°$. The results indicated a reduction of 0.315 in $C_{L_\alpha = 0}$ and 0.216 in $C_{L_{MAX}}$. The drag increase at $1.3V_s$ was 0.008. High-angle-of-attack pitch characteristics were essentially similar to those of the basic configuration.

Two-Segment Flaperon Replacement

For several runs, the single-segment flaperon was replaced with a two-segment flaperon. The effects of the change were evaluated at landing and takeoff flap deflections. The increases in corresponding $C_{L_{MAX}}$ values were 0.061 and 0.039, respectively. Small changes in pitching moment were also indicated. The drag values indicated essentially no change due to the two-segment replacement for the single-slot flaperon.

MODEL LB-486B

CONFIGURATION $B_{2A} W_{3B} X_{2B} N_{2A} P_{2A} Z_{1A} H_{1A} V_{1A}$

MACH = 0.20

RN_{MAC} = 5.11 x 10^6

δ_{FLAP} = 25/12

SYM	RUN	SLAT TRIM CONFIGURATION
O	21	BASIC (SIDE OF FUS AND OVER PYLON)
□	22	OUTBD TRIM (NEAR FUSELAGE)
◇	23	OUTBD TRIM AND ISLAND AT PYLON
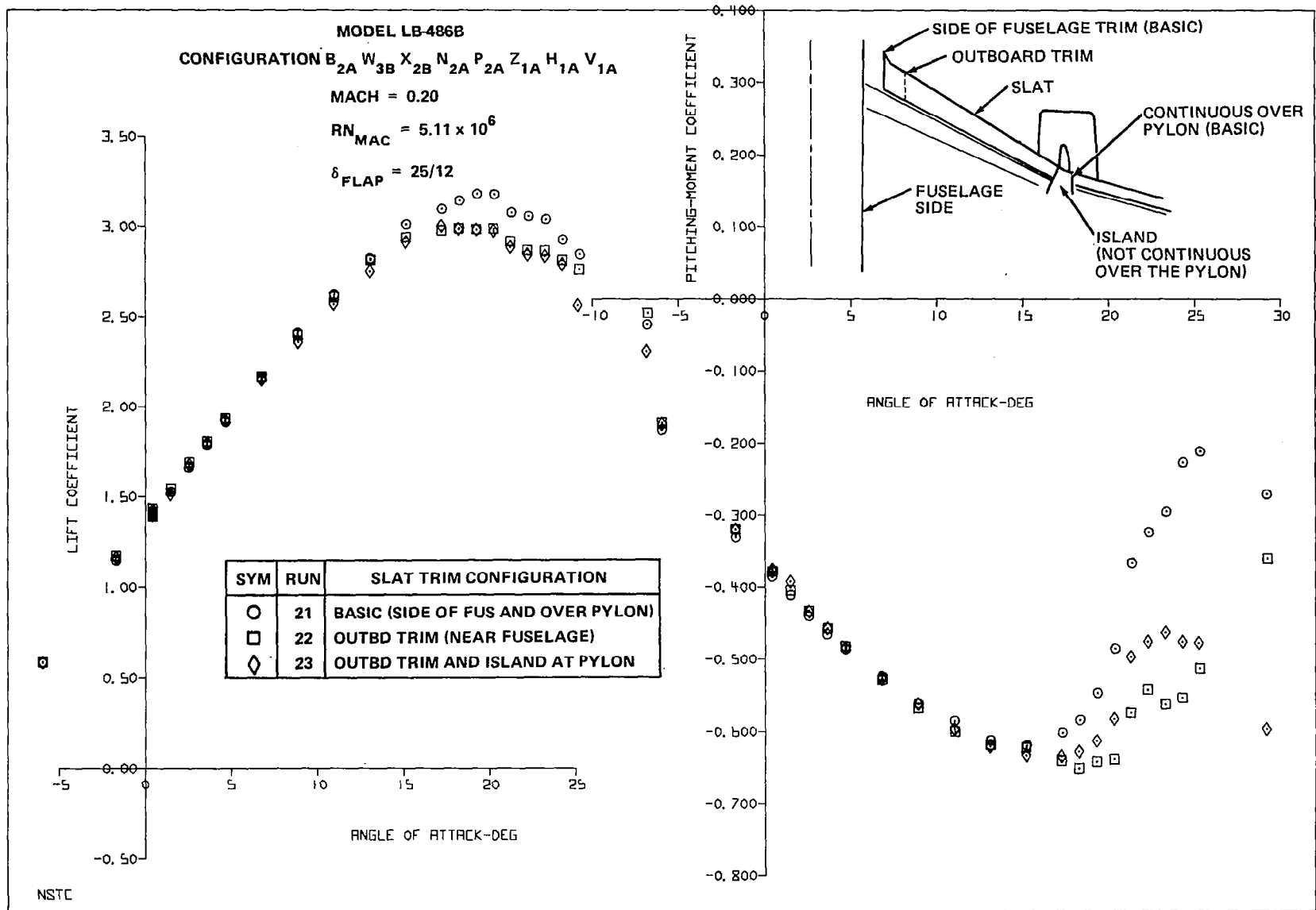
A. LIFT AND PITCHING MOMENT

FIGURE 23. EFFECT OF SLAT TRIM WITH LANDING FLAPS
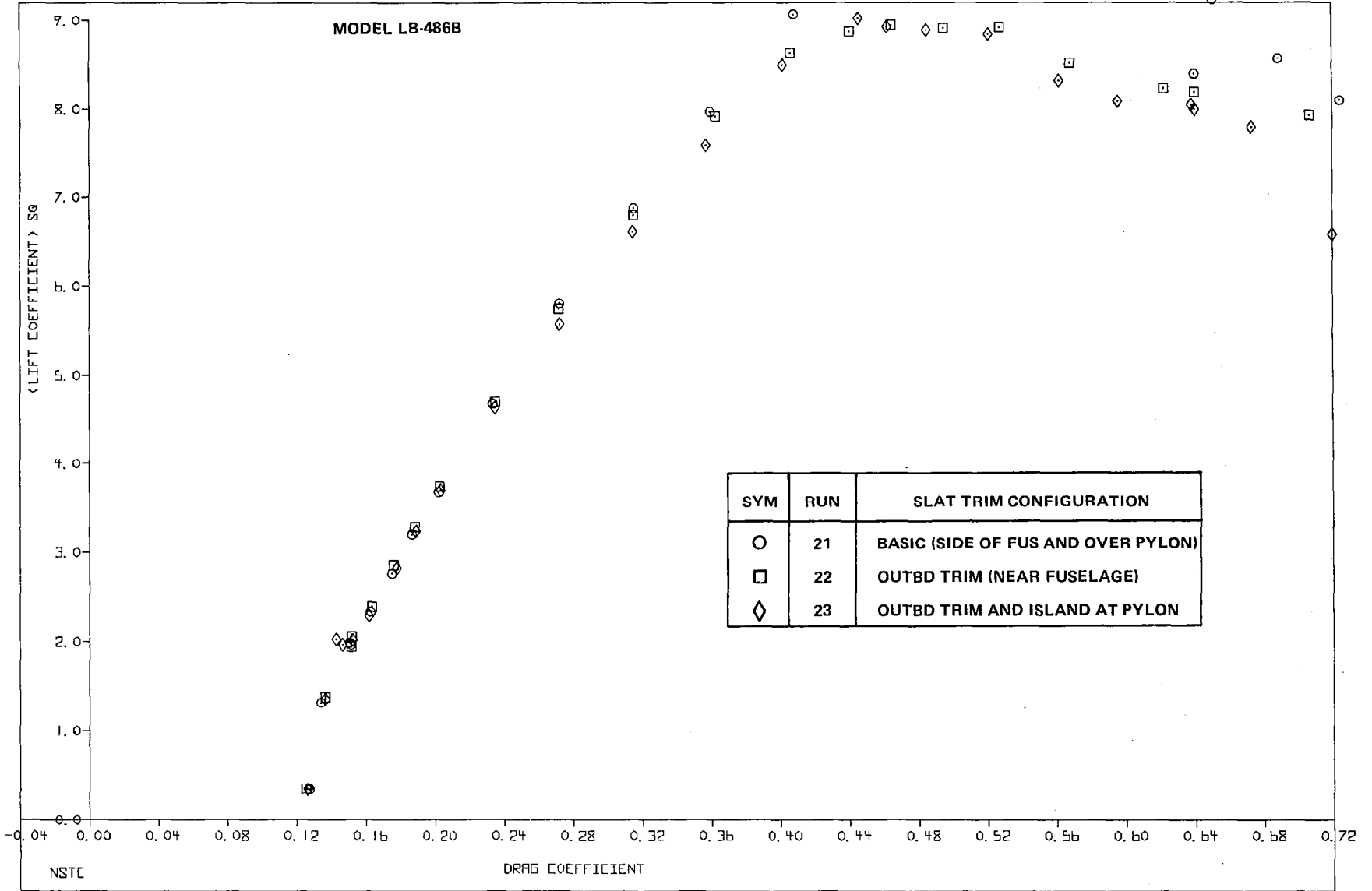
FIGURE 23. EFFECT OF SLAT TRIM WITH LANDING FLAPS

Differential Flap Deflection

A 35°/12° (main flap/auxiliary flap) inboard flap deflection combined with a 25°/12° outboard flap deflection was also tested to determine the effect on the low-speed characteristics. Results compared with those of the basic 25°/12° two-segment flap deflection indicated a small reduction in $C_{L_{MAX}}$ (-0.046) and slightly more positive pitching moments. The increased inboard flap deflection did not produce a smaller inboard stall angle and the associated stall improvements. The differential flap deflection did result in a drag increase of 0.0180 for the C_L range of interest.

Ames 12-Foot and Langley V/STOL Tunnel Comparisons

During the Phase I wind-tunnel tests in the Ames 12-Foot Pressure Tunnel, several configurations were tested at high Reynolds number as well as at atmospheric conditions. Two of these configurations were also tested in the Langley V/STOL facility for comparison. The tandem strut support system was utilized in both cases. Figure 24 presents the lift and pitching-moment comparison at the atmospheric condition for the slat with two-segment takeoff flap configuration. The data presented have been corrected for tunnel wall effects, but not for strut tare effects since these would be the same for both wind tunnels. Good agreement between the Ames and Langley data is shown for the lift coefficient up to the angle of attack for stall. Some differences are noted in the post-stall region. The pitching-moment data show differences for most of the angle-of-attack range. This was also typical of the VCK configuration used for comparison. Comparison of the drag characteristics indicated differences of 0.0050 to 0.0070 for the configurations evaluated. The Ames wall corrections are considered a possible source of these differences.

MODEL LB-486B & C

MACH = 0.20

RN_{MAC} = 1.14 x 10^6

HORIZONTAL TAIL-OFF
LANDING GEAR OFF

SLAT (15°/25°) + TWO-SEGMENT FLAP (5°/10°)

SYMBOL	FACILITY
△	AMES 12-FOOT
O	LANGLEY V/STOL
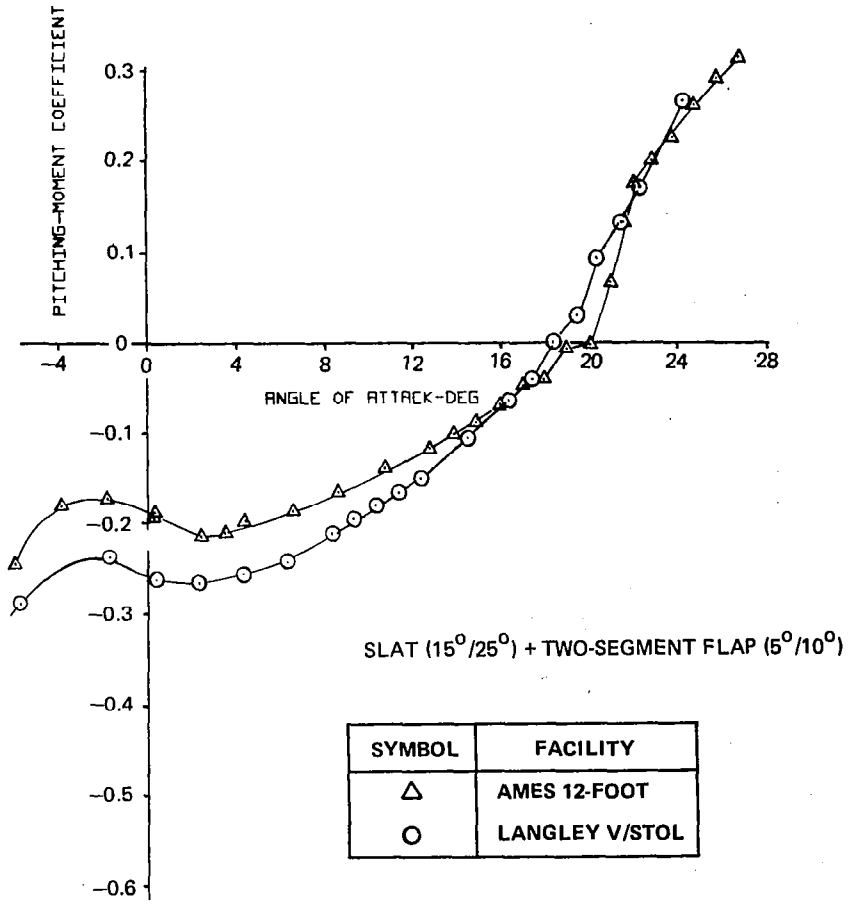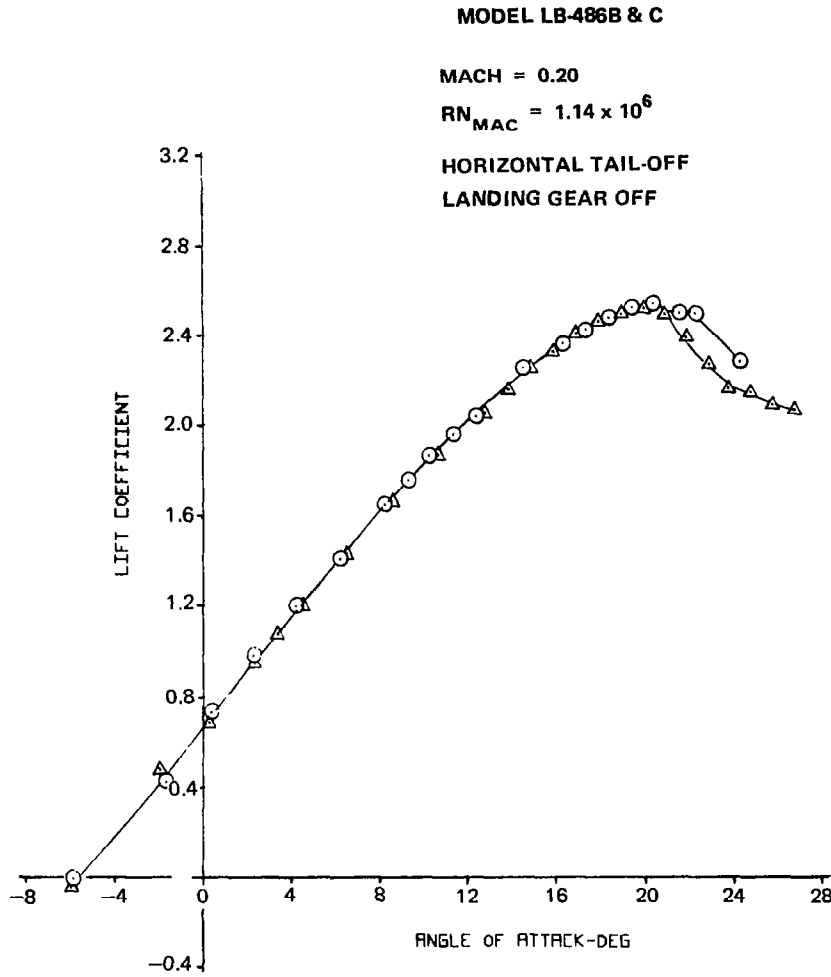
LIFT AND PITCHING MOMENT

FIGURE 24. AMES 12-FOOT AND LANGLEY V/STOL COMPARISON

PART II
NARROW BODY
ATMR-TYPE MODEL

**LB-507A MODEL
INSTALLED IN AMES
12-FOOT PRESSURE TUNNEL**

PART II
NARROW BODY ATMR-TYPE MODEL

LB 507A MODEL DESCRIPTION

A 5.59-percent-scale full-span model of the ATMR aircraft was used for this program. This model is shown in Figure 25. The configuration notation data, dimensional data, and grid position definition are presented in Appendixes D, E, and F, respectively. The model included a high-aspect-ratio supercritical wing, variable-position leading-edge slats, an inboard short-chord FCK, two-segment trailing-edge flaps, wing and high-lift surface pressure instrumentation, and a remotely driven horizontal stabilizer. The outboard ailerons and wing spoilers also had deflection capabilities. The model instrumentation was equipped with the Douglas internal pitch system. This system was used in conjunction with the Douglas tandem support system and the Task MK IIC internal strain-gage balance.

The model fuselage utilized the LB-506A (high-speed EET model) nose section and glass fiber wing/body fillet. These parts were combined with a new aluminum centerbody and aft section. The constant-diameter hollow center section was machined on the upper and lower surfaces and internally to provide clearance for the Douglas 10.16-cm (4-in.) balance housing and internal pitch system. Other instrumentation housed in the fuselage included two 6-pac scanivalve modules in the nose, two electrolytic bubbles measuring the angle of the balance axis, and an electrolytic bubble pack to measure the fuselage angle of attack.

The wing for this model (Figure 26) consisted of right- and left-hand panels which were joined together and to the fuselage by means of a wing splice plate. The wing had removable leading and trailing edges to allow for the attachment of high-lift devices, and had movable control surfaces. The wing also included pressure instrumentation at four spanwise locations, and had a trailing-edge pressure port at one inboard span location. A diagram of the high-lift system and the lateral control surfaces is provided in Figure 27.

MODEL LB-507A

DIMENSIONS IN CENTIMETERS (INCHES)
MODEL SCALE UNLESS OTHERWISE SPECIFIED

2°

43.774
(17.234)

X_{MAC} = 46.007
(18.113)

68.481
(26.961)

TRAPEZOIDAL AREAS:

S_{REF} = 0.464 m^2 (5.000 FT^2)

S_H = 0.113 m^2 (1.231 FT^2)

S_V = 0.086 m^2 (0.931 FT^2)

L_H = 124.412
(48.981)

$Y_{\overline{c}/4}$ = 136.876
(53.888)

L_V = 100.952
(39.745)

227.063
(89.395)

24.079
(9.480) DIA

37.203
(14.647)

13.485
(5.309)

FRP

248.694
97.911

Y = 0

13.553
(5.336)

262.247
(103.247)
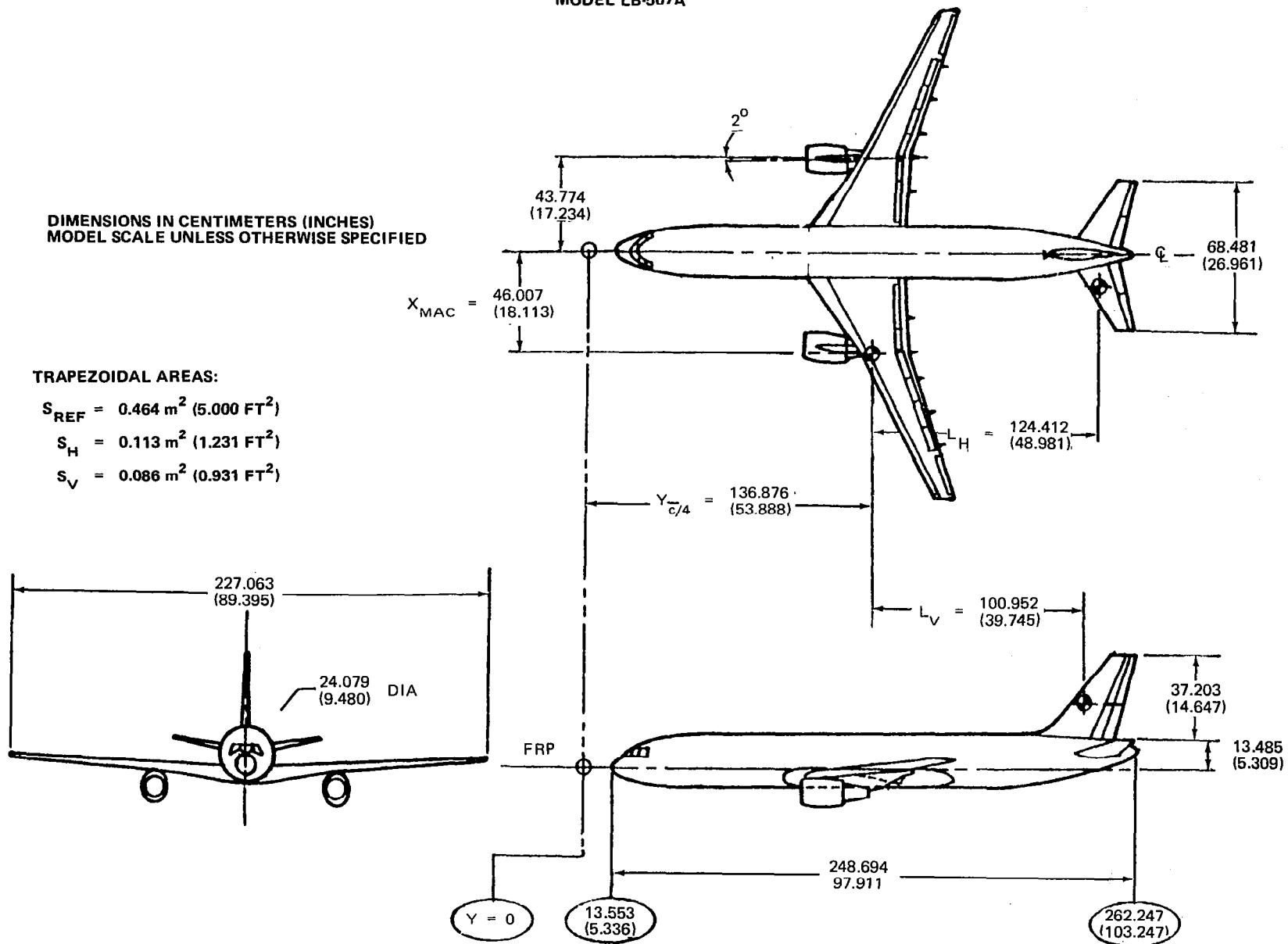
FIGURE 25. LB-507A MODEL THREE VIEW

TRAPEZOIDAL WING CHARACTERISTICS

S_{REF} = 0.464 m^2 (5.000 FT^2)

$\Lambda_{c/4}$ = 26.000 DEG

T.R. = λ = 0.275

AR = 11.10

MAC = 2.103 cm (8.922 IN.)

b/2 = 113.532 cm (44.698 IN.)

DIHEDRAL = Γ = 5.000 DEG

DIMENSIONS IN CENTIMETERS (INCHES)
MODEL SCALE UNLESS OTHERWISE NOTED
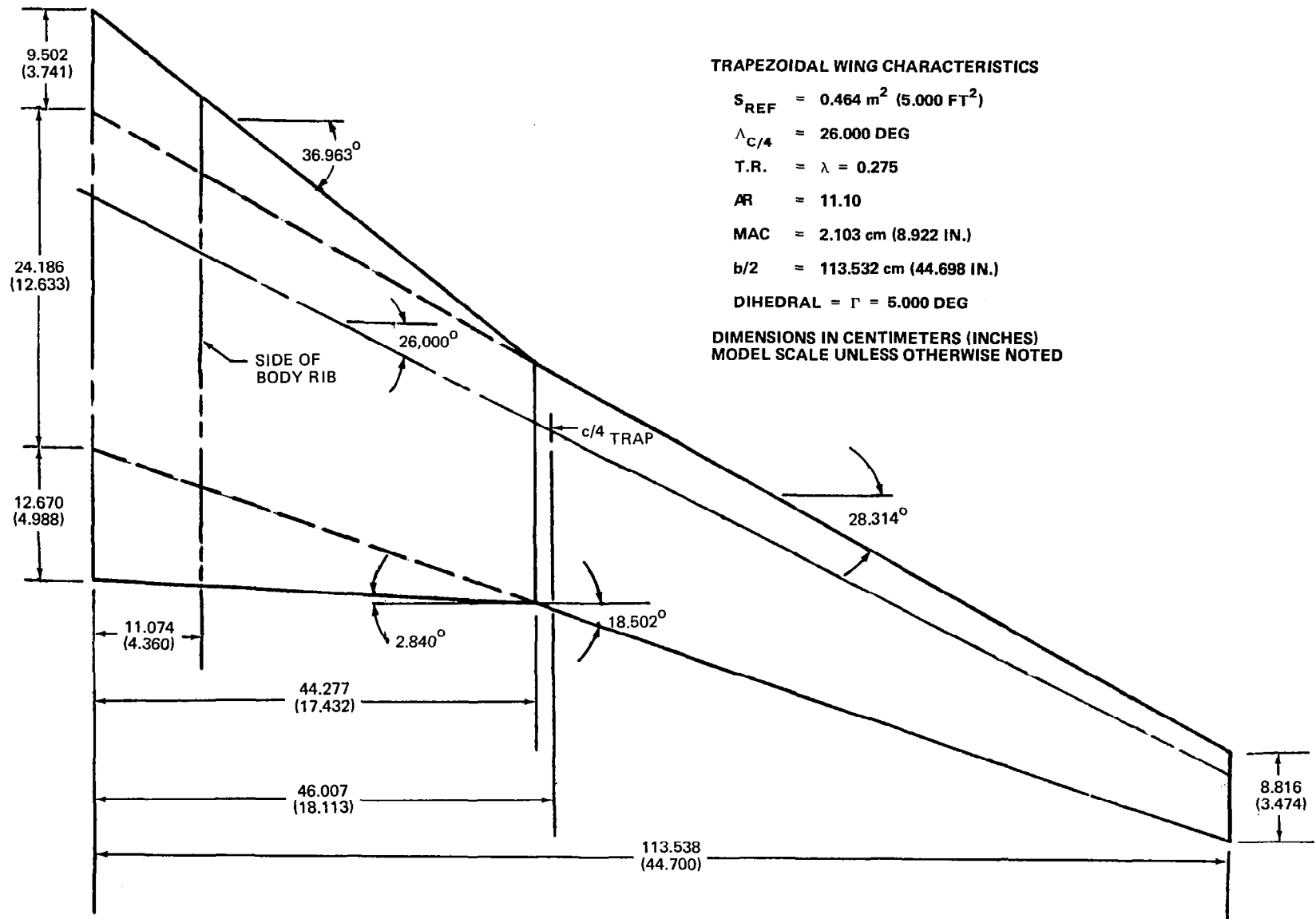
FIGURE 26. LB-507A WING (W$_{1B}$)

58

MODEL LB-507A

DIMENSIONS IN CENTIMETERS (INCHES)
MODEL SCALE

14.625
(5.758)
X_W

42.880
(16.882)
X_W

44.795
(17.636)
X_W

INBD SLAT
L_{3A}

OUTBD SLAT L_{4A}

OUTBD SPOILER f_{2A}

AILERON
a_{1A}

113.106
44.530
X_W

11.643
(4.584)
X_W

INBD FLAP
F_{1A}/F_{2A}

INBD SPOILER
f_{1A}

44.409
17.484
X_W

OUTBD FLAP
F_{3A}/F_{4A}

91.178
(35.897)
X_W

113.939
(44.858)
X_W
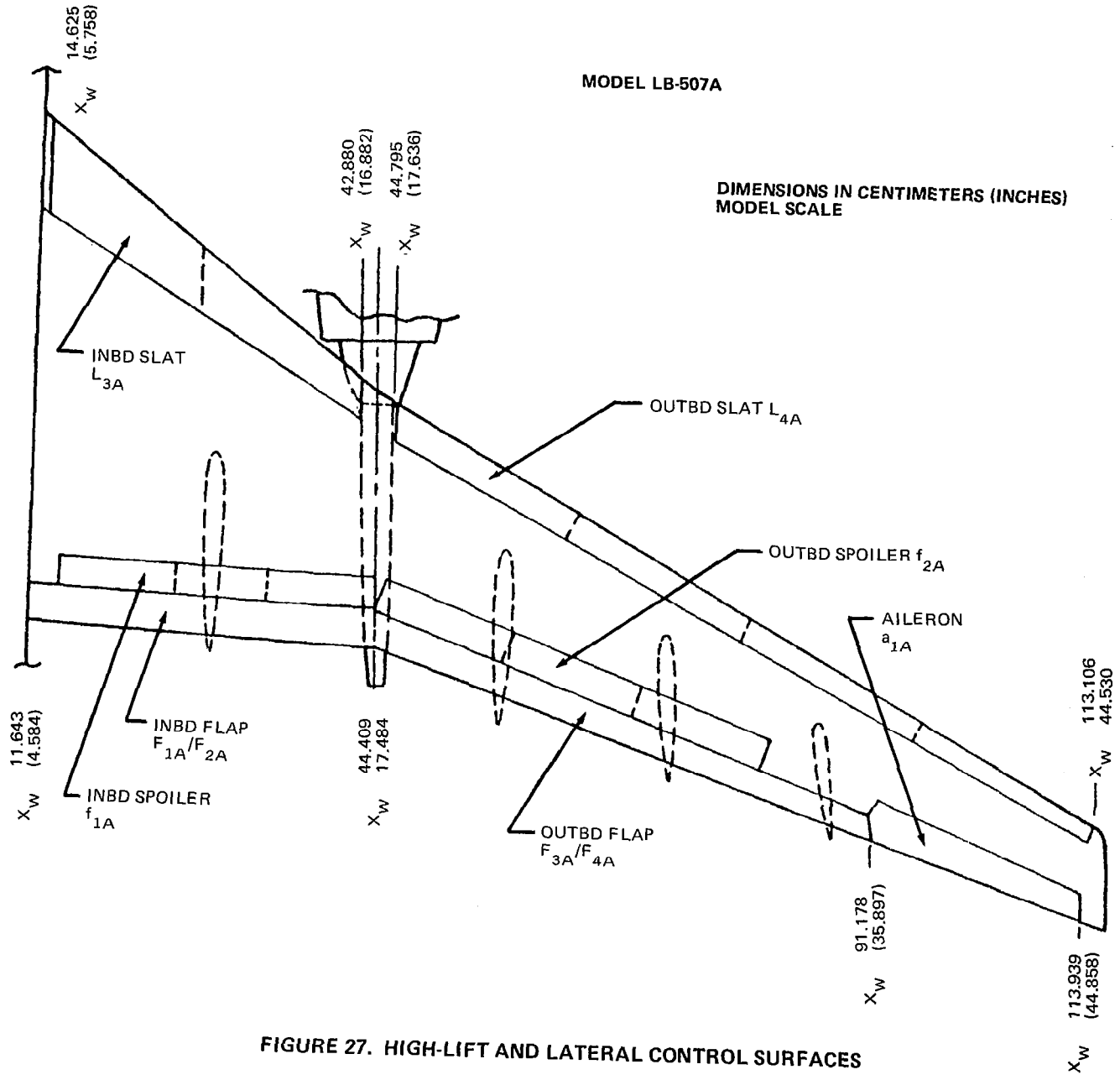
FIGURE 27. HIGH-LIFT AND LATERAL CONTROL SURFACES

The model utilized the X_{1B} fillet which was developed for the high-speed Model LB-506A. The glass fiber fillet was modified on the lower surface to provide access holes for the Douglas tandem support system.

The model was equipped with one set of inboard and one set of outboard leading-edge slats. The slats were attached by rigged brackets to a WUSS leading edge which was interchangeable with the cruise leading edge. Brackets were available to rig the inboard slats at three different positions. At one of these three positions, a set of shims could be installed between the slat brackets and the wing to provide a fourth slat grid position. The definitions of slat gap and overhang are shown in Figure 28 (which is Figure 7 repeated for convenience), the various slat
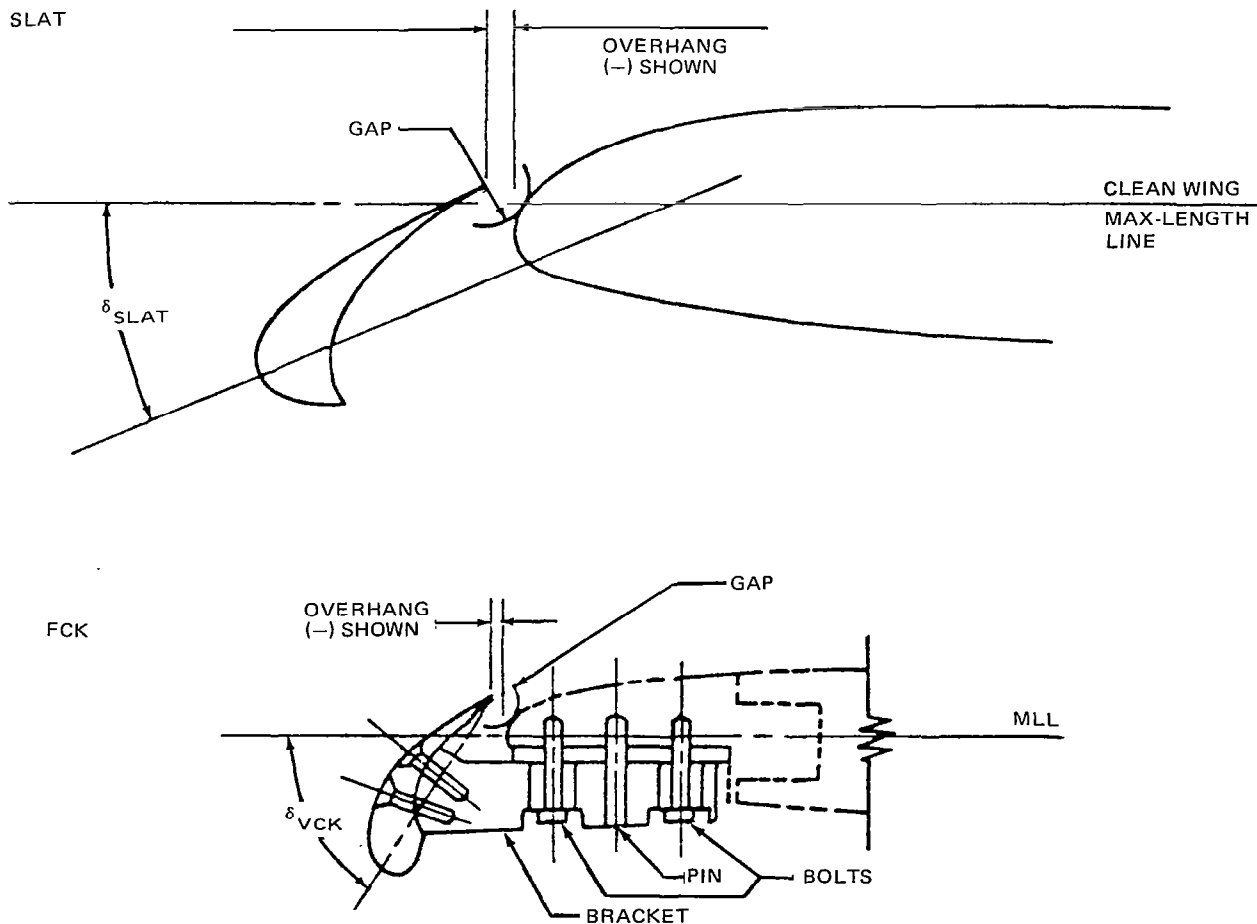
FIGURE 28. LEADING EDGE DEVICE GAP, OVERHANG, AND DEFLECTION DEFINITIONS

deflections and grid positions are provided in Appendix F. The slats also contained pressure instrumentation at four spanwise locations. The inboard leading-edge slat could be replaced with a short-chord fixed-camber Krueger. This FCK could be positioned at two deflection angles with two grid positons at each angle. The FCK did not contain pressure instrumentation.

The trailing-edge high-lift system consisted of 80-percent span two-segment flaps. The flaps were continuous, with no inboard aileron or exhaust gate. They were installed in the desired positions using fixed brackets which attached the main flap to the wing and the auxiliary flap to the main flap. Each forward flap segment could be installed at four deflection angles, and each aft flap segment could be installed at two deflection angles. The bracket attachments were such that the aft flap angles were independent of the forward flap angles, allowing either aft deflection and grid position to be used with all four main flap settings. The exact flap deflections and grid positions are given in Appendix F. The cruise configuration model utilized the same flap linkage fairings as the cruise wing of the high-speed LB-506A. For the flap-deflected case, a new set of fairings was used. The new fairing were set in one position relative to the main flap, and represented the fairing position for maximum fairing deflection. The definitions of the flap gap and overhang are presented in Figure 29.
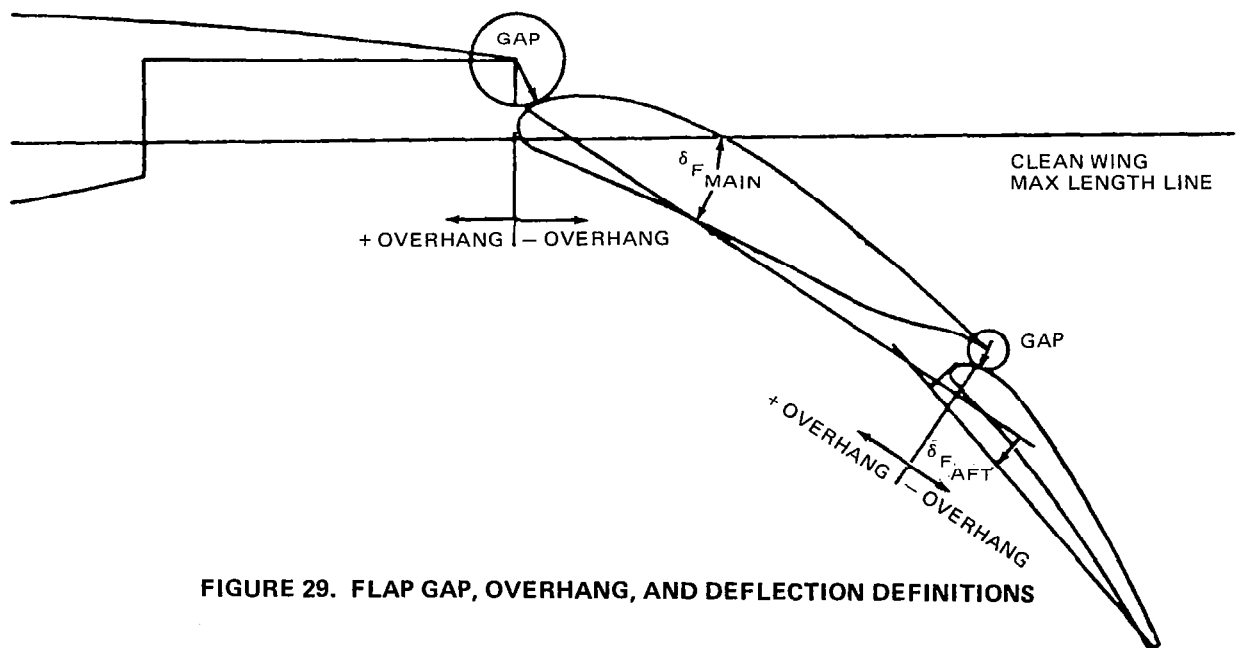
FIGURE 29. FLAP GAP, OVERHANG, AND DEFLECTION DEFINITIONS

The outboard ailerons on this model, attached with fixed brackets, could be manually positioned at several deflection angles. The model was equipped with inboard and outboard spoilers, as shown on the control surface diagram of Figure 27. On the model, a one-piece bent-plate-type spoiler was used to represent the airplane's three inboard panels, and a one piece bent-plate-type spoiler was used to represent the outboard three panels.

A set of landing gear, which included two wing-mounted gear and one nose gear, could be installed on the model for use in the landing or takeoff configuration. The airplane gear wells and gear doors were simulated on the model, and gear well fillers were provided for the gear-up case.

The horizontal and vertical stabilizers from the high-speed LB-506A model were used on this model. The horizontal stabilizer was adapted to a remote-drive and position-indication system, and was modified slightly to match the new aft fuselage lines. The vertical fin was installed on this model such that the exposed area was the same as on model LB-506A. This placed the top of the vertical stabilizer at a different height due to the change in aft fuselage lines. The dorsal fin was also used; however, the contour of the dorsal was changed as shown in Figure 30. Horizontal and vertical stabilizer diagrams are presented in Figures 31 and 32, respectively.

Two wing-mounted nacelles and pylons were used on this model. These parts were the nacelle/pylon combination previously tested on model LB-506A. The flow-through nacelle represented that of the Pratt & Whitney Aircraft JT10D engine. The flap-linkage fairing incorporated into the pylon was modified to allow the fairing to deflect with the flap.

LB-507A INSTRUMENTATION

The instrumentation associated with this model included a six-component internal balance, wing static pressure orifices, a remotely driven horizontal stabilizer, and an internal fuselage pitch system. The internal pitch system and remotely driven horizontal stabilizer required the standard Douglas power supplies, control console, and position readout systems. The control console also included Douglas bubble-pack monitoring equipment.

MODEL LB-507A

D_{2A} DORSAL L.E.

VERT STAB.
(V_{1D})

OLD DORSAL (TYP)

FUS (B_{3B})
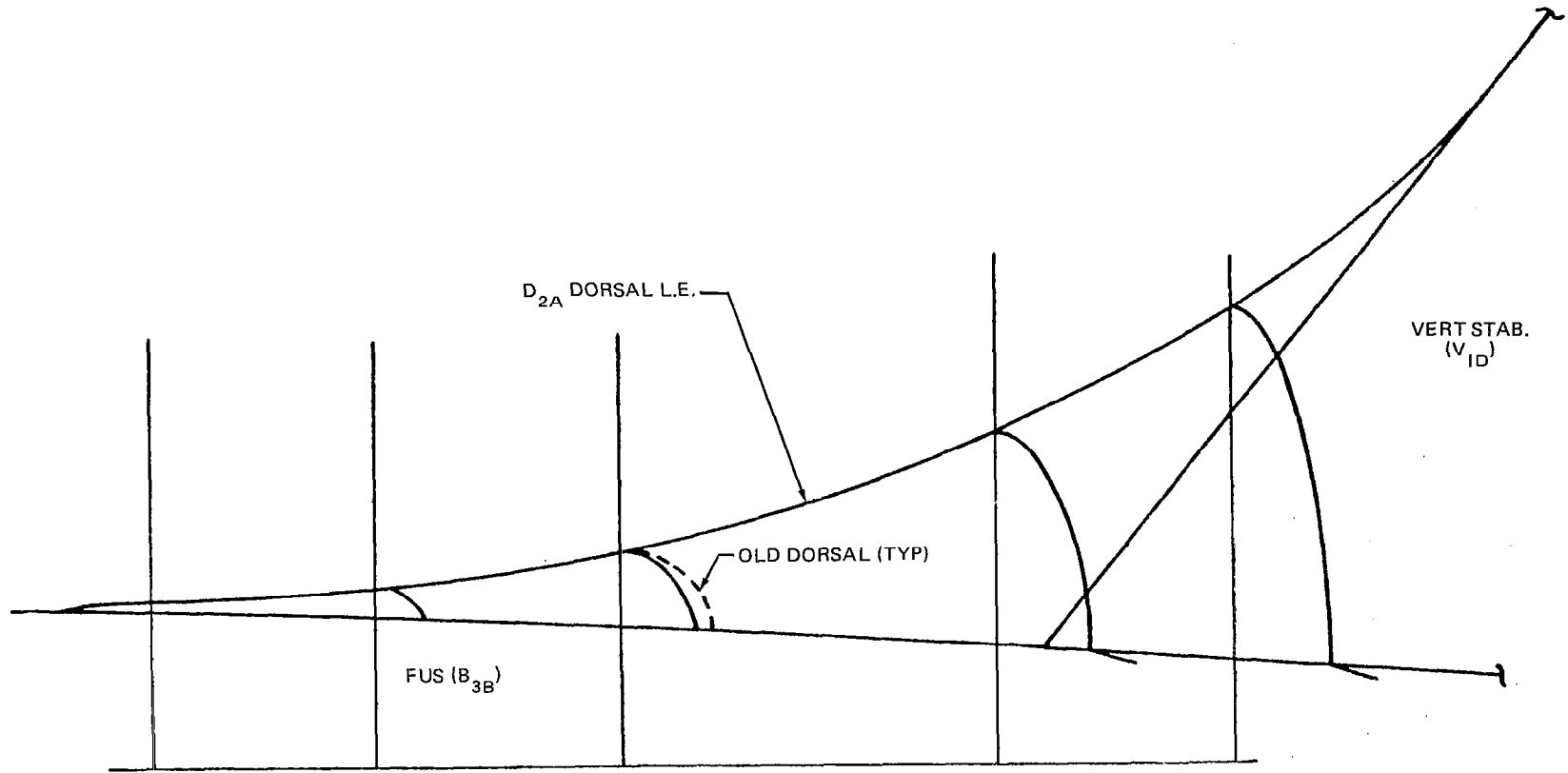
FIGURE 30. DORSAL FIN (D_{2A})

MODEL LB-507A

S_H = 0.114 m² (1.2312 FT²)

AR = 4.10

λ = 0.350

SWEEP $C_{\underline{H}}$ = 30°
          4

Γ_H = 10.0°

0.0

14.371
(5.658)

30°

+X_H

HORIZ STAB.
ORIGIN.

Y = 229.022
    (90.166)

24.745
(9.742)

34.239
(13.480)

8.661
(3.410)

$MAC_{H/4}$
Y_H = 14.484
         (5.7024)

MAC_H = 17.993 (7.084)

PIVOT AXIS 65.42% C_R
Y = 245.209 (96.539)
Z = 6.759 (2.661)

+Y_H

THEORETICAL
TRAILING EDGE

MODEL ACTUAL TRAILING EDGE
(CUT BACK TO ACHIEVE 0.0254 cm
(0.01 INCH) THICK TRAILING EDGE)

DIMENSIONS IN CENTIMETERS (INCHES)
MODEL SCALE
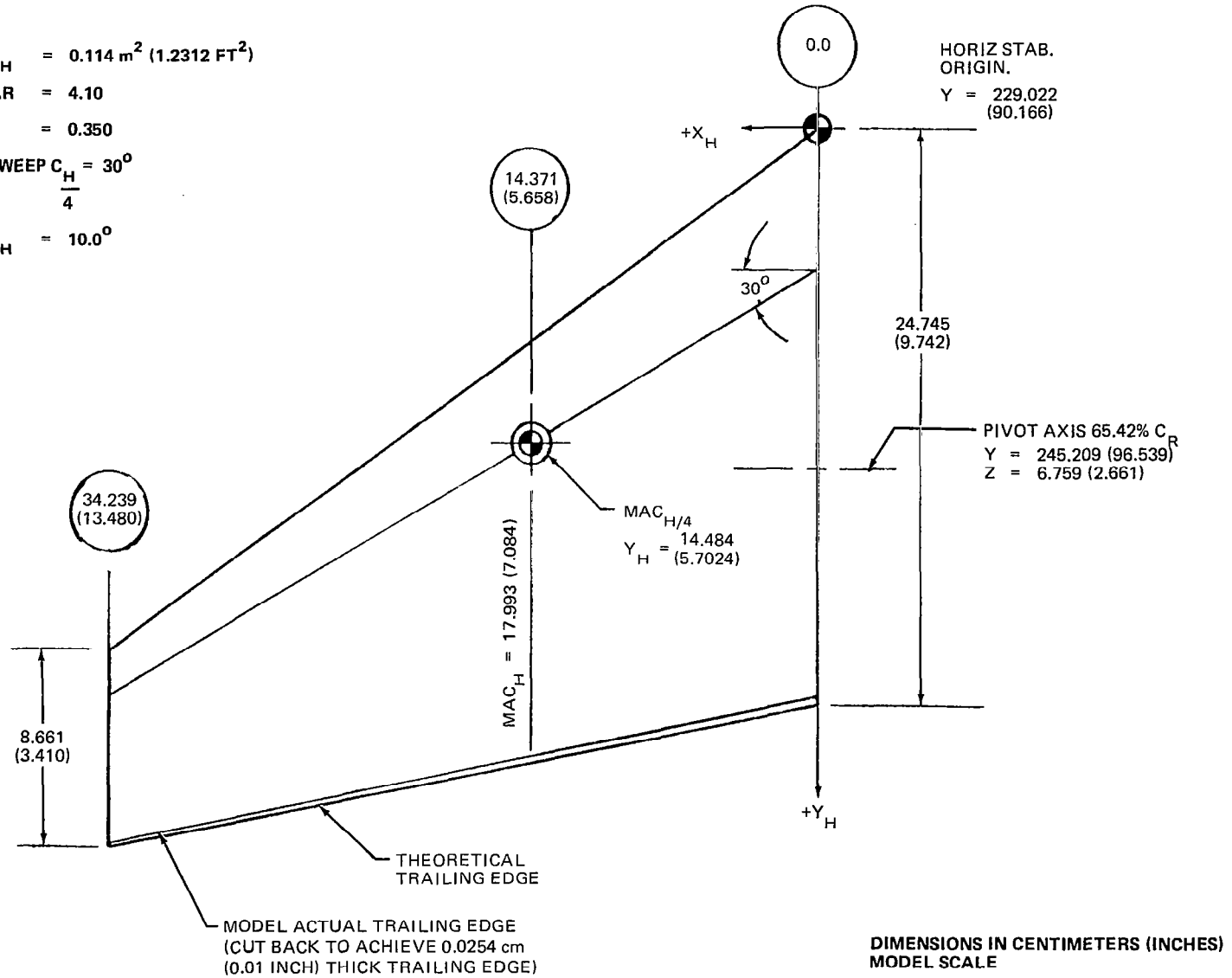
FIGURE 31. HORIZONTAL STABILIZER (H_{1D})

63

MODEL LB-507A

12.057
(4.7469)
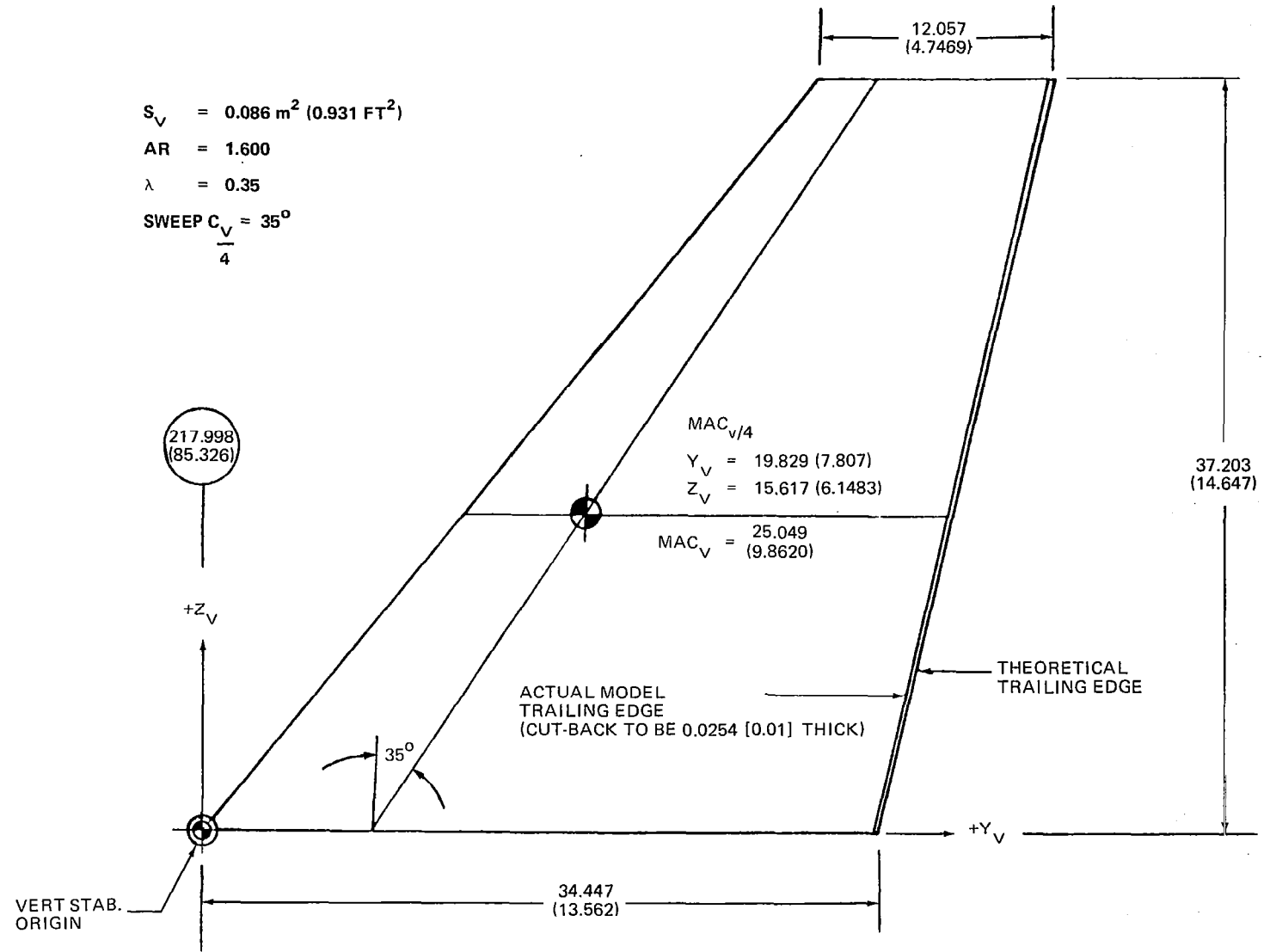
S_V = 0.086 m^2 (0.931 FT^2)

AR = 1.600

λ = 0.35

SWEEP $C_{\underline{V}}$ = 35°

$\dfrac{}{4}$

217.998
(85.326)

$MAC_{v/4}$

Y_V = 19.829 (7.807)

Z_V = 15.617 (6.1483)

MAC_V = $\dfrac{25.049}{(9.8620)}$

37.203
(14.647)

+Z_V

THEORETICAL
TRAILING EDGE

ACTUAL MODEL
TRAILING EDGE
(CUT-BACK TO BE 0.0254 [0.01] THICK)

35°

+Y$_V$

VERT STAB.
ORIGIN

34.447
(13.562)

DIMENSIONS IN CENTIMETERS (INCHES)
MODEL SCALE UNLESS OTHERWISE SPECIFIED

FIGURE 32. VERTICAL STABILIZER (V$_{1D}$)

Aerodynamic forces on the model were measured using the Ames Task Mark IIC, 10.16-cm (4-in.) diameter internal balance. The upper aft balance pin hole was used for this installation.

Pressures over the model wing, aileron, and deflected high-lift system were measured by 12 48-S-type scanivalves arranged in two 6-pac modules mounted in the fuselage nose. Access to the scanivalves was obtained by removing the nose and forward constant sections of the fuselage. In addition to the four complete rows of pressure orifices, one pressure tap was located at the trailing edge of an inboard station (18-percent semispan) to help evaluate any separation that may have occurred (Figure 33).

The angle of attack of the fuselage reference plane was measured using a bubble pack installed in the fuselage nose. From α_{FRP} = -6° to 0°, the model was pitched using the external pitch system. From 0° to +10° angle of attack, the fuselage was pitched using the fuselage internal pitch drive while maintaining the balance at 0°. For angles of attack +10° to +34°, the fuselage was pitched using the external pitch drive with a 10° angle maintained between the balance axis and the fuselage axis.

The horizontal stabilizer incorporated remote drive and a position-indication system. A Douglas control panel and digital readout was provided for use in the tunnel control room.

LB-507A MODEL INSTALLATION

The model was mounted in the Ames 12-Foot Pressure Tunnel using the Douglas tandem support system and the Ames Task Mark II 10.16-cm (4-in.) balance. The balance was attached to the support struts using the Douglas balance pitch block. The installation is depicted in Figure 34.

MODEL LB-507A

% b/2	WING PANEL	NOTES
18	LEFT	T.E. PRESS. ONLY
35	LEFT	
57	LEFT	
72.5	RIGHT	
95	RIGHT	
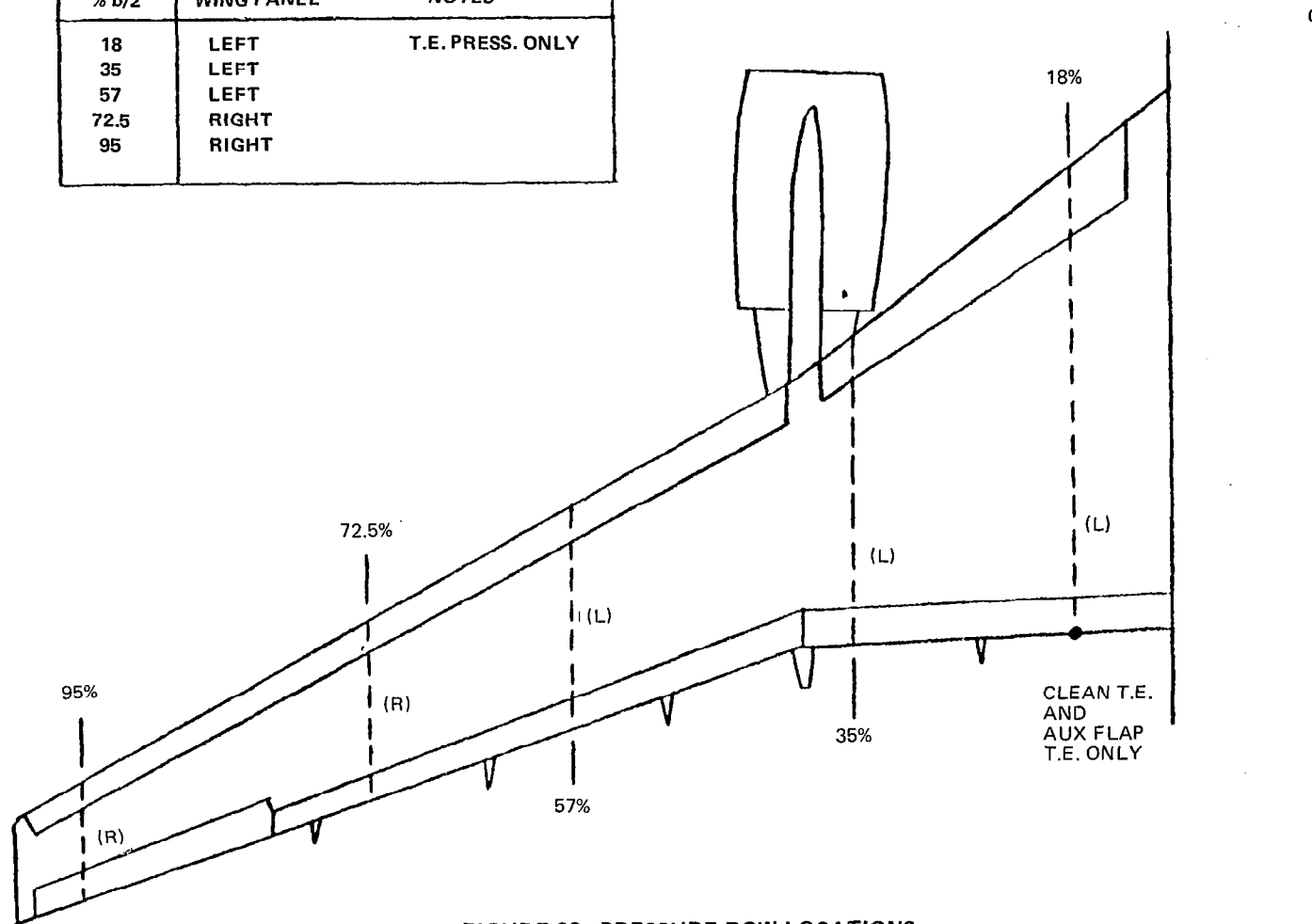
FIGURE 33. PRESSURE ROW LOCATIONS
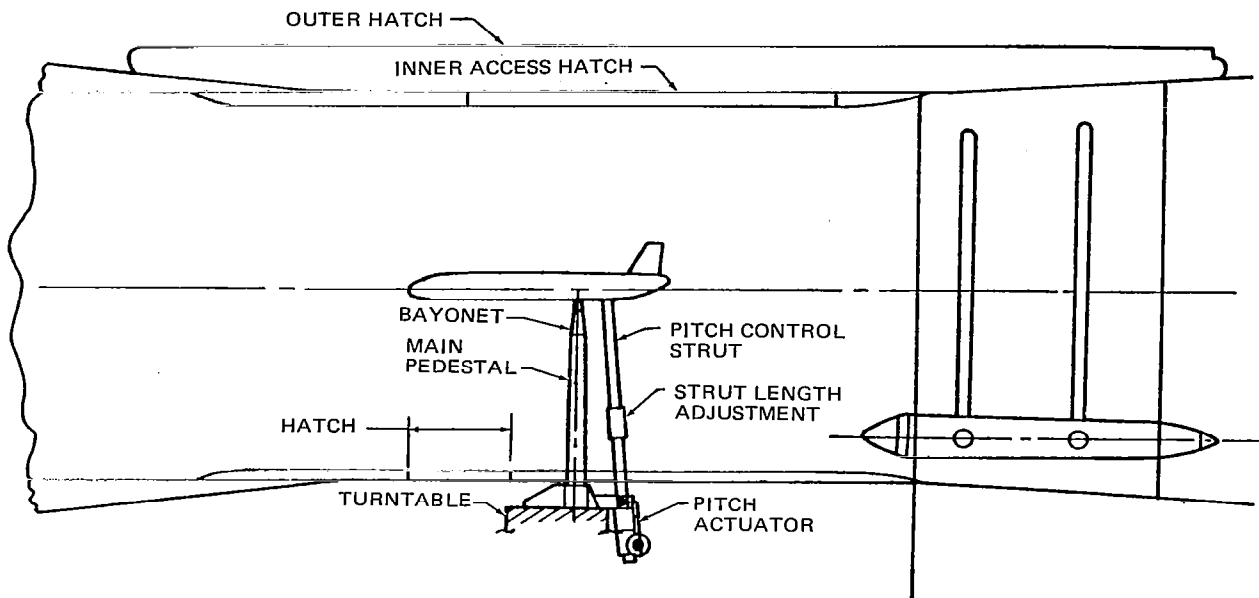
FIGURE 34. INSTALLATION IN NASA AMES 12-FOOT PRESSURE TUNNEL

LB-507A RESULTS AND DISCUSSIONS

Cruise Wing Characteristics

The initial configuration tested was the cruise wing body with the nacelles, pylons, and strakes attached. The basic high-Reynolds-number characteristics (lift, pitching moment, and drag) for the configuration are shown in Figure 35. Two different runs of the same configuration are shown to indicate the repeatability of the data. This figure indicates that a tail-off $C_{L_{MAX}}$ of 1.59 was obtained at the basic test condition of M = 0.20 and RN_{MAC} = 4.61 million. This compared with a maximum value of 1.54 obtained from Phase I testing of the LB-486 model. A direct comparison of the data from the two tests is shown in Figure 36. Besides a higher $C_{L_{MAX}}$, the LB-507A model exhibited better tail-on pitching moments than did the LB-486 model. Though improved, the pitching moments of the LB-507A model still included pitch-up prior to stall. Post-stall pitch-down was abrupt and forceful.

MODEL LB-507A
CONFIGURATION $B_{3B} W_{1B} X_{1B} P_{1C} N_{1C} S_{11F}$
MACH = 0.20
$RN_{MAC} = 4.61 \times 10^6$

SYM	RUN
○	3
□	4
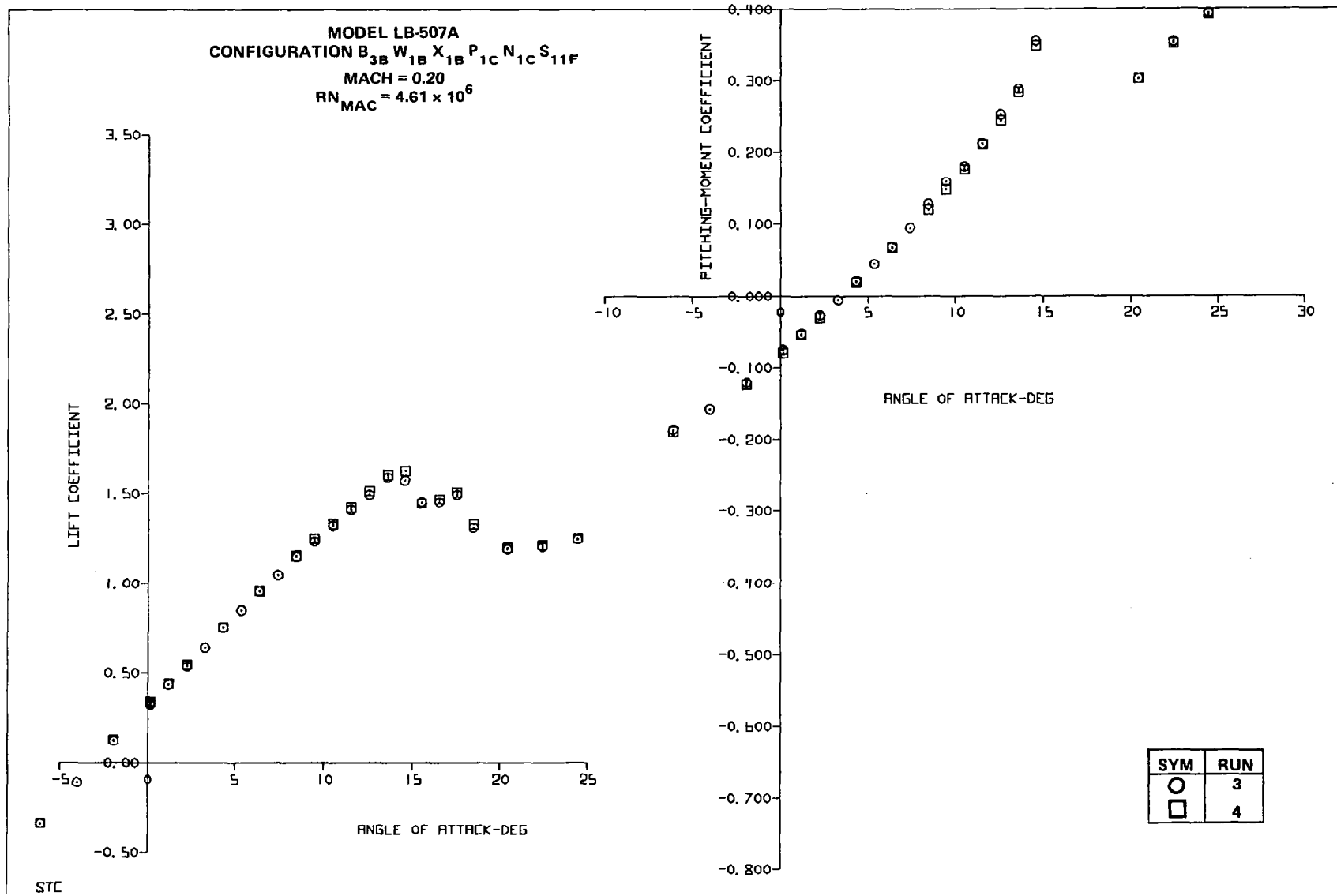
A. LIFT AND PITCHING MOMENT

FIGURE 35. CRUISE WING CHARACTERISTICS AND REPEATABILITY
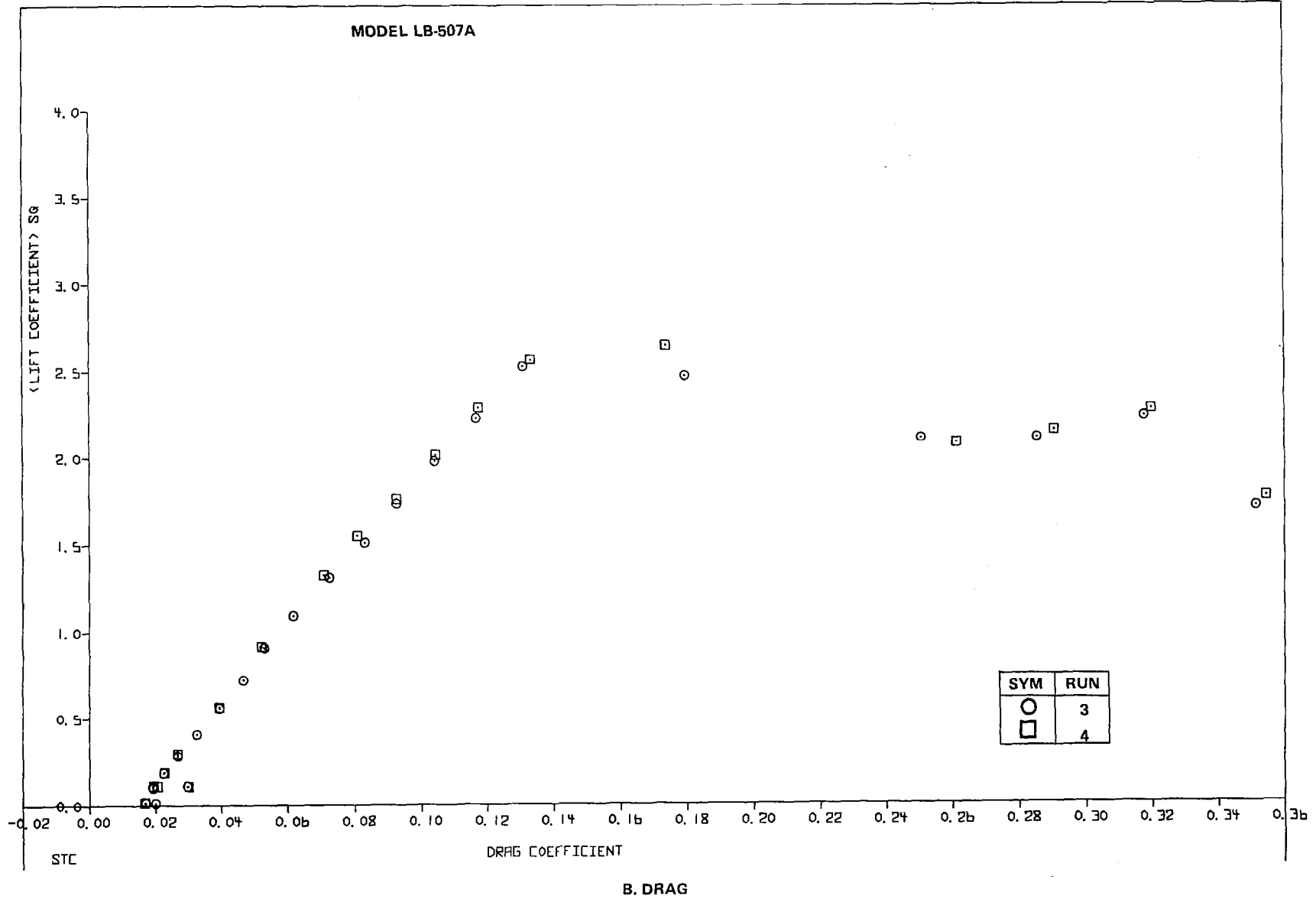
MODEL LB-507A

B. DRAG

FIGURE 35. CRUISE WING CHARACTERISTICS AND REPEATABILITY

MODEL LB-507 A
AND
MODEL LB-486 A
MACH = 0.20
$RN_{MAC} = 4.61 \times 10^6$
NACELLES, PYLONS, STRAKES ON
GEAR OFF

SYM	RUN	TEST	i_H
◯	3	LB-507A	OFF
☐	115	LB-507A	0^0
◇	23	LB-486A	OFF
▽	34	LB-486A	0^0
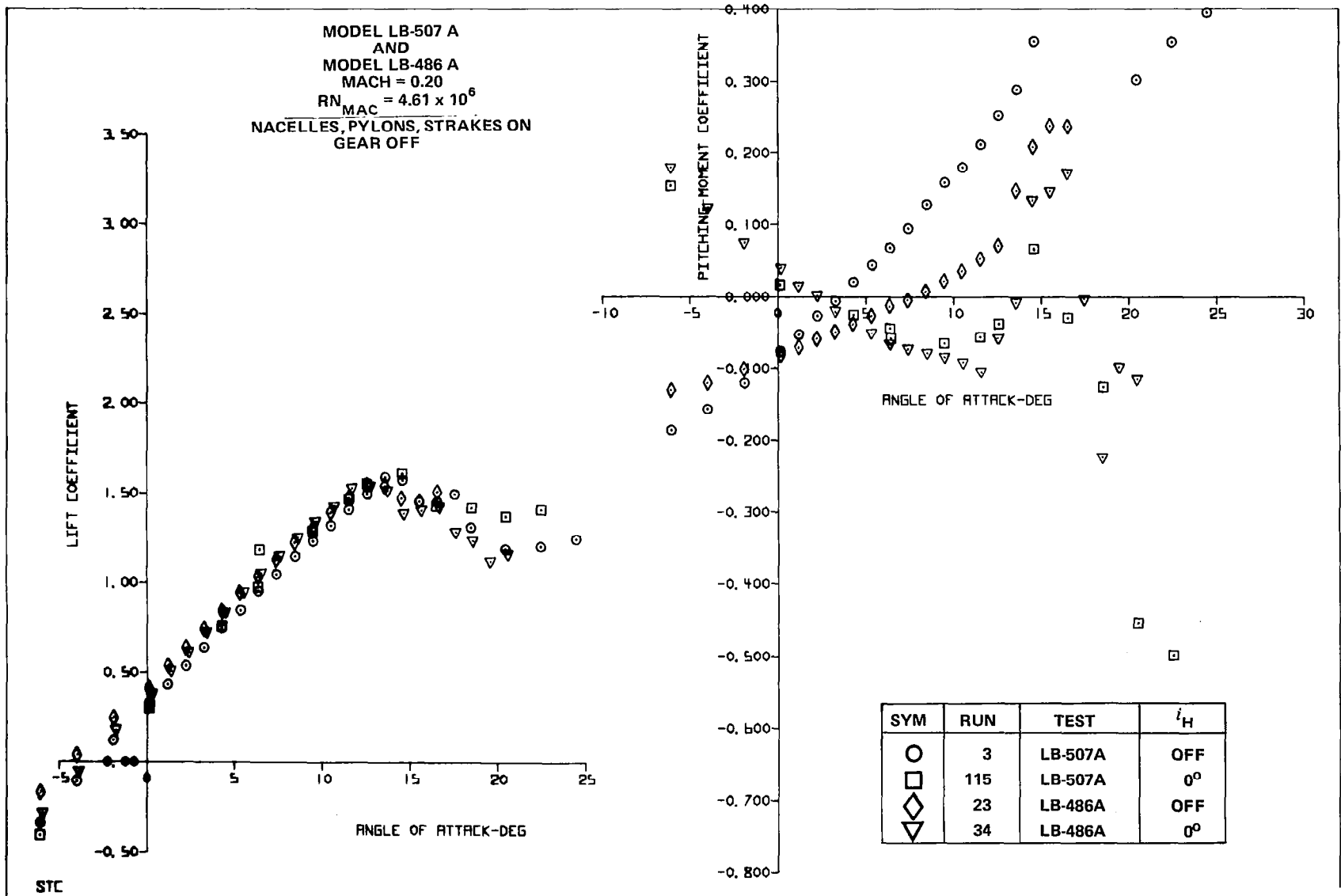
A. LIFT AND PITCHING MOMENT

FIGURE 36. COMPARISON OF LB-507A AND LB-486B CRUISE WING CHARACTERISTICS
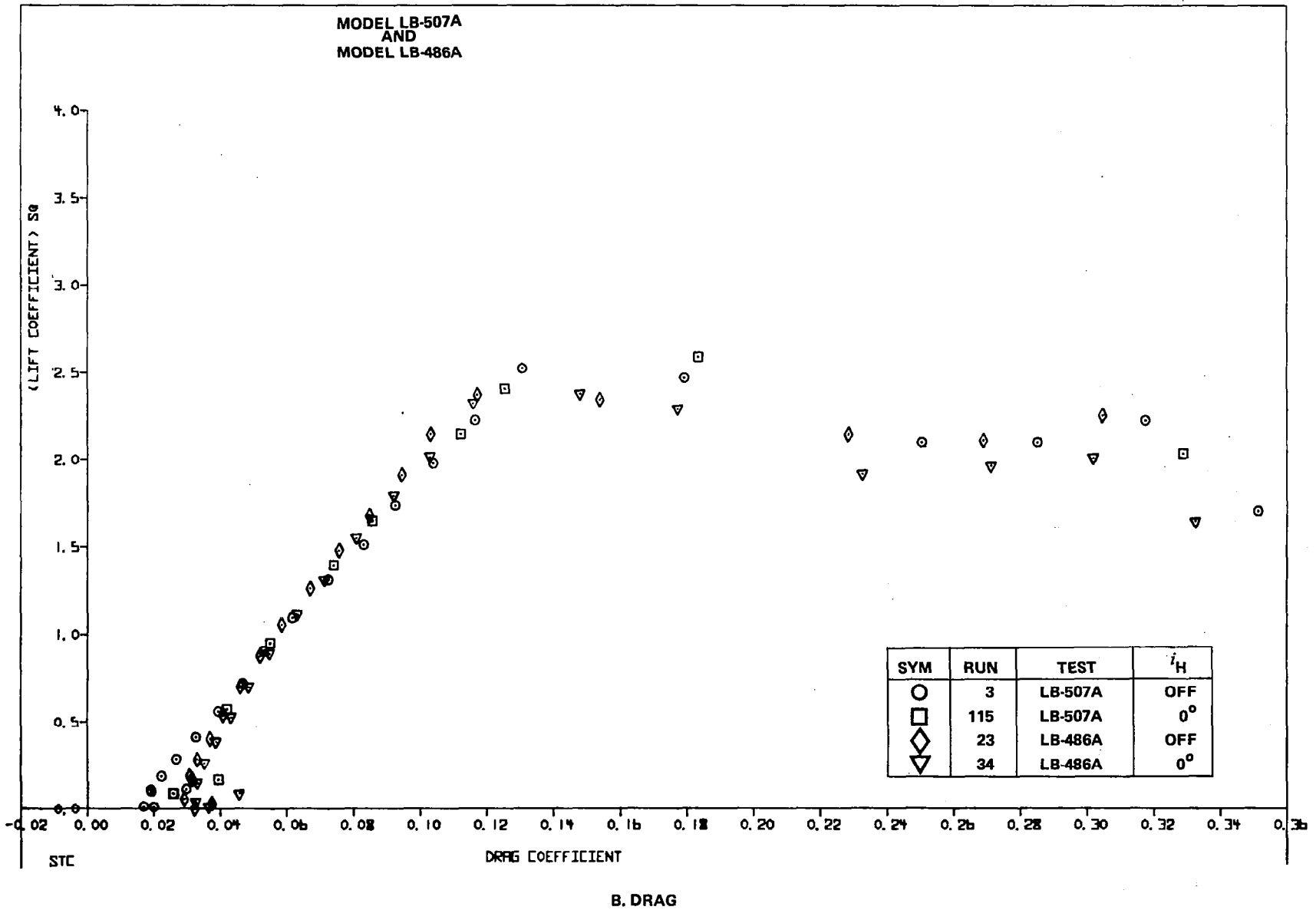
FIGURE 36. COMPARISON OF LB-507A AND LB-486A CRUISE WING CHARACTERISTICS

Mini-tuft pictures of the wing, for a Mach number of 0.20, are presented in Figure 37 for angles of attack before and after $C_{L_{MAX}}$. This figure illustrates the stall phenomena of this high-aspect-ratio wing at RN_{MAC} = 4.61 million. As was the case with the LB-486 model, the outboard wing panel stalled prior to the inboard panel. The inboard panel stalled completely (separated to the leading edge) at an angle approximately 6^0 higher than the outboard stall angle. Figure 38 presents the chordwise pressure distributions of the four streamwise pressure rows for $\alpha C_{L_{MAX}}$ (13.61^0), and 1^0 and 3^0 past $\alpha C_{L_{MAX}}$. At $\alpha C_{L_{MAX}}$, suction peaks are evident for all spanwise locations. Slightly negative trailing-edge pressure coefficients are noted for this condition at all spanwise stations. Large spanwise flow angles are indicated in the corresponding tuft photo for the trailing-edge region. At α_{FRP} = 14.59^0 (1^0 past stall), the 72.5-percent semispan station plot indicates separation near the leading edge. At α_{FRP} = 16.54^0 (2^0 past stall), the 57-, 72.5-, and 95-percent semispan stations are separated at the leading edge. On the other hand, the inboard station was still heavily loaded.

Reynolds number and Mach number effects.- The cruise wing configuration was also tested at Mach = 0.20 at various reference chord Reynolds numbers, ranging from 1.14 million (atmospheric conditions for the Ames facility) to 4.61 million. Test results are presented in Figure 39. Comparing the results of the lowest Reynolds number run to the highest Reynolds number data shows that $C_{L_{MAX}}$ was reduced from 1.59 to 1.31, $\alpha C_{L_{MAX}}$ was reduced from 14.5^0 to 13.6^0, and the magnitude of the post-stall lift loss is decreased. A positive C_M shift was apparent for angles of attack prior to stall, but the configuration still exhibited the same pitch variations for the angles just after $C_{L_{MAX}}$. The maximum value of L/D was reduced from 20.02 to 15.62 by the decrease in Reynolds number. Figure 39 suggests that $C_{L_{MAX}}$ will not increase significantly, due to Reynolds number effects, as the Reynolds number is increased from the highest wind tunnel value to flight conditions.
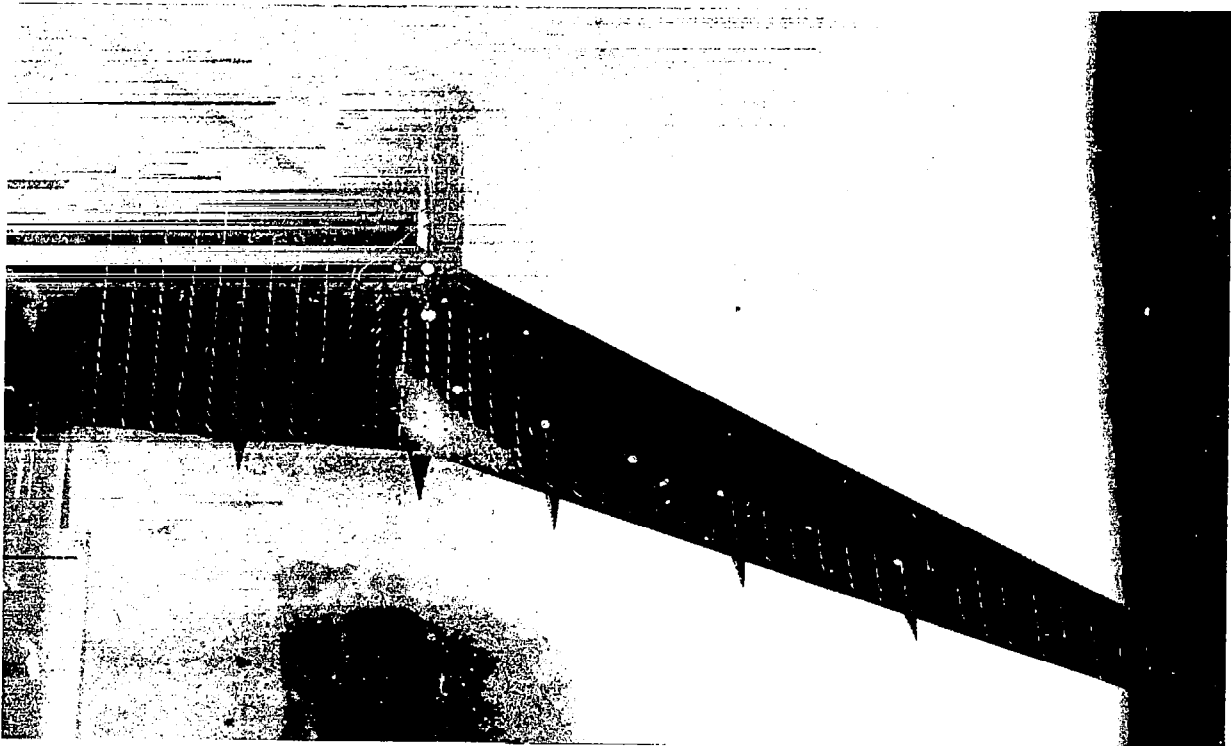
A. $\alpha_{FRP} = 12.58^{O}$
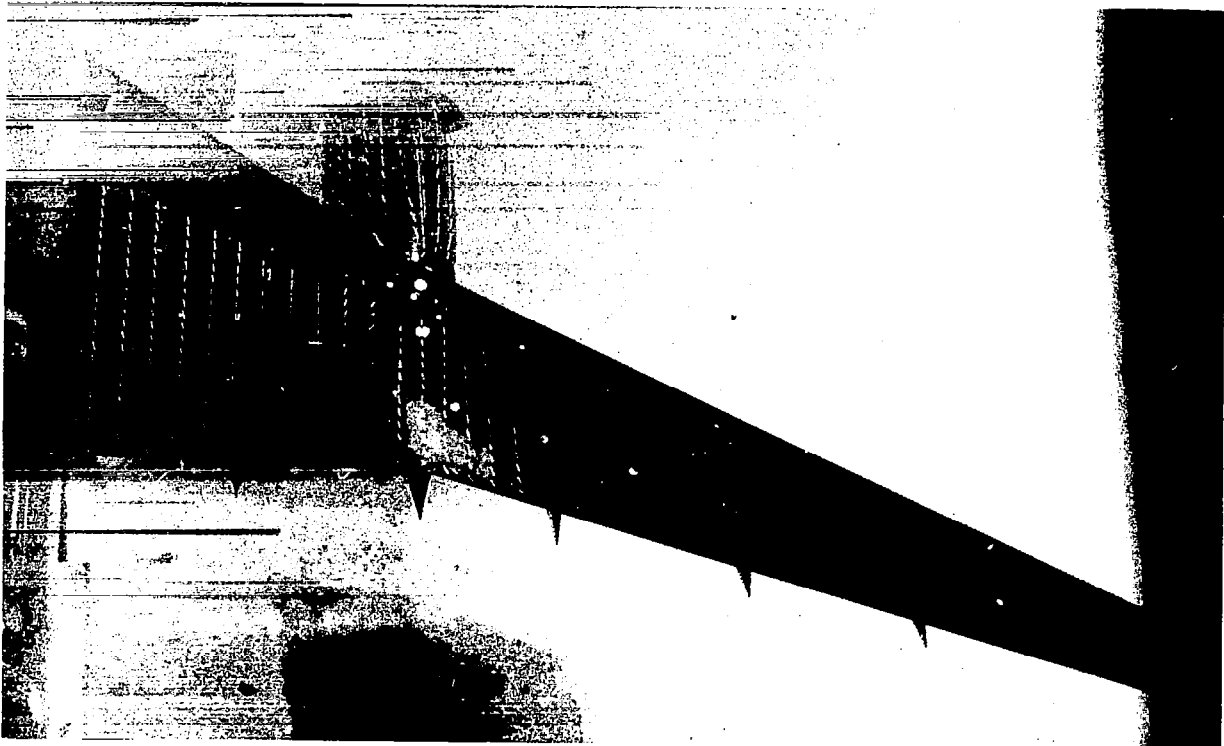
B. $\alpha_{FRP} = 13.61^{O}$ ($\alpha_{C_{L_{MAX}}}$)

FIGURE 37. MINI-TUFT PHOTOS FOR CRUISE WING/BODY WITH NACELLES (RUN 3) (CONTINUED)
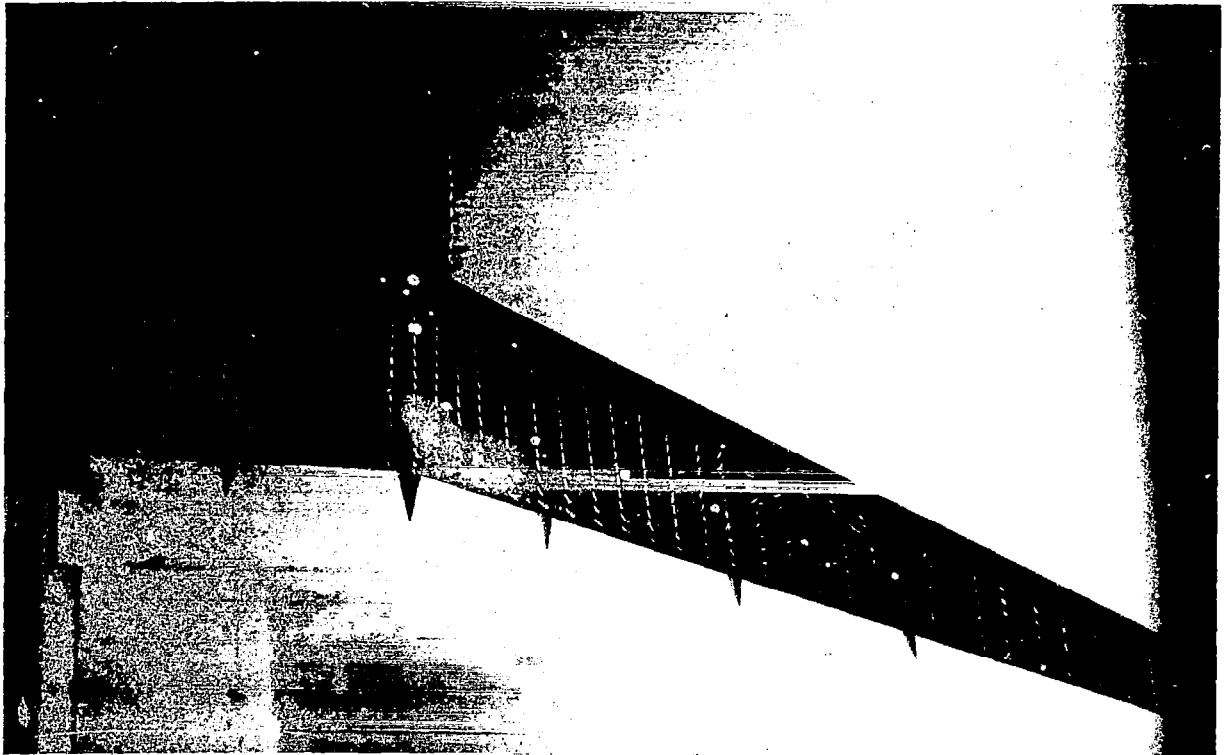
C. $\alpha_{FRP} = 14.59°$

D. $\alpha_{FRP} = 16.54°$

FIGURE 37. MINI-TUFT PHOTOS FOR CRUISE WING/BODY WITH NACELLES (CONTINUED)

E. $\alpha_{FRP} = 18.49°$

F. $\alpha_{FRP} = 20.44°$
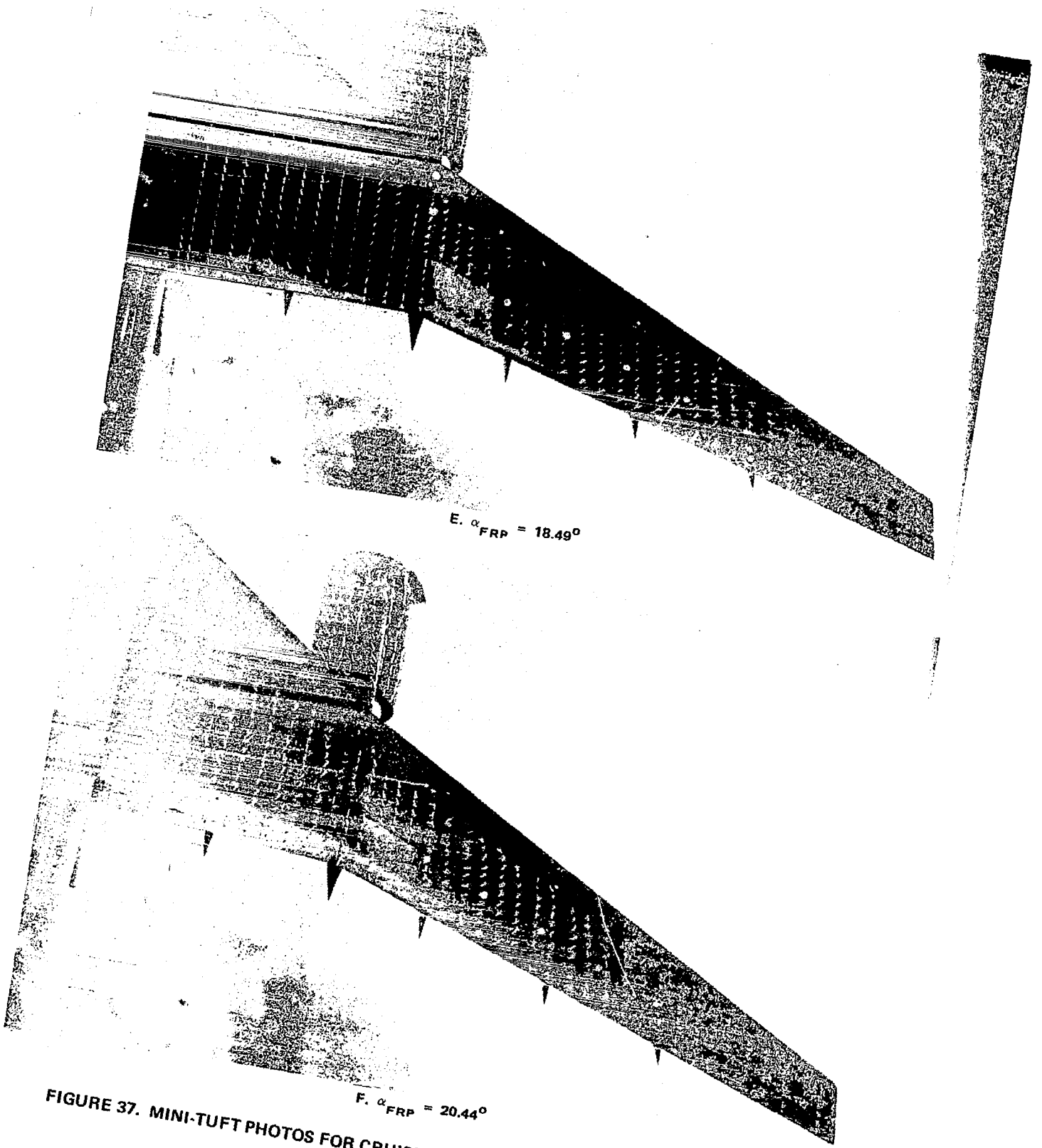
FIGURE 37. MINI-TUFT PHOTOS FOR CRUISE WING/BODY WITH NACELLES (CONCLUDED)

MODEL LB-507A
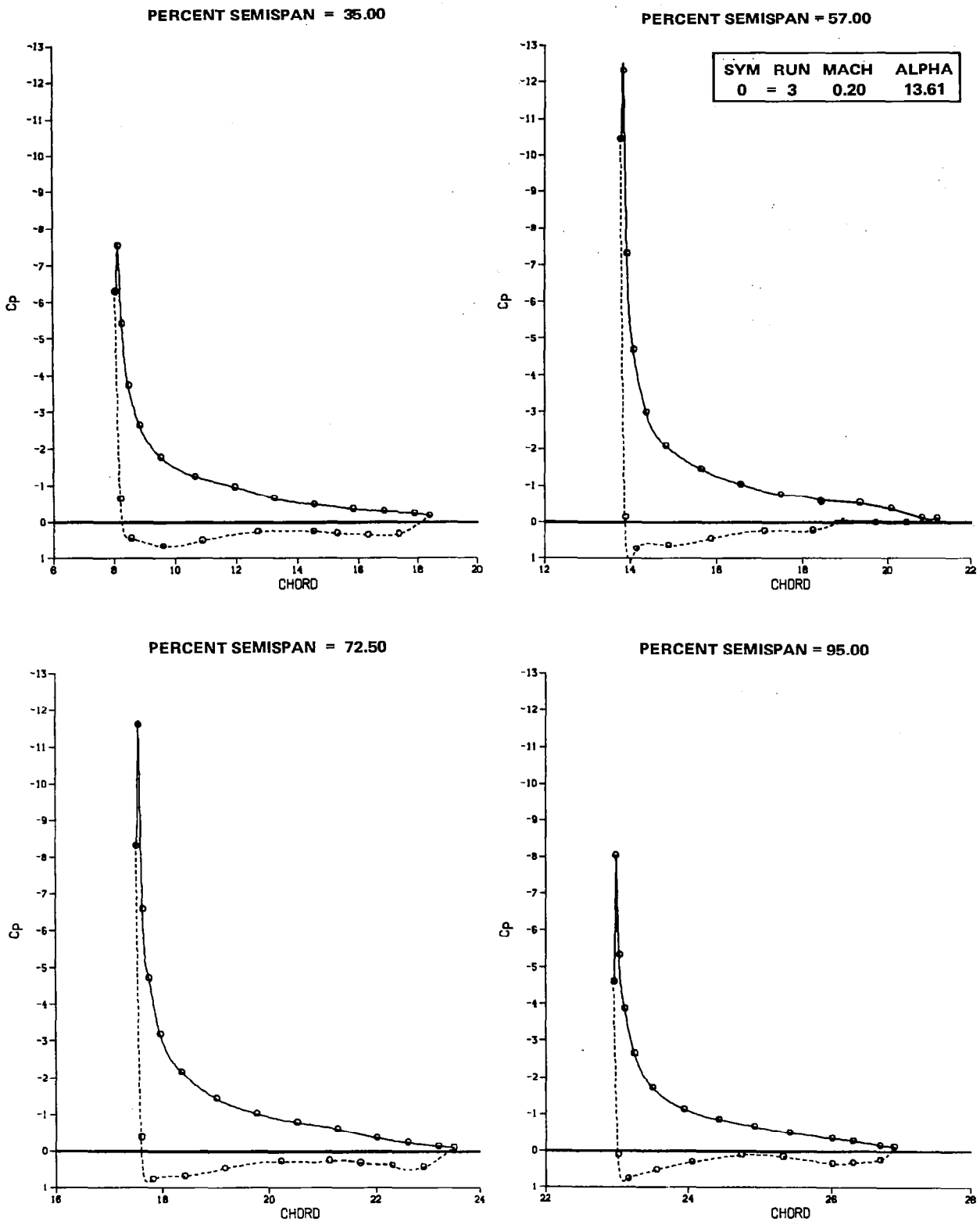
FIGURE 38. CHORDWISE PRESSURE DISTRIBUTIONS OF CRUISE WING WITH NACELLES, PYLONS, AND STRAKES ATTACHED

MODEL LB-507A
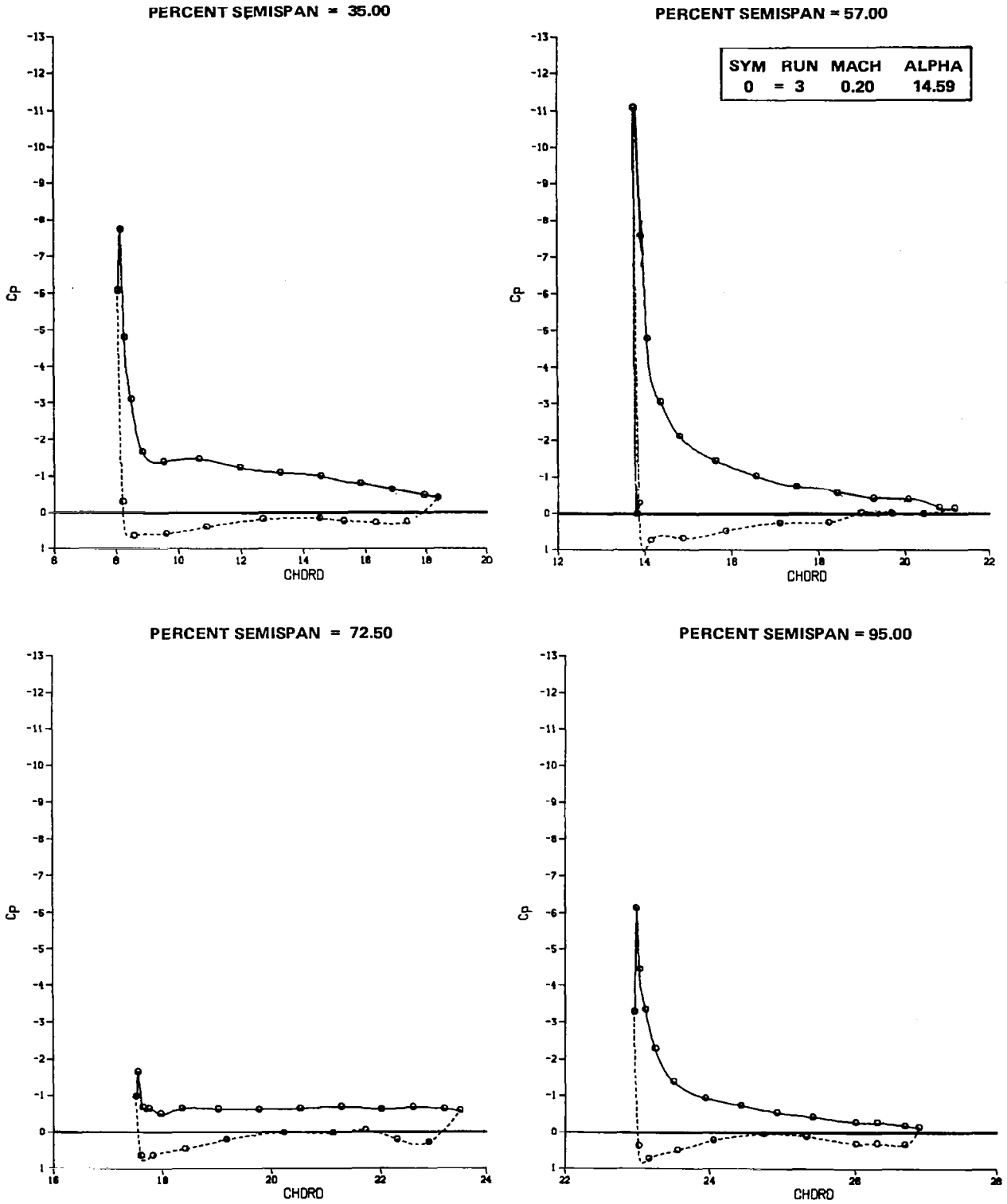
PERCENT SEMISPAN = 35.00

PERCENT SEMISPAN = 57.00

SYM	RUN	MACH	ALPHA
0	= 3	0.20	14.59

PERCENT SEMISPAN = 72.50

PERCENT SEMISPAN = 95.00

B. $\alpha_{FRP} = 14.59^o$

FIGURE 38.   CHORDWISE PRESSURE DISTRIBUTIONS OF CRUISE WING WITH NACELLES, PYLONS, AND STRAKES ATTACHED (CONTINUED)

77
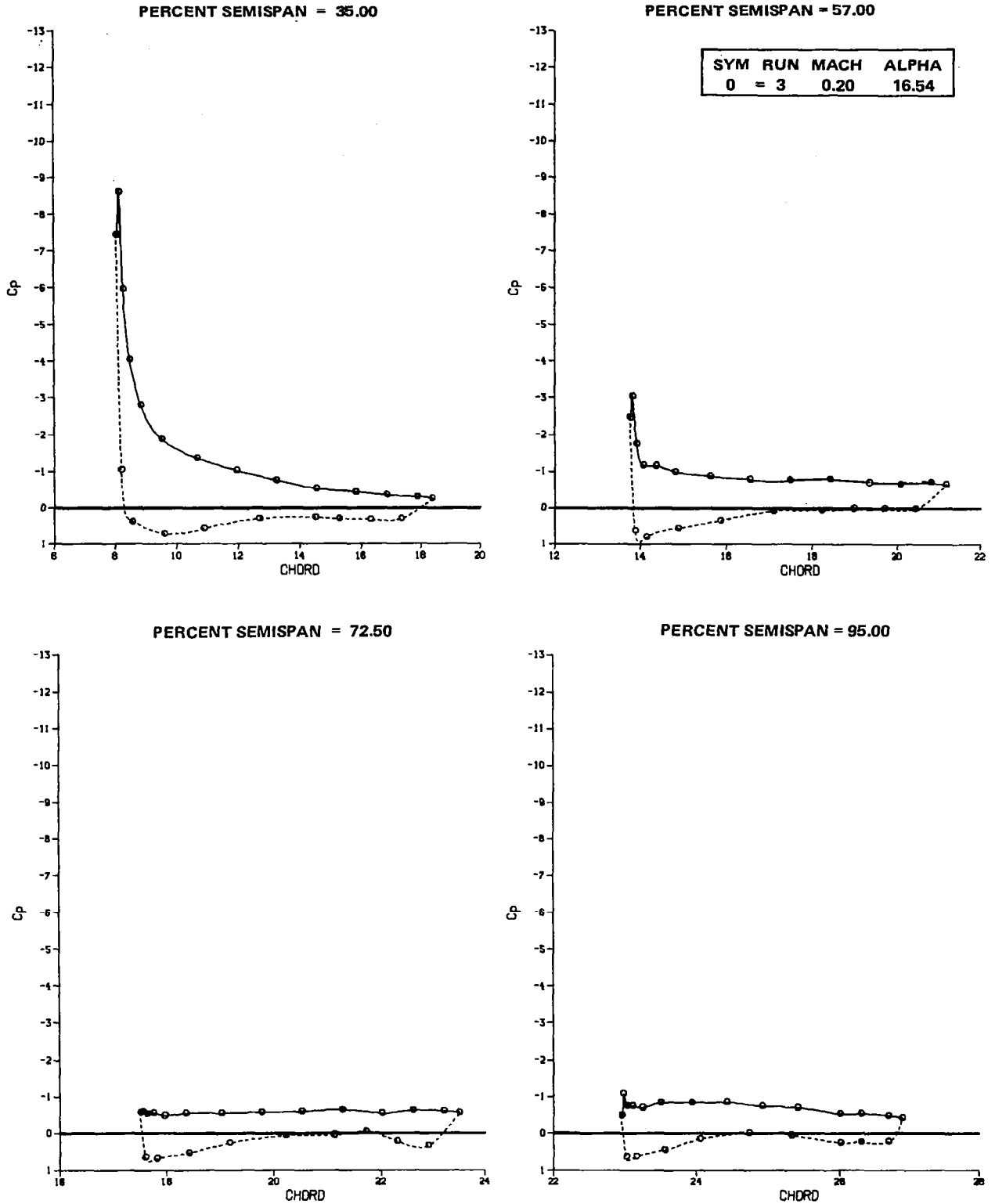
MODEL LB-507A

FIGURE 38. CHORDWISE PRESSURE DISTRIBUTIONS OF CRUISE WING WITH NACELLES, PYLONS, AND STRAKES ATTACHED (CONCLUDED)

MODEL LB-507A
CONFIGURATION $B_{3B} W_{1B} X_{1B} P_{1C} N_{1C}$
MACH = 0.20
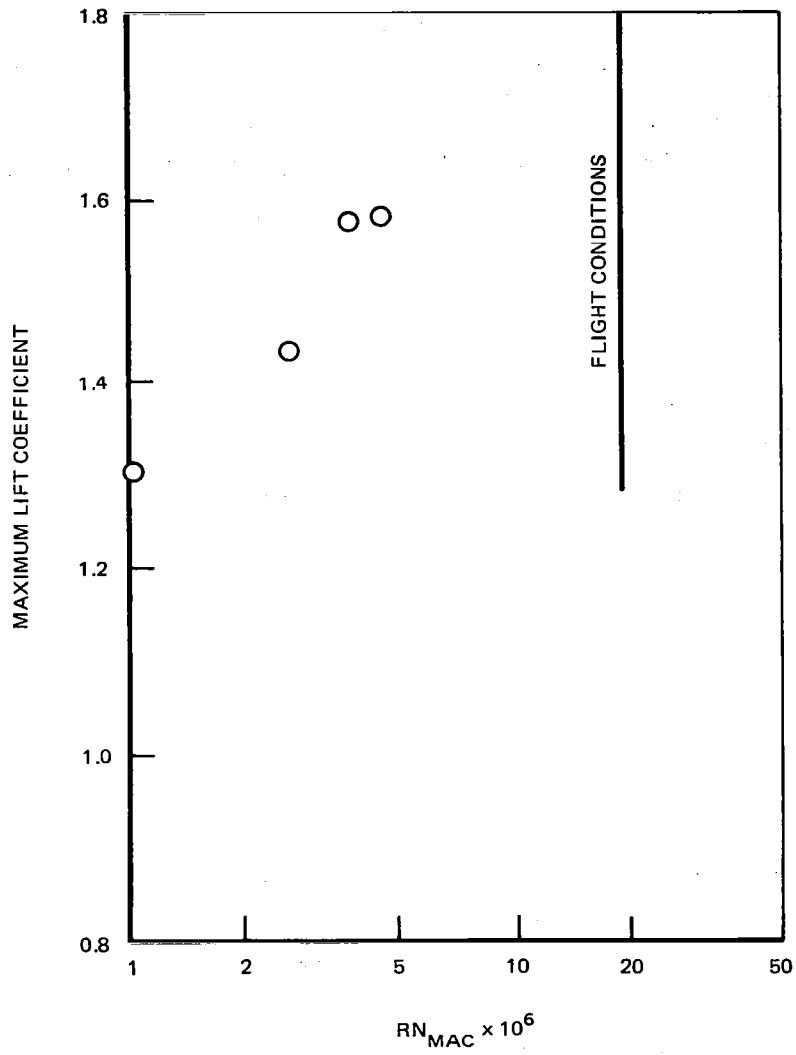
FIGURE 39.   EFFECT OF REYNOLDS NUMBER ON MAXIMUM LIFT OF CRUISE WING

Figure 40 presents the influence of Mach number on the same configuration. These data were obtained at a reference chord Reynolds number of 2.60 million. The effect of Mach number was to decrease $C_{L_{MAX}}$ ($C_{L_{MAX}}$ = 1.44, 1.40, and 1.34 at Mach = 0.20, 0.26, and 0.32, respectively). Also, increased Mach number tended to decrease the angle of attack for the outboard stall.

Nacelle/pylon/strake effects.- The effects of the nacelles, pylons, and strakes are shown in Figure 41. Removal of the nacelles and pylons resulted in a decrease in $C_{L_{MAX}}$ from 1.59 to 1.47. The pitching-moment curves show the nacelles and pylons to be destabilizing prior to stall and stabilizing after stall. The drag increment at $1.2V_s$ due to the nacelles, pylons, and strakes was 0.0171 and they reduced the L/D from 20.3 to 16.3. Mini-tuft photos for the nacelles-off and pylons-off case are shown in Figure 42. Below $C_{L_{MAX}}$, improvements in local flow, compared to the configuration with nacelles, were evident aft of the nacelle location. Outboard separation patterns were similar for the nacelles on and off cases; however, comparison of Figures 42 and 37 show that the presence of the nacelles retarded flow separation on the wing region aft of the nacelles.

Chordwise pressure distributions for the configuration with the nacelles and pylons removed are presented in Figure 43. The angles of attack selected are stall (11.55°) and higher. At the α_{FRP} of 13.55°, the 72.5-percent semispan station shows a collapse of the suction peak, while the 95-percent semispan station shows only a modest increase in $C_{P_{min}}$ and mild trailing-edge separation. At a 1° higher angle of attack, the suction peak of the 57-percent semispan station collapsed. The most outboard station remains reasonably well attached up to 16.5° angle of attack, the same angle as the nacelles on case.

From the standpoint of low-speed clean-wing characteristics, the addition of strakes to the nacelles is detrimental from both a lift and pitching-moment standpoint. This detriment is illustrated in Figure 44. Addition of the strakes reduced the tail-off clean-wing $C_{L_{MAX}}$ from 1.62 to 1.59 and increased the pre-stall nose-up moments.

MODEL LB-507A
CONFIGURATION $B_{3B} W_{1B} X_{1B} P_{1C} N_{1C} S_{11F}$
$RN_{MAC} = 2.60 \times 10^6$

LIFT COEFFICIENT

ANGLE OF ATTACK-DEG

PITCHING-MOMENT COEFFICIENT

ANGLE OF ATTACK-DEG

MACH	SYM	RUN
0.20	○	7
0.26	□	8
0.32	◇	9

STC
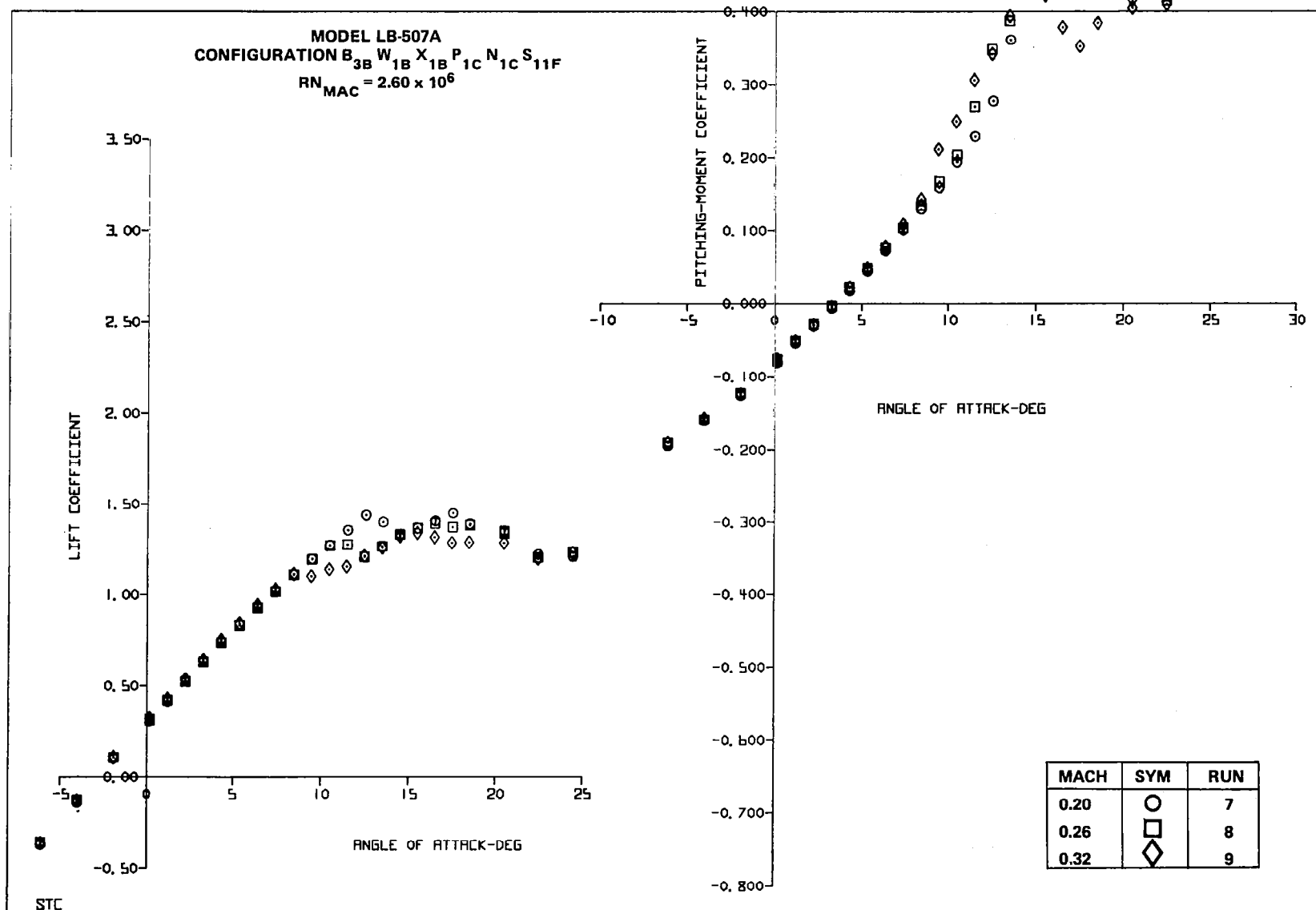
A. LIFT AND PITCHING MOMENT

FIGURE 40. EFFECT OF MACH NUMBER ON CRUISE WING

MODEL LB-507A

FIGURE 40. EFFECT OF MACH NUMBER ON CRUISE WING

MODEL LB-507A
CONFIGURATION $B_{3B} W_{1B} X_{1B}$
MACH = 0.20
$RN_{MAC} = 4.61 \times 10^6$

N&P	SYM	RUN
ON	O	3
OFF	□	113

STC
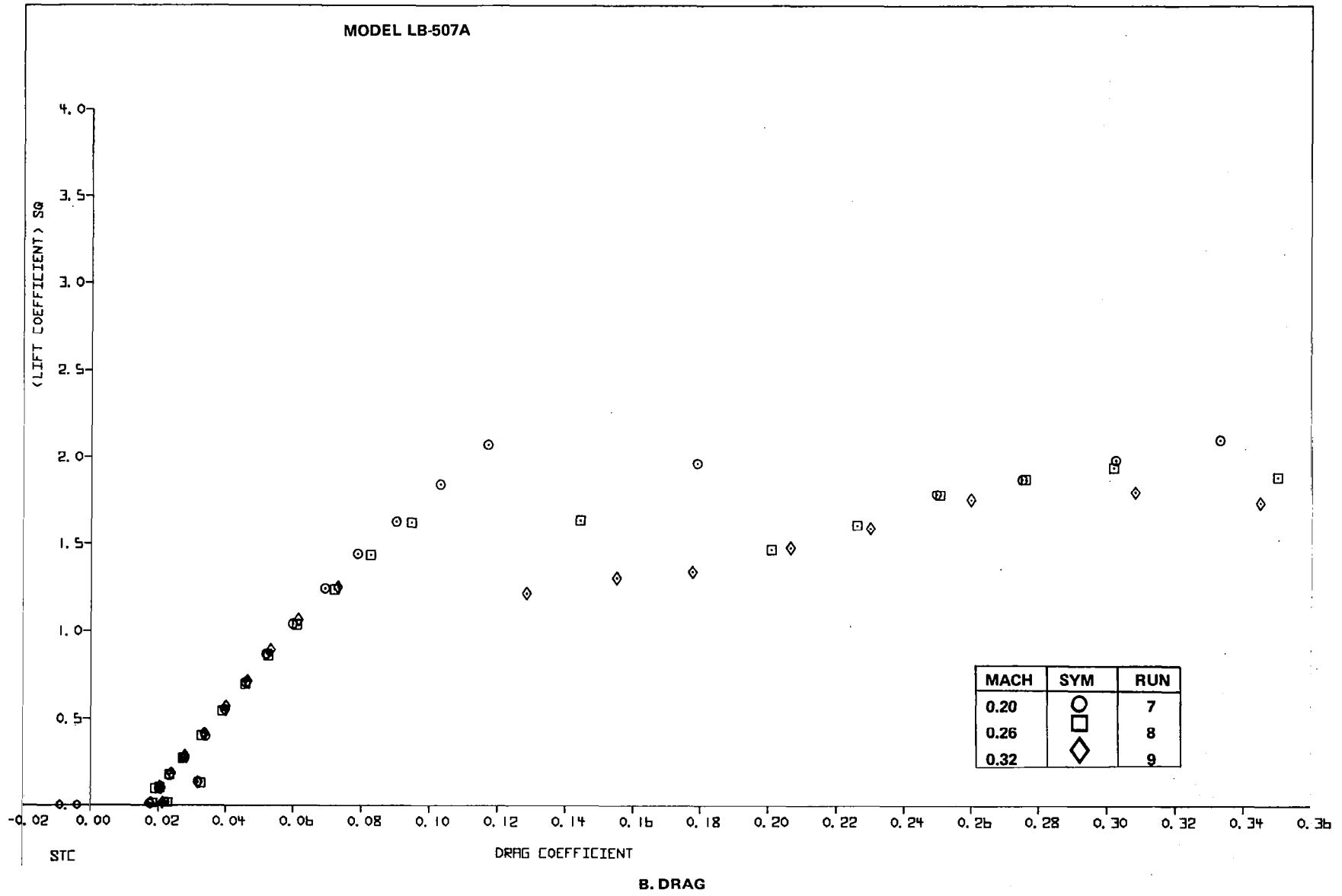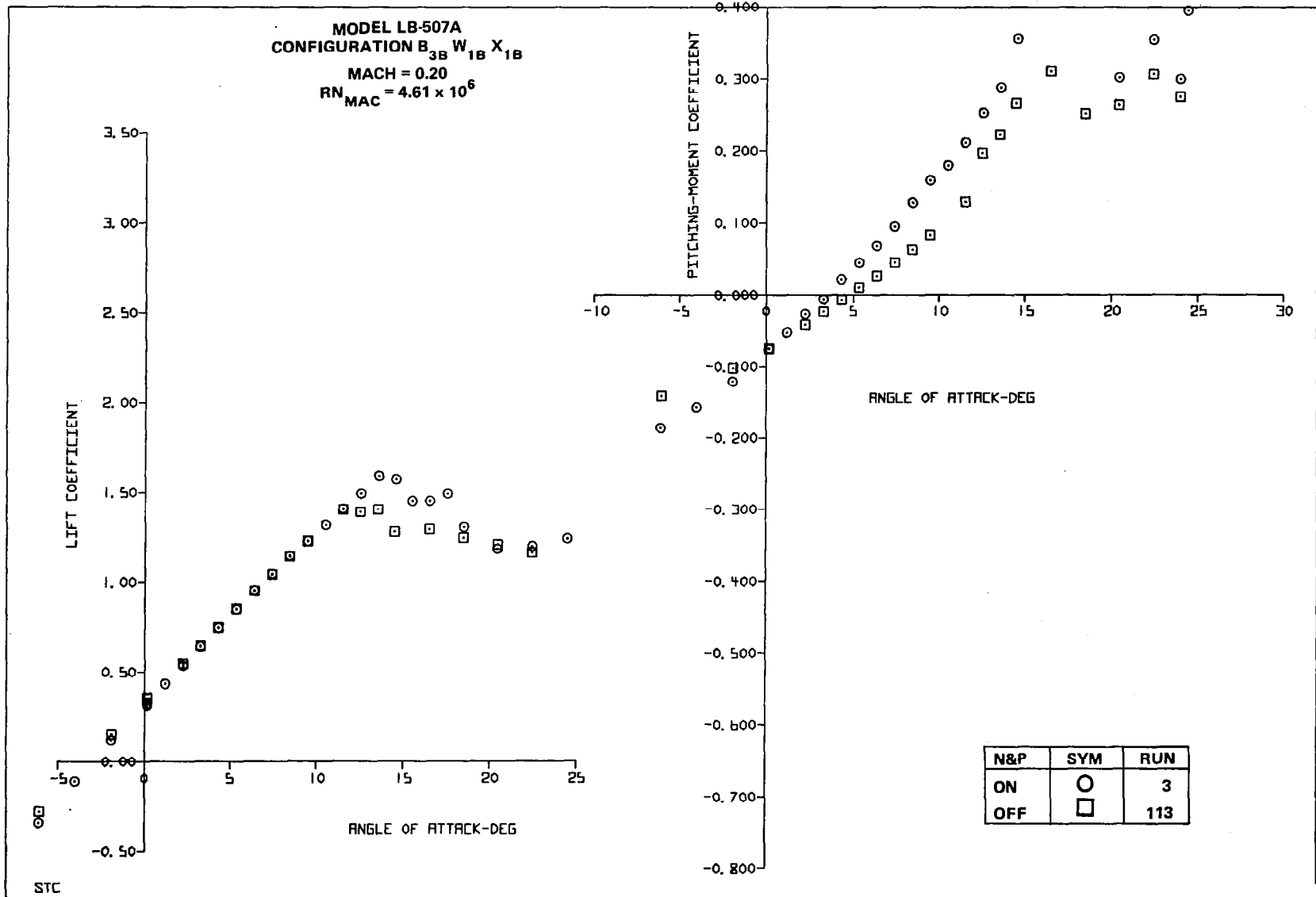
A. LIFT AND PITCHING MOMENT

FIGURE 41. EFFECT OF NACELLES AND PYLON ON CRUISE WING
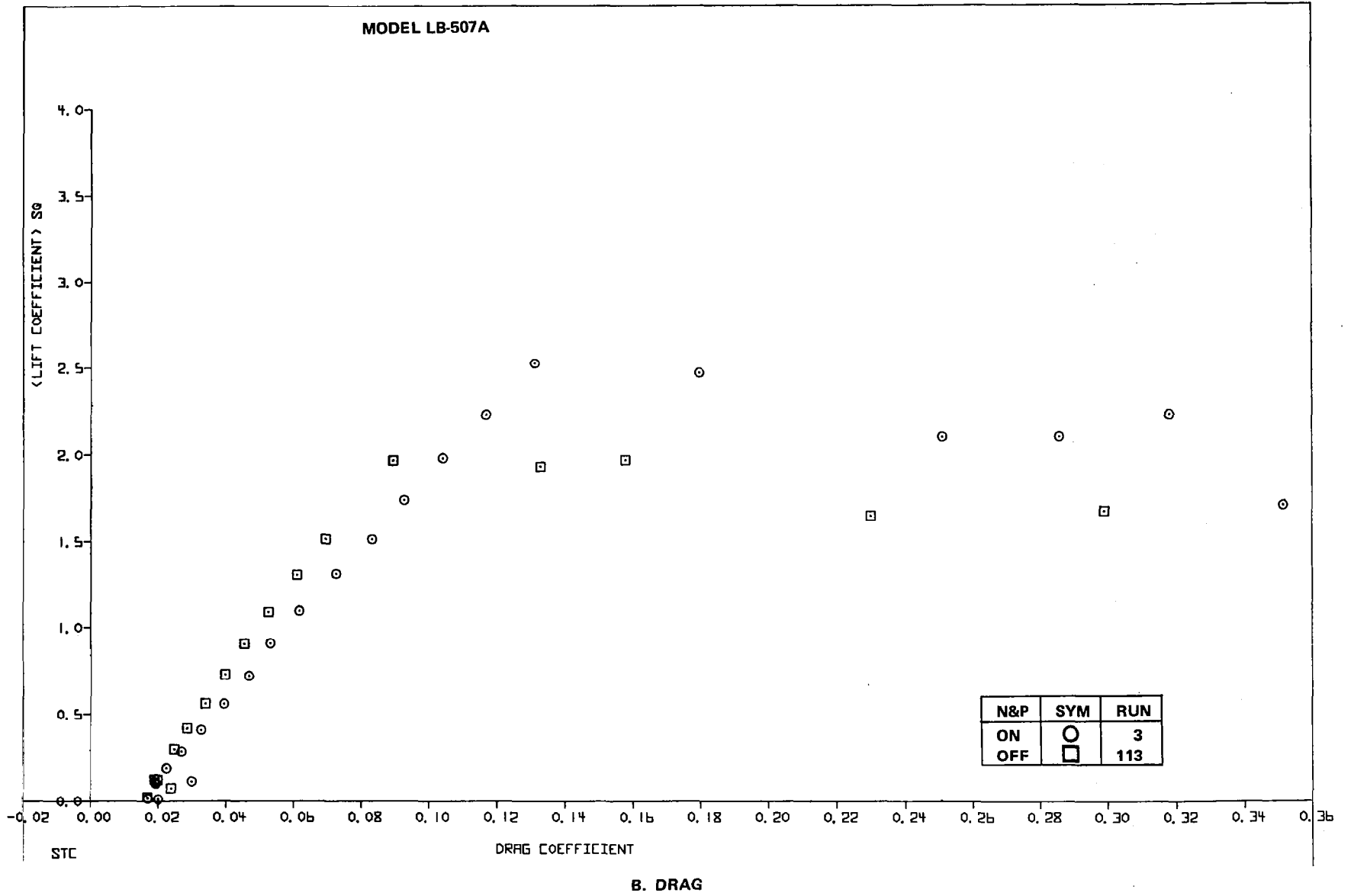
FIGURE 41. EFFECT OF NACELLES AND PYLON ON CRUISE WING
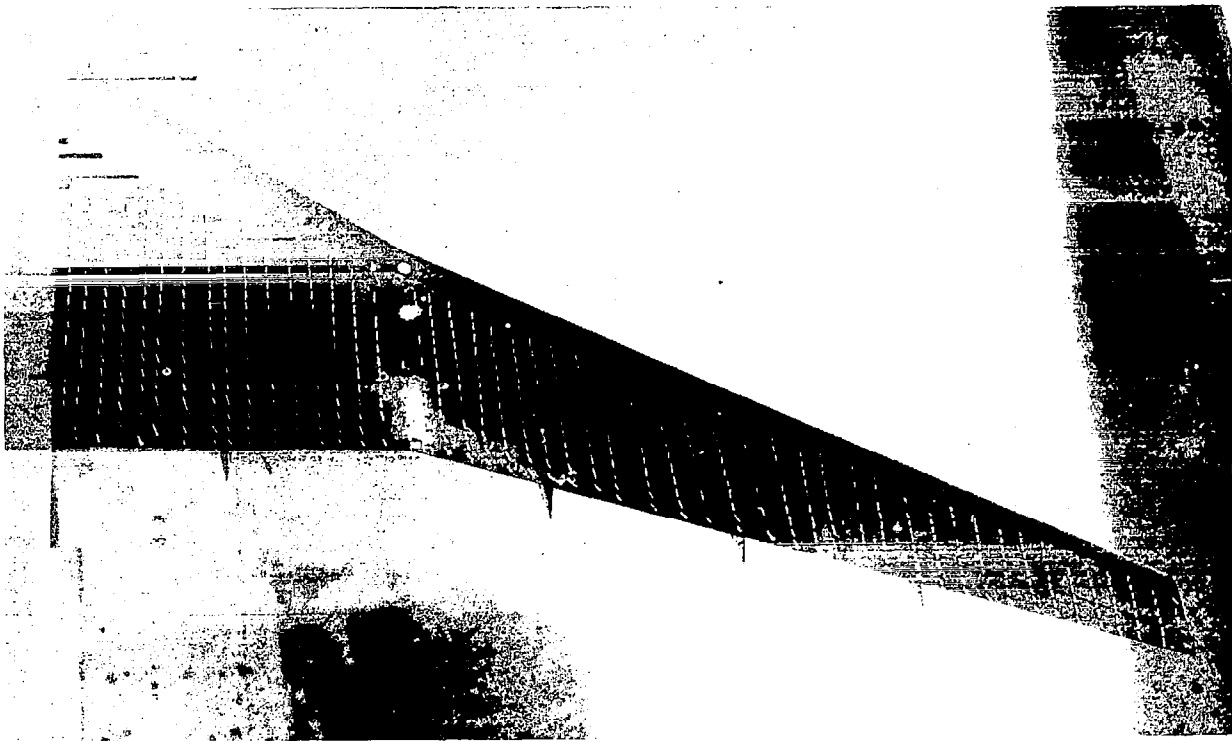
A. $\alpha_{FRP} = 12.54°$
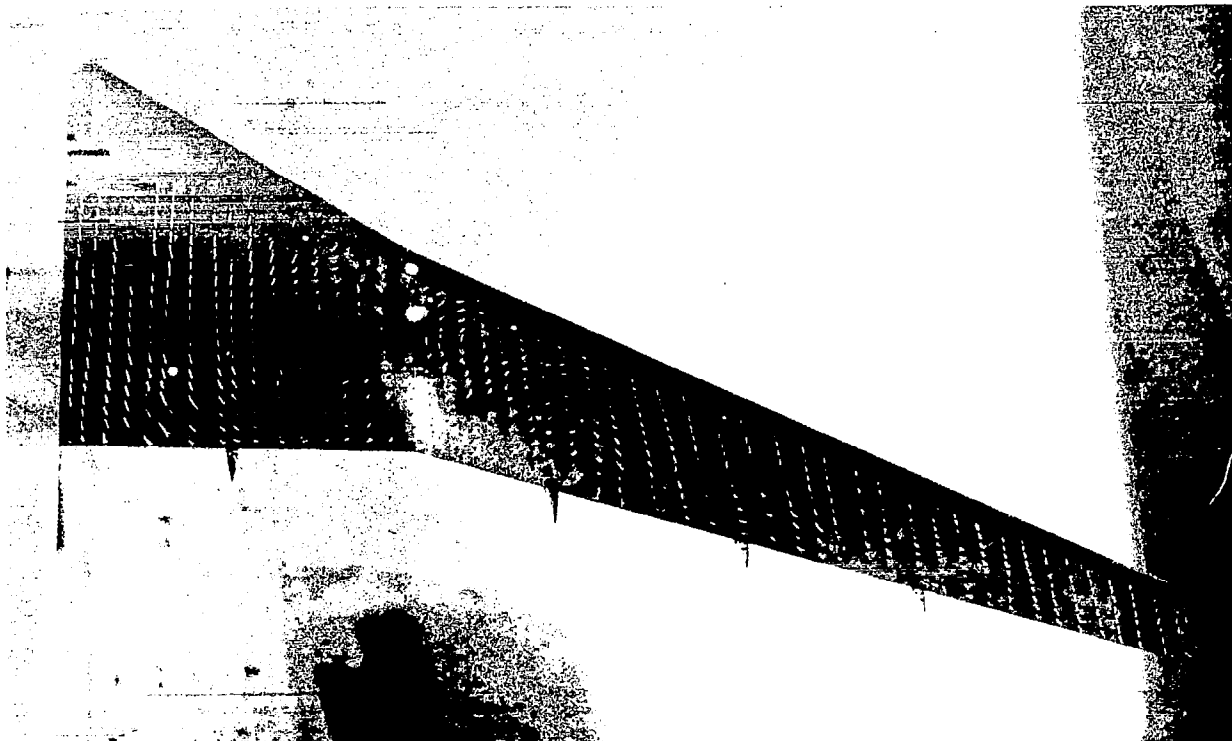
B. $\alpha_{FRP} = 13.55°$ ($\alpha_{C_{LMAX}}$)

FIGURE 42. MINI-TUFT PHOTOS FOR CRUISE WING/BODY (RUN 113)
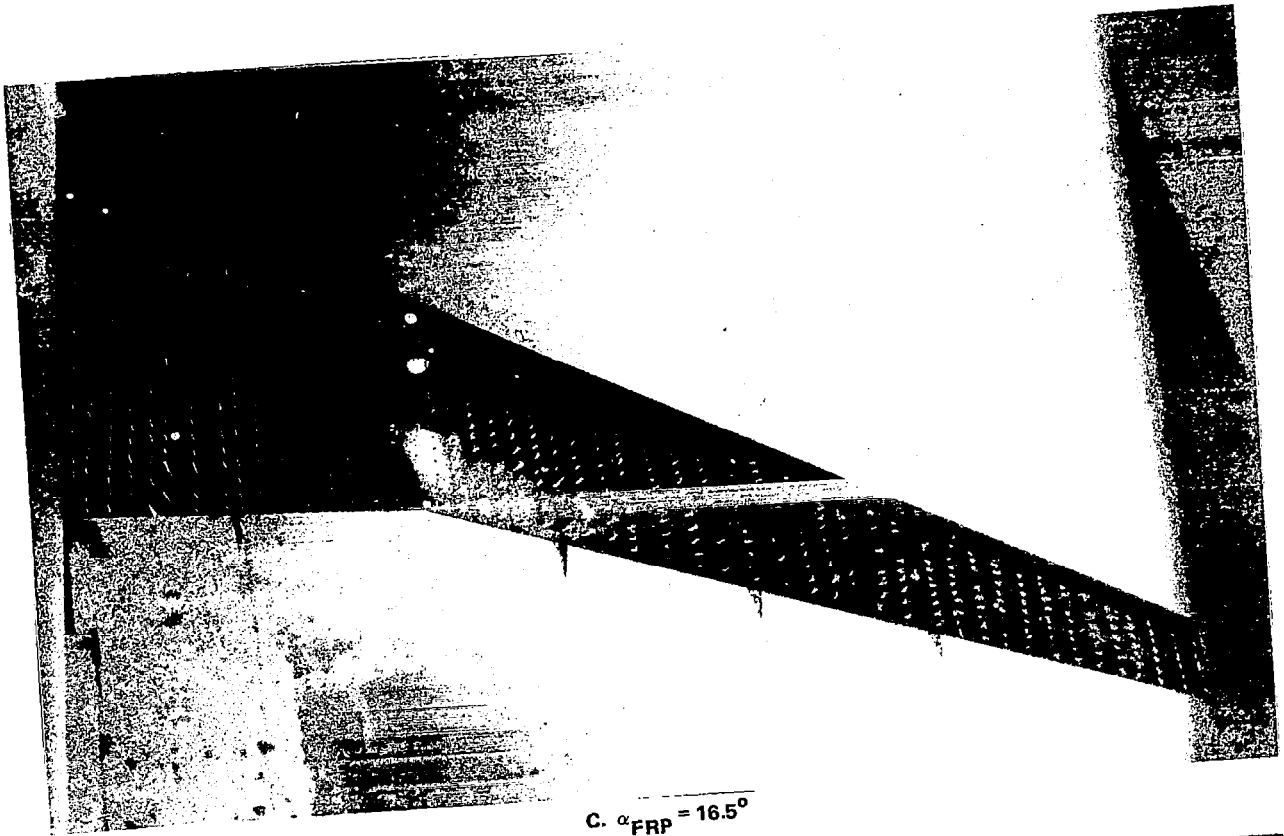
C. $\alpha_{FRP} = 16.5°$
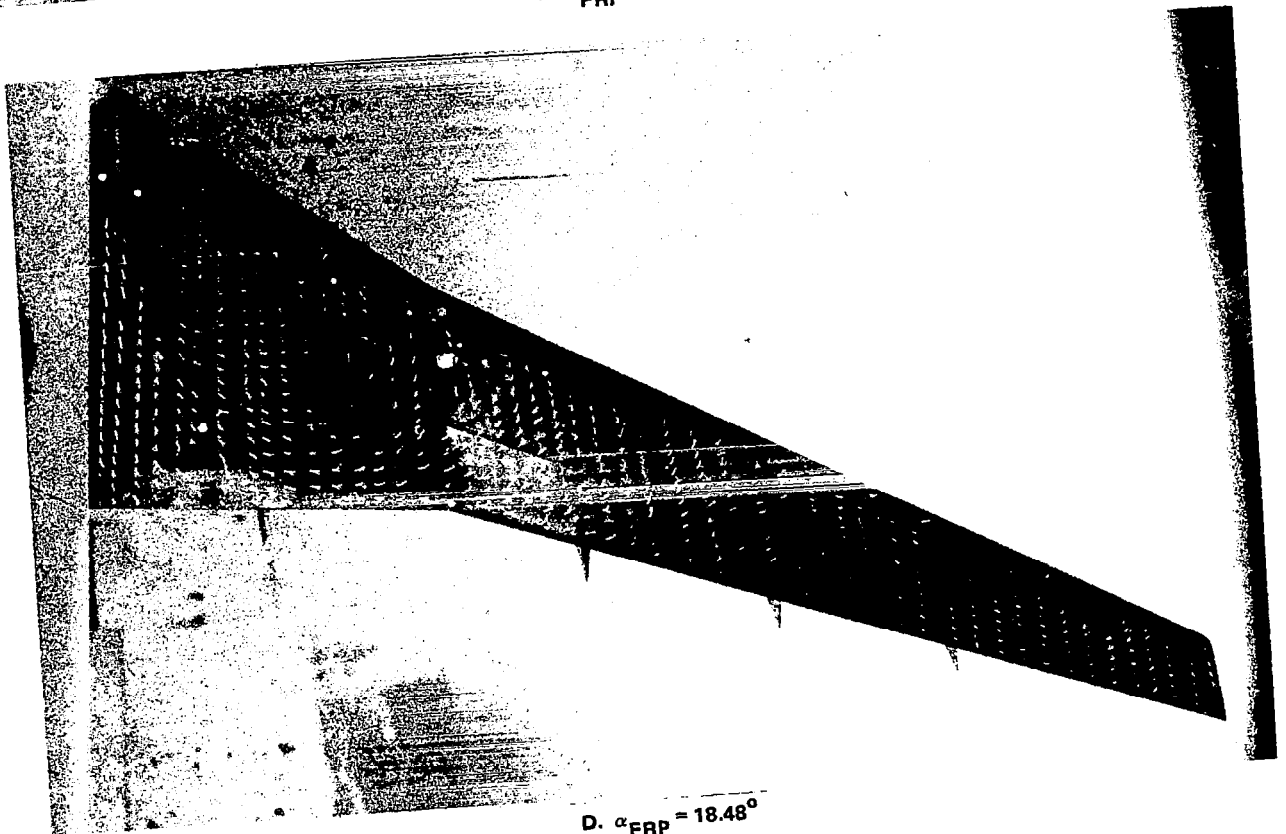
D. $\alpha_{FRP} = 18.48°$

FIGURE 42. MINI-TUFT PHOTOS FOR CRUISE WING/BODY (CONCLUDED)

PERCENT SEMISPAN = 35.00

PERCENT SEMISPAN = 57.00

SYM	RUN	MACH	ALPHA
0 =	113	0.20	11.55

PERCENT SEMISPAN = 72.50

PERCENT SEMISPAN = 95.00
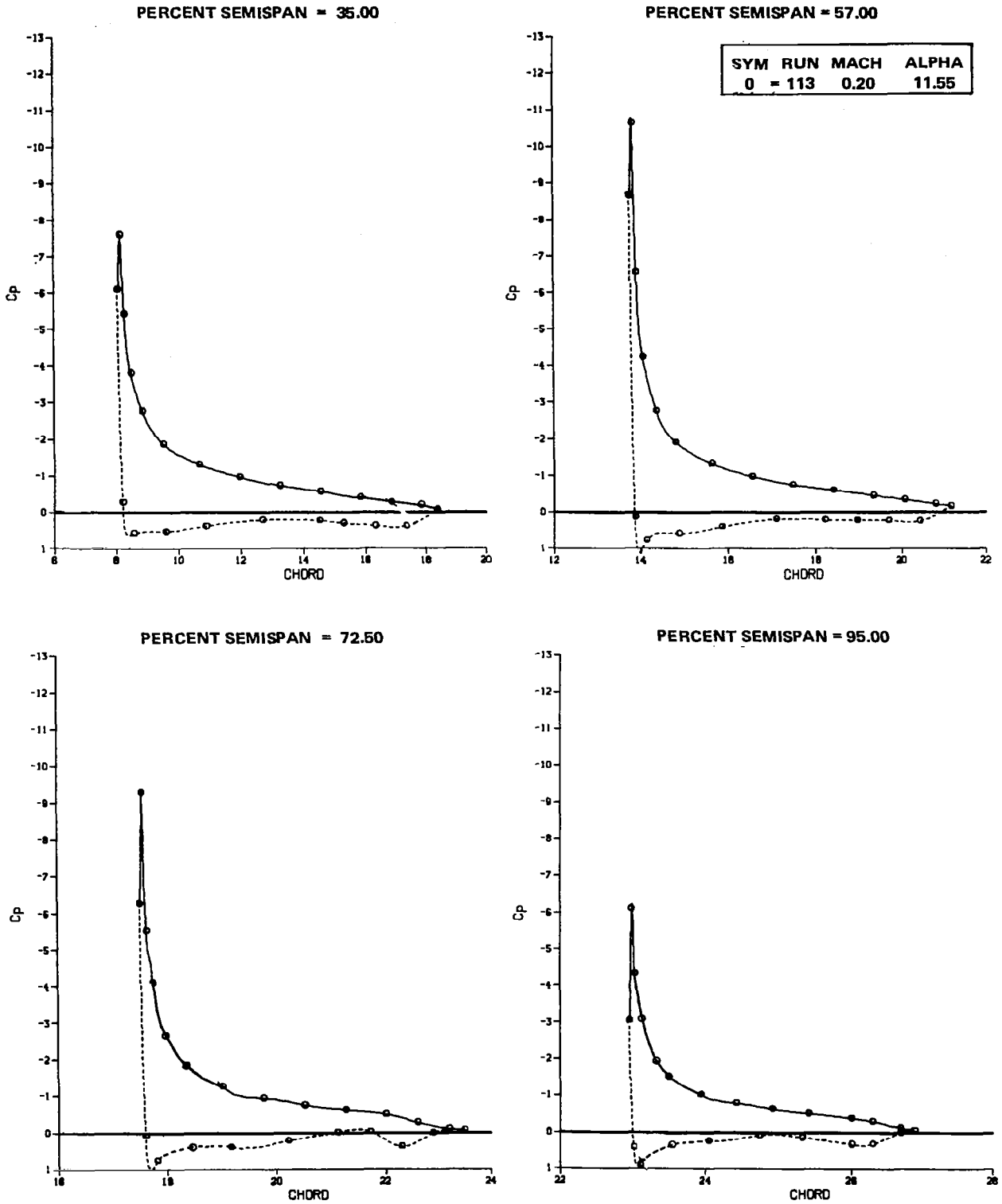
A. $a_{FRP} = 11.55°$ $(a_{C_{L_{MAX}}})$

FIGURE 43.   CHORDWISE PRESSURE DISTRIBUTIONS OF CRUISE WING
WITHOUT NACELLES AND PYLONS

PERCENT SEMISPAN = 35.00

PERCENT SEMISPAN = 57.00

SYM	RUN	MACH	ALPHA
0 =	113	0.20	13.55

PERCENT SEMISPAN = 72.50

PERCENT SEMISPAN = 95.00
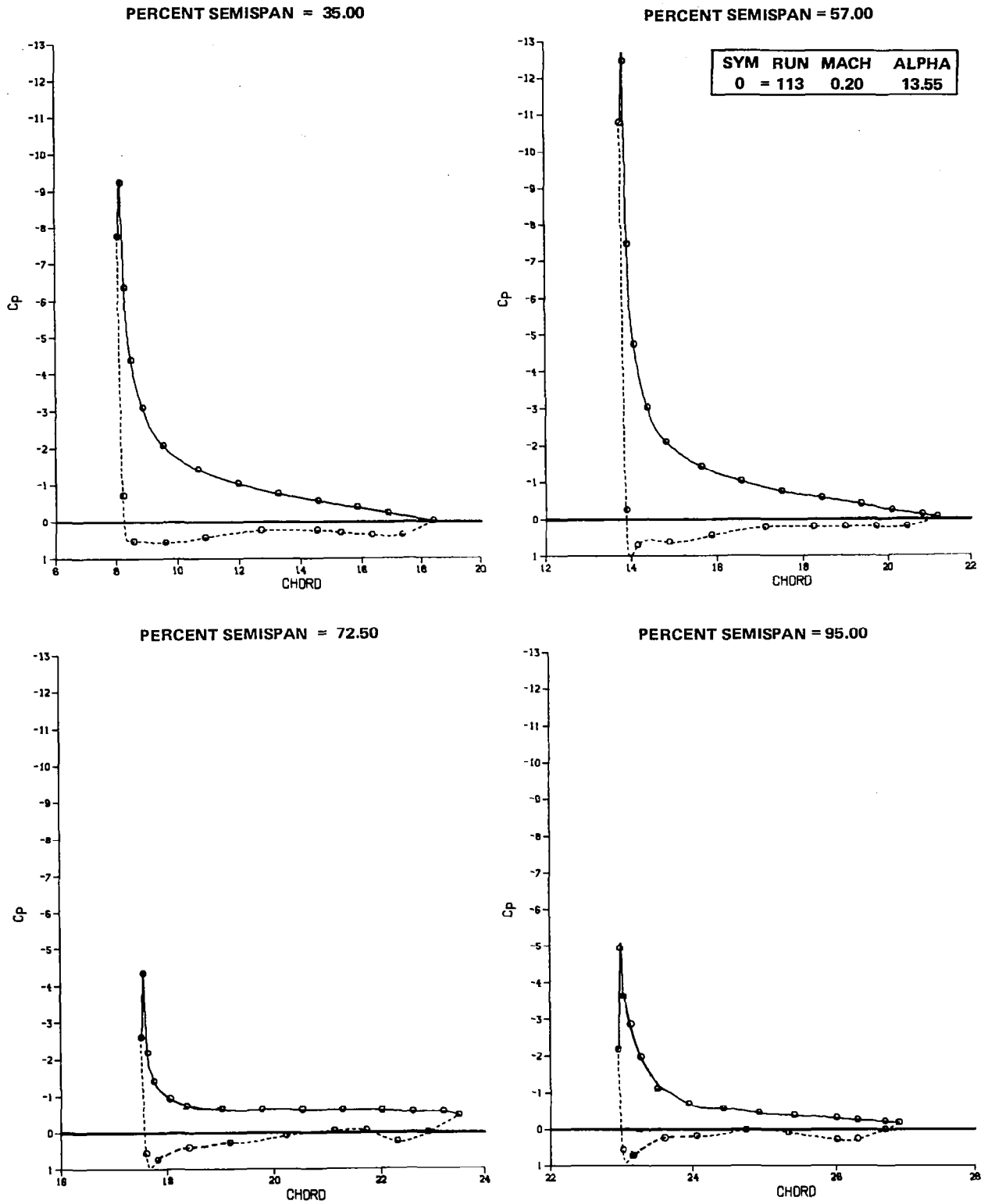
B. $\alpha_{FRP} = 13.55^{o}$

FIGURE 43. CHORDWISE PRESSURE DISTRIBUTIONS OF CRUISE WING WITHOUT NACELLES AND PYLONS (CONTINUED)

MODEL LB-507A
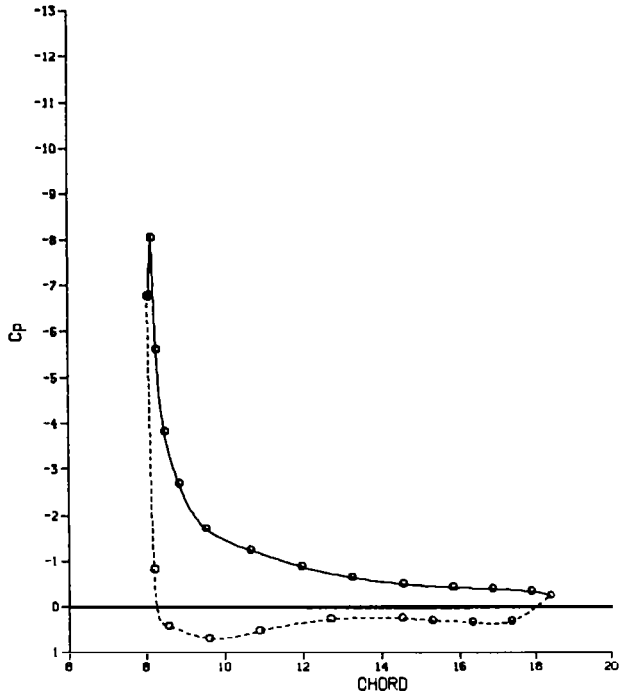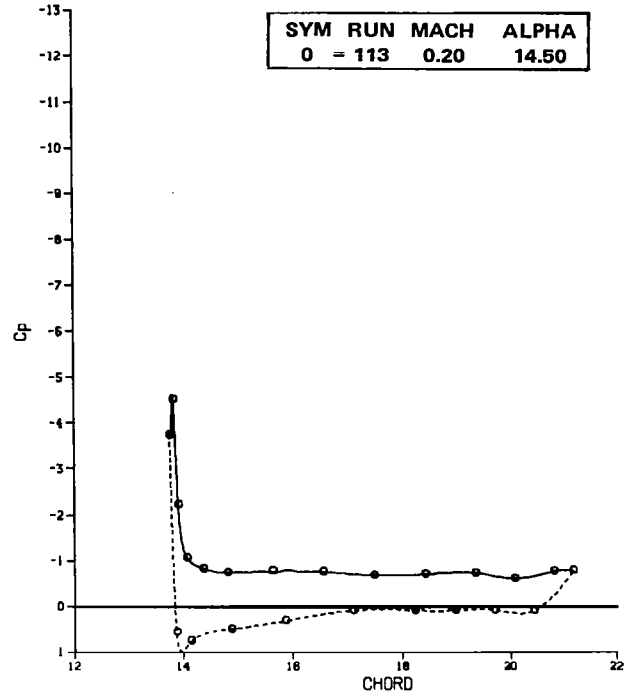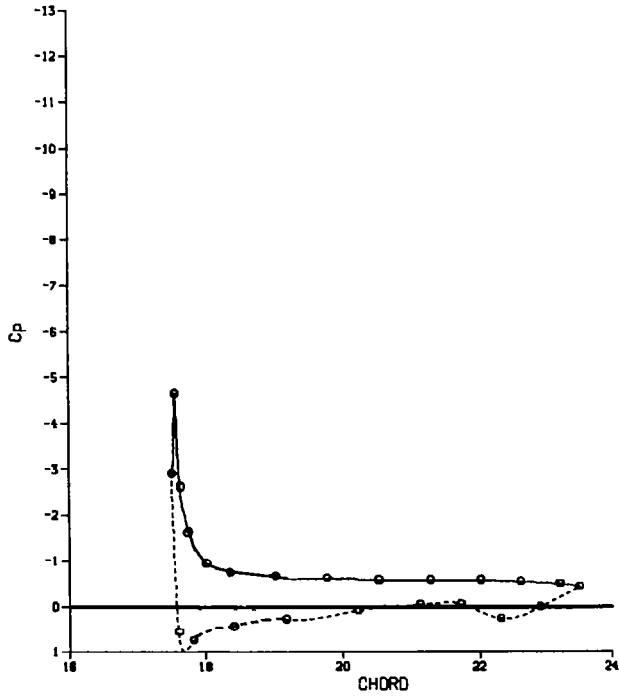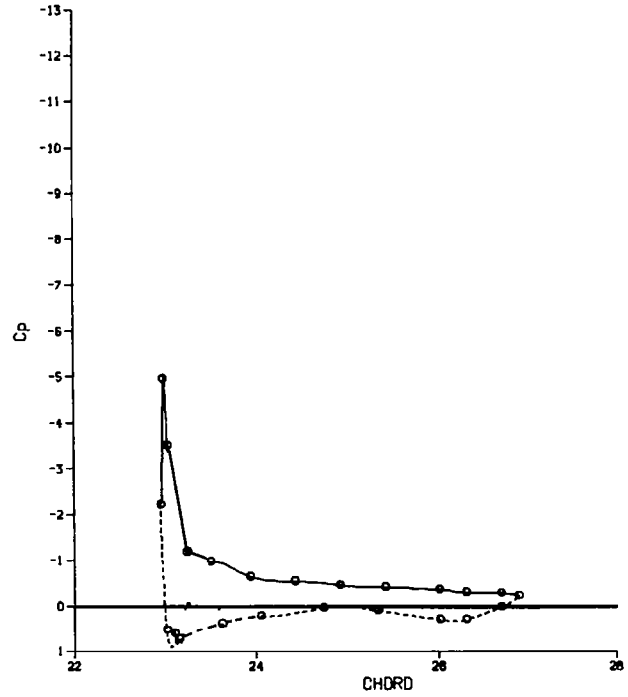
c. $a_{FRP} = 14.50°$

FIGURE 43. CHORDWISE PRESSURE DISTRIBUTIONS OF CRUISE WING
WITHOUT NACELLES AND PYLONS ATTACHED (CONTINUED)

PERCENT SEMISPAN = 35.00

PERCENT SEMISPAN = 57.00

SYM	RUN	MACH	ALPHA
0 =	113	0.20	16.50

PERCENT SEMISPAN = 72.50

PERCENT SEMISPAN = 95.00
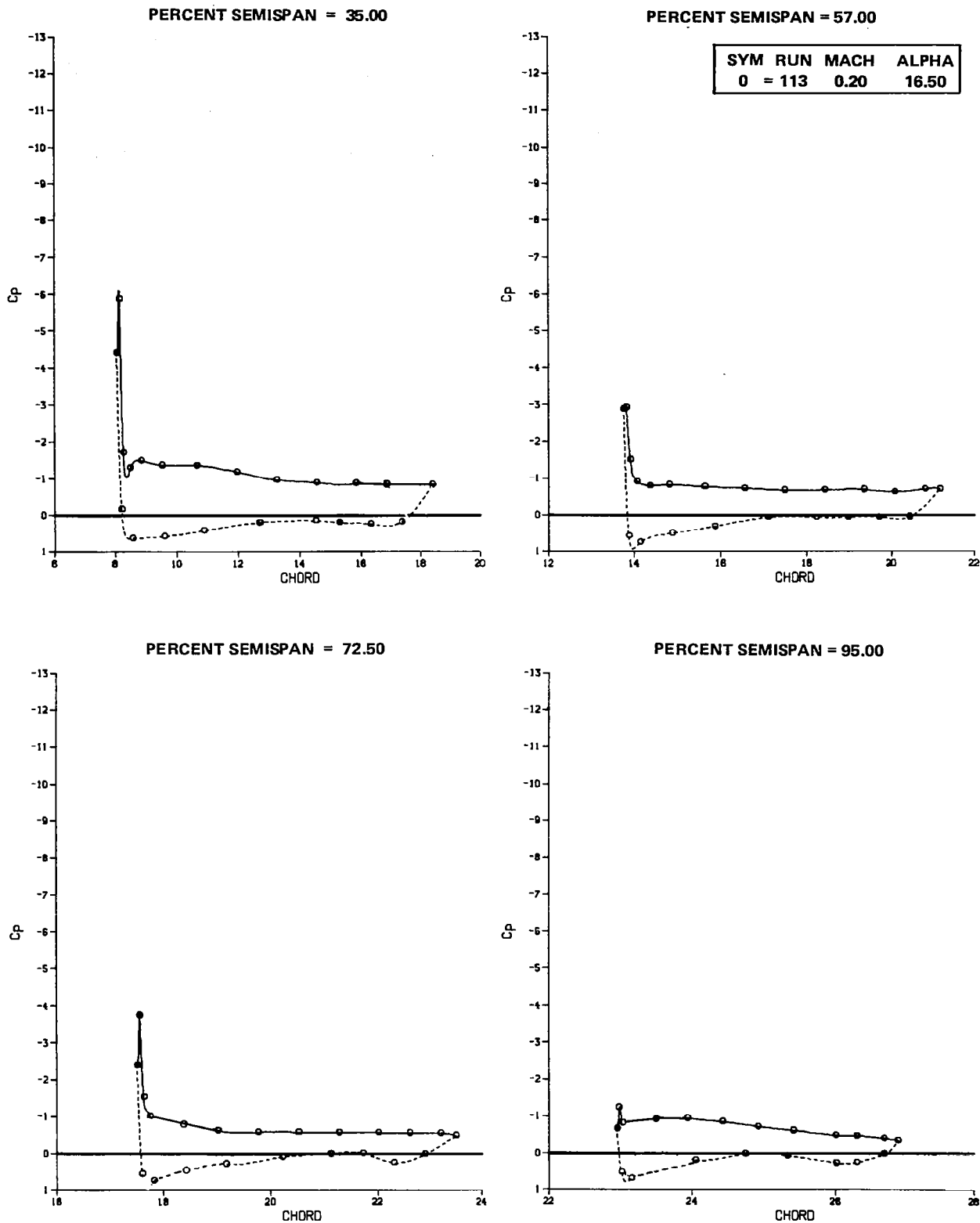
D. $a_{FRP} = 16.50°$

FIGURE 43. CHORDWISE PRESSURE DISTRIBUTIONS OF CRUISE WING
WITHOUT NACELLES AND PYLONS (CONCLUDED)

CONFIGURATION $B_{38} W_{1B} X_{1B} P_{1C} N_{1C} S_{11F}$

MACH = 0.20

$RN_{MAC} = 4.61 \times 10^6$

LIFT COEFFICIENT

PITCHING-MOMENT COEFFICIENT

ANGLE OF ATTACK-DEG

ANGLE OF ATTACK-DEG

STC

STRAKES	SYM	RUN
ON	○	3
OFF	□	10
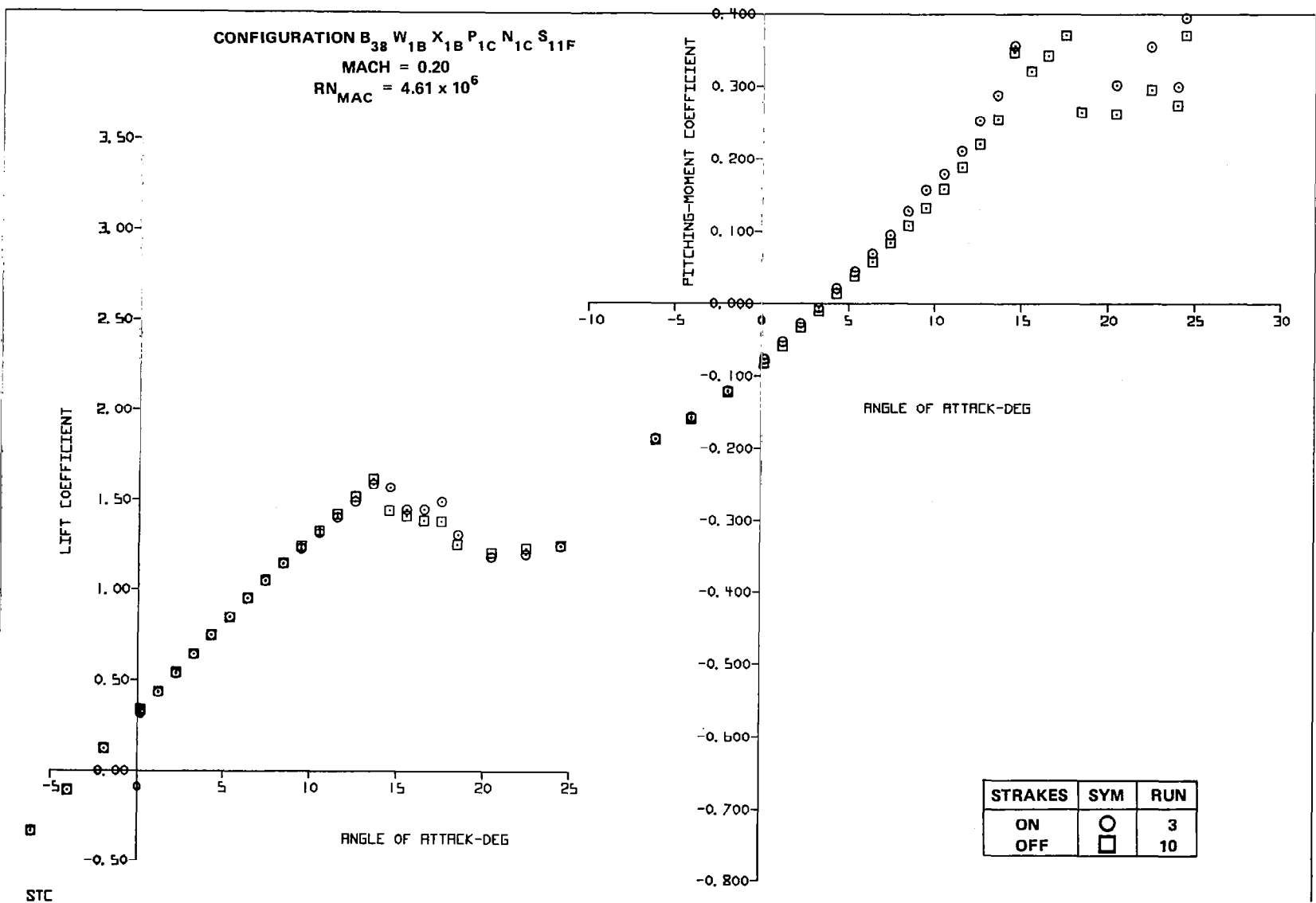
A. LIFT AND PITCHING MOMENT

FIGURE 44. EFFECT OF STRAKES ON CRUISE

MODEL LB-507A
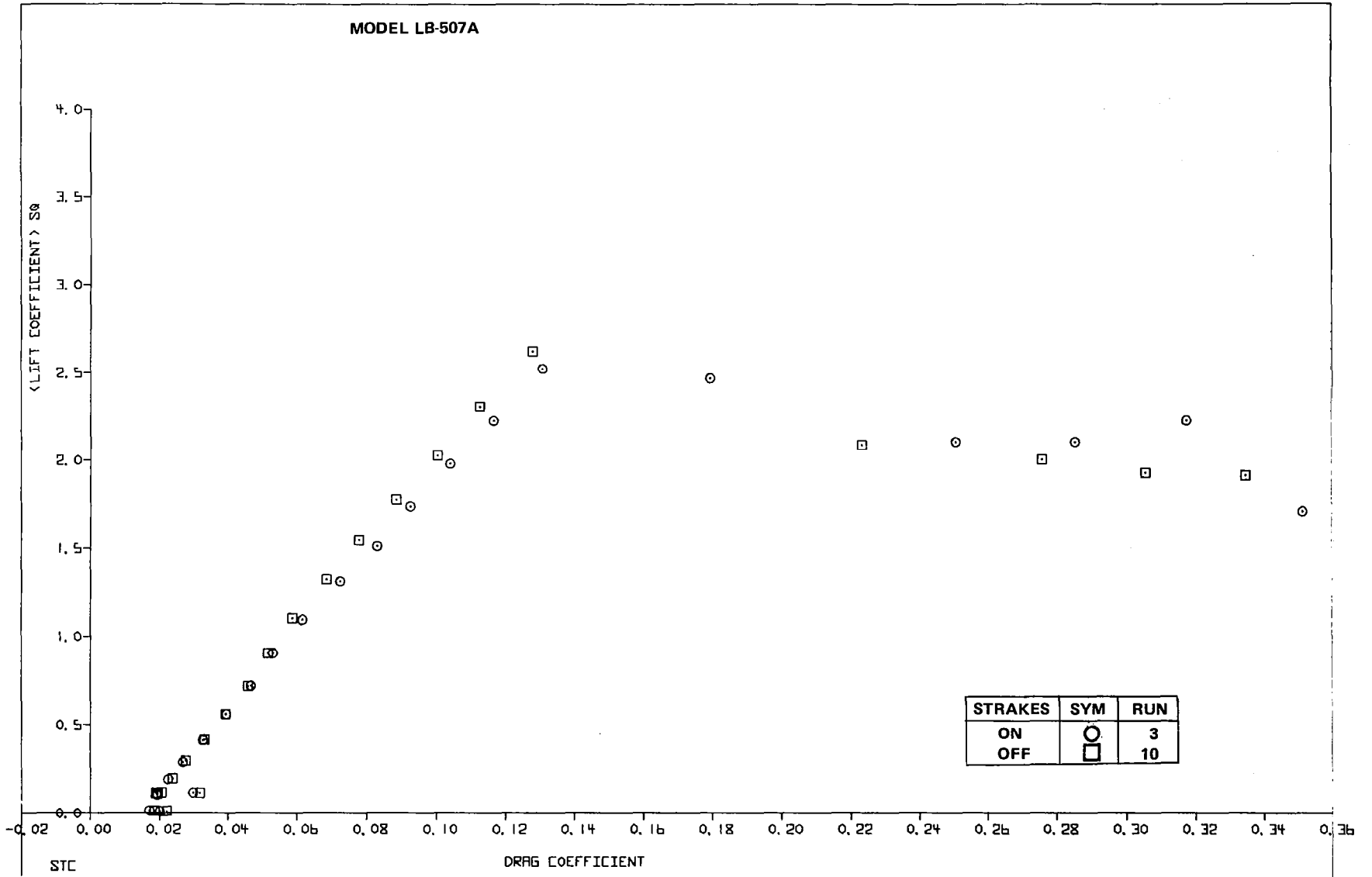
B. DRAG

FIGURE 44. EFFECT OF STRAKES ON CRUISE

Landing Configuration Characteristics

The primary landing configuration consisted of:

1. a two-segment flap deflected at $25^0/12^0$ (main flap/auxiliary flap)
2. a slotted, leading edge, outboard slat deflected at 27^0
3. a slotted slat or short-chord FCK inboard.

The grid optimization studies for the inboard slat and inboard FCK are shown in Figures 45 and 46, respectively. A comparison of the best slat position versus the two best FCK positions is presented in Figure 47. The best pitching-moment characteristics were those associated with the FCK deflected at 70^0. This configuration also resulted in the highest tail-off $C_{L_{MAX}}$ of the test, 3.08. Deflecting the FCK at 55^0 decreased the $C_{L_{MAX}}$ from 3.08 to 2.94, decreased the stall angle from 17.2^0 to 15.2^0, and degraded the post-stall pitching moments. The inboard slat configuration had a $C_{L_{MAX}}$ value between the two FCK values and exhibited the most undesirable pitching moment trends of the group.

Reynolds number and Mach effects.- The effect of Reynolds number on the maximum-lift coefficient of the landing FCK configuration is shown in Figure 48. Unlike the trends for the cruise wing, the trends for the landing configuration suggest that the $C_{L_{MAX}}$ of the landing configuration will increase beyond the wind tunnel values as the Reynolds number is increased from the highest wind tunnel value to flight Reynolds number. Any effort to extrapolate the data to arrive at an estimated $C_{L_{MAX}}$ value for flight conditions would be unwise in light of the distinct break in the $C_{L_{MAX}}$ versus Reynolds number curve for the cruise wing (Figure 39).

The effect of Mach number on the maximum-lift coefficient for the same landing configuration is depicted in Figure 49. Again the trends of the cruise wing differed slightly from those of the landing configuration. Whereas $C_{L_{MAX}}$ of the cruise wing decreased monotonically with Mach number, the $C_{L_{MAX}}$ of the landing configuration increased slightly as the Mach number was increased from 0.20 to 0.26. As the Mach number was further increased to 0.32, the $C_{L_{MAX}}$ of the landing configuration decreased from 2.88 to 2.79.

CONFIGURATION B_{3A} W_{1B} X_{1B} P_{1C} N_{1C} S_{11F}

MACH = 0.20

RN_{MAC} = 4.61 x 10^6

δ_{FLAP} = 25/12.5

INBOARD	OUTBOARD		
δ_{SLAT}	δ_{SLAT}	SYM	RUN
12B	27B	○	17
12A	27A	□	19
8A	27A	◇	20
8B	27A	⬠	21
12B	27A	△	22
12C	27A	▽	23

STC
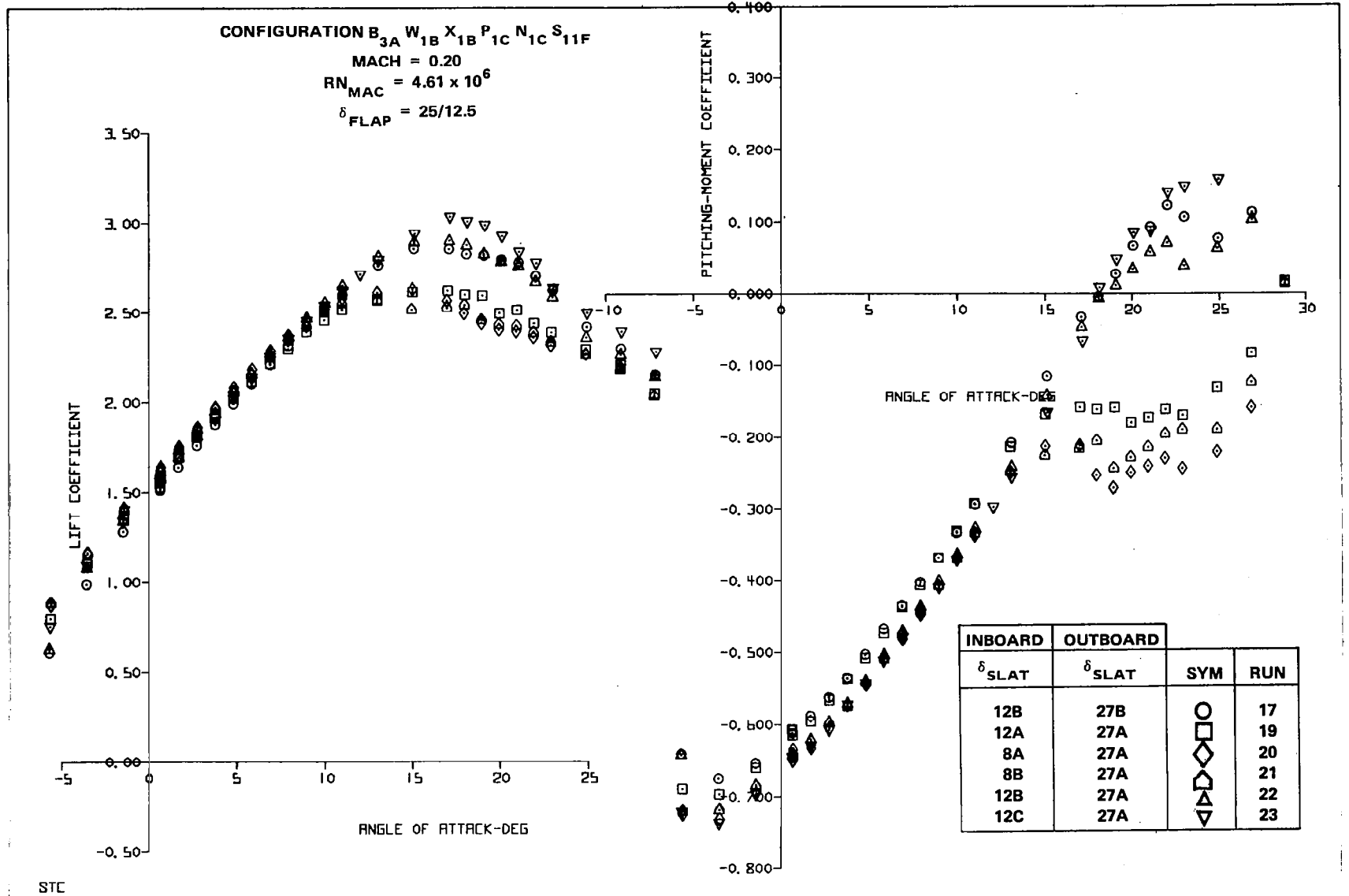
A. LIFT AND PITCHING MOMENT

FIGURE 45. LANDING SLAT GRID OPTIMIZATION

B. DRAG

FIGURE 45. LANDING SLAT GRID OPTIMIZATION

The chart area shows:

MODEL LB-507A

Y-axis: (LIFT COEFFICIENT) SQ

X-axis: DRAG COEFFICIENT

STC

INBOARD	OUTBOARD	SYM	RUN
δ_{SLAT}	δ_{SLAT}		
12B	27B	○	17
12A	27A	□	19
8A	27A	◇	20
8B	27A	⬠	21
12B	27A	△	22
12C	27A	▽	23

MODEL LB-507A

CONFIGURATION $B_{3B} W_{1B} X_{1B} N_{1C} P_{1C} S_{11F}$

MACH = 0.20

$RN_{MAC} = 4.61 \times 10^6$

$\delta_{FLAP} = 25/12.5$

$\delta_{LE} = XX/27A$

δ_{FCK}	SYM	RUN
50A	○	34
55B	□	35
70A	◇	36
70B	△	37

STC
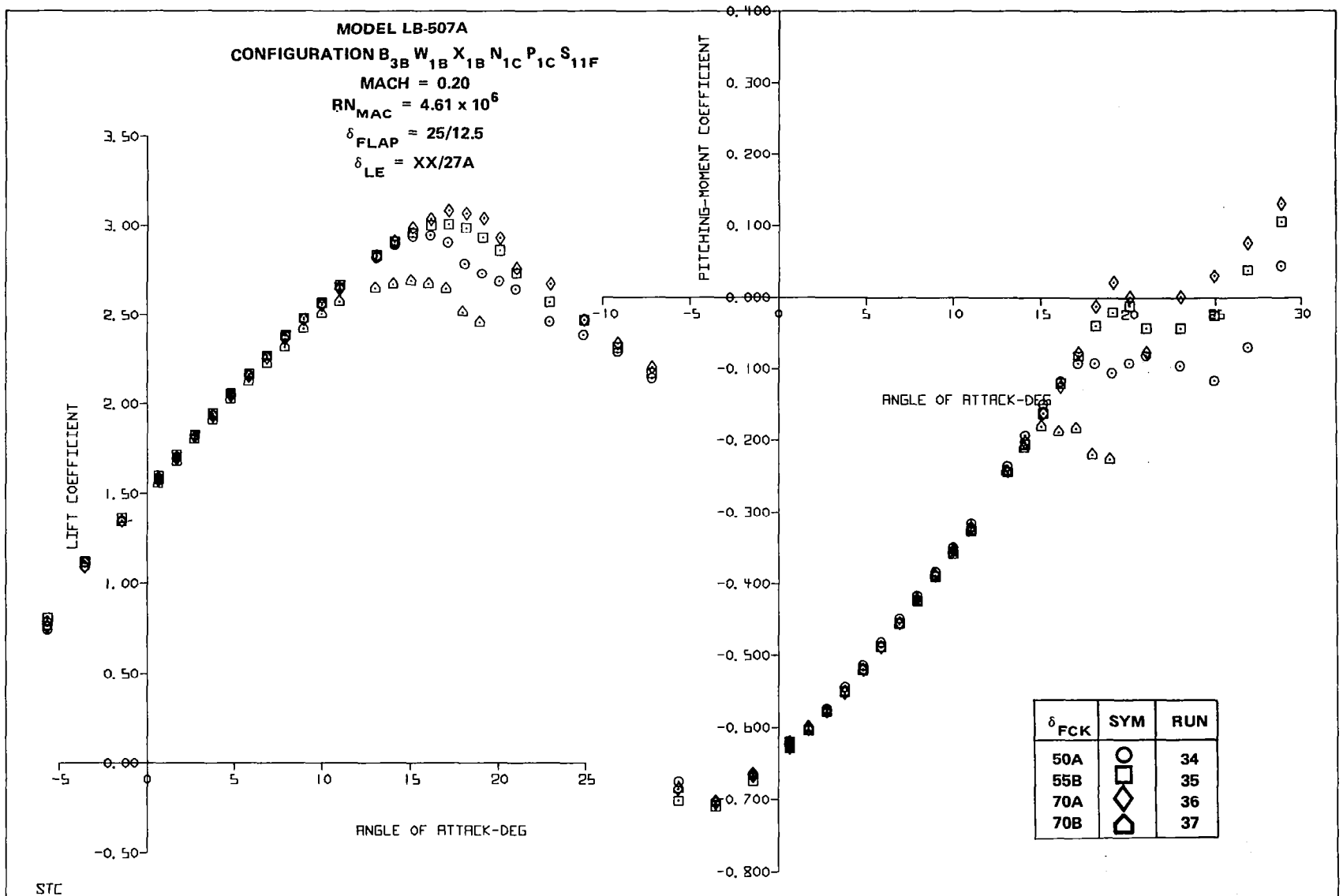
A. LIFT AND PITCHING MOMENT

FIGURE 46. FCK OPTIMIZATION WITH LANDING FLAPS

B. DRAG

FIGURE 46. FCK OPTIMIZATION WITH LANDING FLAPS

MODEL LB-507A
CONFIGURATION $B_{3B} W_{1B} X_{1B} P_{1C} N_{1C} S_{11F}$
MACH = 0.20
$RN_{MAC} = 4.61 \times 10^6$
$\delta_{FLAP} = 25/12.5$

DEVICE	δ_{LE}	SYM	RUN
SLAT/SLAT	12C/27A	◯	23
FCK/SLAT	55A/27A	□	34
FCK/SLAT	70A/27A	◇	36

STC
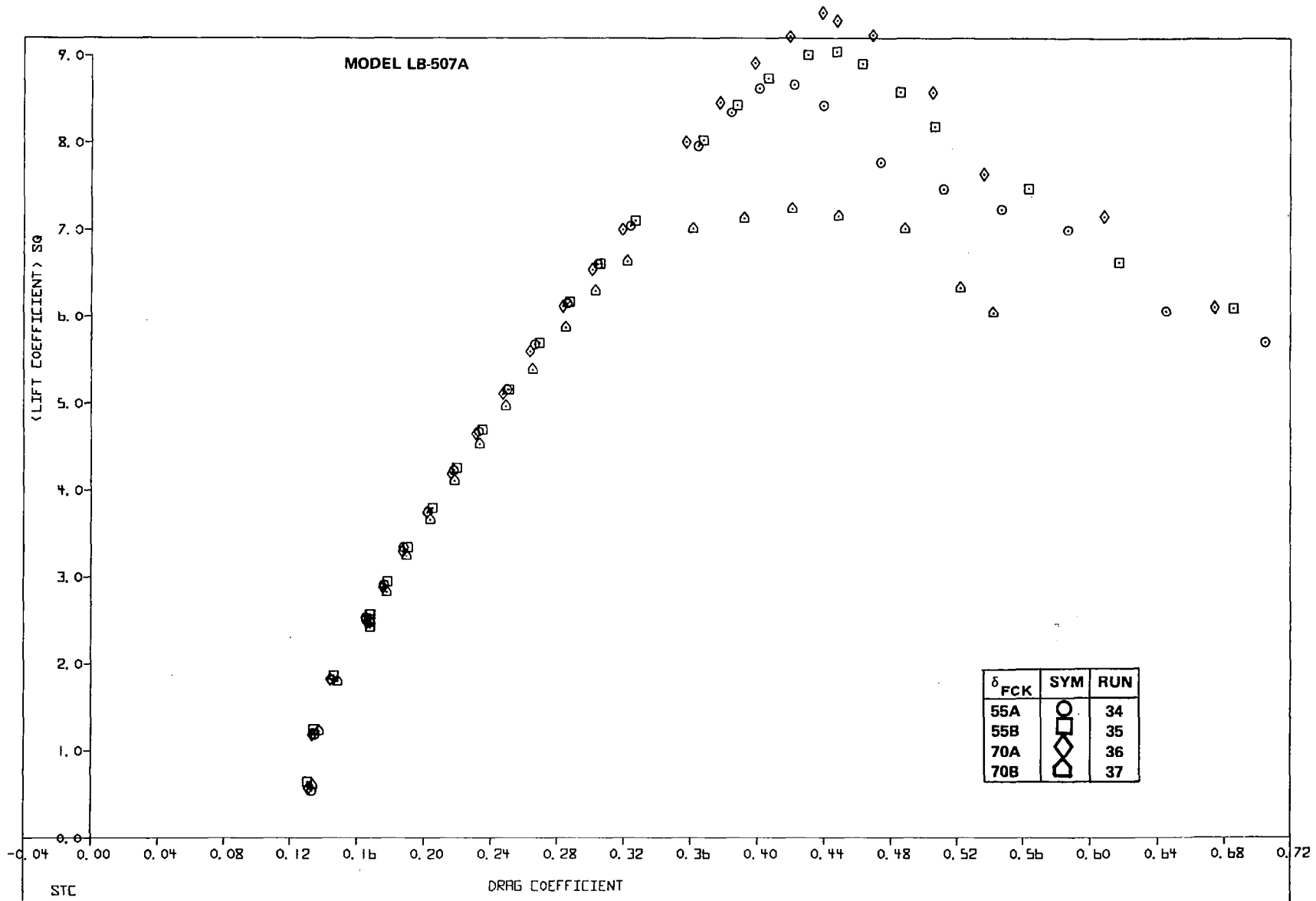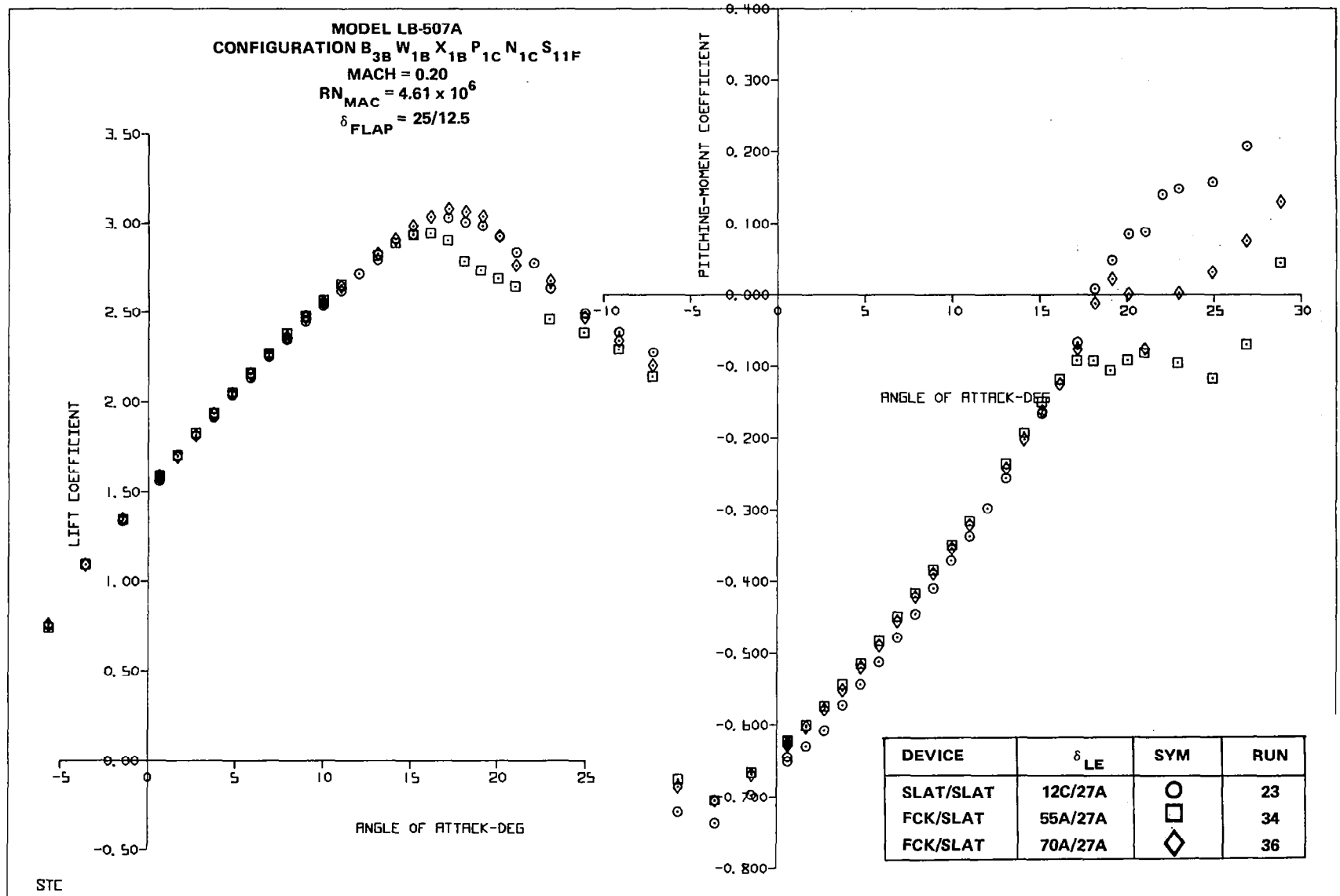
A. LIFT AND PITCHING MOMENT

FIGURE 47. FCK AND SLAT COMPARISON WITH LANDING FLAPS
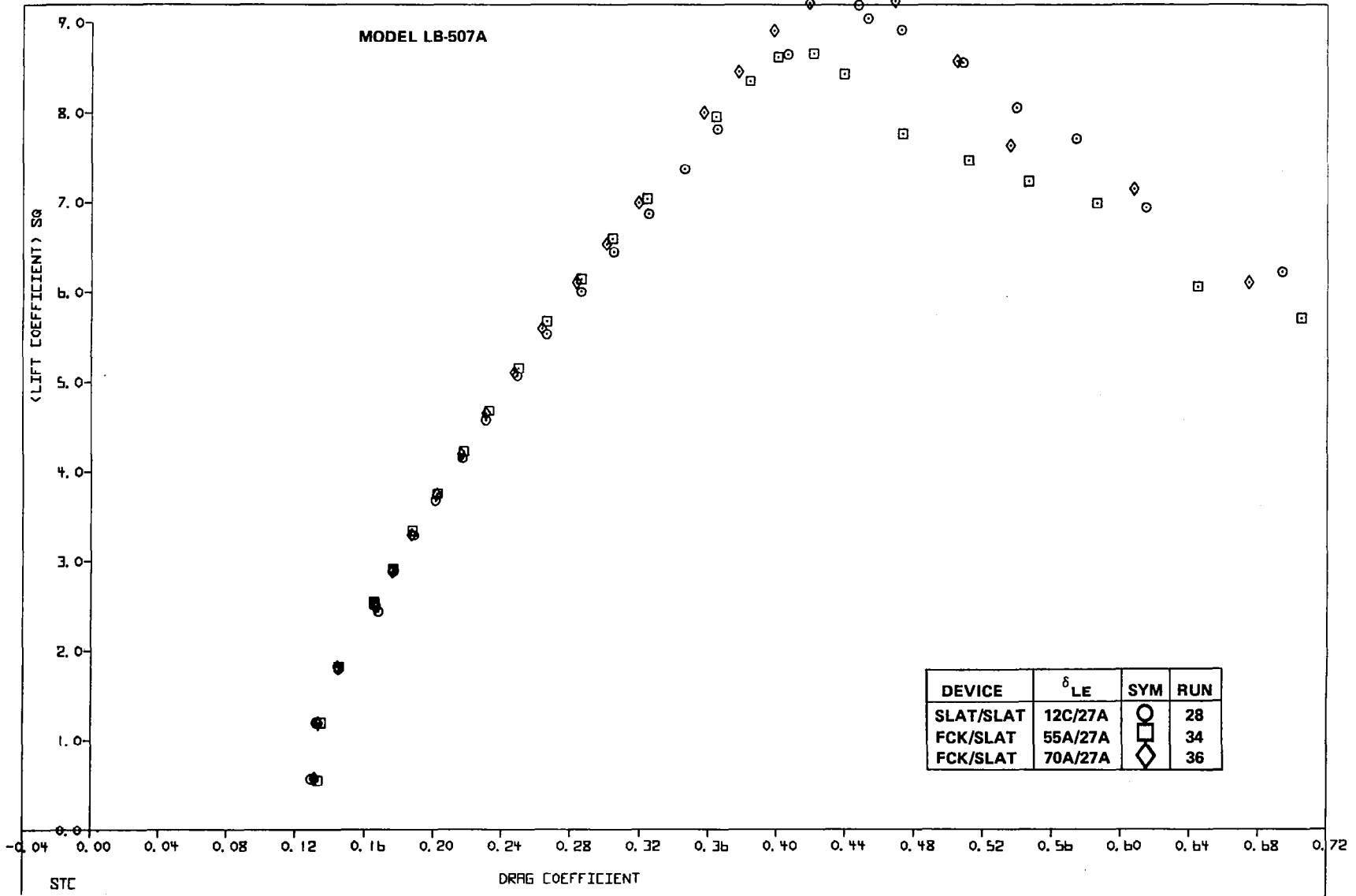
FIGURE 47. FCK AND SLAT COMPARISON WITH LANDING FLAPS

MODEL LB-507A
CONFIGURATION $B_{3B} W_{1B} X_{1B} P_{1C} N_{1C}$
MACH = 0.20

δ_{LE} = 70A/27A
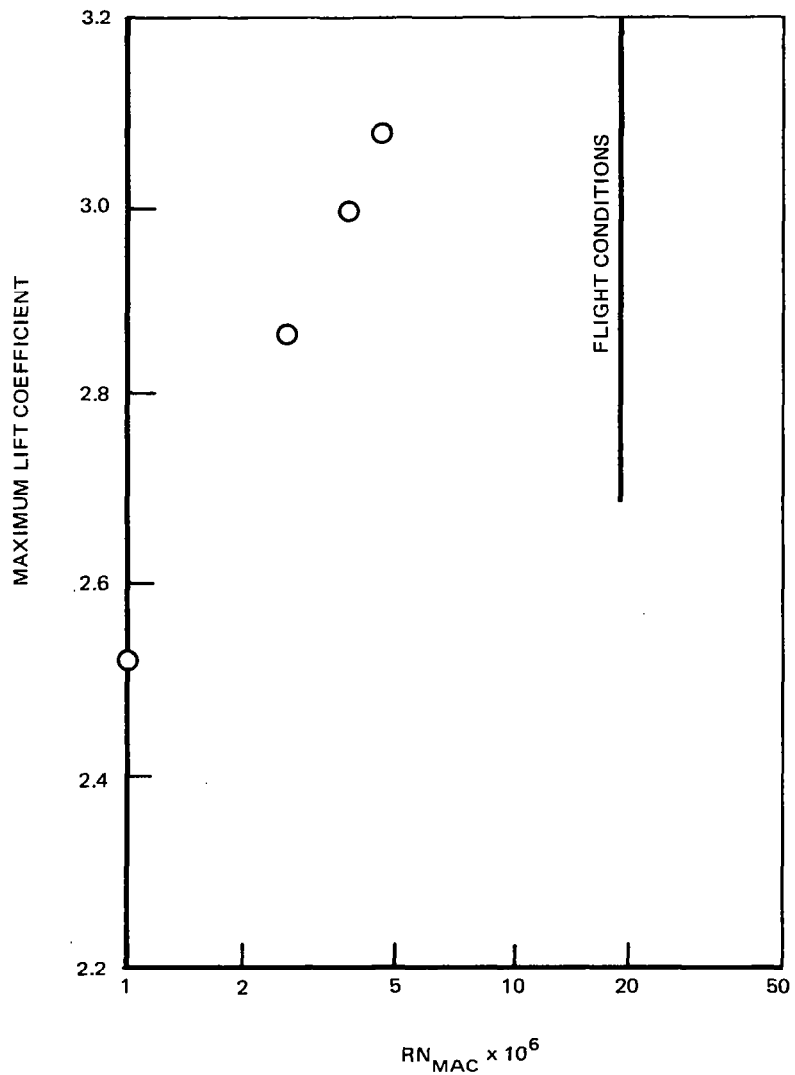
δ_{FLAP} = 25/12.5

FIGURE 48. EFFECT OF REYNOLDS NUMBER ON MAXIMUM LIFT OF LANDING FCK/SLAT
CONFIGURATION

MODEL LB-507A

CONFIGURATION B_{3B} W_{1A} X_{1B} P_{1C} N_{1C} G_{1A}

RN_{MAC} = 2.89 x 10^6

δ_{LE} = 70/27A

δ_{FLAP} = 25/12.5

TAIL OFF, GEAR DOWN
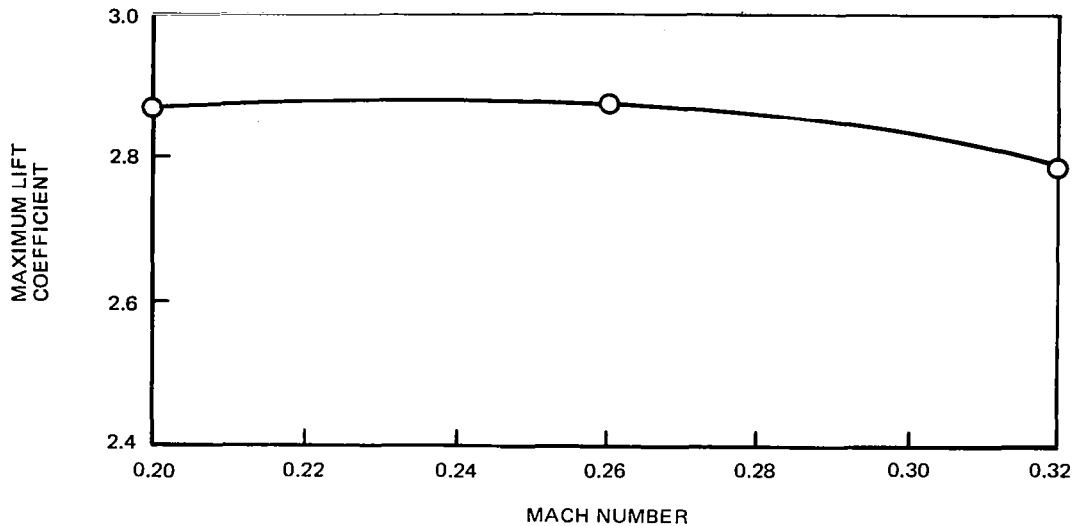
FIGURE 49. EFFECT OF MACH NUMBER ON $C_{L_{MAX}}$ LANDING FCK/SLAT CONFIGURATION

Nacelles/pylons/strakes effect.- Figure 50 shows the effects of having the nacelles, pylons, and strakes on the landing configuration with the slat inboard. The nacelles and pylons had a degrading effect on the post-stall

pitching moments in that their addition eliminated the post-stall pitch-down that was present (tail-off) with the nacelles and pylons off. The nacelles and pylons had no significant effect on the maximum lift value for this particular configuration.

The nacelle strakes, which were added to increase the $C_{L_{MAX}}$ of the inboard slat configurations, were effective in that respect. The tail-on data of Figure 51 showed that the strakes increased the tail-on $C_{L_{MAX}}$ of the inboard slat configuration from 2.94 to 3.08. As might be expected, the strakes degraded the pitching-moment characteristics. Figure 52 shows that the strakes had very little impact on the inboard FCK configuration.

MODEL LB-507A
CONFIGURATION B$_{3B}$ W$_{1B}$ X$_{1B}$
MACH = 0.20
RN$_{MAC}$ = 4.61 × 10^6
δ_{LE} = 12C/27A
δ_{FLAP} = 25/12.5

LIFT COEFFICIENT

ANGLE OF ATTACK-DEG

PITCHING-MOMENT COEFFICIENT

ANGLE OF ATTACK-DEG

STC

N&P	SYM	RUN
ON	O	23
OFF	□	103
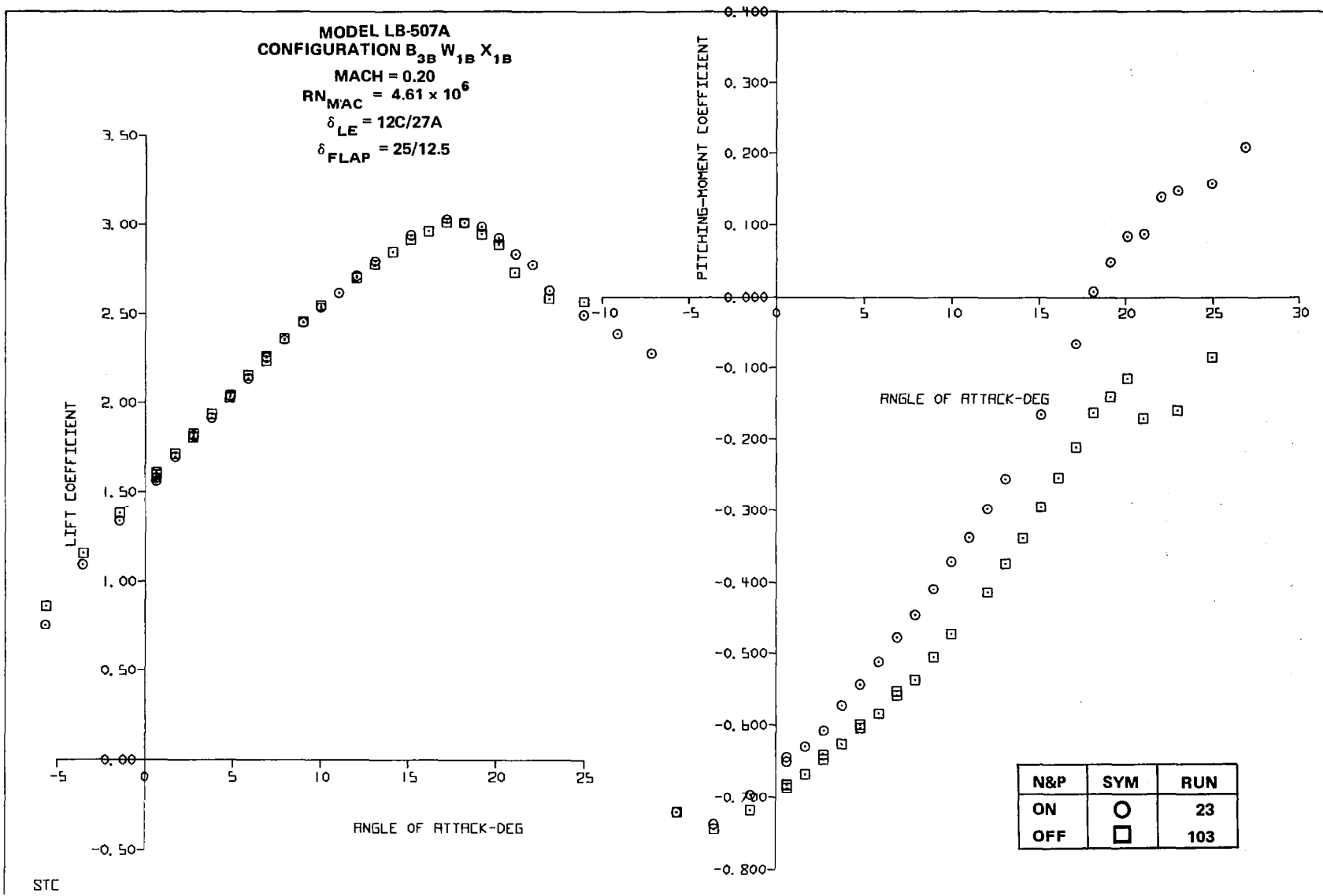
A. LIFT AND PITCHING MOMENT

FIGURE 50. EFFECT OF NACELLES AND PYLONS ON LANDING SLAT CONFIGURATION
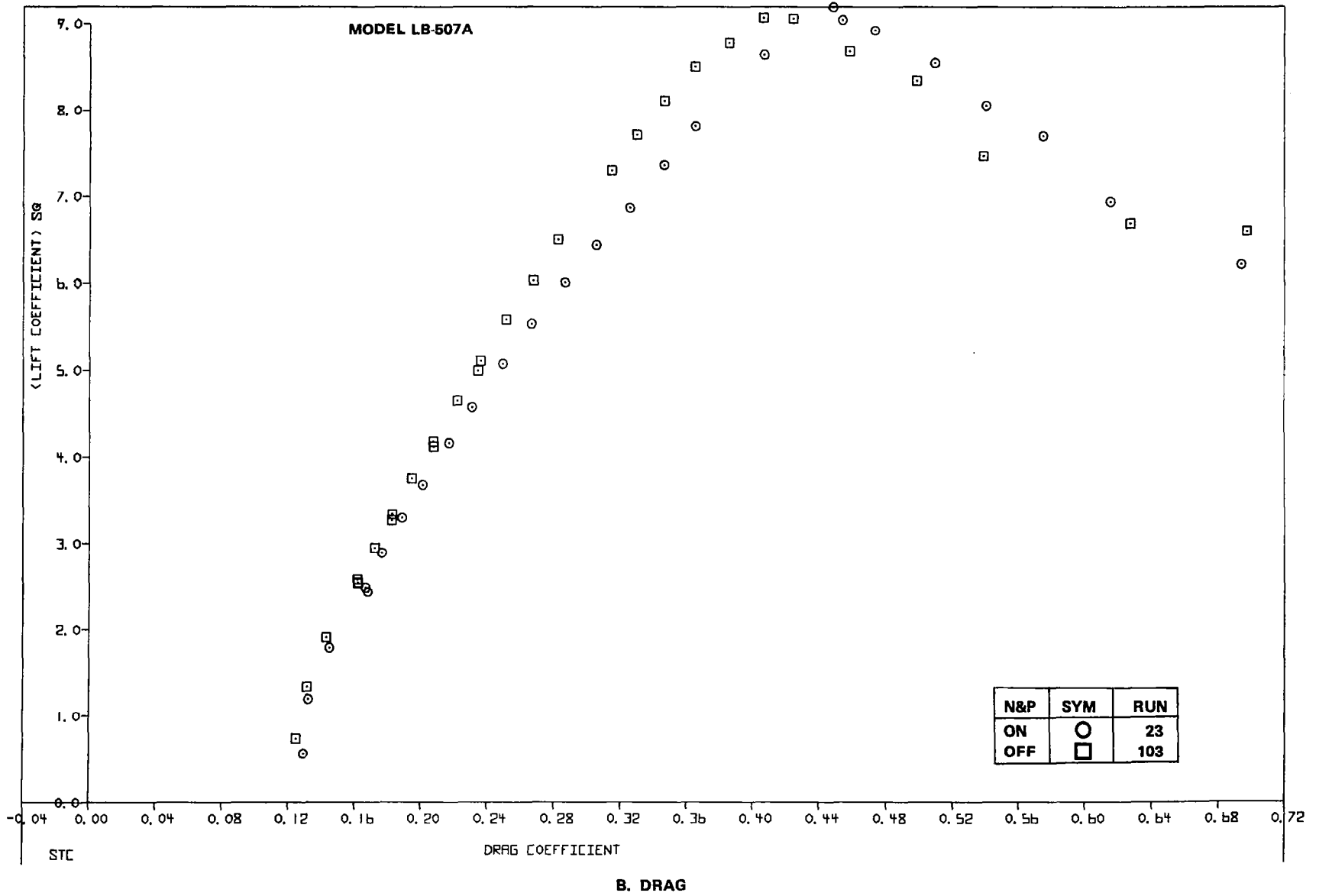
FIGURE 50. EFFECT OF NACELLES AND PYLONS ON LANDING SLAT CONFIGURATION
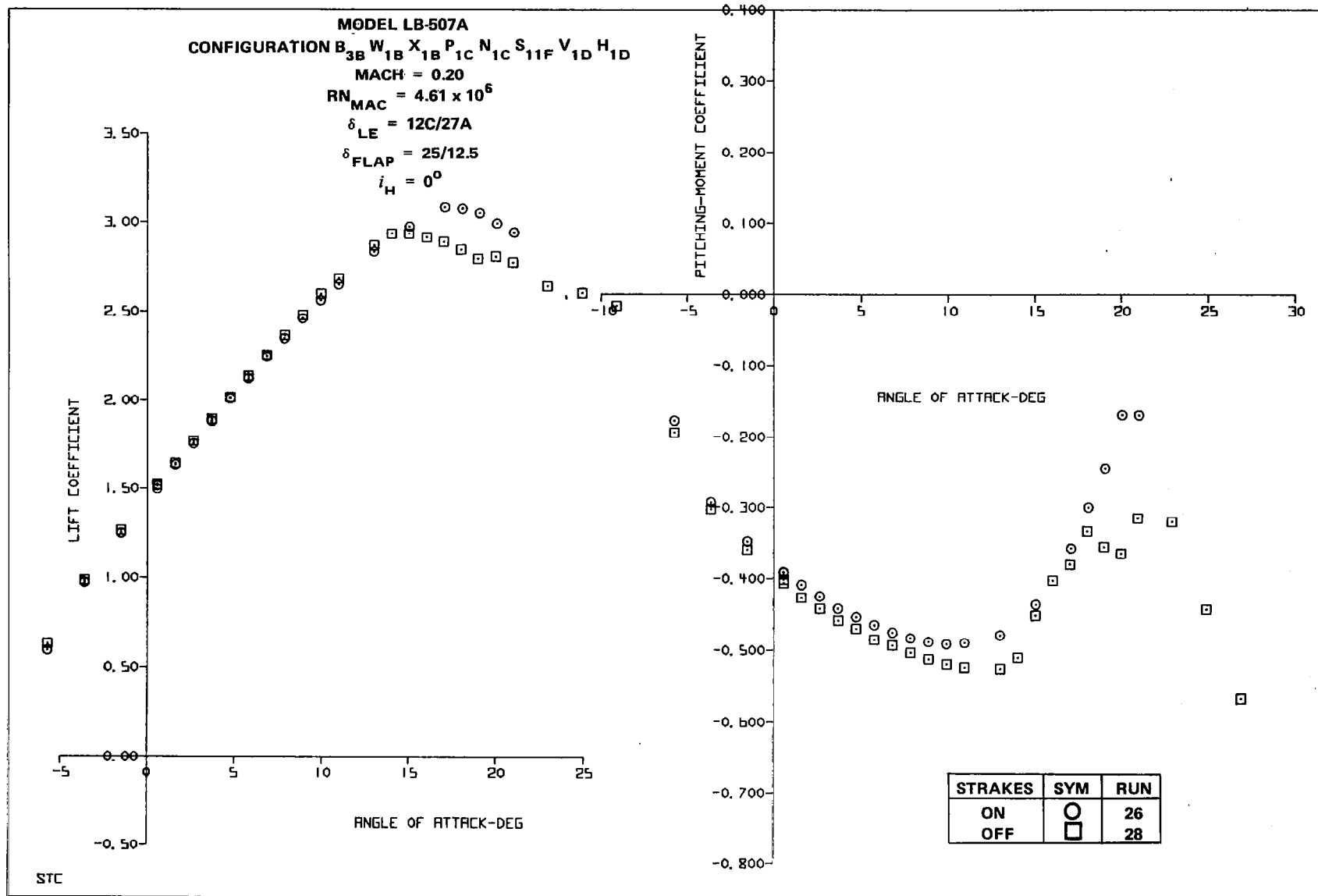
A. LIFT AND PITCHING MOMENT

FIGURE 51. EFFECT OF STRAKES ON LANDING SLAT CONFIGURATION

MODEL LB-507A

STRAKES	SYM	RUN
ON	○	26
OFF	□	28

B. DRAG

FIGURE 51. EFFECT OF STRAKES ON LANDING SLAT CONFIGURATION

MODEL LB-507A

CONFIGURATION $B_{3B} W_{1B} X_{1B} P_{1C} N_{1C} S_{11F} V_{1D} H_{1D}$

MACH = 0.20

RN_{MAC} = 4.61 x 10^6

δ_{LE} = 70A/27A

δ_{FLAP} = 25/12.5

i_H = 0°

PITCHING-MOMENT COEFFICIENT

LIFT COEFFICIENT

ANGLE OF ATTACK-DEG

ANGLE OF ATTACK-DEG

STC

STRAKES	SYM	RUN
ON	◯	48
OFF	☐	49
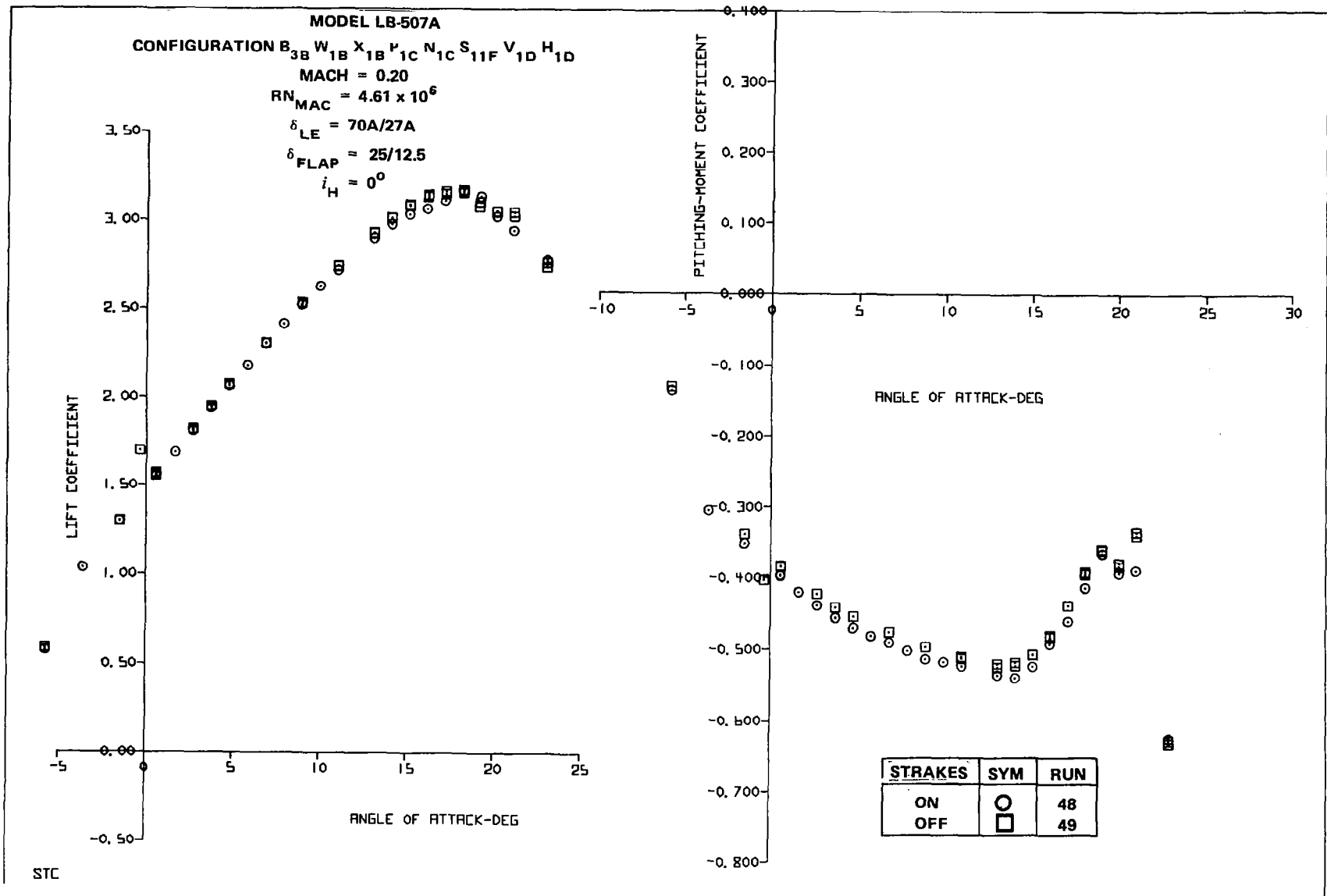
A. LIFT AND PITCHING MOMENT

FIGURE 52. EFFECT OF STRAKES ON LANDING FCK CONFIGURATION
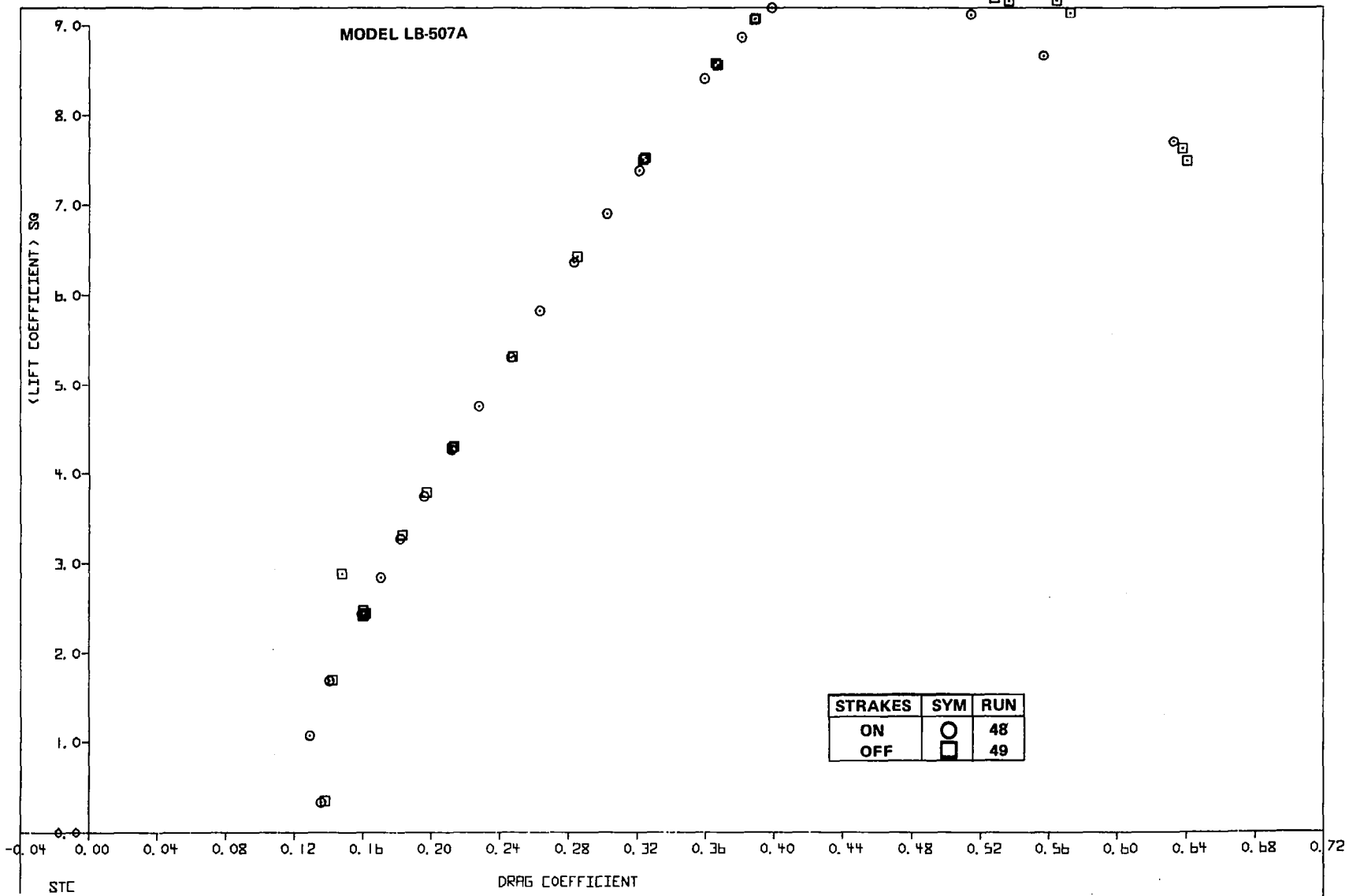
FIGURE 52. EFFECT OF STRAKES ON LANDING FCK CONFIGURATION

Large inboard flap deflection effect.- In addition to testing the baseline landing flap deflection of 25°/12.5°, a deflection of 35°/10° was tested at two different grid positions. The original grid position included a negative overhang of 1%, and resulted in a slight reduction in $C_{L_{MAX}}$ from that of the baseline deflection (Figure 53). Analysis of the mini-tuft photos (Figure 54) and the trailing-edge pressures (Figure 55) indicated that the large deflection caused separation in the trailing-edge region. In order to reduce the extent of trailing-edge separation, a new grid position including a positive overhang of 1 percent was created by extending the spoiler trailing edge. As the mini-tuft photos and trailing-edge pressures show, the positive overhang was effective in reducing trailing-edge separation problems. $C_{L_\alpha = 0}$ increased by nearly 0.20 and $C_{L_{MAX}}$ increased compared to the baseline but only by 0.03. The large deflection did, however, result in a large drag increment at $1.3V_s$ (0.0405 and 0.0270 for the negative and positive overhang cases, respectively).

Takeoff Configuration Characteristics

Most of the work accomplished with takeoff configurations was directed toward the use of sealed (zero gap) slats. The advantage of the sealed slat is that it results in appreciably higher L/D values. The disadvantages are that it provides lower values of $C_{L_{MAX}}$ and can result in poor stalling characteristics, particularly if a small amount of yaw is present at stall. Figure 56 compares data for the slotted and sealed outboard slats with an FCK deflected at 55° inboard. The slat grid 20A was completely sealed, the grid 20B had a small gap, and the grid 27A had a normal gap. As the gap was decreased, the tail-off $C_{L_{MAX}}$ decreased from 2.55 to 2.40 and the pitching moments became more positive. The L/D values at $1.2V_s$, on the other hand, increased from 11.97 to 12.87. The mini-tuft photographs of Figure 57 clearly show the earlier separation of the outboard panel for the sealed slat configuration.

MODEL LB-507A
CONFIGURATION $B_{3B} W_{1B} X_{1B} P_{1C} N_{1C} S_{11F}$
MACH = 0.20
$RN_{MAC} = 4.61 \times 10^6$
$\delta_{LE} = 12C/27A$

LIFT COEFFICIENT

ANGLE OF ATTACK-DEG

PITCHING-MOMENT COEFFICIENT

ANGLE OF ATTACK-DEG

δ_{FLAP}	O.H.	SYM	RUN
35/10	−1%	○	31
35/10	+1%	□	104
25/12.5		◇	23

STC
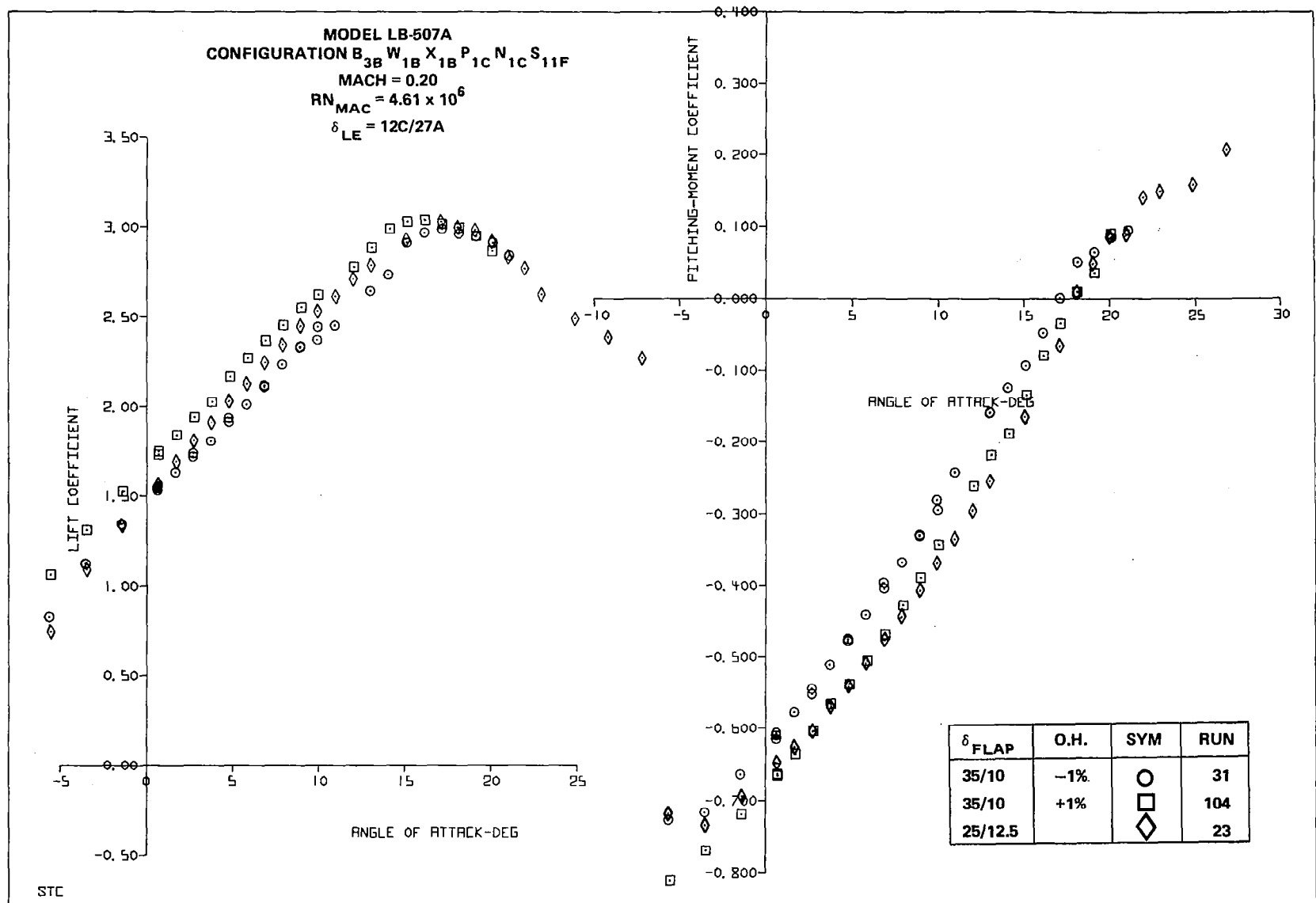
A. LIFT AND PITCHING MOMENT

FIGURE 53. EFFECT OF LARGE FLAP DEFLECTION

109
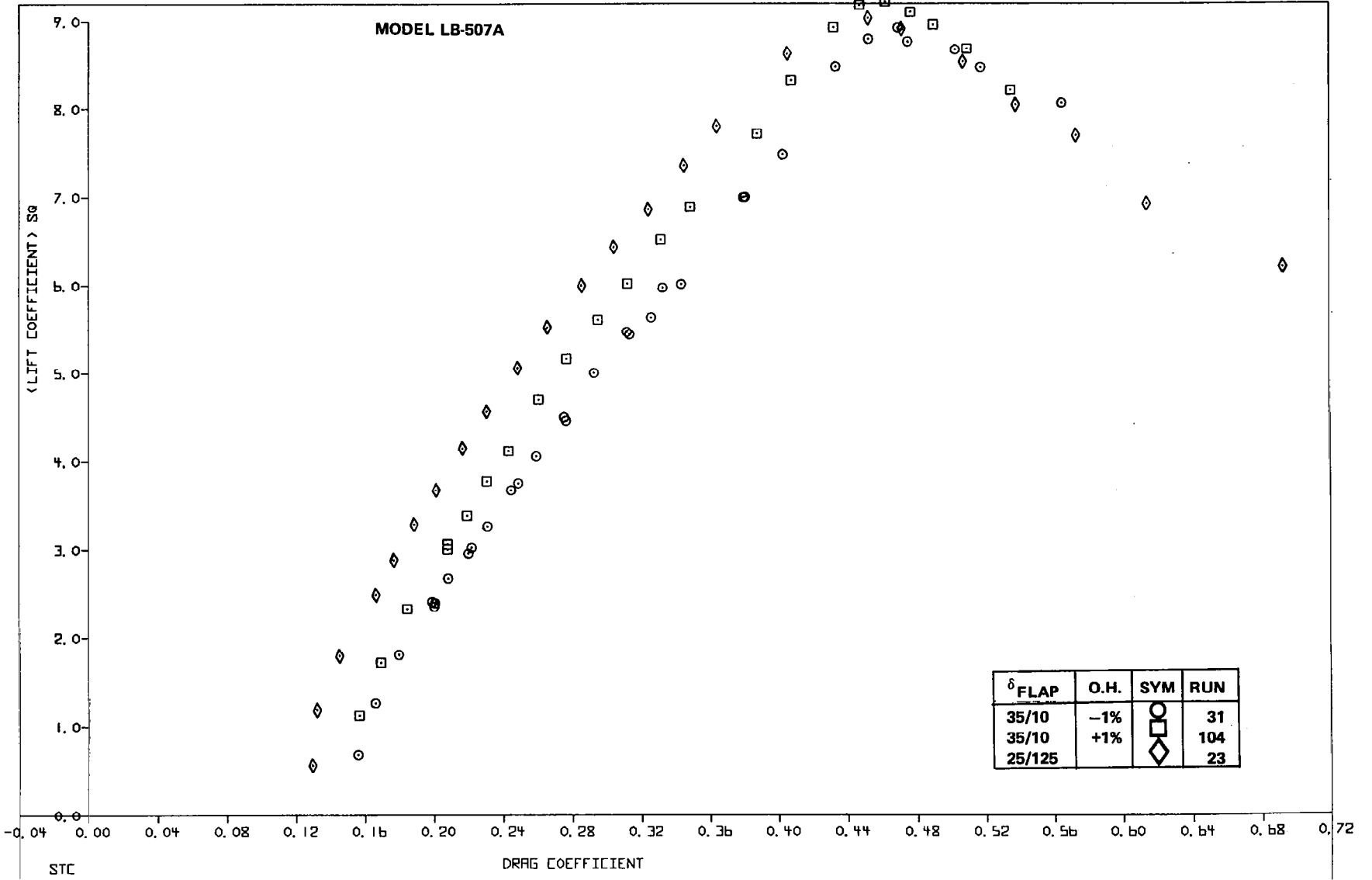
FIGURE 53. EFFECT OF LARGE FLAP DEFLECTION
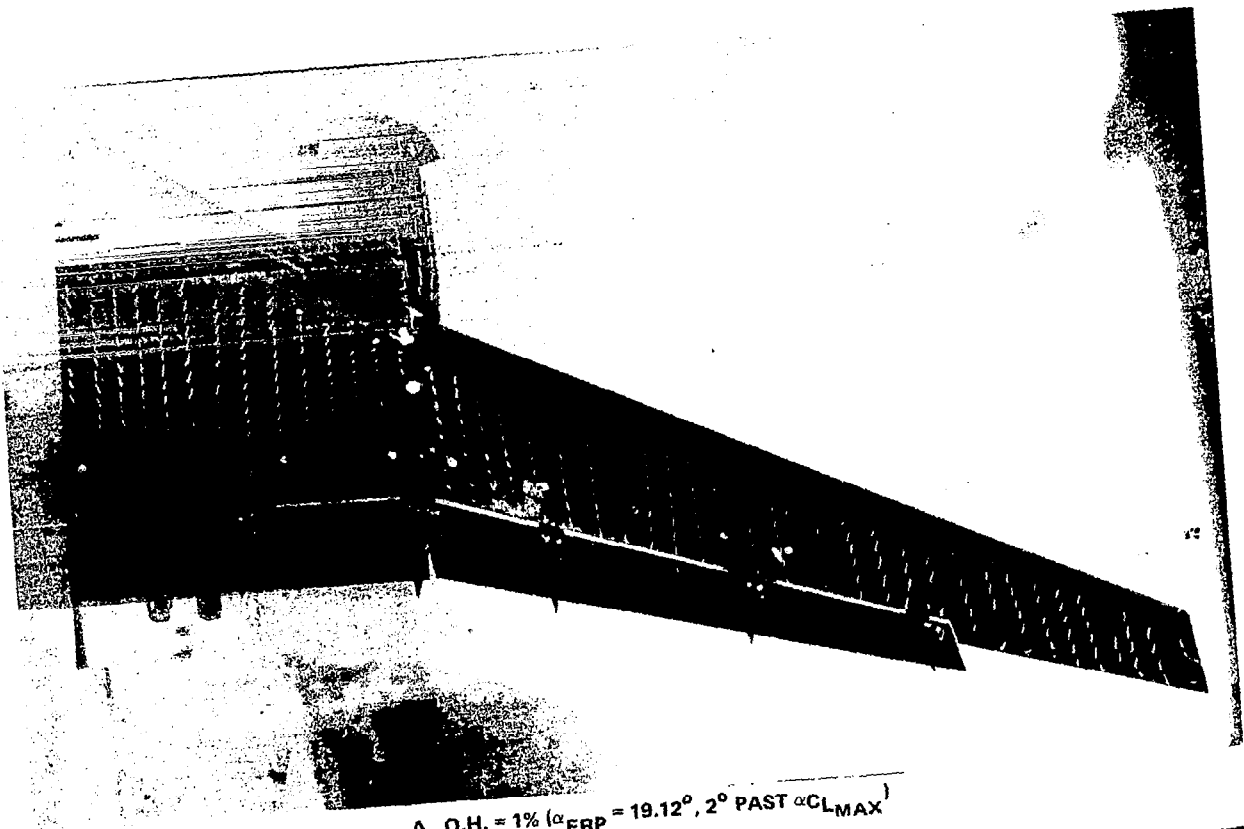
A. O.H. = 1% (α_{FRP} = 19.12°, 2° PAST $\alpha_{C_{L_{MAX}}}$)
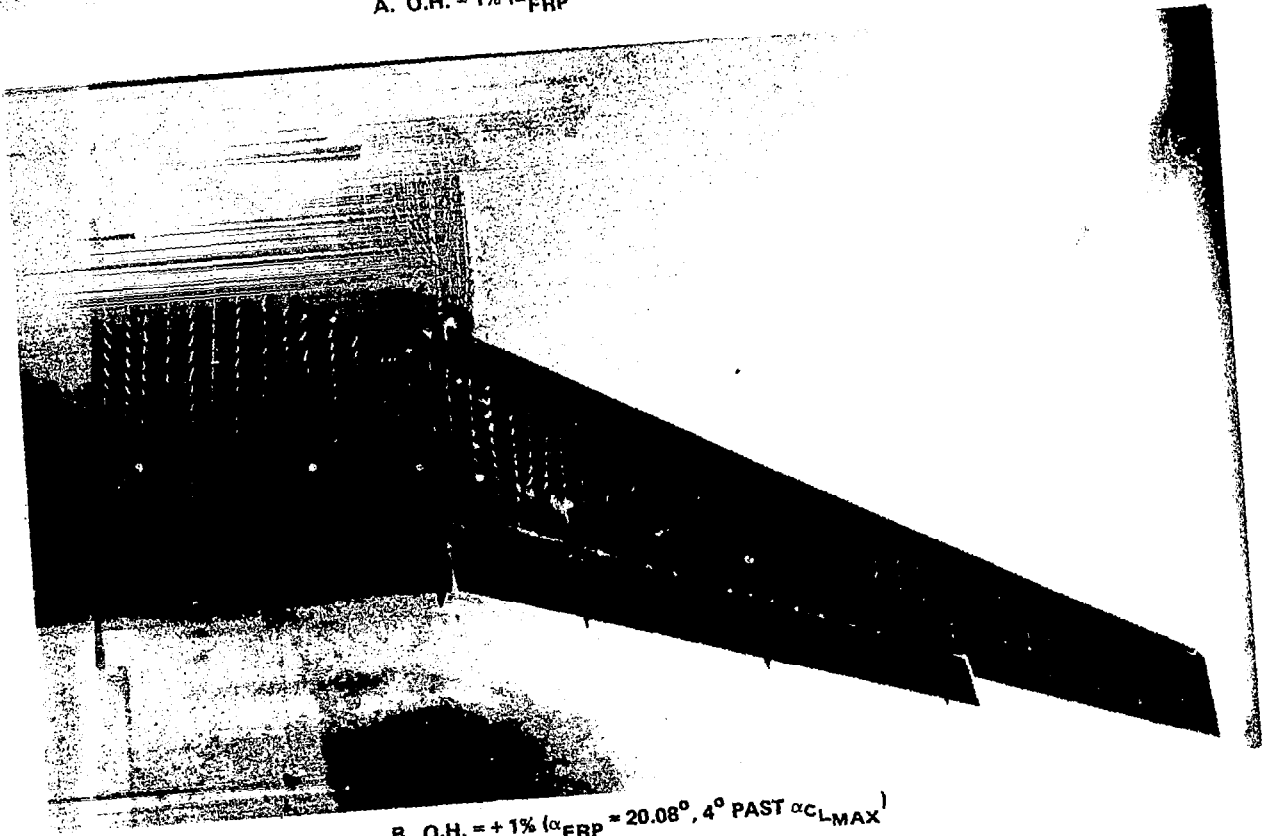
B. O.H. = + 1% (α_{FRP} = 20.08°, 4° PAST $\alpha_{C_{L_{MAX}}}$)

FIGURE 54. MINI-TUFT PHOTOS FOR 35° FLAP DEFLECTION CONFIGURATIONS

111

MODEL LB-507A
CONFIGURATION B_{3B} W_{1A} X_{1A} P_{1C} N_{1C}
M = 0.20
RN_{MAC} = 4.61 x 10^6
δ_{LE} = 12C/27A
TAIL OFF
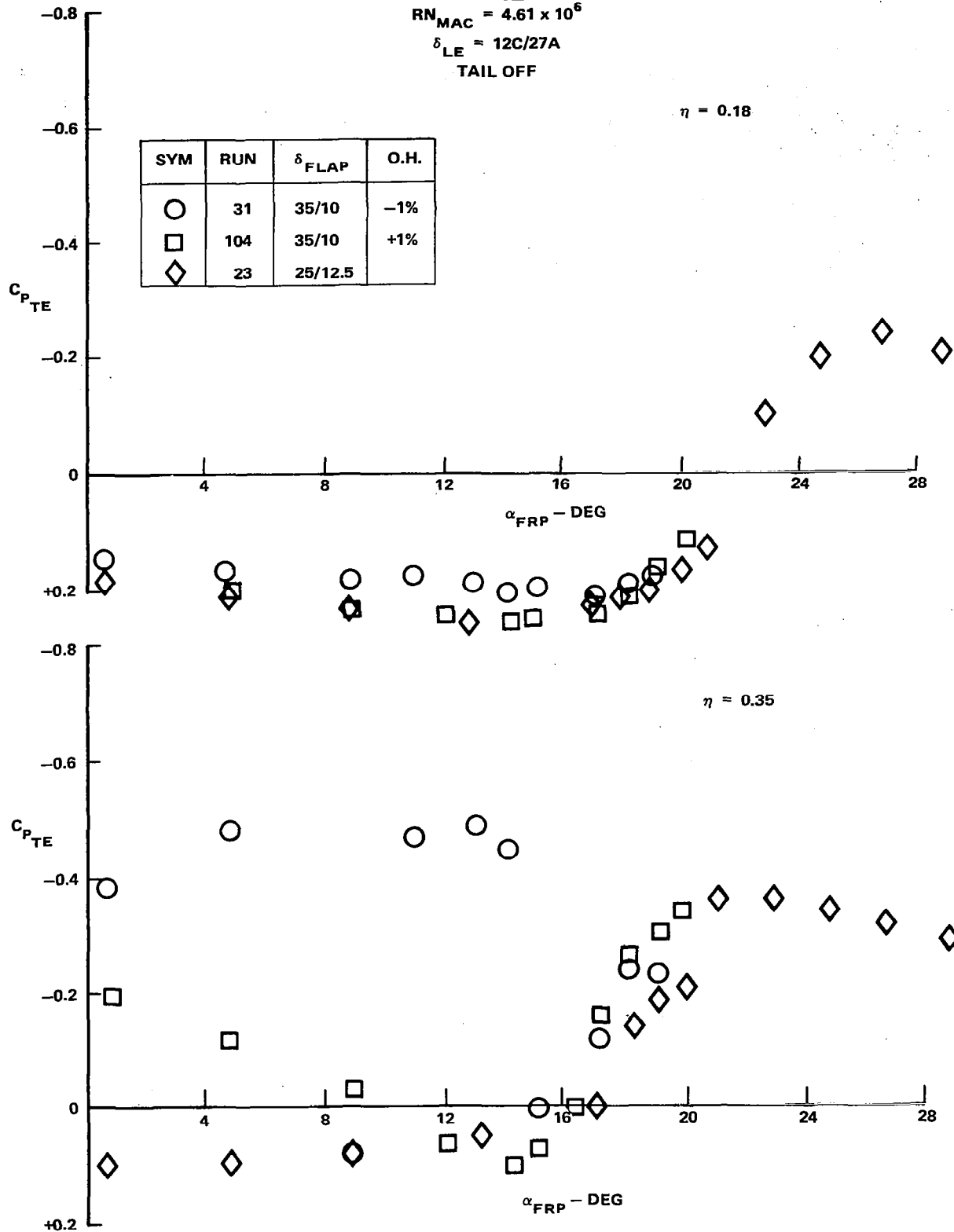
FIGURE 55. EFFECT OF LARGE FLAP DEFLECTION ON TRAILING EDGE PRESSURES

112
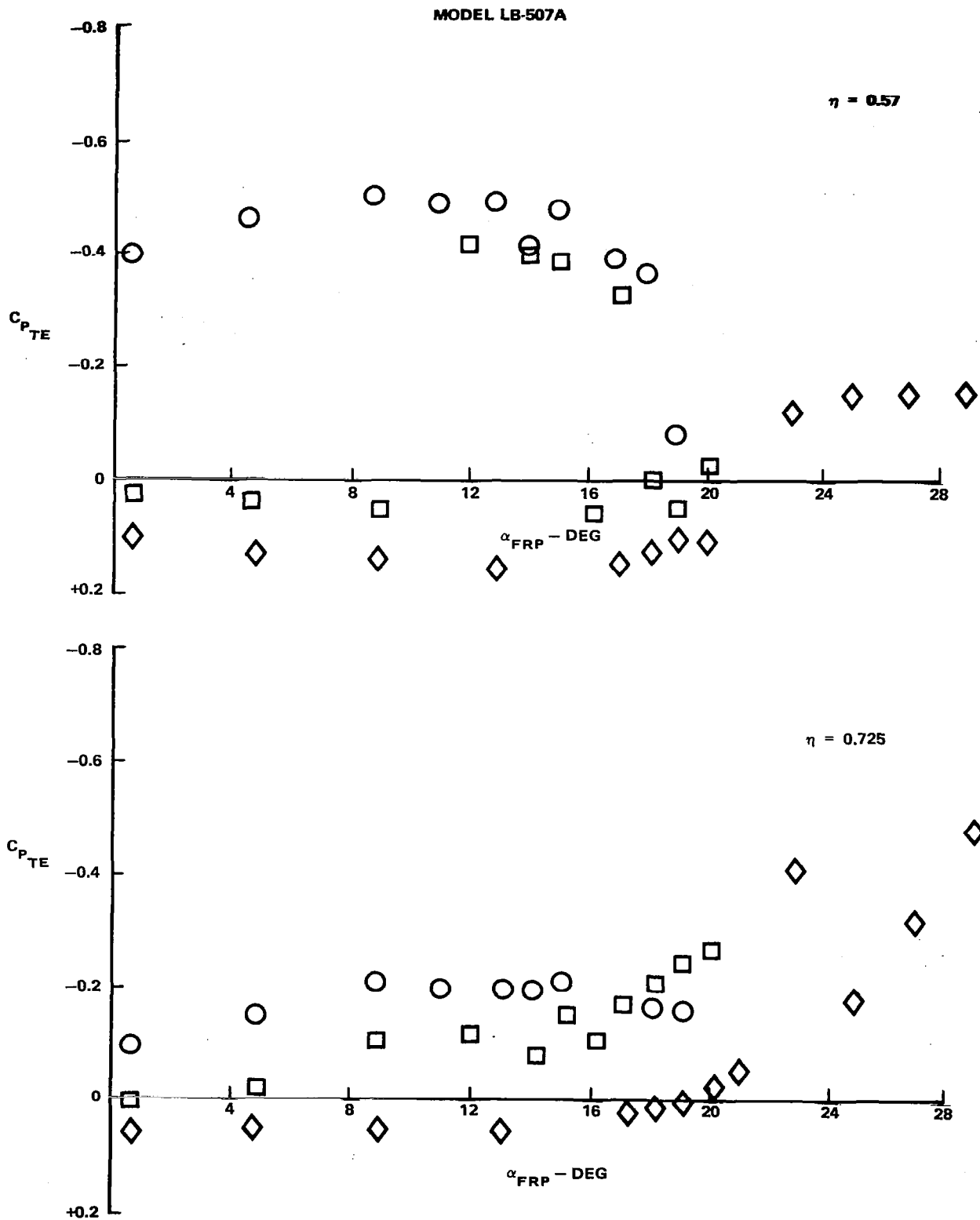
FIGURE 55. EFFECT OF LARGE INBOARD FLAP DEFLECTION ON TRAILING EDGE PRESSURES
(CONCLUDED)

MODEL LB-507A
CONFIGURATION $B_{3B} W_{1B} X_{1A} P_{1C} N_{1C} S_{11F}$

MACH = 0.20
$RN_{MAC} = 4.61 \times 10^6$
$\delta_{FLAP} = 5/10$

SYM	RUN	δ_{FCK}	δ_{SLAT}
◯	64	55A	27A
☐	65	55A	20B
◇	66	55A	20A
△	67	0	20A

STC
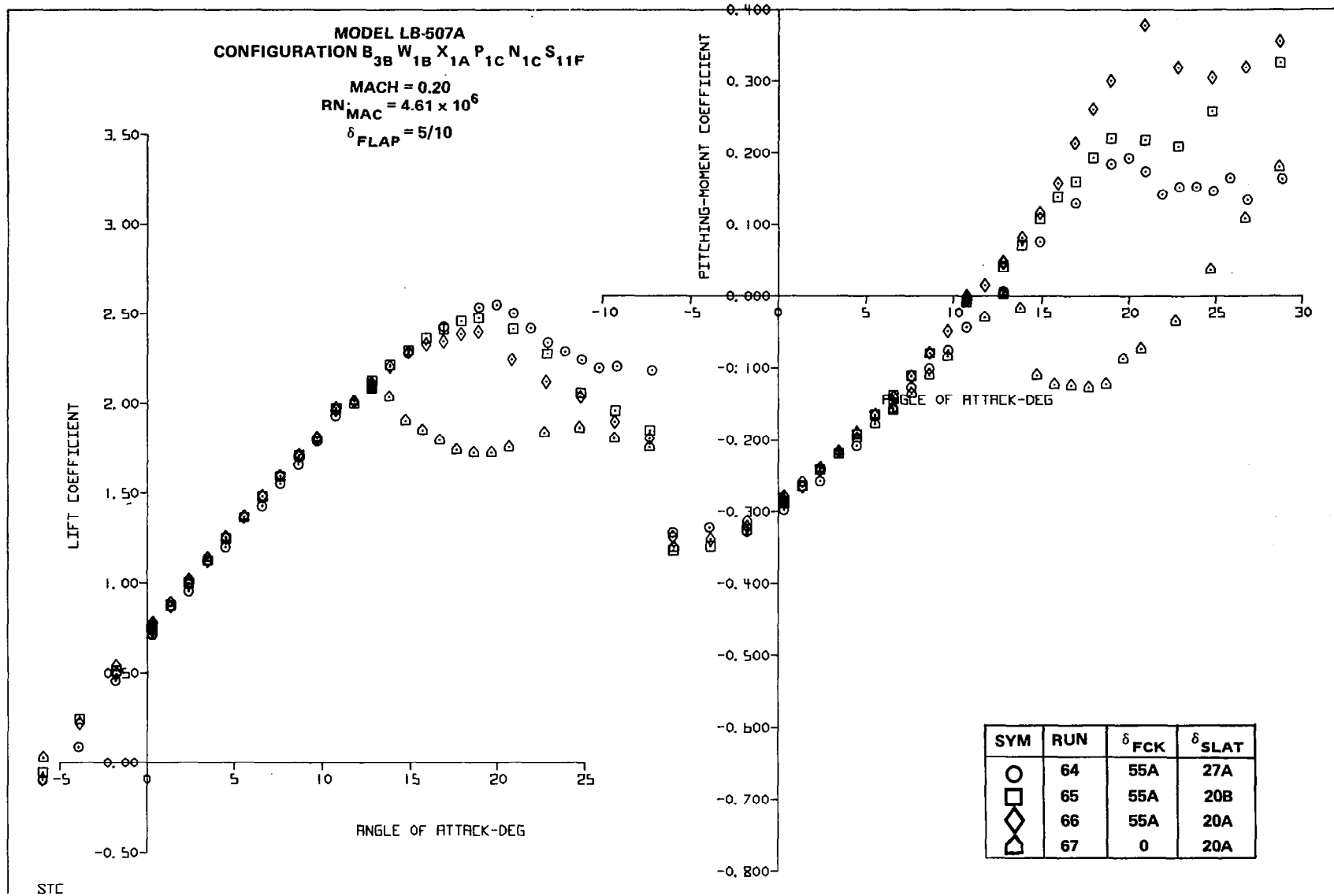
A. LIFT AND PITCHING MOMENT

FIGURE 56. OUTBOARD SLAT GRID OPTIMIZATION WITH FCK INBOARD
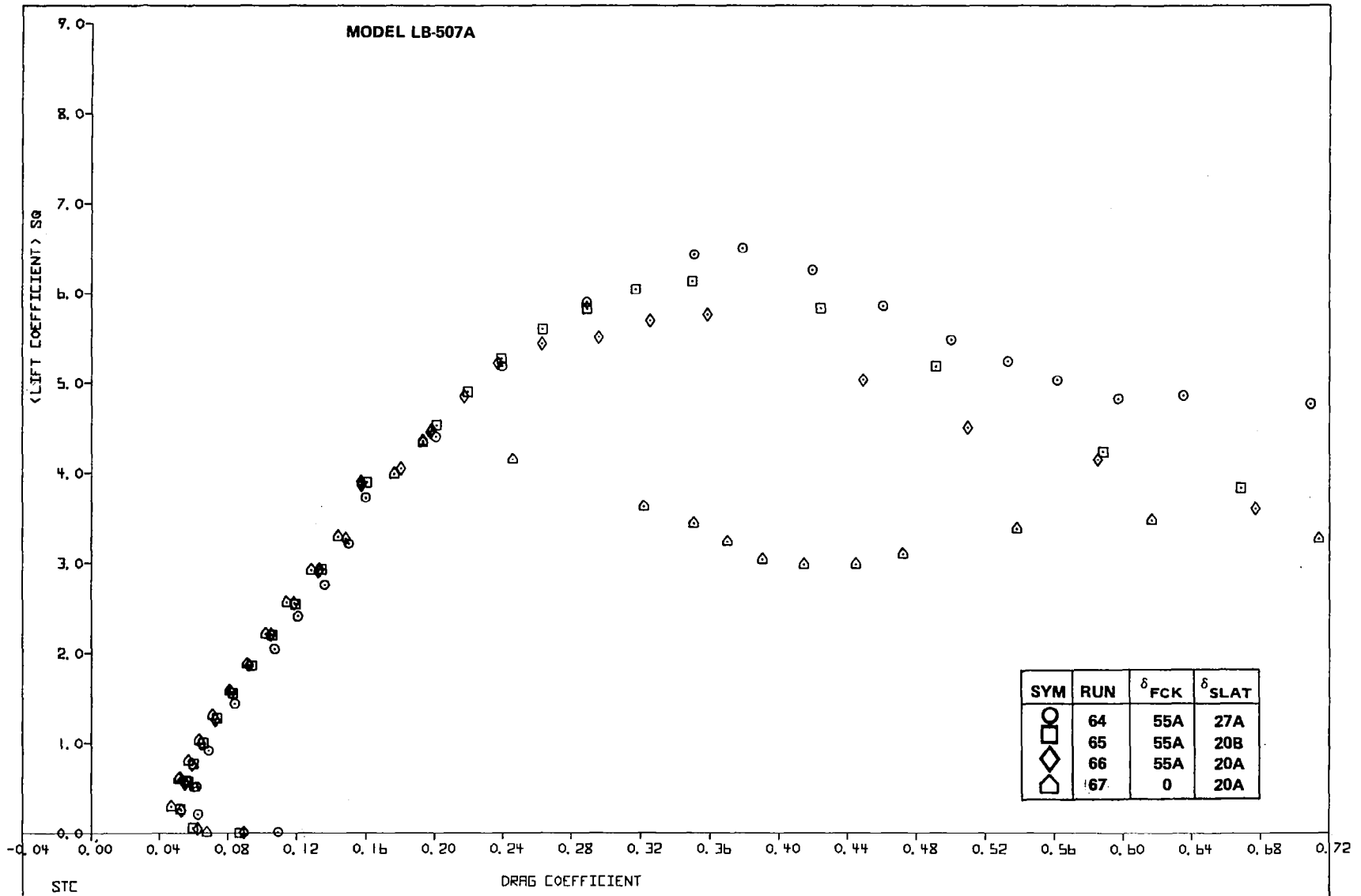
FIGURE 56. OUTBOARD SLAT GRID OPTIMIZATION WITH FCK INBOARD

B. DRAG
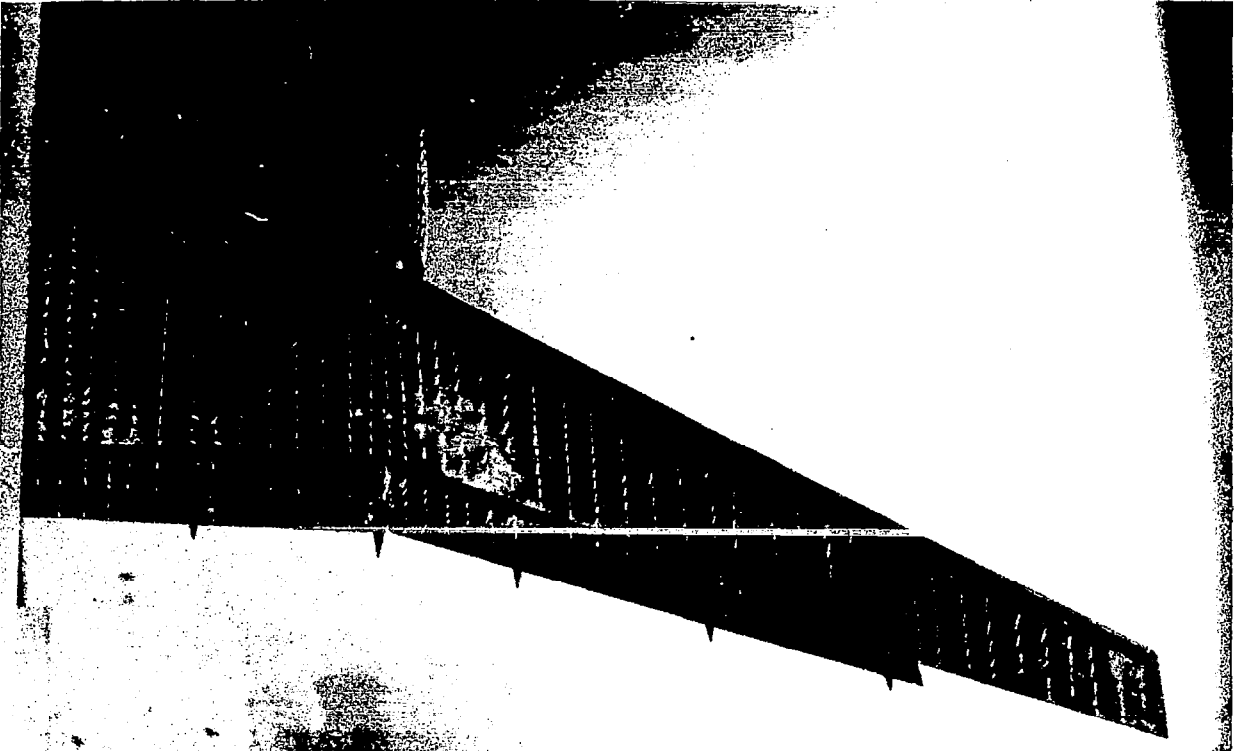
A. SLOTTED SLAT OUTBOARD, $\alpha_{FRP} = 20.94^{o}$
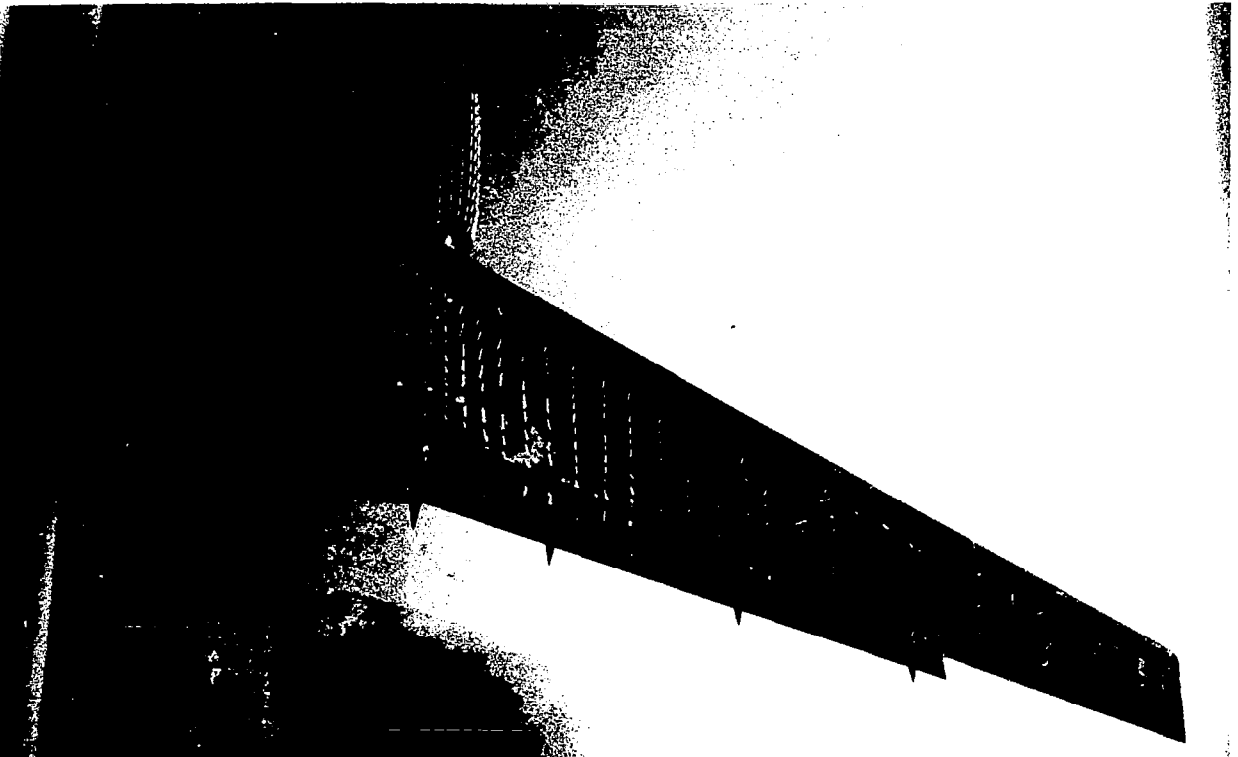
B. SEALED SLAT OUTBOARD, $\alpha_{FRP} = 20.85^{o}$

FIGURE 57. MINI-TUFT PHOTO OF TAKEOFF CONFIGURATION SHOWING EFFECT OF OUTBOARD SEALED SLAT

Figure 58 compares the results of a sealed slat outboard with three different inboard leading-edge configurations: a slotted FCK, a sealed slat, and a clean leading edge. Because of the early stall of the inboard wing not protected by a leading-edge device, the $C_{L_{MAX}}$ of the clean configuration was very low (2.09) and the pitching moments were very well behaved. The $C_{L_{MAX}}$ of the inboard sealed-slat configuration was 2.24 while that of the slotted FCK was 2.40. The pitching-moment trends of the FCK and the sealed slat were similar: both showed nose-down moments just after stall, even in the absence of a tail. The respective values of L/D at $1.2V_s$ for the inboard clean leading edge, sealed slat, and FCK are 14.59, 13.50, and 13.57, respectively.

One concern with the sealed slats is that they can result in lateral instability when stall occurs under a yawed condition. This tendency is illustrated in Figure 59. With a sealed slat outboard, the inboard sealed-slat configuration became laterally unstable at α_{FRP} = 19°; the FCK at α_{FRP} = 17.5°. However, with a slotted slat outboard, the FCK/slat configurations remained laterally stable throughout the angle-of-attack range investigated (Figure 60).

Strakes effects.- Figure 61 shows that the addition of nacelle strakes to the takeoff configuration with sealed slats inboard and outboard caused only small changes in the lift and drag characteristics. The $C_{L_{MAX}}$ increment due to the strakes in conjunction with takeoff flaps and slats, 0.06, was less than half that for the landing flaps and slats case, 0.14. As was the case with clean wing and landing configurations, the strakes were detrimental to the pitching-moment characteristics.

Mach number and Reynolds number effects.- Figures 62 and 63 show the effect of Mach number and Reynolds number, respectively, on the aerodynamic characteristics of the takeoff configuration with an FCK inboard and a sealed slat outboard. As the Mach number was increased from 0.20 to 0.32, $C_{L_{MAX}}$ decreased from 2.20 to 2.15 and the pitching moments degraded slightly. Below $C_{L_{MAX}}$, the drag polar was insensitive to Mach number. The $C_{L_{MAX}}$ versus Reynolds number curve of Figure 63 suggests that the maximum lift coefficient will continue to increase as the Reynolds number increases towards the flight value.

MODEL LB-507A

CONFIGURATION $B_{3B} W_{1B} X_{1B} P_{1C} N_{1C} S_{11F}$

MACH = 0.20

RN_{MAC} = 4.61 x 10^6

δ_{LE} = XX/20A

δ_{FLAP} = 5/10

SYM	RUN	INBOARD LE DEVICE		δ
○	66	FCK		55A
□	67	CLEAN		
◇	83	SEALED SLAT		8A

STC
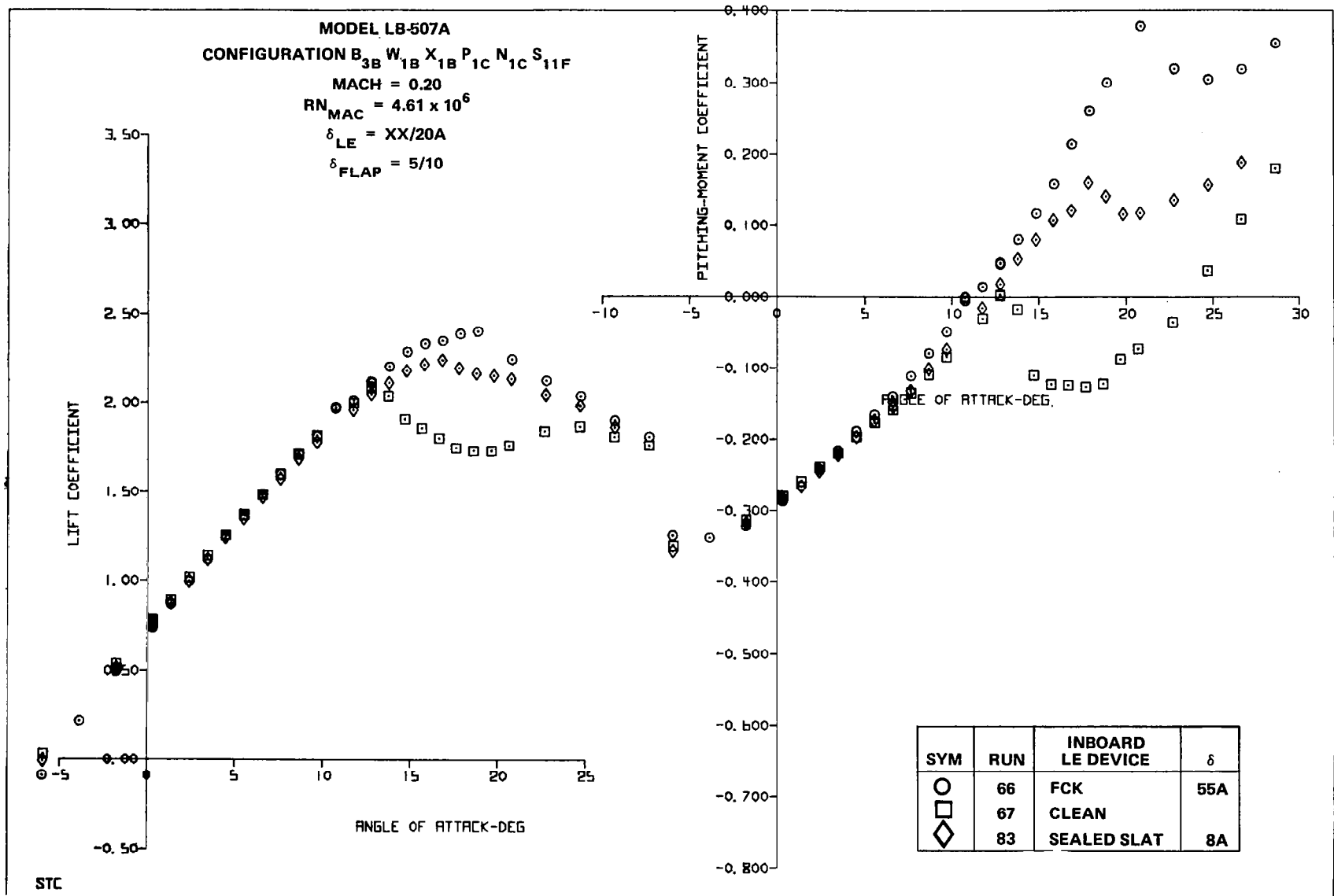
A. LIFT AND PITCHING MOMENT
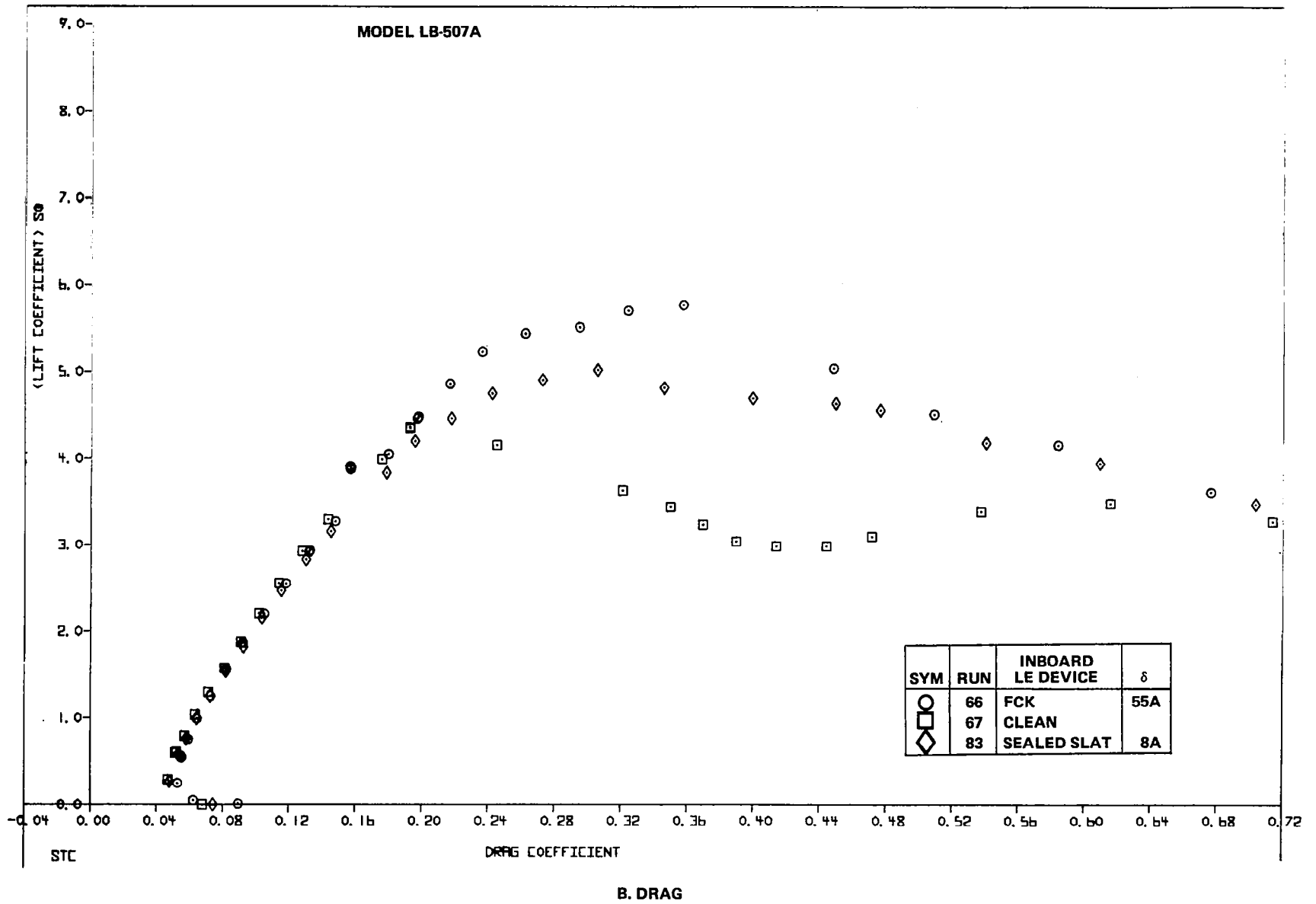
FIGURE 58. EFFECT OF INBOARD LEADING EDGE DEVICE WITH A SEALED SLAT OUTBOARD

FIGURE 58. EFFECT OF INBOARD LEADING EDGE DEVICE WITH A SEALED SLAT OUTBOARD

MODEL LB-507A
CONFIGURATION $B_{3B} W_{1B} X_{1B} P_{IC} N_{IC} H_{1A} V_{1A}$
MACH = 0.20
$RN_{MAC} = 4.61 \times 10^6$
$\delta_{FLAP} = 25/10$
$i_H = 0°$

STABLE

$(\Delta C_\ell)_{\Delta\beta=-5°}$

$C_{L_{MAX}}$

$\delta_{LE} = 55A/20A$
$\delta_{LE} = 8A/20A$
$\delta_{LE} = CLEAN/20A$

0.05

0.04

0.02

−10   −5   0   5   10   15   20   25   30

STABLE

−0.03

$(\Delta C_n)_{\Delta\beta=-5°}$

$C_{L_{MAX}}$

$C_{L_{MAX}}$

−0.02

−0.01

−10   −5   0   5   10   15   20   25   30

ANGLE OF ATTACK (DEG)
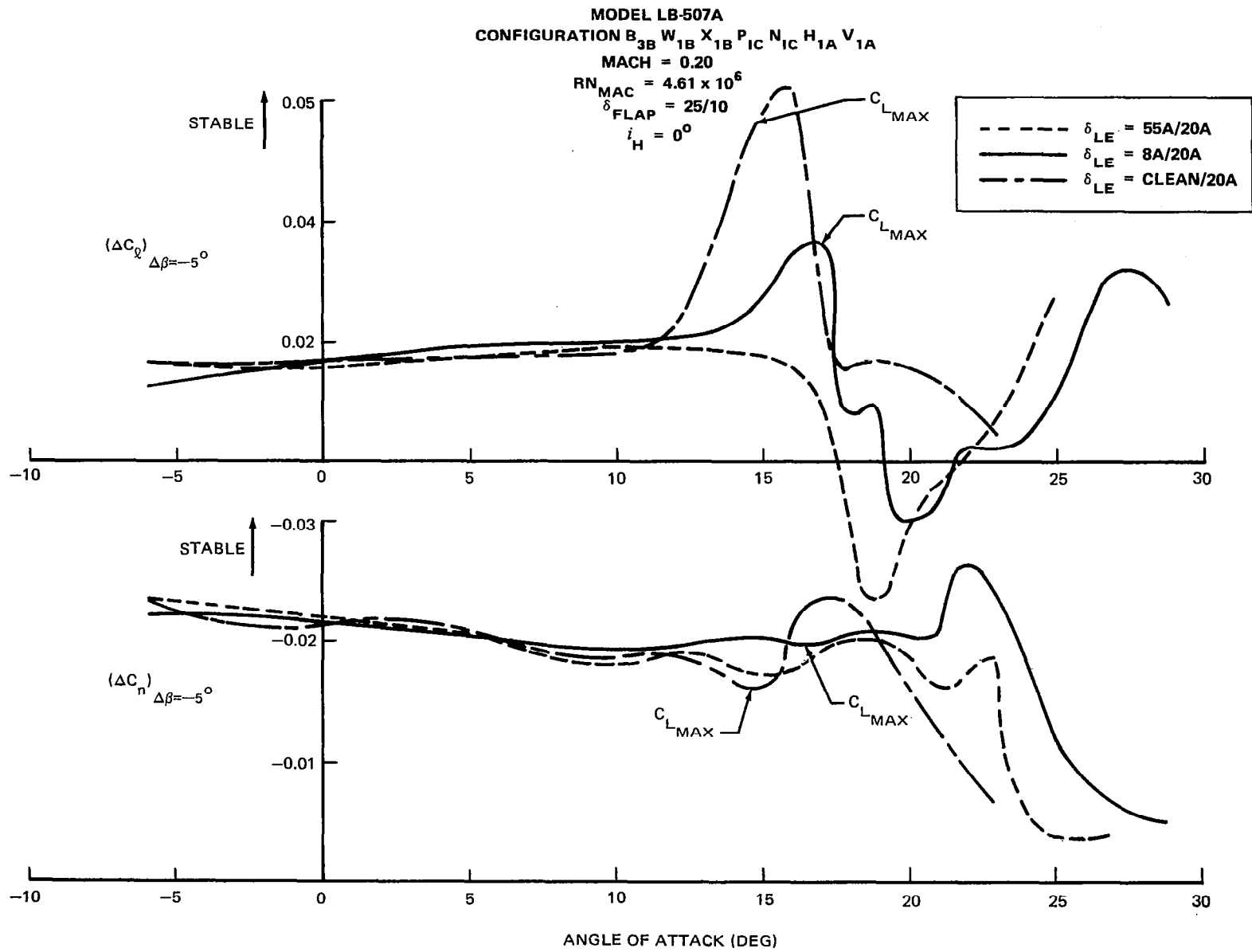
FIGURE 59.   EFFECT OF SLATS ON ROLLING AND YAWING MOMENTS THROUGH STALL
WITH SIDESLIP

MODEL LB-507A
CONFIGURATION B_{3B} W_{1B} X_{1B} P_{IC} N_{IC} G_{1A}
MACH = 0.20
RN_{MAC} = 4.61 x 10^6
δ_{FLAP} = 25/12°

STABLE

$(\Delta C_\ell)_{\Delta\beta=-5°}$

δ_{LE} = 70A/27A
δ_{LE} = 55A/27A

$C_{L_{MAX}}$

$C_{L_{MAX}}$

ANGLE OF ATTACK (DEG)
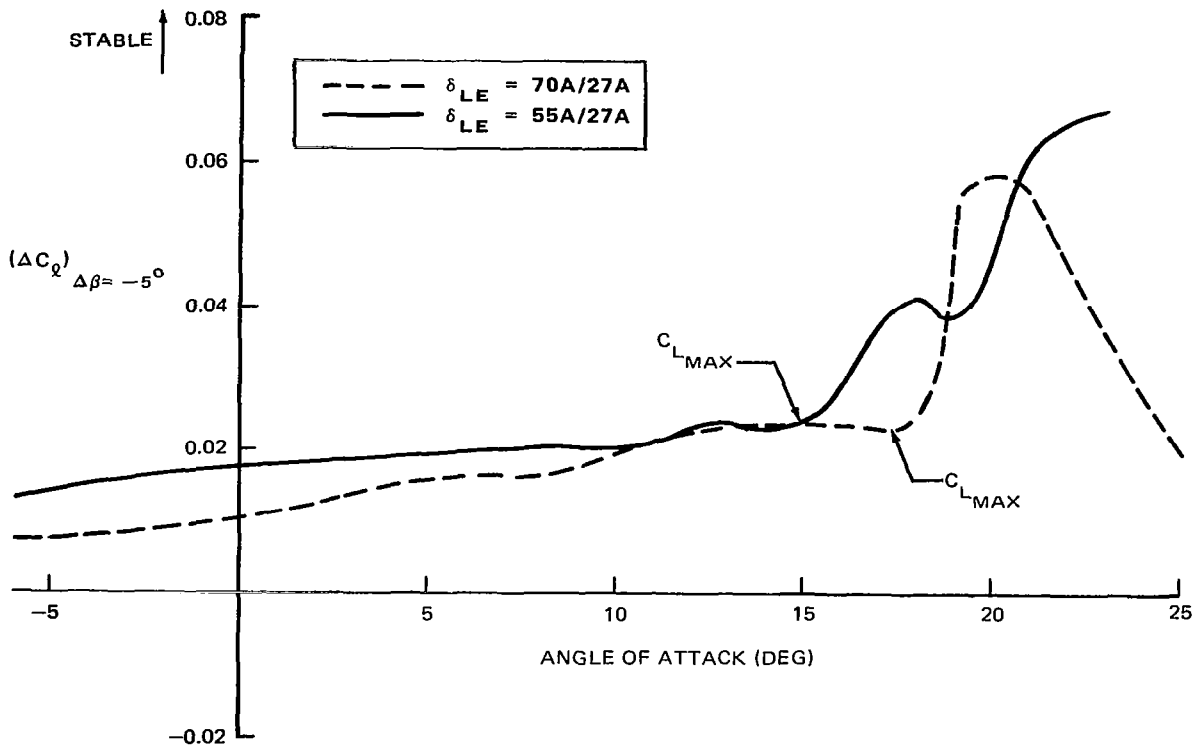
FIGURE 60. EFFECT OF INBOARD FCK SLAT DEFLECTION ON ROLLING MOMENT THROUGH STALL WITH SIDESLIP

121

MODEL LB-507A

CONFIGURATION $B_{3B} W_{1B} X_{1B} P_{1C} N_{1C} S_{11F} V_{1D} H_{1D}$

MACH = 0.20

$RN_{MAC} = 4.61 \times 10^6$

$\delta_{LE} = 8A/20A$

$\delta_{FLAP} = 5/10$

$i_H = 0$

LIFT COEFFICIENT

ANGLE OF ATTACK-DEG

PITCHING-MOMENT COEFFICIENT

ANGLE OF ATTACK-DEG

STC

STRAKES	SYM	RUN
ON	O	72
OFF	□	77
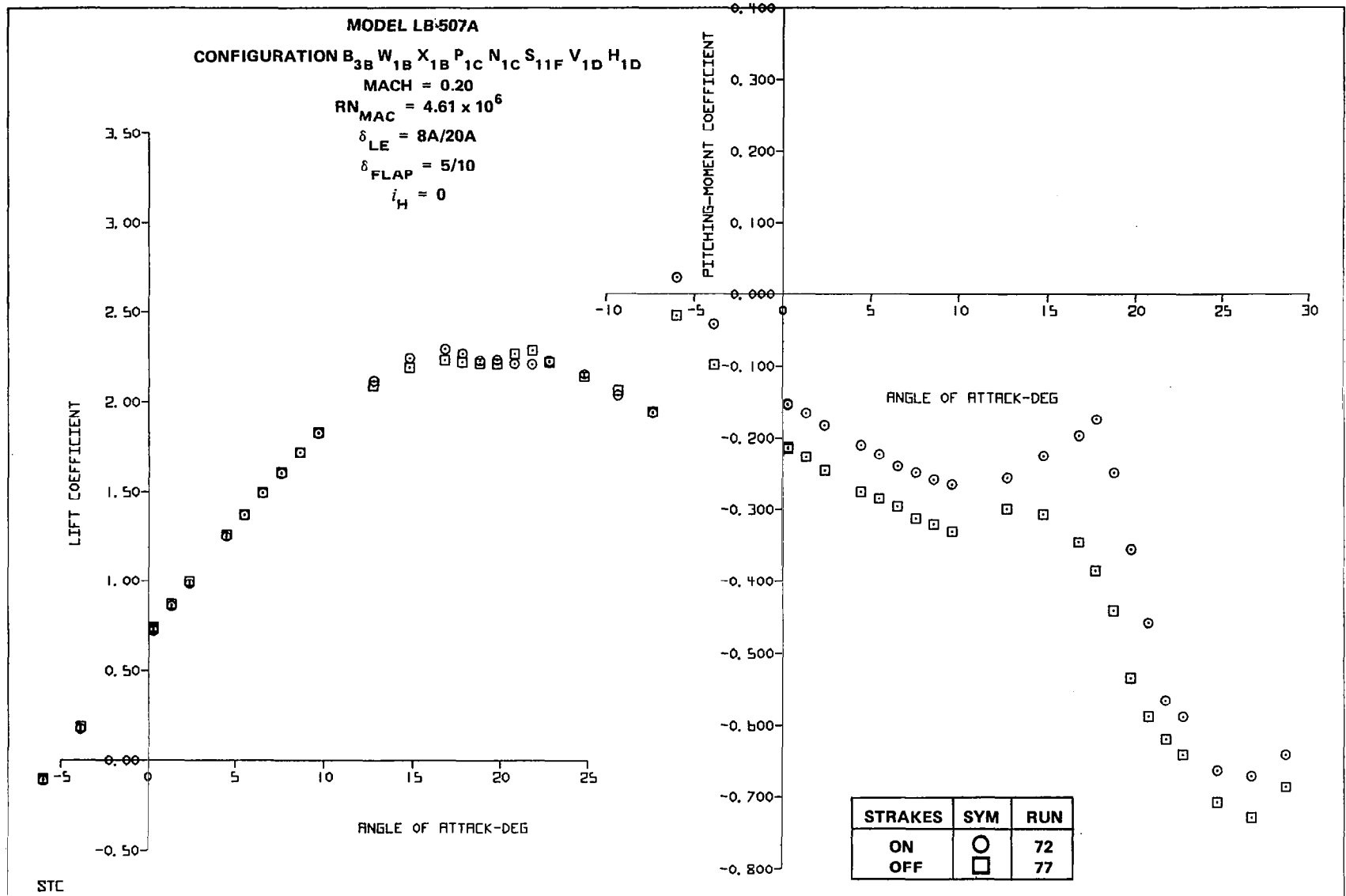
A. LIFT AND PITCHING MOMENT

FIGURE 61. EFFECT OF STRAKES WITH TAKEOFF FLAPS AND SEALED SLATS
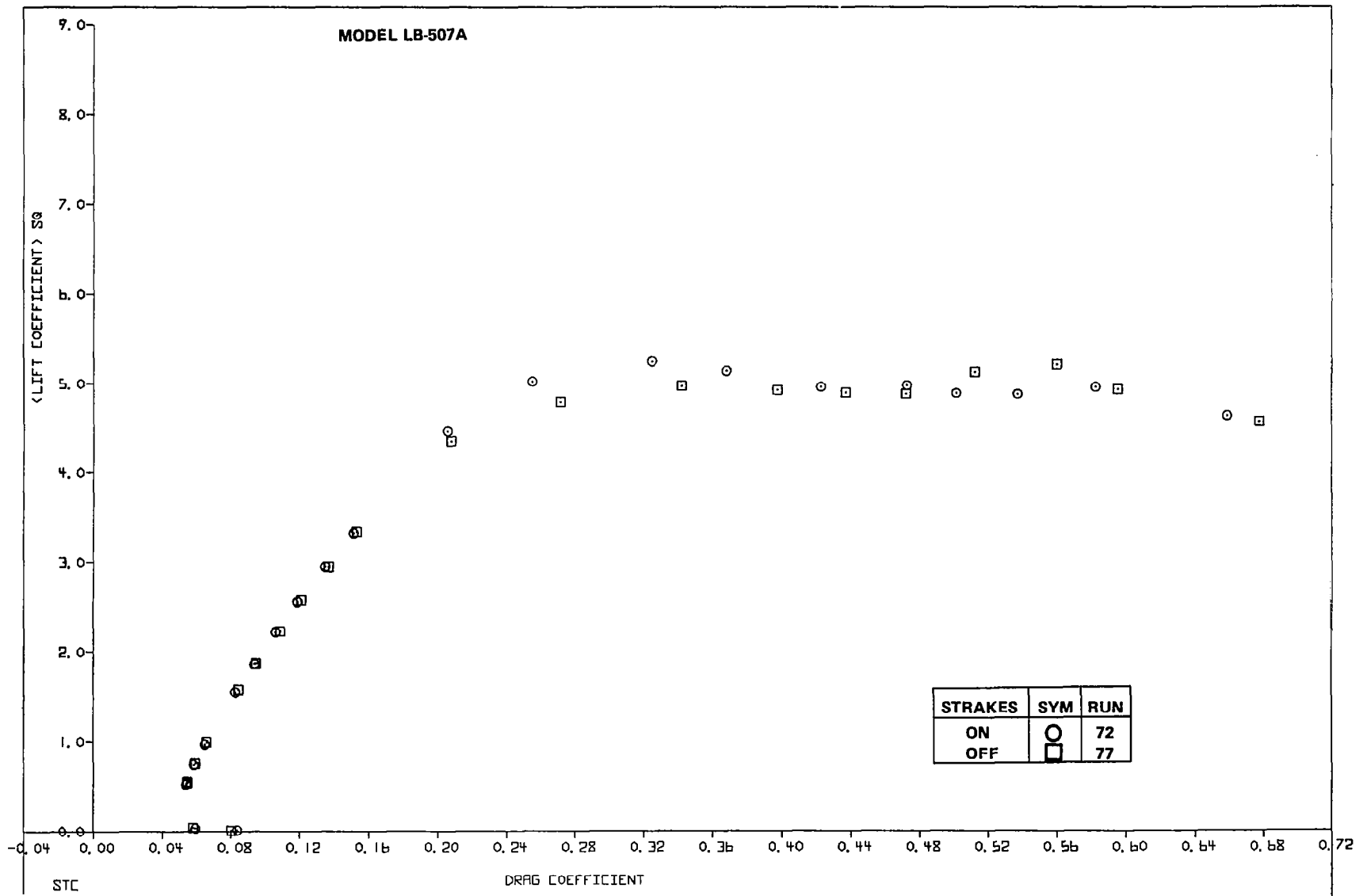
FIGURE 61. EFFECT OF STRAKES WITH TAKEOFF FLAPS AND SEALED SLATS

MODEL LB-507A
CONFIGURATION $B_{3B} W_{1B} X_{1B} N_{1C} P_{1C} S_{11F}$

$RN_{MAC} = 2.60 \times 10^6$

$\delta_{FLAP} = 5/10$

$\delta_{LE} = 55A/20A$

SYM	RUN	MACH	$C_{L\,MAX}$
◯	87	0.20	2.20
□	88	0.26	2.20
◇	89	0.32	2.15

STC
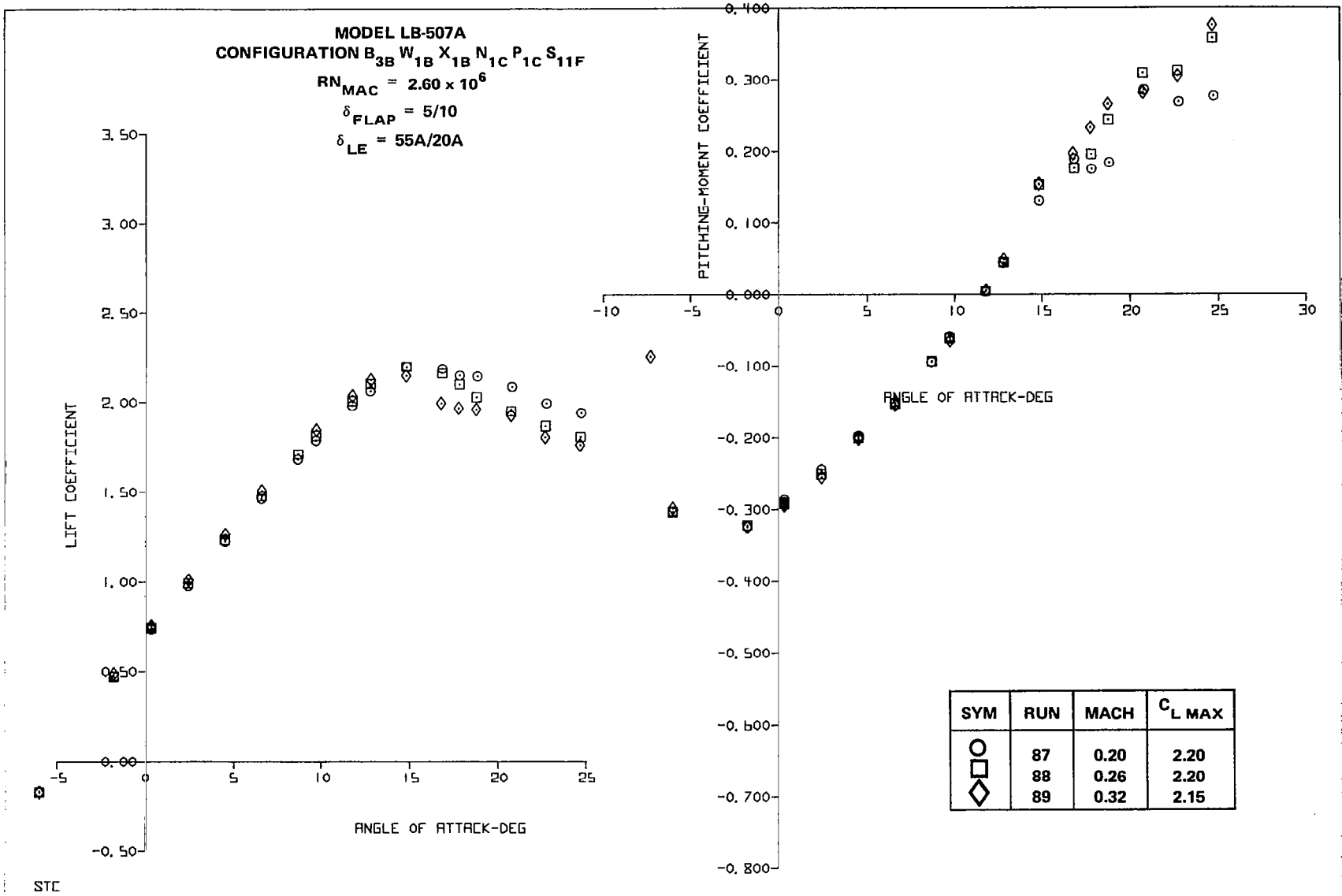
A. LIFT AND PITCHING MOMENT

FIGURE 62. EFFECT OF MACH NUMBER ON TAKEOFF FCK/SLAT CONFIGURATION
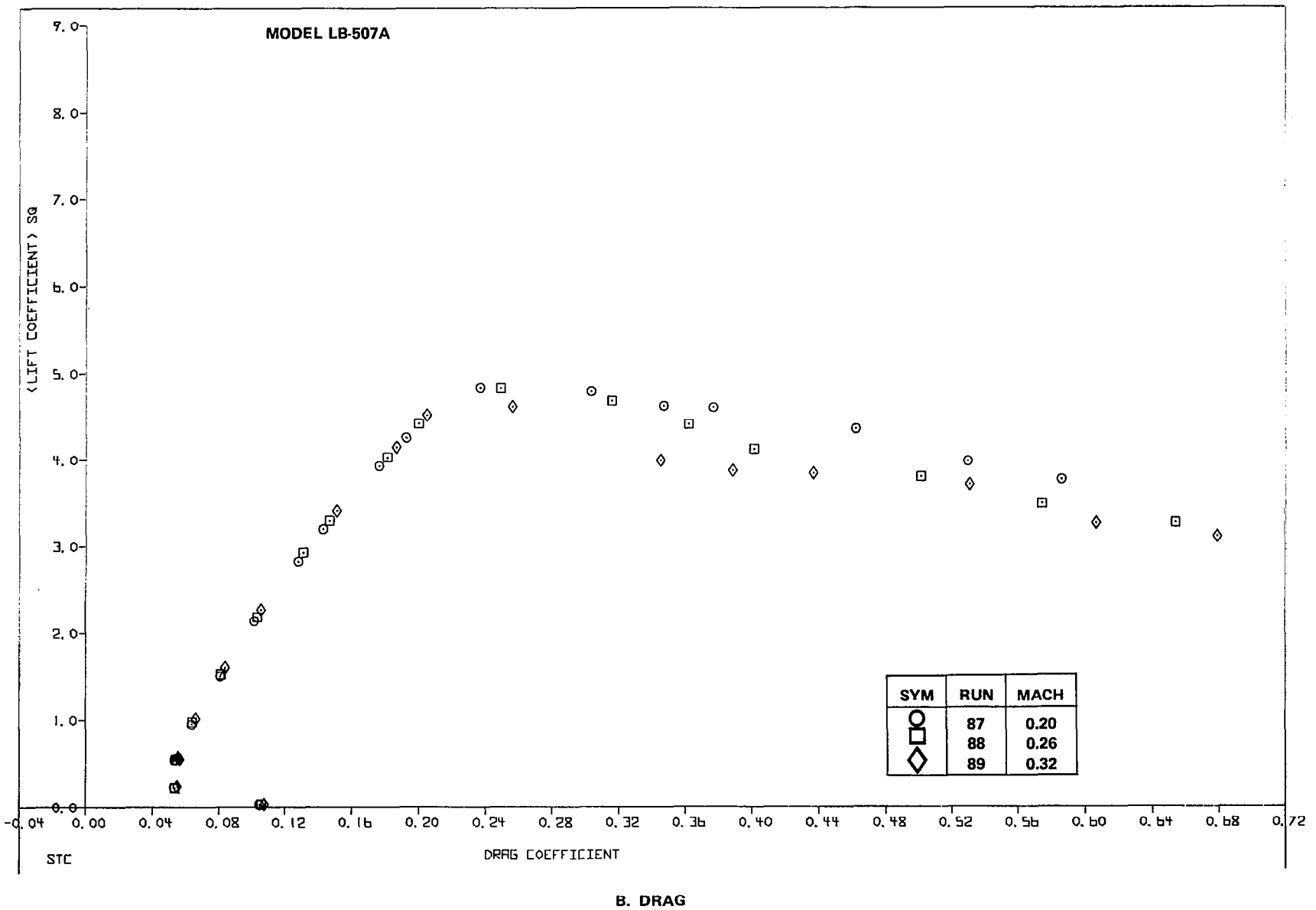
B. DRAG

FIGURE 62. EFFECT OF MACH NUMBER ON TAKEOFF FCK/SLAT CONFIGURATION

MODEL LB-507A
CONFIGURATION $B_{3B} W_{1B} X_{1B} P_{1C} N_{1C}$
MACH = 0.20
δ_{LE} = 55A/20A
δ_{FLAP} = 5/10
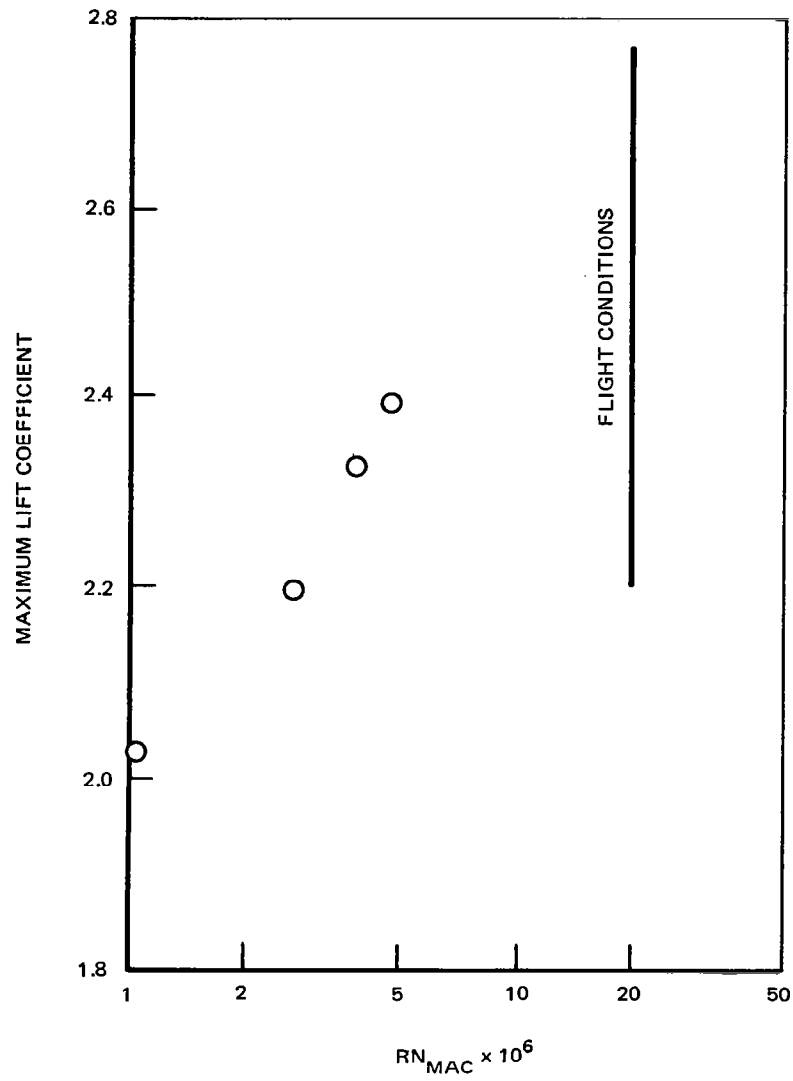
FIGURE 63. EFFECT OF REYNOLDS NUMBER ON MAXIMUM LIFT OF TAKEOFF FCK/SLAT CONFIGURATION

Alternative Flap Settings.- In addition to the primary takeoff flap setting of $5°/10°$, two other takeoff flap settings ($0°/0°$ and $15°/10°$) were tested. Figure 64 presents the basic aerodynamic characteristics for the $15°/10°$ flap setting with a variety of leading-edge-device combinations. The highest $C_{L_{MAX}}$ was associated with the slat/slat configuration. The best pitching moment was associated with the FCK/slotted slat configuration. The highest L/D values were associated with use of a sealed slat outboard.

The basic aerodynamic characteristics of the aircraft with a clean trailing edge are presented in Figure 65 for several leading-edge device combinations. The combinations investigated included a sealed slat outboard with an FCK or sealed slat inboard, and a slotted slat outboard with a clean leading edge inboard. This latter configuration was representative of an auto-slat system. Also shown are the characteristics of the cruise wing, for reference. The pitching-moment curves show the obvious aerodynamic benefit of an auto-slat system in improving stall behavior. Figure 66 summarizes the L/D values for the takeoff configurations.

Aileron and Spoiler Characteristics

Aileron effectiveness is presented for takeoff and landing configurations in Figures 67 and 68, respectively. At pre-stall angles of attack, the aileron effectiveness was well behaved for most angles of attack, but near the stall angle the effectiveness of the upward deflected aileron diminished. The shape of the rolling moment curve with aileron deflection indicates, for all flap settings, that the negative deflections (TEU) were more effective than the positive deflections (TED). In many cases, the incremental rolling moment obtained was more than twice as large as the corresponding value for positive aileron deflection. (Good data for the landing flaps, with positive aileron deflections are not available.)

MODEL LB-507A
CONFIGURATION $B_{3B} W_{1B} X_{1B} P_{1C} N_{1C} S_{11F}$
MACH = 0.20
$RN_{.MAC}$ = 4.61 × 10^6
δ_{FLAP} = 15/10

SYM	RUN	LE DEVICE	δ_{LE}
○	96	SLAT/SLAT	12C/27A
□	99	FCK/SLAT	55A/27A
◇	100	FCK/SEALED SLAT	55A/20A
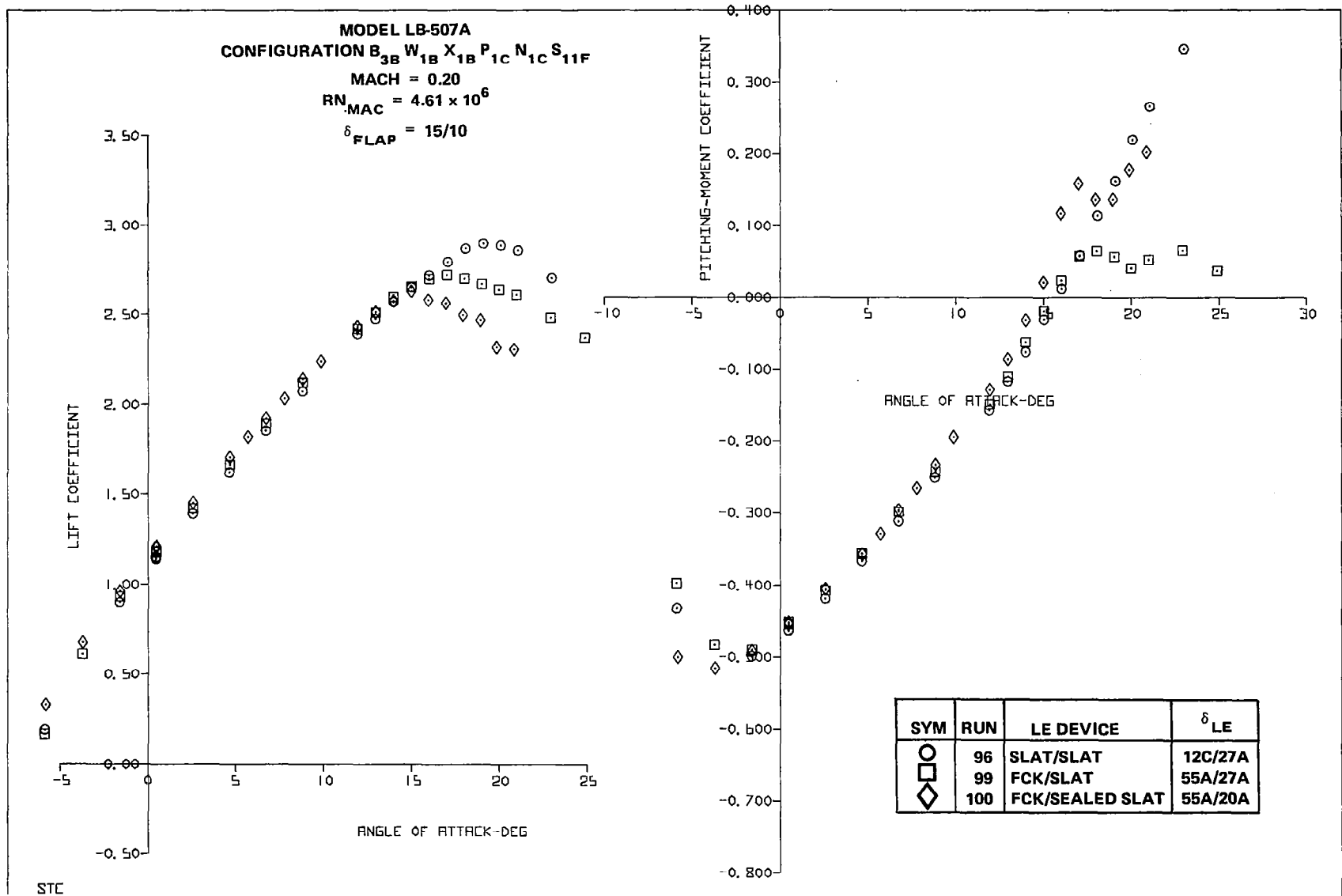
A. LIFT AND PITCHING MOMENT

FIGURE 64. AERODYNAMIC CHARACTERISTICS OF THE 15°/10° FLAP CONFIGURATIONS
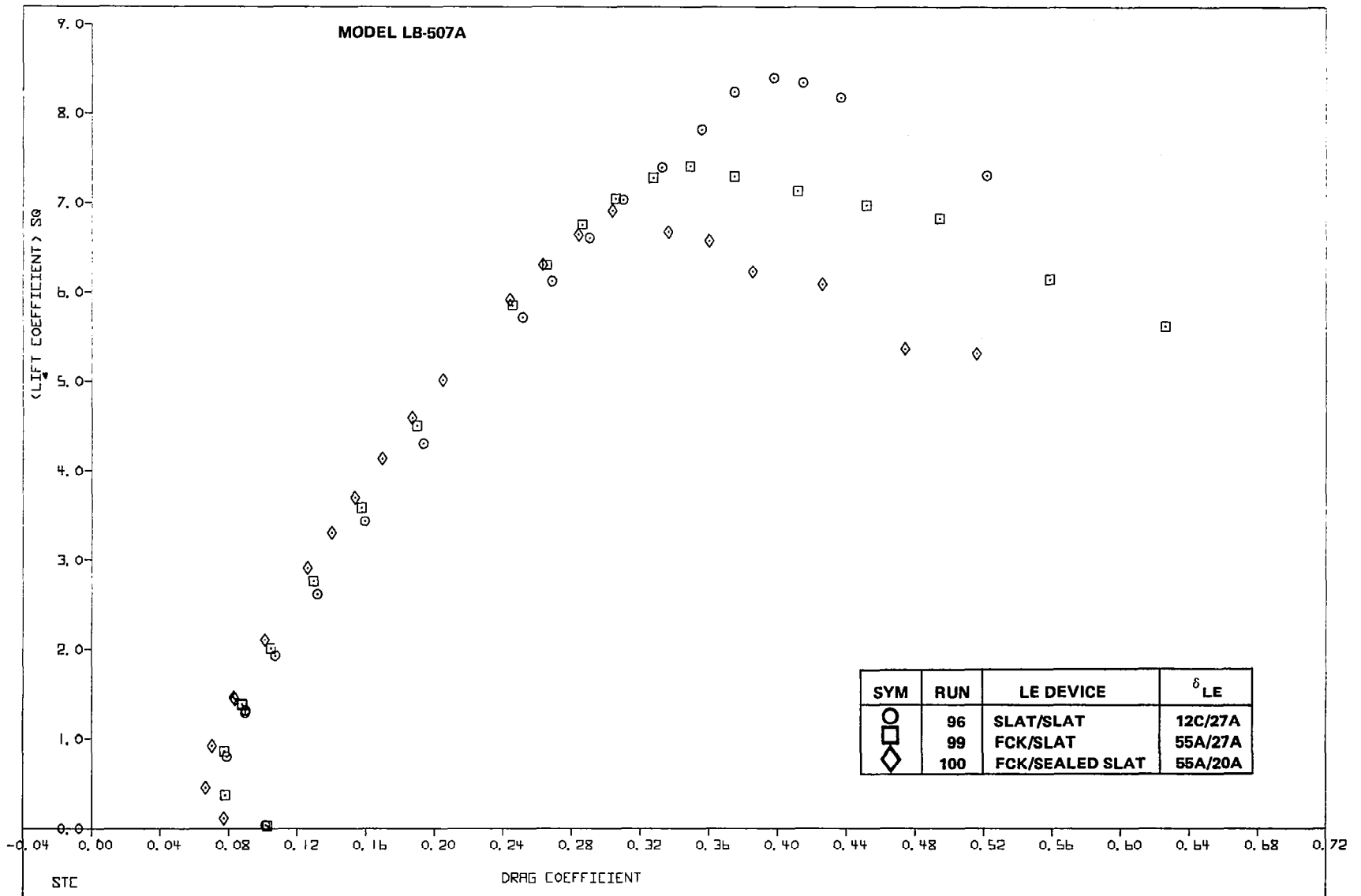
STC

B. DRAG

FIGURE 64. AERODYNAMIC CHARACTERISTICS OF THE 15°/10° FLAP CONFIGURATIONS

MODEL LB-507A

CONFIGURATION $B_{3B} W_{1B} X_{1B} P_{1C} N_{1C} S_{11F}$

MACH = 0.20

$RN_{MAC} = 4.61 \times 10^6$

TAIL OFF

SYM	RUN	LE DEVICE	δ_{LE}
◯	3	CLEAN/CLEAN	0/0
▢	106	CLEAN/SLAT	0/27A
◇	109	FCK/SEALED SLAT	55A/20A
△	110	SEALED SLAT/SEALED SLAT	8A/20A

STC
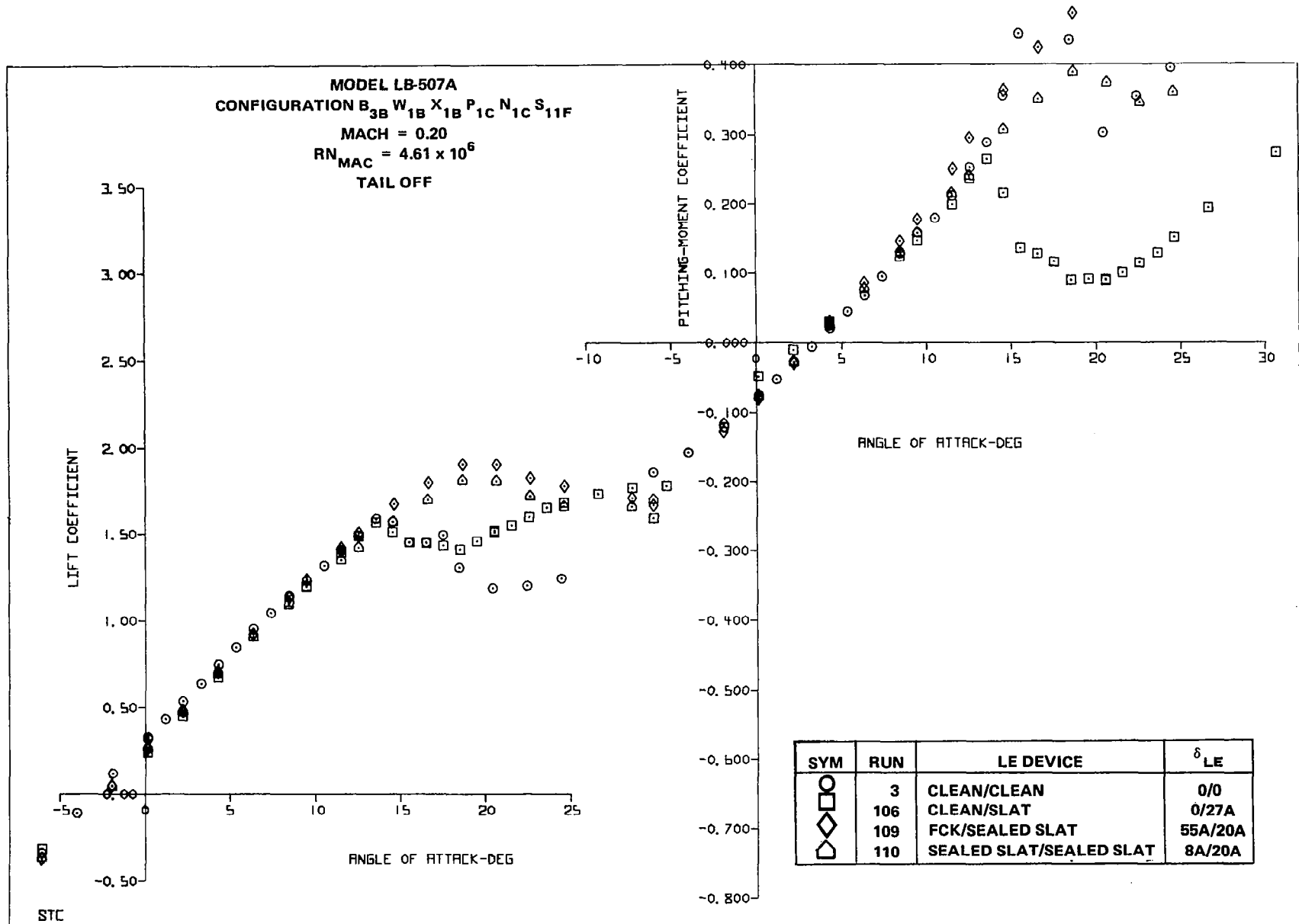
A. LIFT AND PITCHING MOMENT

FIGURE 65. AERODYNAMIC CHARACTERISTICS OF CLEAN TRAILING EDGE CONFIGURATIONS
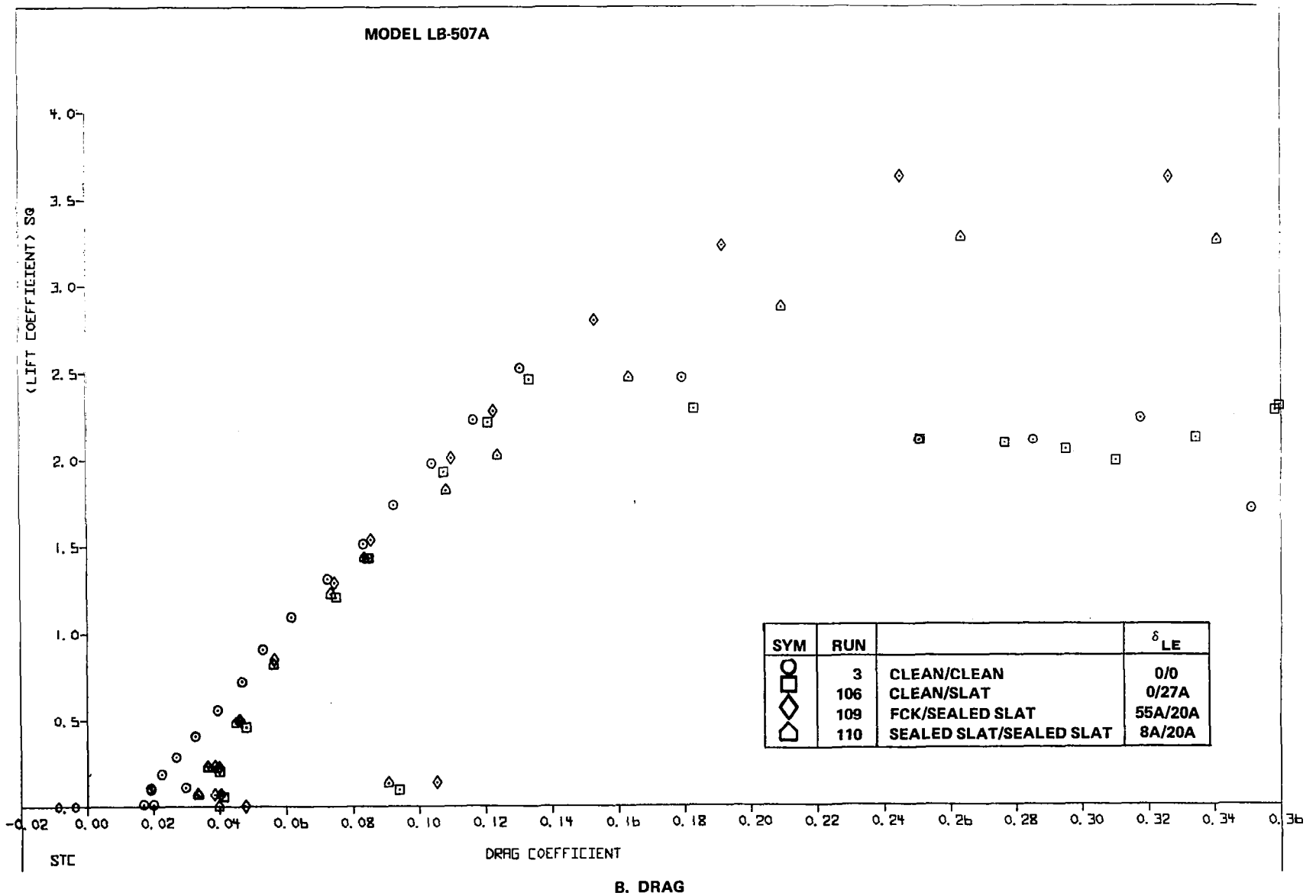
MODEL LB-507A

FIGURE 65. AERODYNAMIC CHARACTERISTICS OF CLEAN TRAILING EDGE CONFIGURATIONS

MODEL LB-507A

CONFIGURATION $B_{3B} W_{1B} X_{1B} P_{1C} N_{1C} S_{11_F}$

MACH = 0.20

$RN_{MAC} = 4.61 \times 10^6$

SYMBOL	δ_{LE} INBD/OUTBD	LE DEVICE INBD/OUTBD	δ_{FLAP} MAIN/AUX
——————	$8°/20°$	SLAT*/SLAT*	0/0, 5/10, 15/10
— — — —	$55°/20°$	FCK/SLAT*	0/0, 5/10, 15/10
——*—*	$12°/27.5°$	SLAT/SLAT	0/0, 5/10, 15/10
——*—*	$55°/27.5°$	FCK/SLAT	0/0, 5/10, 15/10
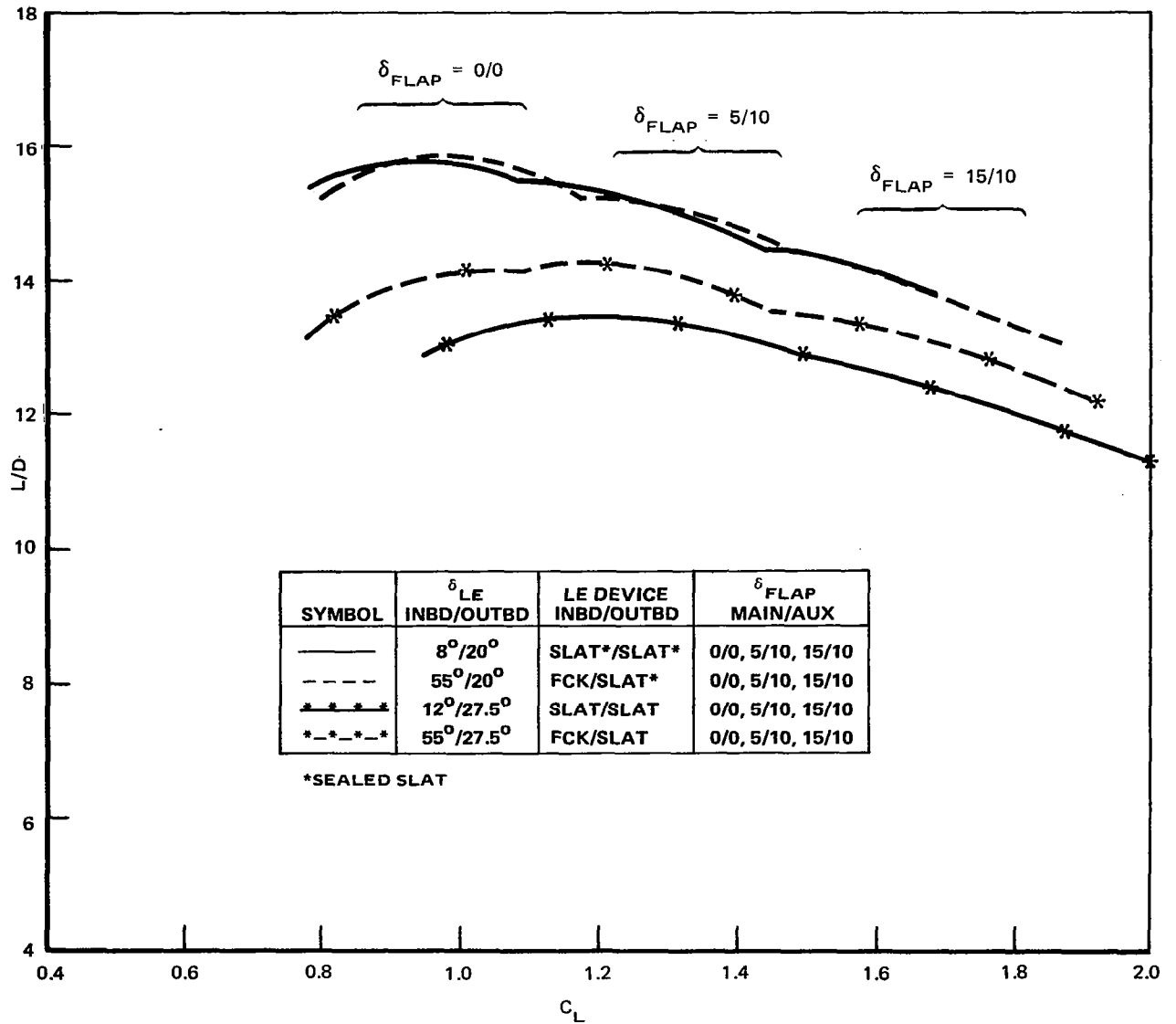
*SEALED SLAT

FIGURE 66. TAKEOFF L/D SUMMARY

MODEL LB-507A
CONFIGURATION $B_{3B} W_{1B} X_{1B} P_{1C} N_{1C} V_{1D} H_{1D}$
MACH = 0.20
RN_{MAC} = 4.61 x 10^6
δ_{LE} = 8A/20A
δ_{FLAP} = 5/10
i_H = 0
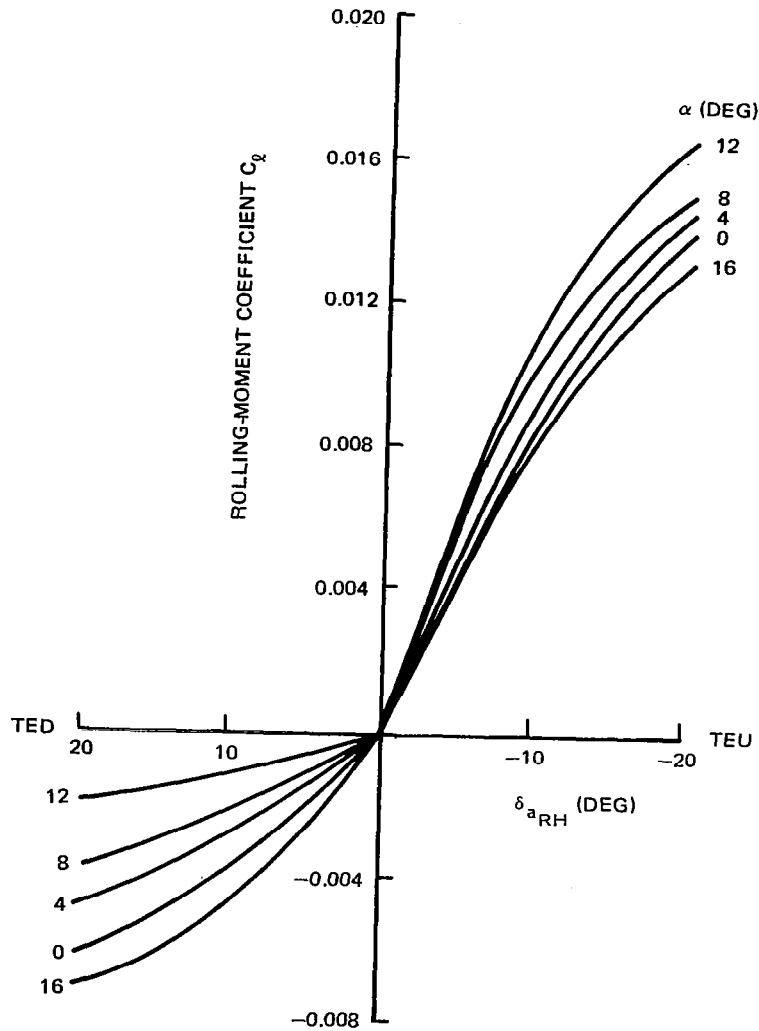
FIGURE 67. ROLLING-MOMENT COEFFICIENT DUE TO AILERON DEFLECTION FOR SEALED SLAT TAKEOFF CONFIGURATION

MODEL LB-507A

CONFIGURATION $B_{3B} W_{1B} X_{1B} P_{1C} N_{1C} S_{11F} V_{1D} H_{1D} G_{1A}$

MACH = 0.20

RN_{MAC} = 4.61 x 10^{6}

δ_{LE} = 55A/27A

δ_{FLAP} = 25/12.5

i_H = 0
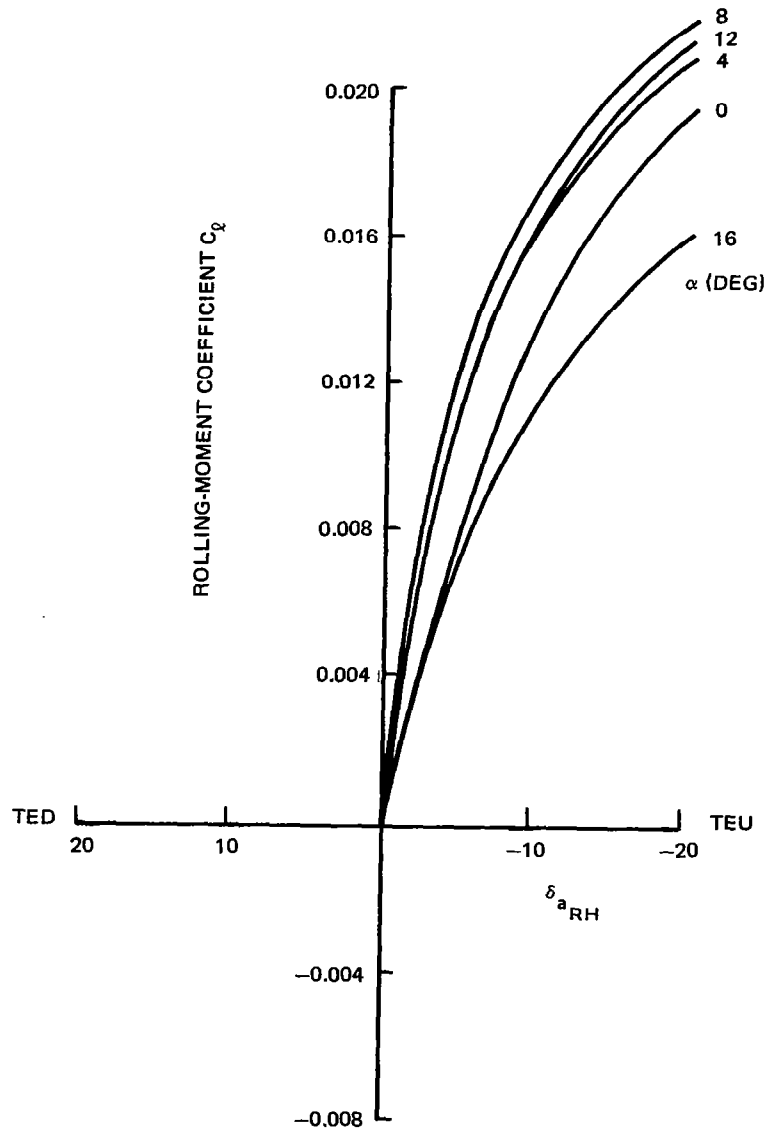
FIGURE 68. ROLLING-MOMENT COEFFICIENT DUE TO AILERON DEFLECTION FOR THE FCK/SLAT LANDING CONFIGURATION

Spoiler effectiveness for takeoff and landing configurations is presented in Figures 69 and 70, respectively. The spoiler data indicated well-behaved characteristics for both configurations, with increasing effectiveness shown for increased flap deflections. The spoiler arrangement consisted of large chord panels compatible with space available aft of the rear spar, and spoiler span corresponding to flap span. This powerful spoiler configuration was needed because of the reduced-roll-rate capability associated with the high-aspect-ratio wings.

The effect of symmetrical spoiler deflection with landing flap deflection is shown in Figure 71. These results were obtained for out-of-ground-effect conditions. The large spoiler chord and spanwise extent was very effective in reducing the lift and increasing the drag; however, a significant positive pitching-moment shift was also apparent. While the reduction in lift and increase in drag would result in greater deceleration on the ground, the positive increment of pitching moment would tend to unload the nose wheel. The ground effect on pitching moment, lift, and drag, with the spoilers deflected, should be obtained in a future test program.

Landing Gear Effects

The effects of the landing gear are shown in Figure 72. The gear increased C_D by 0.0245 and decreased L/D at $1.3V_s$ (at C_L = 1.864) from 11.55 to 9.92.

MODEL LB-507A
CONFIGURATION B_{3B} W_{1B} X_{1B} P_{1C} N_{1C} S_{11F} H_{1D} V_{1D}
MACH = 0.20
δ_{LE} = 8A/20A
δ_{FLAP} = 5/10
i_H = 0°

δ_{SP}	RN_{MAC}
−5	4.61×10^6
−30	3.72×10^6

SYM	α_{FRP}
◯	0
☐	4
◇	8
△	12
☆	16

ROLLING-MOMENT COEFFICIENT C_ℓ

SPOILER DEFLECTION (DEG)
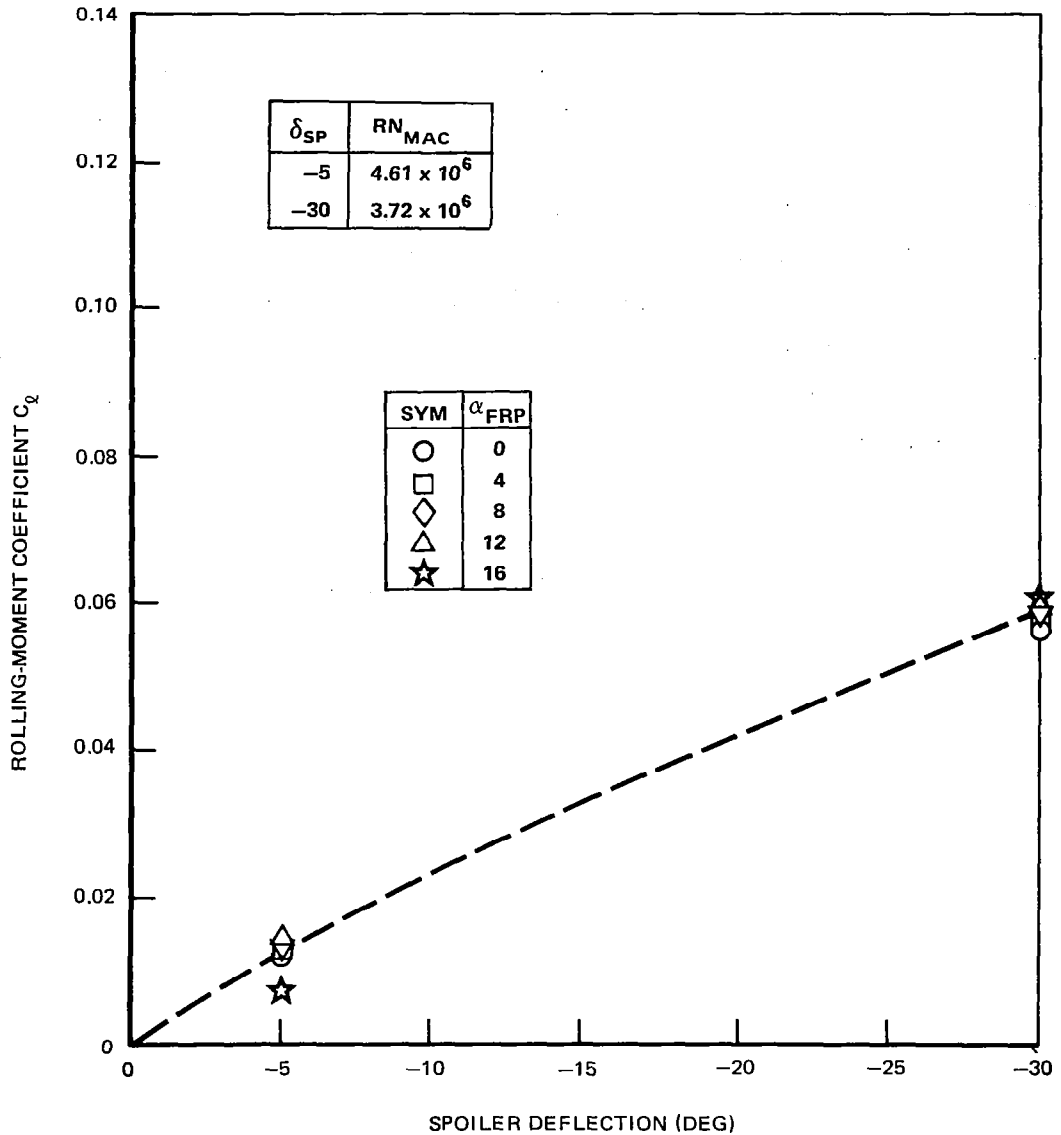
FIGURE 69. ROLLING-MOMENT COEFFICIENT DUE TO SPOILER DEFLECTION FOR THE SEALED SLAT TAKEOFF CONFIGURATION

136

MODEL LB-507A

CONFIGURATION B_{3B} W_{1B} X_{1B} P_{1C} N_{1C} S_{11F} H_{1D} V_{1D} G_{1A}

MACH = 0.20

δ_{LE} = 55A/27A

δ_{FLAP} = 25/12.5

i_H = 0°

δ_{SP}	RN_{MAC}
−5	4.61×10^6
−30	3.72×10^6

SYM	α_{FRP}
○	0
□	4
◇	8
△	12
☆	16
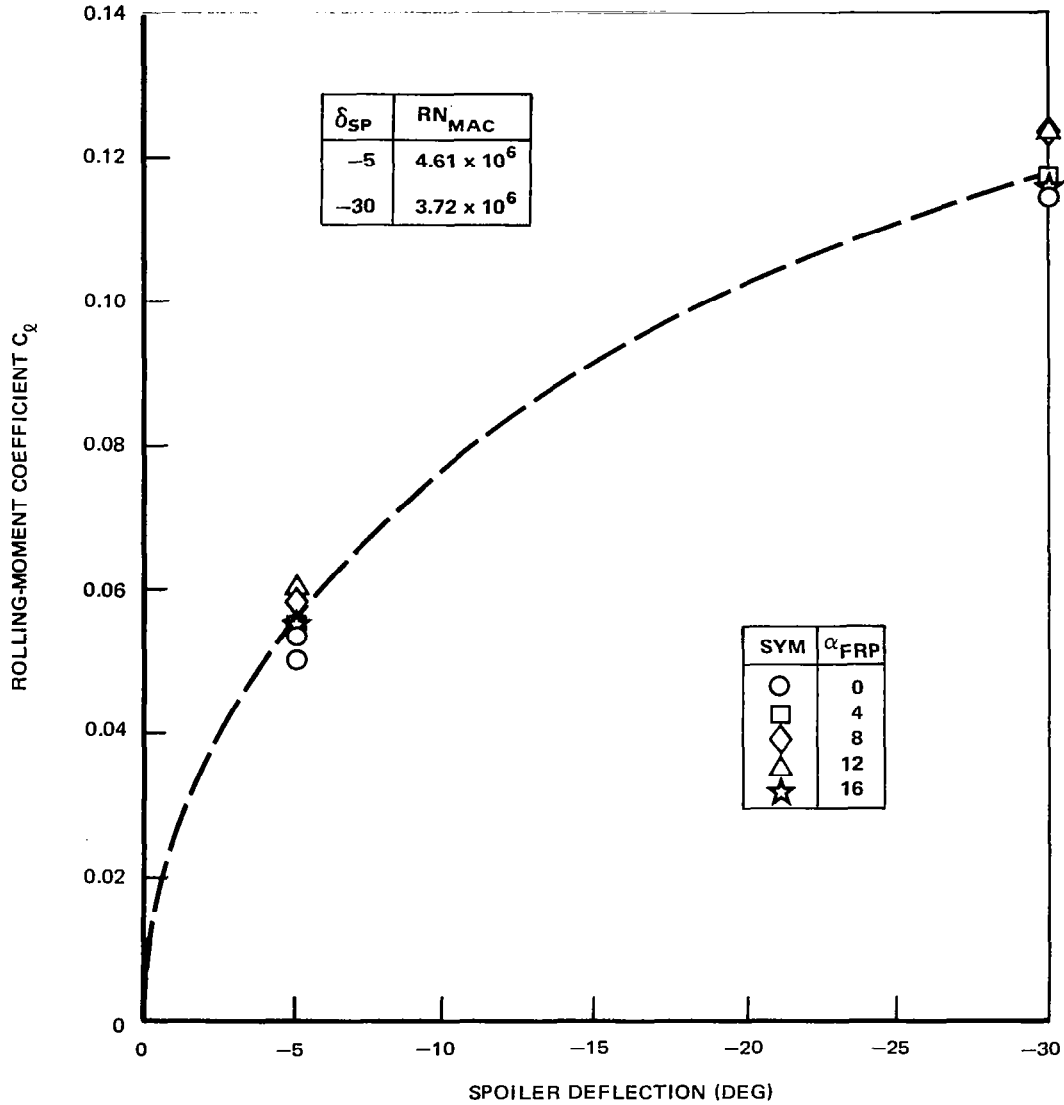
FIGURE 70. ROLLING-MOMENT COEFFICIENT DUE TO SPOILER DEFLECTION FOR THE FCK/SLAT LANDING CONFIGURATION

137

MODEL LB-507A
CONFIGURATION B_{3B} W_{1B} X_{1B} N_{1C} P_{1C} S_{11F} G_{1A}
MACH = 0.20
RN_{MAC} = 4.61 x 10^6
δ_{LE} = 55A/27A
δ_{FLAP} = 25/12.5

SYM	RUN	δ_{SP}
O	51	0/0
□	61	−60/−60

STC
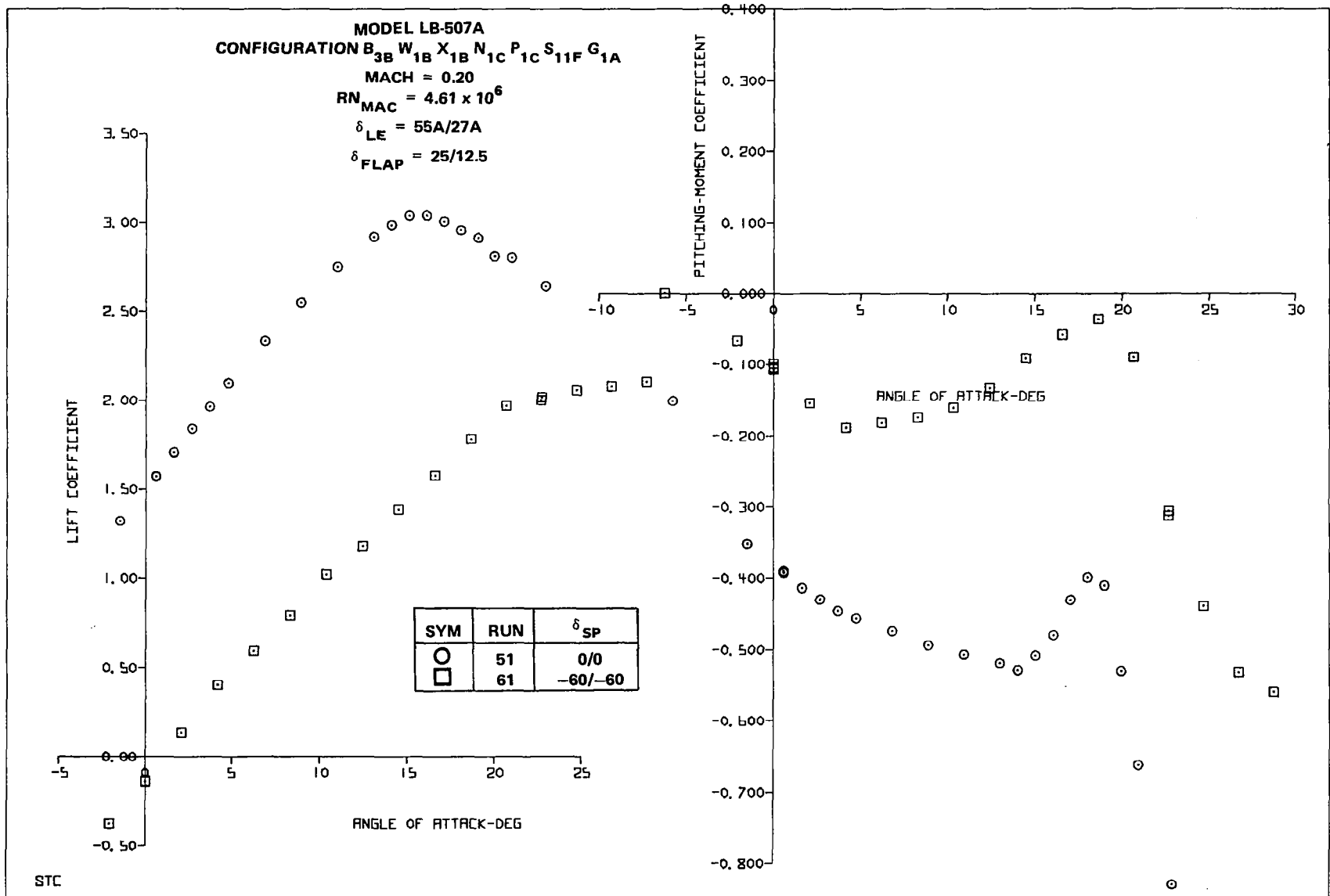
A. LIFT AND PITCHING MOMENT

FIGURE 71. EFFECT OF SYMMETRICAL SPOILER DEFLECTION
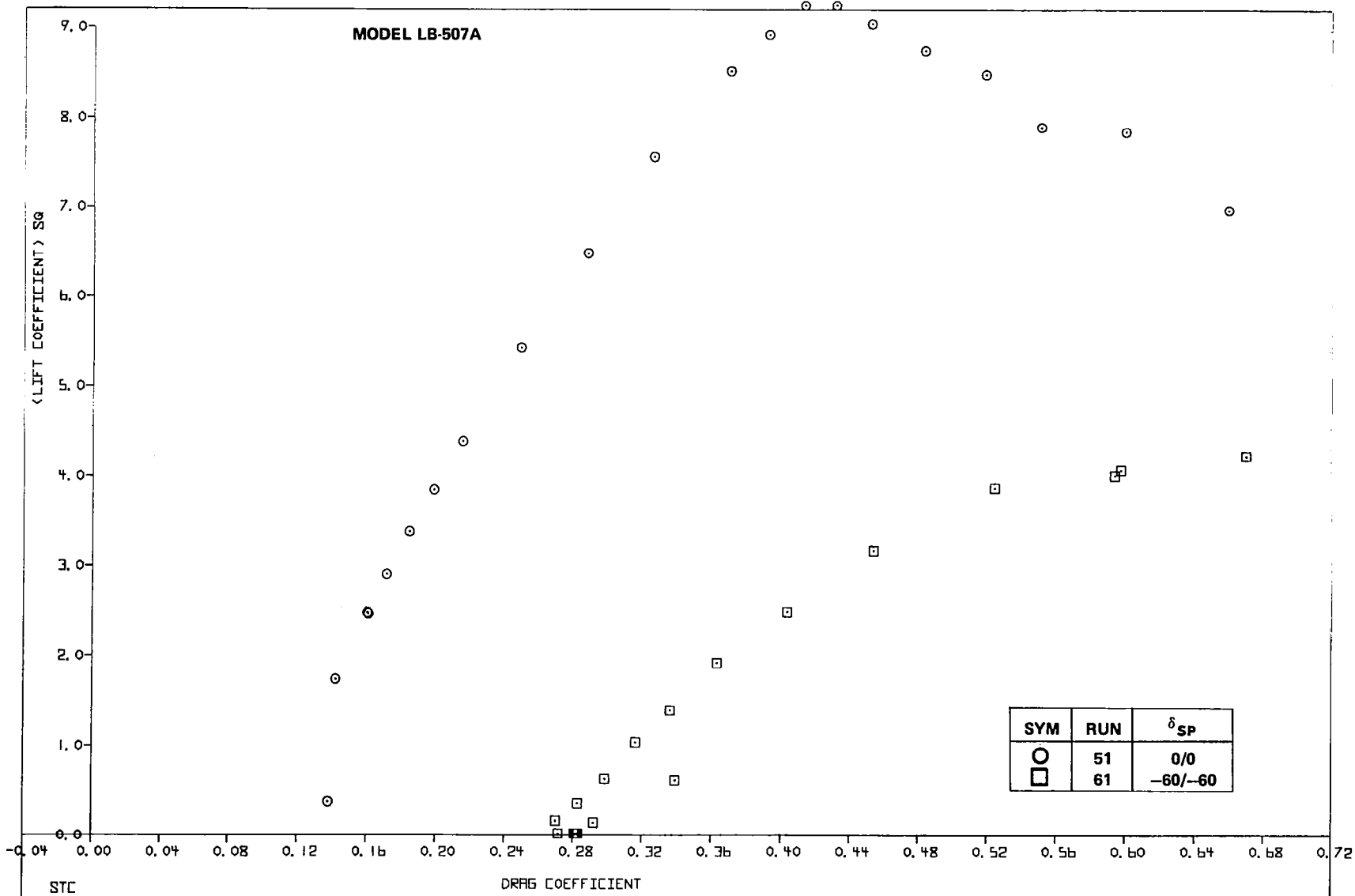
FIGURE 71. EFFECT OF SYMMETRICAL SPOILER DEFLECTION

MODEL LB-507A

CONFIGURATION $B_{3B} W_{1B} X_{1B} N_{1C} P_{1C} S_{11F}$

MACH = 0.20

RN_{MAC} = 4.61 x 10^6

δ_{LE} = 70A/27A

δ_{FLAP} = 25/12.5

LIFT COEFFICIENT

3.50

3.00

2.50

2.00

1.50

1.00

0.50

0.00

-0.50

ANGLE OF ATTACK-DEG

-5   0   5   10   15   20   25

STC

PITCHING-MOMENT COEFFICIENT

0.400

0.300

0.200

0.100

0.000

-0.100

-0.200

-0.300

-0.400

-0.500

-0.600

-0.700

-0.800

ANGLE OF ATTACK-DEG

-10   -5   0   5   10   15   20   25   30

SYM	RUN	GEAR
○	36	ON
□	46	OFF
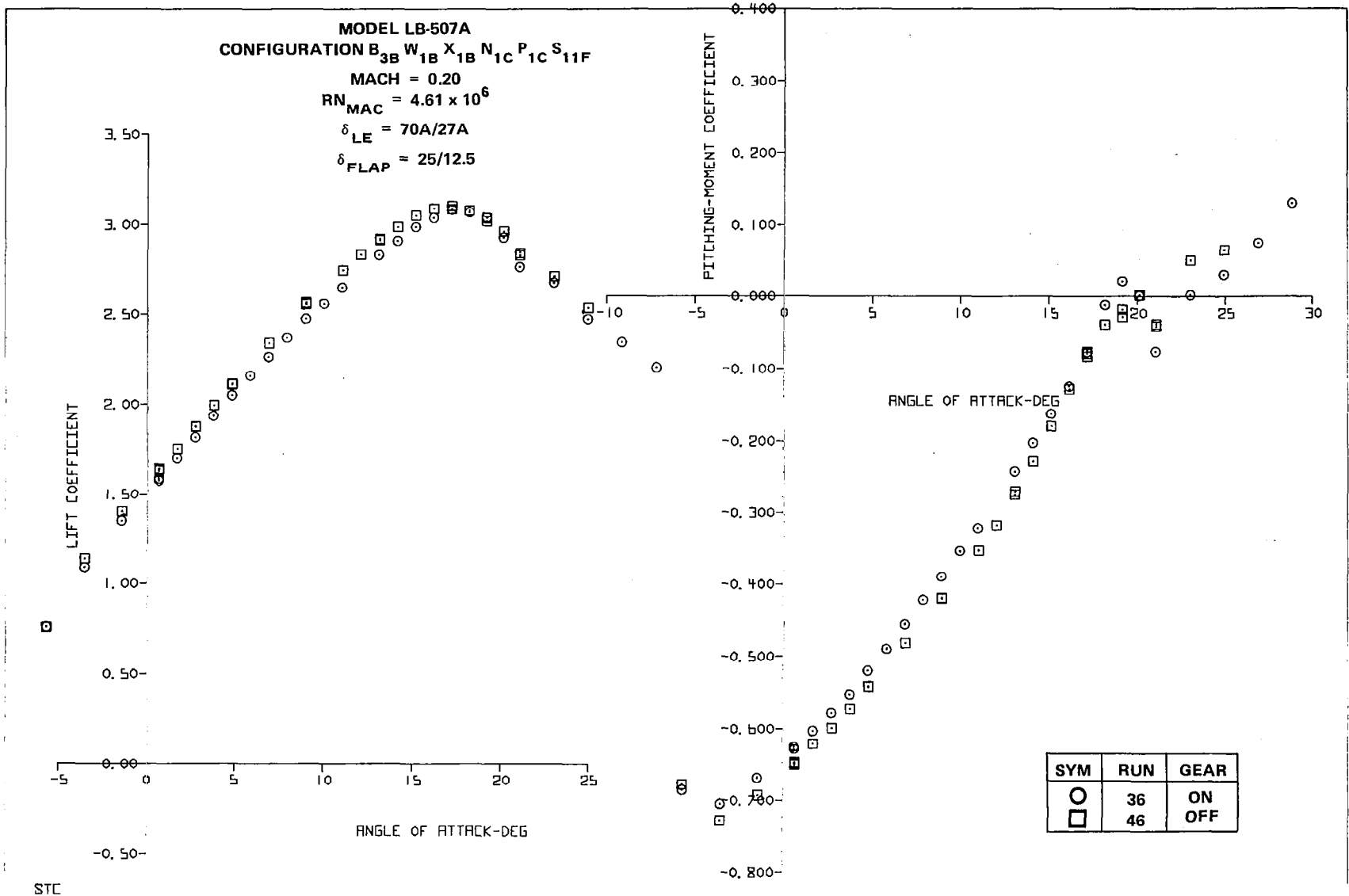
A. LIFT AND PITCHING MOMENT

FIGURE 72. EFFECT OF LANDING GEAR
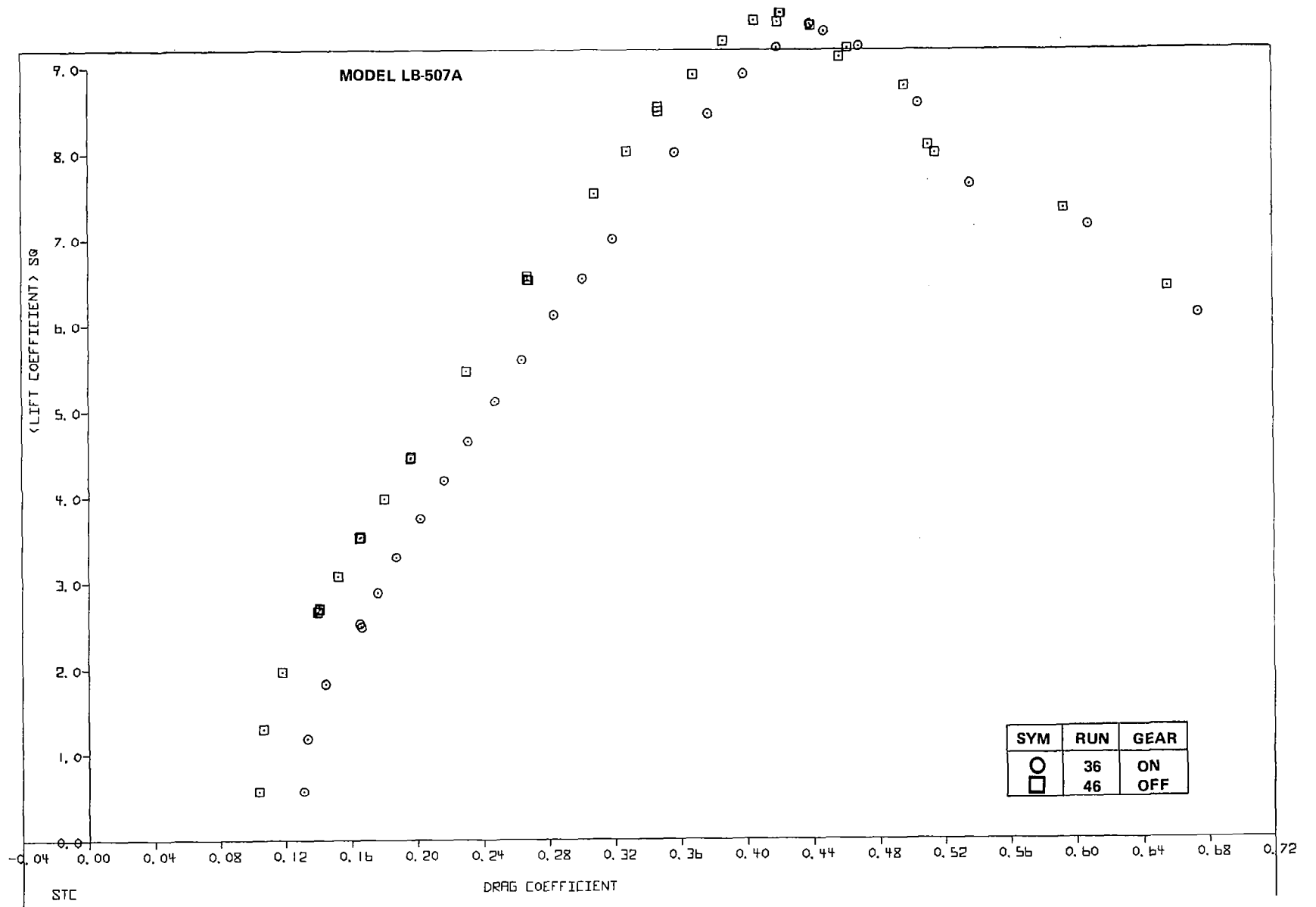
B. DRAG

FIGURE 72. EFFECT OF LANDING GEAR
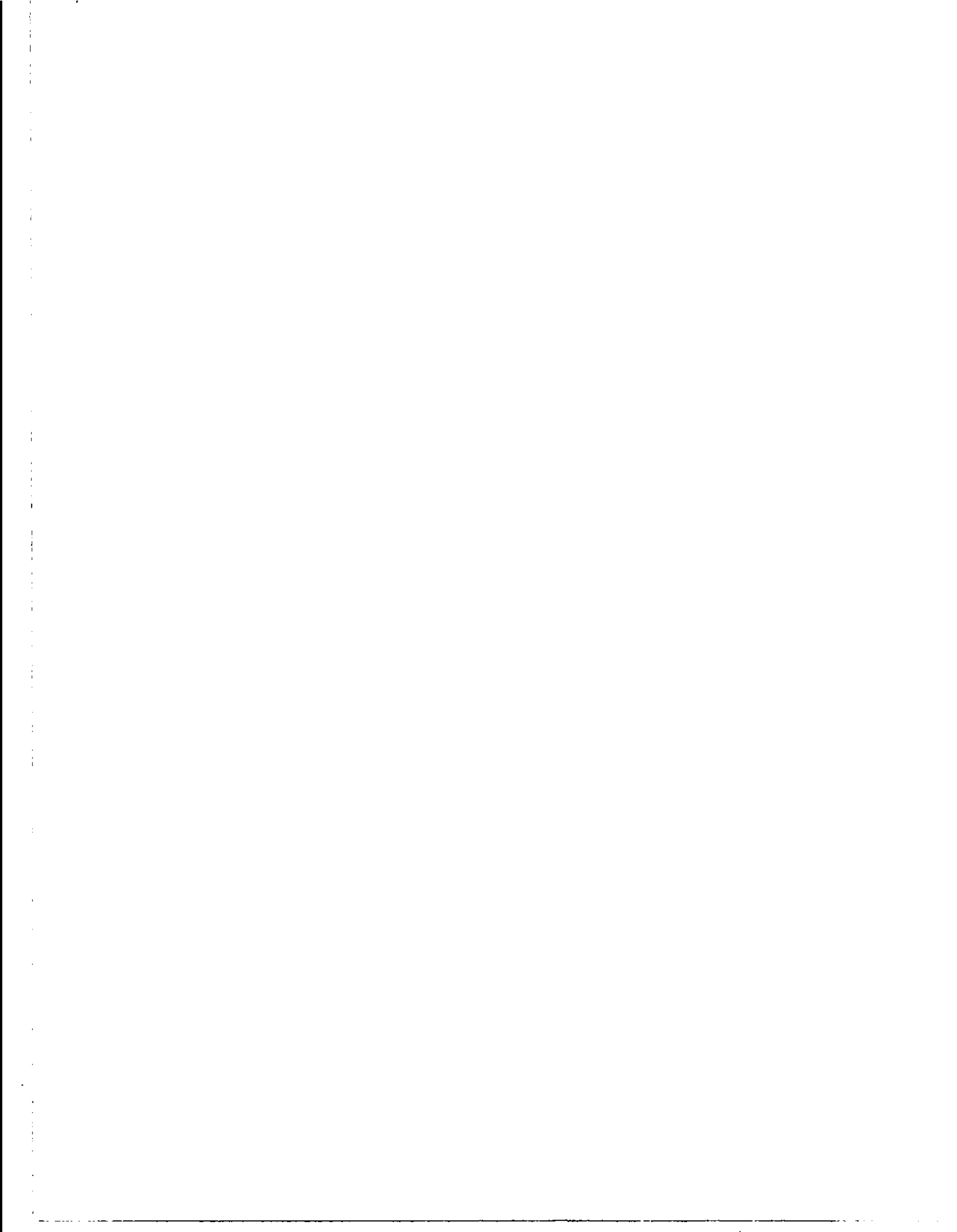
CONCLUSIONS AND RECOMMENDATIONS
Conclusions

As a result of wind tunnel testing conducted at the NASA Ames 12-Foot Pressure Tunnel and the NASA Langley V/STOL Tunnel, the objectives set for the EET Phase II investigation of high-lift systems for advanced transports have been accomplished. This combined NASA/Douglas research effort has demonstrated the aerodynamic benefits of advanced-technology high-lift systems, has established a comprehensive data base for analysis of developing methods, and has identified future development areas.

The following conclusions are drawn from the LB-486 data:

1. Reduced VCK deflections, compared to those employed during Phase I testing, provided no benefit in terms of additional $C_{L_{MAX}}$ or improved stalling characteristics.

2. With takeoff flaps, use of a sealed outboard slat with a clean leading edge inboard provided significant improvement in L/D and pitching-moment characteristics compared to the basic slat configuration. This configuration resulted in a significant penalty in $C_{L_{MAX}}$. Use of an inboard sealed or small-gap slat at an intermediate deflection is a candidate for future low-speed testing.

3. The full-span FCK offered no obvious advantages in high-lift performance compared to either a full span VCK or a full-span slat; however, an FCK (especially a short-chord FCK) inboard, used in conjunction with a slat outboard, provided the greatest improvement in stalling behavior with only a relatively small loss in $C_{L_{MAX}}$.

4. The revised slat-trim configurations tested showed less improvement in pitching-moment characteristics and a larger loss in $C_{L_{MAX}}$ than the short-chord FCK/slat (inboard/outboard) combination.

5. The use of a single-segment flaperon in place of the high-speed aileron significantly increased $C_{L_{MAX}}$ without penalizing L/D or pitching-moment characteristics. Replacement of the single-segment flaperon with a two-segment flaperon resulted in an additional small increment in maximum lift.

6. Comparison of aerodynamic data for equivalent configurations in the Ames 12-Foot Pressure Tunnel and the Langley V/STOL Tunnel indicated generally good agreement for the lift characteristics. The comparisons indicated differences in pitching moment and drag.

The following conclusions are drawn from the LB-507 data:

1. For the high Reynolds number test condition, the cruise wing achieved a tail-off $C_{L_{MAX}}$ of 1.59 and an L/D at $1.2V_s$ of 20.02. Pitch characteristics were influenced by changes in Mach and Reynolds number.

2. The optimization of the leading-edge devices indicated superior $C_{L_{MAX}}$ and pitching moments for the configurations with an inboard FCK; the L/D values for the inboard sealed-slat and FCK configurations were equivalent. The sealed-slat configurations exhibited lateral instability near stall under a yawed condition. Improvement in aerodynamic performance and pitch characteristics could result from further leading-edge-device optimization studies.

3. Testing of the highly deflected flap (35°/10°) indicated little increase in $C_{L_{MAX}}$, but a large increment in drag.

4. Mach and Reynolds number effects were studied during the test program for selected configurations. $C_{L_{MAX}}$, pitching moments, and L/D values tended to improve with increasing Reynolds number and decreasing Mach number. Extrapolation of the wind tunnel data to flight Reynolds numbers suggested further increases in maximum lift are possible.

5. The nacelles and pylons increased the cruise wing $C_{L_{MAX}}$ by 0.1; the $C_{L_{MAX}}$ increment on the flaps-deflected configuration was nearly zero. The presence of the nacelles and pylons tended to be a post-stall stabilizing influence.

6. The strakes, which were added to improve the C_{Lmax} of the slatted configurations, were effective in that respect. The additional C_{Lmax} for the inboard slat configuration with landing flaps was 0.14; for the takeoff flaps, 0.06. The strakes did not, on the other hand, increase the maximum lift values of the cruise wing nor of the FCK configurations. In all cases, the strakes were detrimental to the longitudinal stability.

7. Aileron effectiveness studies indicated that, for all flap settings, negative deflections (trailing edge up) were more effective than positive deflections (trailing edge down). In some cases, the incremental rolling moment obtained with the negative aileron deflections was more than twice that obtained with the corresponding value for positive aileron deflection.

8. The effect of spoiler deflection on roll characteristics increased as flap deflection increases. Symmetrical spoiler deflections for landing flap settings were very effective in reducing lift and increasing drag.

Recommendations

Analysis of the Phase II study data has identified those areas where continued work could result in further improvement of the technology. The potential for improvement has been noted in the following low-speed aerodynamic characteristics: pitching moments for high-lift configurations and increases in maximum lift for both landing and takeoff configurations. It is therefore recommended that future studies include the following:

1. The use of small gaps to improve the pitching-moment characteristics of slat configurations without decreasing L/D.

2. The use of a slat that has a larger slot near the pylon than near the fuselage, to increase the section $C_{L_{MAX}}$ of the inboard wing panel, and to promote a more rapid inboard lift loss after stall.

3. Additional testing of the inboard short-chord FCK, in order to increase the configuration L/D by reducing deflection and/or closing the gap.

4. High-lift testing in ground effect at high Reynolds number.

5. Reduced landing slat deflections to increase $C_{L_{MAX}}$.

6. Higher-Reynolds-number testing to determine $C_{L_{MAX}}$ and pitching-moment trends at conditions more closely matching those of flight.

APPENDIX A
LB-486 A,B,C
CONFIGURATION NOTATION

B_{2A} — Simulates the DC-X-200 Model D-969N-21 fuselage. Full-scale dimensions: Length = 42.29 m (138.8 ft); constant section diameter = 602 cm (237 in.). The aft fuselage tail cone uses the DC-10 model parts. The fuselage is configured for tandem strut support system.

W_{3B} — Simulates the DC-X-200 Model D-969N-21 wing and is lofted to represent the airplane wing with a 1-g load. Full scale dimensions: S_W = 212.597 m^2 (2288.457 ft^2); b_W = 47.252 m (155.027 ft); aspect ratio = 10.502; λ = 0.1407; MAC = 5.351 m (17.555 ft). The model wing has a removable leading edge, full-span VCK flap, trailing-edge two-segment flap, outboard aileron on one side, and spoilers. The wing is constructed of Armco 17.4 steel and contains five rows of pressure orifices.

X_{2B} — Wing-fuselage fillet for $B_{2A}W_{3B}$.

H_{1A} — Horizontal stabilizer for DC-X-200 (slab surface).

V_{1A} — Vertical stabilizer for DC-X-200 (slab surface).

N_{2A} — Flow-through, short core cowl nacelle configuration (2).

P_{2A} — New pylons for mating N_{2A} to wing W_{2B} (2).

Z_{1A} — Nacelle strake configuration (attaches to N_{2A}, 2 each nacelle).

G_{1A} — Main and nose landing gear defined for the DC-X-200 airplane. Main gear wheel wells with gear extended are not provided.

a_{2A} The outboard aileron with inboard trim at X_W = 89.020 cm (35.047 in.) and outboard trim at X_W = 109.480 cm (43.102 in.). The hingeline is located at 75% C.

f_1, f_2 Inboard spoiler segments fabricated as individual parts. Superscript R = right side, L = left side, None = both sides.

f_{1A}, f_{2A} f_1 and f_2 inboard 0^0 spoilers with sheet metal aft extension. Trailing-edge step is filled with wax and faired (LB-486A). This assembly was refurbished and the T.E. step filled with potting (LB-486C).

$f_3, f_4,$
f_5, f_6 Outboard spoiler segments fabricated as one piece.

L_{1A} Leading-edge slat inboard of X_W = 36.367 cm (14.318 in.) and support at nominal gap = 2.25% C, O.H. = 2.0% C, and δ_{SLAT} = 25^0.

L_{2A} Leading-edge slat outboard of X_W = 36.367 cm (14.318 in.) and supported at nominal gap = 2.25% C, O.H. = 2.0% C, and δ_{SLAT} = 35^0.

L_{3A} Leading-edge variable-camber Krueger inboard of wing station X_W = 36.367 cm (14.318 in.) and supported at the nominal gap = 2.82% C, O.H. = -0.725% C, and δ_{VCK} = 55^0.

L_{4A} Leading-edge variable-camber Krueger outboard of wing station X_W = 36.367 cm (14.318 in.) and supported at the nominal gap = 3.5% C, O.H. = 1.0% C, and δ_{VCK} = 55^0.

L_{5a} The inboard VCK extension to the fuselage.

L_{6A} The VCK section at the pylon interruption.

F_{1A} Inboard main flap of a two-segment flap with inboard trim at X_W = 13.868 cm (5.460 in.) and outboard trim at X_W = 30.793 cm (12.123 in.).

F_{2A} Inboard aft flap of a two-segment flap trimmed to match F_{1A} and supported from F_{1A}.

F_{3A} A single-slot flaperon with inboard trim at X_W = 30.793 cm (12.123 in.) and outboard trim at X_W = 43.411 cm (17.091 in.).

F_{4A} Outboard main flap of a two-segment flap with inboard trim at X_W = 43.411 cm (17.091 in.) and outboard trim at X_W = 89.020 cm (35.047 in.).

F_{5A} Outboard aft flap of a two-segment flap trimmed to match F_{4A} and supported from F_{4A}.

X_W, Y_W Wing coordinates (spanwise, chordwise).

α_{FRP} Angle of attack, in degrees, of the fuselage reference plane relative to the equivalent free airstream. Nose up is positive.

δ_a Aileron deflection, in degrees. Positive deflection is trailing edge down.

$\delta_{F_{AFT}}$ Aft flap deflection, in degrees (see Figure 51).

$\delta_{F_{MAIN}}$ Main flap deflection, in degrees (see Figure 51).

δ_{SLAT} Slat deflection, in degrees (see Figure 48).

δ_{VCK} VCK deflection, in degrees (see Figure 48).

i_H Incidence angle, in degrees, of the horizontal stabilizer H_{1A} Positive deflection is trailing edge down.

Summary Code

S_1 $B_{2A}W_{3B}X_{2B}a_{2A}$. Body + cruise wing.

S_2 $B_{2A}W_{3B}X_{2B}N_{2A}P_{2A}Z_{1A}L_{3A}L_{4A}F_{1A}F_{2A}F_{3A}F_{4A}F_{5A}$
$a_{2A}f_{1, 2, 2A}$ $f_{1A, 2A, 3, 4, 5, 6}$. Body+flapped wing+VCK
leading-edge device+flaps+nacelles, pylons, and nacelle strakes
+VCK filler blocks.

S_3 $S_2 - W_{3B} + W_{3D}$. Configuration S_2 - VCK filler blocks.

S_4 $S_2 - W_{3B} + W_{3D} - f_{1,2} + f_{1A}f_{2A}$. Configuration
S_3+inboard spoiler trailing-edge extensions.

S_5 $B_{2A}W_{3B}X_{2B}N_{2A}P_{2A}Z_{1A}L_{1A}L_{2A}F_{1A}F_{2A}F_{3A}F_{4A}F_{5A}$
a_{2A} $f_{1A}, f_{2A}, f_3, f_4, f_5, f_6$. Body+flapped wing
+slat and WUSS leading-edge+flaps+nacelles, pylons, and nacelle
strakes.

APPENDIX B

LB-486A,B,C

DIMENSIONAL DATA

COMPONENT	UNITS	MODEL	SCALE
FUSELAGE (B_{2A})			
Length	cm (in.)	198.77	(78.255)
Maximum width	cm (in.)	28.293	(11.139)
Maximum height	cm (in.)	28.293	(11.139)
WING (W_{3B})			
Area	m^2 (ft^2)	0.4696	(5.055)
Span	m (ft)	2.221	(7.286)
Mean aerodynamic chord	m (ft)	0.251	(0.825)
Root chord (trapezoidal wing)	cm (in.)	37.076	(14.597)
Total root chord	cm (in.)	51.895	(20.431)
Tip chord (trapezoidal wing)	cm (in.)	5.217	(2.054)
Total tip chord	cm (in.)	9.27	(3.65)
Aspect ratio		10.502	
Taper ratio		0.1407	
Spanwise station of MAC	cm (in.)	41.580	(16.370)
Fuselage station of 25% MAC	cm (in.)	160.28	(63.102)
Sweepback of 25% C_W	deg	28.57	
Dihedral("lg")	deg	4.5	
HORIZONTAL STABILIZER (H_{1A})			
Area	m^2 (ft^2)	0.1298	(1.397)
Span	cm (in.)	70.234	(27.651)
MAC	cm (in.)	19.91	(7.839)
Root chord	cm (in.)	27.384	(10.781)

COMPONENT	UNITS	MODEL	SCALE
HORIZONTAL STABILIZER (H_{1A}) (continued)			
Tip chord	cm (in.)	9.583	(3.773)
Aspect ratio		3.800	
Taper ratio		0.35	
Sweepback of 25% chord	deg	30.0	
Dihedral	deg	10.0	
Fuselage station of 25% H_{MAC}	cm (in.)	247.36	(97.384)
Tail length (25% W_{MAC} to 25% H_{MAC})	cm (in.)	87.076	(34.282)
VERTICAL STABILIZER (V_{1A})			
Area	m^2 (ft^2)	0.099	(1.060)
Span	cm (in.)	39.700	(15.630)
MAC	cm (in.)	26.731	(10.524)
Root chord	cm (in.)	36.759	(14.472)
Tip chord	cm (in.)	12.87	(5.065)
Aspect ratio		1.6	
Taper ratio		0.35	
Sweepback of 25% chord	deg	35.0	
Tail length(25% W_{MAC} to 25% V_{MAC})	cm (in.)	82.301	(32.402)
OUTBOARD AILERON (a_{2A})			
Area aft of hingeline	cm^2 (in^2)	54.4	(8.44)
Span	% b/2	18.4	
Chord aft of hingeline	% C_W	25.0	
SPOILER (f_1,f_2)			
Area (each)	cm^2 (in^2)	47.2	(7.32)
Span (each)	cm (in.)	13.2	(5.18)

COMPONENT	UNITS	MODEL SCALE	
SPOILER (f_3, f_4, f_5, f_6)			
Area (total, one side)	cm^2 (in^2)	104.660	(16.222)
Span (total, one side)	cm (in.)	43.835	(17.258)
NACELLE (N_{2A})			
Length	cm (in.)	32.00	(12.60)
Maximum cowl height	cm (in.)	13.7	(5.38)
Inlet diameter (fan cowl)	cm (in.)	9.85	(3.88)
Exit area (gas generator)	cm^2 (in^2)	6.86	(1.06)
Incidence of thrust line to FRP	deg	1.6	
Toe in	deg	1.8	

APPENDIX C
LB-486A,B,C GRID NOTATION

SLAT GRID NOTATION
All gaps and overhangs are percent of local wing chord
Dimensions are model scale

δ_{SLAT}	$X_W = 14.140$ cm (5.567 in.)		$X_W = 36.367$ cm (14.138 in.)		NOTATION
	GAP	O.H.	GAP	O.H.	
25°	2.25	-2.0	2.25	-2.0	L_{1AA}
25°	1.50	-1.0	1.50	-1.0	L_{1AB}
25°	3.25	-2.0	3.25	-2.0	L_{1AC}
15°	2.25	-2.0	2.25	-2.0	L_{1AD}
15°	1.50	-1.0	1.50	-1.0	L_{1AE}
15°	3.25	-2.0	3.25	-2.0	L_{1AF}
5°	$\simeq$ 0.0	+7.54	$\simeq$ 0.0	+4.65	L_{1AG}
35°	2.25	-2.0	2.25	-2.0	L_{2AA}
35°	1.50	-1.0	1.50	-1.0	L_{2AB}
35°	3.25	-2.0	3.25	-2.0	L_{2AC}

APPENDIX C (continued)

LB-486A,B,C GRID NOTATION

SLAT GRID NOTATION

All gaps and overhangs are percent of local wing chord

Dimensions are model scale

	$X_W = 36.367$ cm (14.138 in.)		$X_W = 89.020$ cm (35.047 in.)		
δ_{SLAT}	GAP	O.H.	GAP	O.H.	NOTATION
25^0	2.25	-2.0	2.25	-2.0	L_{2AD}
25^0	1.50	-1.0	1.50	-1.0	L_{2AE}
25^0	3.25	-2.0	3.25	-2.0	L_{2AF}
20^0	$\simeq 0$	+2.0	$\simeq 0$	+2.0	L_{2AG}

LB-486A,B,C GRID NOTATION

VCK GRID NOTATION
All gaps and overhangs are percent of local wing chord
Dimensions are model scale

X_W = 14.140 cm (5.567 in.)			X_W = 36.367 cm (14.138 in.)			
δ_{VCK}	GAP	O.H.	δ_{VCK}	GAP	O.H.	NOTATION
51.318°	2.82	-0.725	55°	3.5	-1	L_{3AA}
51.318°	2.82	-1.725	55°	3.5	-2	L_{3AB}
51.318°	1.82	-0.725	55°	2.5	-1	L_{3AC}
51.318°	1.82	-0.275	55°	2.5	0	L_{3AD}

X_W = 36.367 cm (14.318 in.)			X_W = 111.274 cm (43.809 in.)			
55°	3.5	-1	55°	3.5	-2	L_{4AA}, L_{4AB}
55°	2.5	-1	55°	2.5	0	L_{4AC}, L_{4AD}

X_W = 14.140 cm (5.567 in.)			X_W = 36.367 cm (14.318 in.)			
41.318°	2.82	-0.725	45°	3.5	-1	L_{3AE}
41.318°	0.82	-0.725	40°	0.5	-1	L_{3AF}

VCK GRID NOTATION
All gaps and overhangs are percent of local wing chord
Dimensions are model scale

	X_W = 14.140 cm (5.567 in.)			X_W = 36.367 cm (14.318 in.)		
δ_{VCK}	GAP	O.H.	δ_{VCK}	GAP	O.H.	NOTATION
41.318^0	1.82	-0.725	45^0	2.5	-1	L_{3AG}
41.318^0	1.82	-0.725	45^0	2.5	0	L_{3AH}

	X_W = 36.367 cm (14.318 in.)			X_W = 111.274 (43.809 in.)		
45^0	3.5	-1	45^0	3.5	-1	L_{4AE}, L_{4AF}
45^0	2.5	-1	45^0	2.5	-1	L_{4AG}, L_{4AH}

LB-486A,B,C GRID NOTATIONS

FCK GRID NOTATIONS

All gaps and overhangs are percent of local wing chord

Dimensions are model scale

X_W = 14.140 cm (5.567 in.)			X_W = 36.368 cm (14.318 in.)			
δ_{FCK}	GAP	O.H.	δ_{FCK}	GAP	O.H.	NOTATION
31.065°	2.82	-0.725	35°	3.5	-1.0	L_{7AA}
31.065°	1.82	-0.725	35°	3.5	-1.0	L_{7AB}
31.065°	0.33	-0.33	35°	0.5	-0.5	L_{7AC}
35°	2.5	-1.0	35°	1.5	-1.0	L_{8AA}, L_{8AB}
35°	0.5	-0.5	35°	0.5	-0.5	L_{8AC}
31.065°	2.82	-0.725	45°	3.5	-1.0	L_{7AD}
31.065°	1.82	-0.725	45°	2.5	-1.0	L_{7AE}
31.065°	0.33	-0.33	45°	0.5	-0.5	L_{7AF}

X_W = 36.368 cm (14.318 in.)			X_W = 111.036 cm (43.715 in.)			
45°	2.5	-1.0	45°	2.5	-1.0	L_{8AD}
45°	1.5	-1.0	45°	1.5	-1.0	L_{8AE}

FCK GRID NOTATIONS

All gaps and overhangs are percent of local wing chord
Dimensions are model scale

X_W = 36.367 cm (14.318 in.)			X_W = 111.036 cm (43.715 in.)			
δFCK	GAP	O.H.	δFCK	GAP	O.H.	NOTATION
45^0	0.5	-0.5	45^0	0.5	-0.5	L_{8AF}
51.065^0	2.82	-0.725	55^0	3.5	-1.0	L_{7AG}
51.065^0	1.82	-0.725)	55^0	2.5	-1.0	L_{7AH}
51.065^0	0.33	-0.33	55^0	0.5	-0.5	L_{7AJ}

X_W = 36.368 cm (14.318 in.)			X_W = 111.036 cm (43.715 in.)			
55^0	2.5	-1.0	55^0	2.5	-1.0	L_{8AG}
55^0	1.5	-1.0	55^0	1.5	-1.0	L_{8AH}
55^0	0.5	-0.5	55^0	0.5	-0.5	L_{8AJ}

X_W = 14.140 cm (5.567 in.)			X_W = 36.368 cm (14.318 in.)			
50^0	0.05	-0.5	50^0	0.05	-0.5	L_{9AA}
60^0	0.05	-0.5	60^0	0.05	-0.5	L_{9AB}
70^0	0.05	-0.5	70^0	0.05	-0.5	L_{9AC}

MAIN FLAP GRID NOTATION

All gaps and overhangs are percent of local wing chord
Dimensions are model scale

Inboard Flap and Flaperon Grid

	X_W = 14.140 cm (5.567 in.)		X_W = 43.411 cm (17.091 in.)		
δF_{MAIN}	GAP	O.H.	GAP	O.H.	NOTATION
	1.3	3.2	2.5	6.0	F_{1AA}
5°	0.8	3.2	1.5	6.0	F_{1AB}
	0.8	2.2	1.5	4.0	F_{1AC}
	1.3	2.2	2.5	4.0	F_{1ADD}
	1.6	1.1	3.0	2.0	F_{1AE}
15°	1.3	2.2	2.5	4.0	F_{1AF}
	0.8	2.2	1.5	4.0	F_{1AG}
	0.8	1.1	1.5	2.0	F_{1AH}
	1.6	0.0	3.0	0.0	F_{1AJ}
25°	1.3	0.0	2.5	0.0	F_{1AK}
	1.3	0.5	2.5	1.0	F_{1AL}
	0.8	0.5	1.5	1.0	F_{1AM}
	1.9	1.1	3.5	-2.0	F_{1AN}
35°	1.3	0.0	2.5	0.0	F_{1AP}
	1.3	0.5	2.5	1.0	F_{1AR}
	1.1	0.5	2.0	1.0	F_{1AS}

MAIN FLAP GRID NOTATION
All gaps and overhangs are percent of local wing chord
Dimensions are model scale

OUTBOARD FLAP GRID

δF_{MAIN}	$X_W = 43.411$ cm (17.091 in.)	$X_W = 89.020$ cm (35.047 in.)		
		GAP	O.H.	NOTATION
5°		2.5	6.0	F_{4AA}
		1.5	6.0	L_{4AB}
		1.5	4.0	F_{4AC}
		2.5	4.0	F_{4AD}
15°		3.0	2.0	F_{4AE}
		2.5	4.0	F_{4AF}
		1.5	4.0	F_{4AG}
		1.5	2.0	F_{4AH}
25°		3.0	0.0	F_{4AJ}
		2.5	0.0	F_{4AK}
		2.5	1.0	F_{4AL}
		1.5	1.0	F_{4AM}
35°		3.5	-2.0	F_{4AN}
		2.5	0.0	F_{4AP}
		2.5	1.0	F_{4AR}
		2.0	1.0	F_{4AS}

APPENDIX C (Concluded)
LB-486A,B,C GRID NOTATION

AFT FLAP GRID NOTATION
All gaps and overhangs are percent of local wing chord
Dimensions are model scale

FLAPERON DIFFERENTIAL POSITION

$X_W = 43.411$ cm
(17.091 in.)

$\delta F_{FLAPERON}$	GAP	O.H.	NOTATION
25°	2.5	1.0	F_{3AR}

$X_W = 14.140$ cm (5.567 in.) $X_W = 30.793$ cm (12.123 in.)

δF_{AFT}	GAP	O.H.	GAP	O.H.	NOTATION
7.5°	0.3	0.8	0.4	1.1	F_{2AA}
10°	0.3	0.8	0.4	1.1	F_{2AB}
12.5°	0.4	0.4	0.5	0.5	F_{2AC}
15°	0.4	0.4	0.5	0.5	F_{2AD}

$X_W = 43.411$ cm (17.091 in.) $X_W = 89.020$ cm (35.047 in.)

δF_{AFT}	GAP	O.H.	GAP	O.H.	NOTATION
7.5°	0.5	1.5	0.5	1.5	F_{5AA}
10°	0.5	1.5	0.5	1.5	F_{5AB}
12.5°	0.75	0.75	0.75	0.75	F_{5AC}
15°	0.75	0.75	0.75	0.75	F_{5AD}

APPENDIX D
LB-507A
CONFIGURATION NOTATIONS

B_{3B} -   Fuselage represents the ATMR-11 aft fuselage and center body. The fuselage nose is the same as the one used with fuselage B_{3A}. The fuselage has cutouts for the tandem-strut-support system and wiper for horizontal tail. Fuselage length = 44.2492 m (145.9619 ft). (F.S.), constant section diameter = 4.310 m (14.142 ft). (F.S.).

W_{1B} -   New technology wing, rigged to represent the airplane wing under a "1g" load at test conditions. Full scale trapezoidal dimensions: $S_W = 148.0$ m^2 (1600 ft^2); $b_W = 40.6198$ m (133.267 ft); AR = 11.10; $\lambda = 0.275$; MAC = 4.054 m (13.300 ft); $\Gamma = 5^0$. The model has removable leading and trailing edges, spoilers, outboard ailerons, and four rows of pressure orifices.

X_{1B} -   Wing fuselage fillet for $B_{3B}W_{1B}$ with two strut clearance holes added.

L_{3A} -   Inboard conventional leading-edge slat extends from station X = 2.267 cm (5.758 in.) to $X_W = 6.6464$ cm (16.882 in.). The slat extends in a streamwise direction and the inboard and outboard trims are streamwise. The inboard slat deflections are 8^0 and 12.5^0 (streamwise angle).

L_{4A} -   Outboard conventional leading-edge slat extends from $X_W = 6.943$ cm (17.636 in.) to $X_W = 17.532$ cm (44.530 in.). The slat extends normal to the wing leading edge. The inboard trim is streamwise and the outboard is normal to the wing leading edge. The outboard slat deflections are 20^0 and 27.5^0 (streamwise angle).

L_{5A} - Inboard FCK with inboard trim normal to the wing leading edge at X_W = 2.399 cm (6.093 in.). The outboard trim is such that the Krueger will seal against the pylon. The inboard FCK deflections are 55° and 70°.

F_{1A} - Inboard main flap extends from station X_W = 1.8047 cm (4.584 in.) to X_W = 6.883 cm (17.484 in.). The flap deflections are 5°, 15°, 25°, and 35°. A pressure row is located at X_W = 6.183 cm (15.704 in.) (left hand).

F_{2A} - Inboard auxiliary flap trim station same as F_{1A}. The deflection angles of the auxiliary flap are 10° and 12.5°. The pressure row is located at X_W = 6.183 cm (15.704 in.).

F_{3A} - Outboard main flap extends from station X_W = 6.895 cm (17.514 in.) to X_W = 14.059 cm (35.710 in.) at the flap leading edge and X_W = 14.133 cm (35.897 in.) at the flap trailing edge. The pressure rows are located at X_W = 10.069 cm (25.575 in.) (left hand) and X_W = 12.807 cm (32.530 in.) (right hand). The flap deflections are 5°, 15°, 25°, and 35°.

F_{4A} - Outboard auxiliary flap trim station X_W = 6.895 cm (17.514 in.) to X_W = 14.133 cm (35.895 in.).

a_{1A} - The trim is streamwise aft to 30% C_a at which point the cut slants outboard to permit flap deflection. The aileron outboard trim station at the leading edge is

X_W = 17.661 cm (44.858 in.) and it is a streamwise cut. The aileron deflections available are -20°, -10°, 0°, +10°, and +20°. The aileron does not have a built in seal.

b_{F1B} — Wing flap linkage fairings representing D-3243-11 cruise configuration from LB-506A. Four per side in addition to the fairing incorporated into pylon.

b_{F1C} — b_{F1B} deflected to maximum position to allow flaps to deflect. One position only relative to the main flap.

f_{1A} — One-piece bent plate representing the three inboard spoiler segments having a 8.66 cm (22 in.) constant chord. (F.S.).

f_{2A} — One-piece bent plate representing the three outboard segments having a 7.874 cm (20 in.) constant chord. (F.S.).

G_{1A} — Main and nose landing gear defined for an EET/ACA airplane.

N_{1C} — A 5.59% scale flow through nacelle representing the Pratt & Whitney JT10D engine. This is the same nacelle configuration used with the LB-506A model.

P_{1C} — A 5.59% scale pylon used in conjunction with the W_{1B} wing and the N_{1C} nacelle. The pylon positions the nacelle centerline at +2° with respect to the FRP and toed-in 2° with respect to plane of symmetry. The pylon is the same one used in conjunction with WTM LB-506A.

D_{2A} — Same dorsal profile as D_{1B} with a modified leading edge contour.

H_{1D} — LB-506 H_{1C} horizontal stabilizer modified at inboard end to match B_{3B} fuselage. Remote control position capability. $S = 0.1144 \text{ m}^2$ (1.2312 ft^2); AR = 4.10; $\lambda = 0.350$; sweep $C_{V/4} = 30^0$; $\Gamma = 10.0^0$.

V_{1D} — LB-506 V_{1C} vertical stabilizer modified at the root to match V_{3B} fuselage. $S_V = 0.0865 \text{ m}^2$ (0.9312 ft^2); $A_R = 1.600$; $\lambda = 0.35$; sweep $C_{V/4} = 35^0$.

S_{11F} — Nacelle strakes from DC-10 model LB-246 on N_{1C} nacelle.

APPENDIX E
LB-507A
DIMENSIONAL DATA

COMPONENT	UNITS	MODEL SCALE	
FUSELAGE B_{3B}			
Length	cm (in.)	248.680	(97.908)
Diameter - Constant Section	cm (in.)	24.079	(9.480)
WING W_{1b}			
Trapezoidal gross area	m^2 (ft^2)	.4645	(4.9997)
Sweepback of the quarter chord	deg	26.00	
Taper ratio	-	0.275	
Aspect ratio	-	11.10	
Trapezoidal root chord	cm (in.)	32.090	(12.636)
Tip chord	cm (in.)	8.840	(3.480)
Mean aerodynamic	m (ft)	0.2266	(0.743)
Span	m (ft)	2.271	(7.449)
Spanwise location of MAC_W	cm (in.)	46.007	(18.113)
Dihedral (1g)	deg	5.00	
VERTICAL STABILIZER V_{1D}			
Gross area	m^2 (ft^2)	0.086	(0.931)
Aspect ratio	-	1.6	
Taper ratio	-	0.35	
Sweepback at c/4	deg	35.0	
Theoretical root chord	cm (in.)	34.442	(13.560)
Theoretical tip chord	cm (in.)	12.070	(4.752)
Mean aerodynamic chord	cm (in.)	25.054	(9.864)
Spanwise MAC_V position	cm (in.)	15.616	(6.148)
Horizontal distance from 25% $\overline{c}_W$ to 25% $\overline{c}_V$	cm (in.)	100.952	(39.745)

NOTE: All dimensions listed are in the FRP system.
All angles listed are in the WRP system.

COMPONENT	UNITS	MODEL SCALE	
HORIZONTAL STABILIZER H_{1D}			
Gross area	m^2 (ft^2)	0.1144	(1.231)
Aspect ratio	-	4.10	
Taper ratio	-	0.35	
Sweepback at c/4	deg	30.0	
Span	cm (in.)	68.4886	(26.964)
Theoretical root chord	cm (in.)	24.750	(9.744)
Theoretical tip chord	cm (in.)	8.656	(3.408)
Mean aerodynamic chord	cm (in.)	17.983	(7.080)
Spanwise MAC_H position	cm (in.)	14.371	(5.658)
Fuselage station of $(0.25)MAC_H$	cm (in.)	243.507	(95.869)
Dihedral angle	deg	10.0	
Horizontal distance from 25% c_W to 25% c_H	cm (in.)	124.419	(48.984)
OUTBOARD AILERON (a_{1A})			
Chord aft of hinge line	$\%C_W$	25.0	
Span	cm (in.)	22.793	(8.974)
INBOARD SPOILER (f_{1A})			
Area	cm^2 (in^2)	3.027	(1.192)
Span	cm (in.)	29.538	(11.629)
Chord	cm (in.)	3.124	(1.230)
OUTBOARD SPOILER (f_{2A})			
Area	cm^2 (in^2)	3.453	(1.360)
Span	cm (in.)	37.051	(14.587)
Chord	cm (in.)	2.841	(1.118)

NOTE: All dimensions listed are in the FRP system.
      All angles listed are in the WRP system.

COMPONENT	UNITS	MODEL	SCALE
NACELLE (N_{1C})			
Length	cm (in.)	30.526	(12.018)
Maximum cowl height	cm (in.)	15.728	(6.192)
Inlet diameter (fan cowl)	cm (in.)	9.327	(3.672)
Inlet area (fan cowl)	cm^2 (in^2)	68.284	(10.584)
Exit area (gas generator)	cm^2 (in^2)	16.258	(2.520)
Incidence of thrust line to FRP	deg	2.0	
Toe in	deg	2.0	
LEADING-EDGE SLAT (L_{3A}, L_{4A})			
Span (L_{3A} - Inboard)	cm (in.)	27.150	(10.690)
Span (L_{4A} - Outboard)	cm (in.)	68.199	(26.850)
Effective span	%b/2	82.476	
INBOARD-MAIN FLAP (F_{1A})			
Area	cm^2 (in^2)	170.291	(26.395)
Span	cm (in.)	33.329	(13.122)
Root chord	cm (in.)	5.386	(2.120)
Tip chord	cm (in.)	4.837	(1.904)
Inboard trim (X_W)	cm (in.)	11.643	(4.584)
Outboard trim (X_W)	cm (in.)	44.409	(17.484)
INBOARD-AUXILIARY FLAP (F_{2A})			
Area	cm^2 (in^2)	105.631	(16.373)
Span	cm (in.)	32.766	(12.900)
Root chord	cm (in.)	3.225	(1.270)
Tip chord	cm (in.)	3.225	(1.270)
Inboard trim (X_W)	cm (in.)	11.643	(4.584)
Outboard trim (X_W)	cm (in.)	44.409	(17.484)

NOTE: All dimensions listed are in the FRP system.
All angles listed are in the WRP system.

COMPONENT	UNITS	MODEL	SCALE
OUTBOARD-MAIN FLAP (F_{3A})			
Area	cm^2 (in^2)	181.997	(28.210)
Span	cm (in.)	46.217	(18.196)
Root chord	cm (in.)	4.831	(1.902)
Tip chord	cm (in.)	3.014	(1.187)
Inboard trim (X_W)	cm (in.)	210.168	(17.514)
Outboard trim (X_W)	cm (in.)	90.980	(35.819)
OUTBOARD-AUXILIARY FLAP (F_{4A})			
Area	cm^2 (in^2)	121.052	(18.763)
Span	cm (in.)	46.689	(18.382)
Root chord	cm (in.)	3.124	(1.230)
Tip chord	cm (in.)	2.042	(0.804)
Inboard trim (X_W)	cm (in.)	44.485	(17.514)
Outboard trim (X_W)	cm (in.)	91.403	(35.985)

NOTE: All dimensions listed are in the FRP system.
All angles listed are in the WRP system.

APPENDIX F
GRID NOTATION LB-507A

SLAT GRID NOTATION

All gaps and overhang are percent of local wing chord
Dimensions are model scale

X_W = 11.117 cm X_W = 44.447 cm
(4.377 in.)   (17.499 in.)

δ_{SLAT}	GAP	O.H.	GAP	O.H.
Inboard				
8A	0.15	6.00	0.30	6.00
8B	0.65	6.00	0.80	6.00
12A	0.53	4.00	0.46	4.00
12.5A	1.50	-1.00	1.50	-1.00

X_W = 44.447 cm X_W = 91.173 cm
(17.499 in.)   (35.895 in.)

δ_{SLAT}	GAP	O.H.	GAP	O.H.
Outboard				
20A	0.00	2.00	0.00	2.00
20B	0.50	2.00	0.50	2.00
27.5	2.25	-2.00	2.25	-2.00
27.5B	1.5	-1.00	1.50	-1.00

APPENDIX F (CONTINUED)
GRID NOTATION LB-507A

FCK INBOARD GRID NOTATION

All gaps and overhang are percent of local wing chord
Dimensions are model scale

X_W = 11.117 cm X_W = 44.447 cm
(4.377 in.)   (17.499 in.)

δ_{SLAT}	GAP	OVERHANG
55A	0.75	-0.75
55B	1.50	-1.0
70A	0.75	-0.75
70B	1.5	-1.0

GRID NOTATION LB-507A

INBOARD TWO-SEGMENT FLAP (F_{1A}/F_{2A})

All gaps and overhangs are percent of local wing chord

Dimensions are model scale

$$X_W = 44.447 \text{cm}$$
(17.449 in.)

MAIN δF_{MAIN}	GAP	OVERHANG	AUX δF_{AUX}	GAP	OVERHANG
5.0	1.50	4.0	10.0	0.50	1.50
15.0	1.50	2.00	10.0	0.50	1.50
25	2.50	0.00	12.5	0.75	0.75
35.0	2.50	-1.00	12.5	0.75	0.75

The inboard flap is rigged at the above station, and at the side of fuselage X_W = 11.117 cm, (4.337 in.) with the same physical gap and overhang.

The outboard flap is also rigged to the above percent gap and overhang values at station X_W = 44.447 cm (17.499 in.). At all stations, outboard, the gap and overhang are the same percentages of the local wing chord.

REFERENCES

1. Oliver, Wayne R.: Results of Design Studies and Wind Tunnel Tests of an Advanced High Lift System for an Energy Efficient Transport. NASA CR-159389, 1980.

2. Steckel, Doris K.; Dahlin, John A.; and Henne, Preston A.: Results of Design Studies and Wind Tunnel Tests of High Aspect Ratio Supercritical Wings for an Energy Efficient Transport. NASA CR-159332, October 1980.

3. Crowder, J.P.: Fluorescent Mini-Tufts for Non-Intrusive Flow Visualization. McDonnell Douglas Report MDC-J7374, February 1977.

4. The Staff of Douglas Aircraft Company: Selected Advanced Aerodynmamic and Active Control Concepts Development. Summary Report. NASA CR-3469, 1981.

1. Report No. NASA CR-3523	2. Government Accession No.	3. Recipient's Catalog No.
4. Title and Subtitle WIND TUNNEL TESTS OF HIGH-LIFT SYSTEMS FOR ADVANCED TRANSPORTS USING HIGH-ASPECT-RATIO SUPERCRITICAL WINGS		5. Report Date July 1982
		6. Performing Organization Code
7. Author(s) John B. Allen, Wayne R. Oliver, and Lee A. Spacht		8. Performing Organization Report No. ACEE-17-FR-1608
		10. Work Unit No.
9. Performing Organization Name and Address Douglas Aircraft Company McDonnell Douglas Corporation 3855 Lakewood Boulevard Long Beach, CA 90846		11. Contract or Grant No. NAS1-15327
		13. Type of Report and Period Covered
12. Sponsoring Agency Name and Address National Aeronautics and Space Administration Washington, D.C. 20546		Contractor Report
		14. Sponsoring Agency Code

15. Supplementary Notes

Langley Technical Monitor: Thomas G. Gainer
Final Report

16. Abstract

The wind tunnel testing of an advanced-technology high-lift system for a wide body and a narrow body transport incorporating high-aspect-ratio supercritical wings is described. This testing has added to the very limited low-speed high-Reynolds-number data base for this class of aircraft. The experimental results included the effects on low-speed aerodynamic characteristics of various leading- and trailing-edge devices, nacelles and pylons, ailerons, and spoilers, and the effects of Mach and Reynolds numbers.

17. Key Words (Suggested by Author(s)) Wings High aspect ratio High lift devices Supercritical Lift Lift augmentation Pitching moments High Lift Flow visualization		18. Distribution Statement FEDD Distribution Subject Category 02	
19. Security Classif. (of this report) Unclassified	20. Security Classif. (of this page) Unclassified	21. No. of Pages 188	22. Price